Involvement of peptidergic Edinger-Westphal nucleus in the neurobiology of migraine and acute alcohol exposure

Al-Omari Ammar

Department of Pharmacology and Pharmacotherapy

University of Pécs

Supervisor:

Viktória Kormos, M.D., Ph.D.

Pécs, 2024

Table of contents

Preface

The main objective of this thesis was to examine the involvement of the centrally projecting Edinger-Westphal nucleus in migraine pathogenesis. First, we examined the anatomical evidence to support our hypothesis, moreover, we initially utilized a nitroglycerin-induced migraine mouse model. However, when we examined the acute neuronal activation of this brain area, both nitroglycerin and vehicle (containing alcohol) treatment resulted in a strong activation of the neurons. Therefore, considering the high sensitivity of Edinger-Westphal nucleus to alcohol and taking into account that the vehicle of all commercially available nitroglicerin preparations contains alcohol, we decided to investigate this brain area in an alternative mouse model of migraine (calcitonin gene-related peptide model). Additionally, based on our unexpected results in nitroglicerin-induced migraine model, our focus turned to the role of this brain area in alcohol consumption. The thesis shows the first step of this study: the examination of the Edinger-Westphal nucleus in a mouse model of acute alcohol exposure. In our ongoing project we are managing a free-choice chronic alcohol consumption model, to shed light on the possible role of this brain area in alcohol addiction.

1. Introduction and literature background

1.1. Edinger-Westphal nucleus

The midbrain's Edinger-Westphal nucleus (EW) comprises two distinct cell populations (Kozicz et al., 2011). One group, the preganglionic (cholinergic) division (EWpg), is part of the oculomotor complex and supplies cholinergic parasympathetic preganglionic fibers to the ciliary ganglion, regulating pupil constriction and lens accommodation. The other subdivision, known as centrally projecting Edinger-Westphal nucleus (EWcp), is peptidergic and expresses various neuropeptides including urocortin 1 (UCN1); cocaine and amphetamine-regulated transcript (CART) and cholecystokinin (CCK) among others. Intermingled with the peptidergic cells, some glutamatergic, choline acetyltransferase (CHAT) immunoreactive and tyrosine hydroxylase (TH)-containing neurons were also identified (Kozicz et al., 2003; Zuniga & Ryabinin, 2020; Li & Ryabinin, 2022; Priest et al., 2023) **(Figure 1.)**. The EWcp sends multiple projections to a number of regions through the brain **(Figure 2.)**.

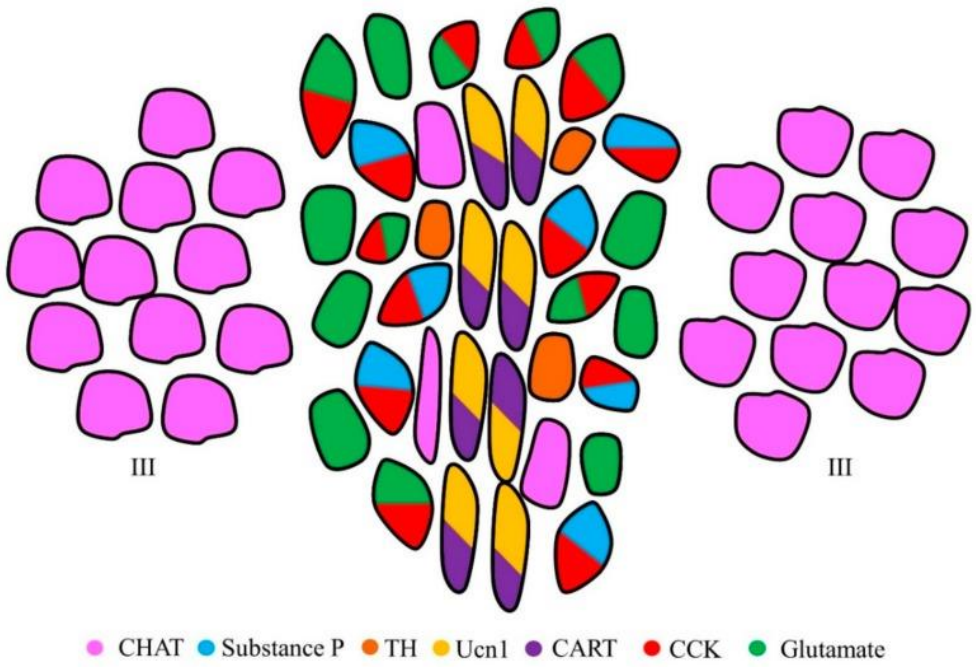

Figure 1. Illustration of the neuropeptides and neurotransmitters known to be expressed in the Edinger-Westphal nucleus (EW). The centrally projecting EW nucleus (EWcp) sits between choline acetyltransferase (CHAT)-expressing cells of the motor nucleus of oculomotor nerve (III). EWcp neurons can be distinguished from the preganglionic EW (EWpg) neurons based on their lack of CHAT expression. The few CHAT-positive neurons within the EWcp most likely represent the EWpg. TH: tyrosine hydroxylase; Ucn1: urocortin 1; CART: cocaine and amphetamine-regulated transcript; CCK: cholecystokinin (Zuniga & Ryabinin, 2020).

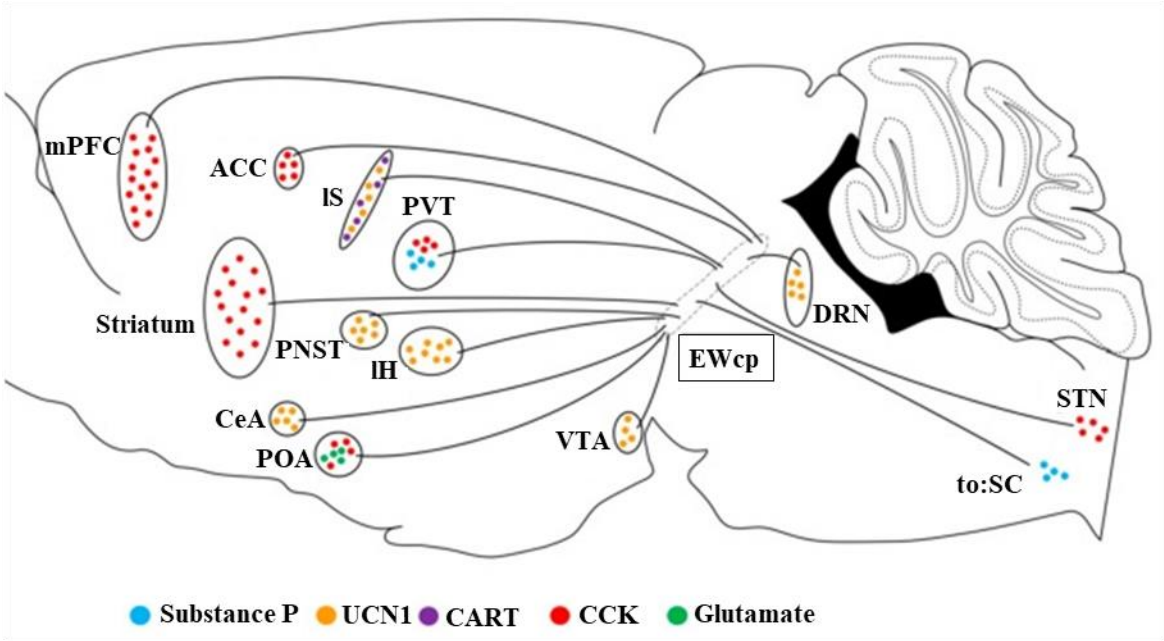

Figure 2. Schematic of central projections arising from the centrally projecting EW nucleus (EWcp). Efferents originating in the EWcp project to a number of regions through the brain. These regions receive specific neuropeptidergic and neurotransmitter inputs from the EWcp. Filled circles denote peptides and neurotransmitters known to be released in that area from the EWcp. Orange circles: urocortin 1 (UCN1); purple circles: cocaine and amphetamine-regulated transcript (CART); blue circles: substance P; red circles cholecystokinin (CCK); green circles: glutamate; ACC: anterior cingulate cortex; BNST: bed nucleus of the stria terminalis; CeA: central nucleus of the amygdala; DRN: dorsal raphe nucleus; lH: lateral hypothalamus; lS: lateral septum; mPFC: medial prefrontal cortex; POA: preoptic area; PVT: paraventricular nucleus of the thalamus; SC: spinal cord; STN: spinal trigeminal nucleus; VTA: ventral tegmental area (Modified based on Zuniga & Ryabinin 2020).

UCN1 is a member of the corticotropin-releasing hormone (CRH) family, which is primarily found in the EWcp (Vaughan et al., 2007). UCN1 binds to both CRH receptors (CRH1R and CRH2R), with a higher affinity for CRH2R over CRH itself (Bale et al., 2002; And & Biol, 2002; Kozicz et al., 2007; Im et al., 2015). UCN1 plays a role in the stress response, reward, appetite control, thermoregulation, and affect the mood status (Fekete et al., 2007; Kormos & Gaszner, 2013; Zuniga & Ryabinin, 2020). CART is a neuropeptide that is known to be involved in energy metabolism (Kristensen et al., 1998.; Elias et al., 2001; Lau et al., 2018) and regulation of feeding, drug reward and addictive behaviors (Vicentic & Jones, 2007; Ong & McNally, 2020; Zuniga & Ryabinin, 2020). Interestingly, UCN1 immunoreactive neurons in the EWcp show a full co-localization with CART. Moreover, our research group previously showed that the EWcp/UCN1 positive neurons are the primary site of expression of the transient receptor potential cation channel subfamily A member 1 (TRPA1) ion channel in the brain **(Figure 3.)**. TRPA1 is a non-selective cation channel which upon activation leads to calcium influx. The

increased intracellular calcium may lead to several types of cellular responses (Julius et al., 2013; Kádková et al., 2017; Talavera et al., 2020). TRPA1 is expressed primarily in the peripheral nervous system and plays a crucial role in several physiological and pathophysiological processes including nociception and inflammatory responses, however its role in the central nervous system (CNS) is less clear yet.

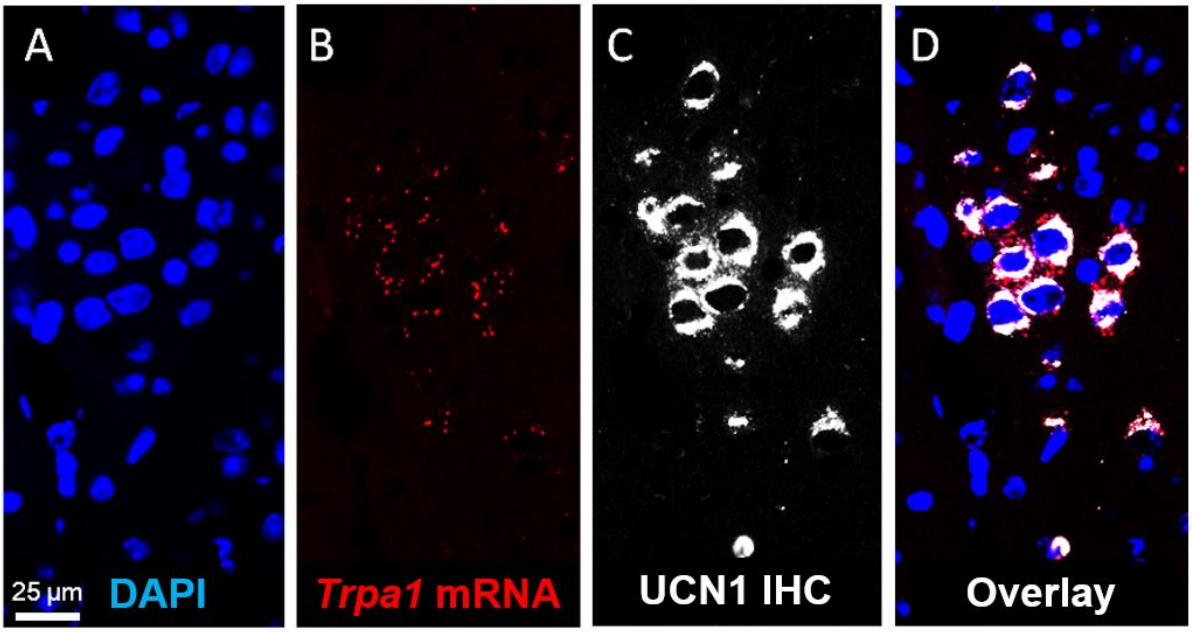

Figure 3. Representative images of transient receptor potential ankyrin 1 (*Trpa1)* mRNA-expressing urocortinergic cells of mouse Edinger-Westphal nucleus. *Trpa1* mRNA (red, B) was visualized by RNAscope *in situ* (ISH) hybridization. Urocortin 1 (UCN1) peptide (white, C) was detected by immunofluorescence. For nuclei, the sections were counterstained with 4′,6-diamidino-2-phenylindole (DAPI) (blue, A). Note the co-localization of *Trpa1* mRNA and UCN1 peptide (D) (Kormos et al., 2022).

1.2. Migraine

Migraine is a neurovascular disorder (Jiang et al., 2019) of primary neuronal dysfunction (Kikkeri & Nagalli, 2022). Migraine is typically manifested as a recurring episode of headache associated with other symptoms of neurological dysfunction in varying admixtures (Goadsby et al., 2018). Episodes of migraine attacks can last for hours up to days and include multiple symptoms such as pulsating headache, nausea, vomiting, photophobia and phonophobia (Wood & Welch, 1993). About one-third of migraineurs experience transient neurological deficits during their attacks, known as migraine aura (Benemei & Dussor, 2019). Before puberty, males are more likely to experience migraine than females. However, when puberty sets in, migraine turns more common in females, and by the late teens, the prevalence of migraine in females is roughly twice that of males. In both sexes, migraine prevalence peaks between the ages of 25 and 55, which are considered to be the most productive years of adulthood (Lipton & Bigal, 2005). Collectively, migraine affects an estimated one billion individuals globally (Ashina et al., 2021), accounting for more disability than all other neurological diseases combined (Vos et al., 2017). While not a life-threatening condition, migraine is an important cause of disability (Stovner et al., 2018) and one of the most common complaints in neurological day-to-day practice (Cutrer & Swanson, 2022).

1.2.1. Neuroanatomy of migraine

Several theories have been proposed to explain the underlying pathomechanism of migraine including the cortical spreading depression (CSD) theory (Harriott et al., 2019), serotonin (5-HT) imbalance theory (Cahill & Murphy, 2004), neurovascular and trigeminovascular theories (Haanes & Edvinsson, 2019). As of today, the most widely accepted theory of migraine is based on the activation and sensitization of the trigeminovascular system. The primary dysregulation of sensory processing will likely result in a constellation of neurological symptoms that affect our senses (Benemei et al., 2017).

The trigeminovascular system is comprised by the meningeal blood vessels and type C as well as type Aδ dendritic axons of first order sensory neurons located in the trigeminal ganglion (TRG) providing nociceptive innervation for intracranial meninges (Ashina et al., 2019). The central (axonic) axon of the pseudounipolar nociceptive TRG cells transmit the pain signals to the spinal trigeminal nucleus (STN) by the fast-acting excitatory neurotransmitter, glutamate. At the same time, when activated, TRG neurons release a variety of neuropeptides from their peripheral and central terminals that are known to play a role in the pathogenesis of migraine.

These include substance P (SP), pituitary adenylate cyclase-activating polypeptide (PACAP), and calcitonin gene-related peptide (CGRP) (Durham et al., 2016; Spekker et al., 2023).

The STN corresponds to a long column of secondary sensory neurons extending from the caudal pontine tegmentum through the entire dorsolateral tegmentum of medulla oblongata till the dorsal horn of rostral cervical spinal cord. The STN is responsible for relaying the protopathic sensory modalities that include perception of pain, temperature and crude touch. Considering that the facial skin, the orbital structures, the nasal and oral cavities are innervated mainly by the trigeminal nerve, the main input arrives from here to the STN. Nevertheless, the STN receives afferents of protopathic type from the middle ear *via* the geniculate ganglion of facial nerve, from the root of tongue, nasal and oral parts of pharynx, through the sensory ganglia of glossopharyngeal nerve moreover from the external acoustic meatus, hypopharynx and larynx *via* sensory vagus ganglia (Stranding et al., 2020; Patel et al., 2024). A rostro-caudal somatotopic arrangement is characteristic for the STN, corresponding to an onion skin pattern on the face starting with the lips in the center. The rostral, oral part (i.e. pontine and upper medullary division of the nucleus) is responsible for the skin of lips and nose. The lower medullary, interpolar part, receives afferents from the skin of chin, cheeks, zygomatic area, eyelids and lower forehead. The upper part of forehead, skin of skalp and, importantly, the meningeal nociception projects to the caudal division of the STN, located in the caudal most medulla oblongata, as well as the first and second cervical spinal cord segments. The second order STN neurons convey the nociceptive signal to the contralateral ventral posteromedial nucleus of the thalamus *via* the trigeminal lemniscus. Third order neurons in the thalamus relay the nociceptive signal through the superior thalamic radiation to the primary somatosensory cortex. The cortical representation area of the meninges is located in the lateral inferior part of the postcentral gyrus in the parietal lobe (a review for neuroanatomy: Edvinsson et al., 2020.)

Diencephalic connections of the STN beyond those to the thalamus, include also hypothalamic afferents. The hypothalamus integrates the pain with viscerosensory information and regulates the basic homeostatic variables mainly by, but not limited to, neural connections to the autonomic nervous system and the neuroendocrine hypothalamo-hypophyseal systems. (Edvinsson et al., 2020).

It has to be noted that the STN sends direct connections to multiple brainstem centers also. Fibers to the rostral ventromedial medulla, and locus coeruleus may control the perception of pain during migraine including the autonomic, endocrine, cognitive and affective symptoms.

The afferents to the ventrolateral periaqueductal gray, nucleus raphe magnus, are particularly important, because these are centers that contribute to the control of the descending antinociceptive serotonergic and noradrenergic systems. The dorsal raphe nucleus (DRN) is also part of the serotonergic midline nuclear complex and its role in pain modulation *via* STN is well-known (Li et al., 1993, Andrade et al., 2013, Rattanawong et al., 2022; Shibata et al., 2022).

The connection of the STN to the CGRP and PACAP-expressing parabrachial nucleus, provides an input of pain information into the higher-order limbic centres including the amygdala, nucleus accumbens among others, that provide the affective value of pain (Almeida et al., 2004).

It's important to note that probably also due to the above summarized anatomical complexity, the exact cause and pathophysiology of migraine are still the subject of ongoing research, and no single mechanism can explain all aspects of this complex condition, highlighting the importance of further research in this area.

1.2.2. Calcitonin gene-related peptide

CGRP is a 37-amino-acid neuropeptide, primarily released from sensory nerves, commonly known for its potent cerebral vasodilative activity (Brain & Grant, 2004). The dilatory effect is facilitated by activation of CGRP receptors, G-protein-coupled heterodimers composed of calcitonin receptor-like receptor (CLR), and receptor activity modifying protein-1 (RAMP1) (McLatchie et al., 1998). The role of CGRP in the pathogenesis of migraine is supported by the large body of preclinical and clinical research results. CGRP is abundant in nociceptive fibers of TRG neurons and can act on CGRP receptors of second-order neurons in the trigeminal nucleus caudalis when released at central nerve endings, providing a connection between the periphery and the central nervous system (Bartsch et al., 2003; Iyengar et al., 2019). CGRP binds with equal affinity to CLR and calcitonin receptor (CTR, encoded by calcitonin receptor mRNA (*Calcr*) gene) when co-expressed with RAMP1. The CLR/RAMP1 complex forms CGRP receptor and CTR/RAMP1 complex creates amylin receptor (AMY1) (Salvatore et al., 2006). CGRP receptor component protein (CRCP) is not necessary for the receptor's activity, but it enhances the efficacy of CGRP (Dickerson et al., 2013).

Activation of the trigeminal system leads to an elevated level of CGRP during migraine attacks (Goadsby et al., 1990), which can be restored to baseline by administration of 5-HT receptor

agonists (triptans), such as sumatriptan and dihydroergotamine (Goadsby & Edvinsson, 1993), concurrent with pain relief (Juhasz et al., 2005).

Although it is generally known that CGRP cannot penetrate the walls of cerebral blood vessels (Edvinsson et al., 2007), several studies have demonstrated that both peripheral (intravenous (i.v.) and intraperitoneal (i.p.)) and central (intracerebroventricular (i.c.v.)) administration of CGRP-induced many migraine-like symptoms in rodents. Additionally, the CGRP-induced migraine-like symptoms were reversed by concomitant administration of sumatriptan or anti-CGRP monoclonal antibodies (Kaiser et al., 2014; Mason et al., 2017; Rea et al., 2018). Therefore, it was reasoned that CGRP can act in both the CNS and peripheral nerves (Raddant & Russo, 2011) **(Figure 4.)**.

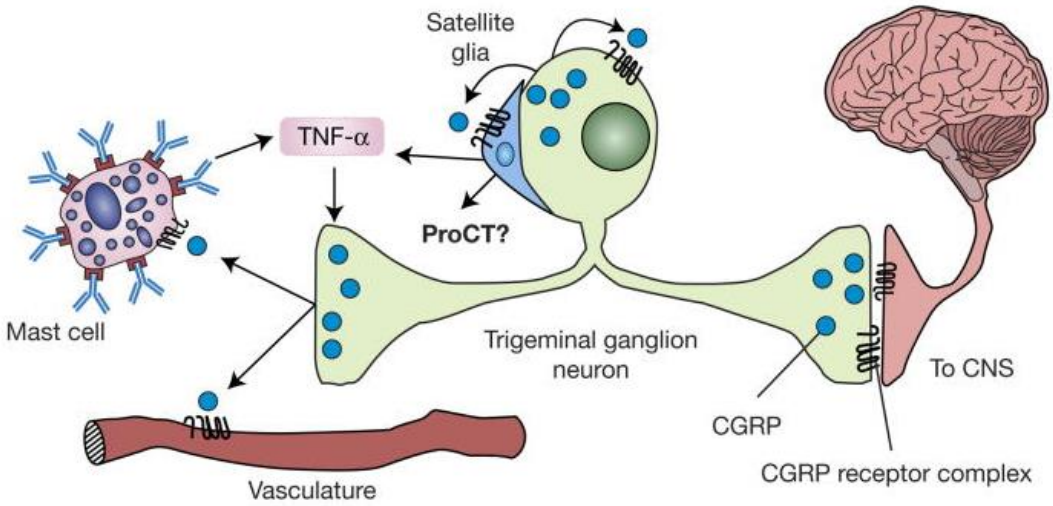

Figure 4. Calcitonin gene-related peptide (CGRP) action at peripheral receptors. CGRP triggers an inflammatory cascade at the periphery. Inflammatory mediators released from mast cells sensitise sensory neurons and promote vascular permeability. Satellite glia influence the local microenvironment within the ganglia by releasing proinflammatory mediators such as tumour necrosis factor α (TNF-α). This can act on trigeminal neurons to increase CGRP synthesis and secretion, setting up a positive-feedback loop, which along with direct actions mediated by CGRP on a subset of trigeminal neurons might contribute to the extended duration of migraine. Satellite glia might also release procalcitonin (proCT), which could also activate CGRP receptors. CNS: central nervous system (Raddant & Russo, 2011).

Human studies have shown that intravenous administration of CGRP can cause migraine headaches in migraineurs (Asghar et al., 2011; Kuburas & Russo, 2023), which can be reversed by systemic intravenous infusion of the CGRP receptor antagonist olcegepant (Olesen et al., 2004). In addition, elevated concentrations of CGRP have been detected in the peripheral blood outside migraine attacks, determining CGRP as a possible biomarker in the diagnosis of chronic

migraine (Cernuda-Morollon et al., 2013). Three anti-CGRP antibodies (eptinezumab, fremantezumab and galcanezumab) and one anti-CGRP receptor antibody (erenumab) have been shown to be therapeutically effective in migraine prevention (Tepper et al., 2018; de Vries & MaassenVanDenBrink, 2019; Schiano di Cola et al., 2023). Their inability to pass the human brain-blood barrier (BBB) suggest a site of action outside the CNS (Edvinsson et al., 2015; Ashina et al., 2017). Potential targets may be the trigeminal system, cerebral blood vessels, and dura mater (Henson et al., 2020). Small molecule CGRP receptor antagonists (gepants), such as atogepant and remegepant, are promising candidates for the treatment of acute migraine (attacks) (Hargreaves & Olesen, 2009) due to their minor molecule nature (Negro & Martelletti, 2019; Henson et al., 2020). They are on the way to becoming the newest class of drugs approved for the treatment of migraine (Dubowchik et al., 2020).

1.2.3. Migraine therapy

Available pharmacological treatment options of migraine differ between countries and include both acute and preventive therapies. According to the International Headache Society Clinical Trials Standing Committee the success of migraine treatments is determined by two clinical outcomes, the freedom from headache pain and the absence of migraine-associated symptoms (i.e. nausea, vomiting, photophobia, or phonophobia) within two hours after treatment (Diener et al., 2019). A wide range of drugs are reported to be suitable for the treatment of acute migraine attacks.

Options of acute therapy:

- Nonsteroidal anti-inflammatory drugs (paracetamol, acetylsalicylic acid, diclofenac and ibuprofen) (Pardutz & Schoenen, 2010).
- Serotonin ($5HT_{1b}$ and $5HT_{1d}$) receptor agonists (Ergot alkaloids, sumatriptan, naratriptan, rizatriptan, almotriptan, eletriptan, frovatriptan) (Yang et al., 2021).
- Serotonin ($5HT_{1f}$) receptor agonist (lasmiditan) (Vila-Pueyo et al., 2021).
- CGRP receptor antagonists (rimegepant and ubrogepant) (Rissardo & Caprara, 2022).

In migraine sufferers for whom acute medication is ineffective, preventive medications are used to reduce the frequency, intensity, or duration of migraine attacks.

Options of preventive therapy:

- Beta-adrenergic receptor antagonists (propranolol, atenolol, bisoprolol, metoprolol, nadolol) (Danesh & Gottschalk, 2019).
- Antiepileptic agents (topiramate, valproate) (Parikh & Silberstein, 2019).
- Antidepressants drugs (amitriptyline, venlafaxine, nortriptyline, duloxetine) (Burch et al., 2019).
- Monoclonal antibodies against CGRP receptor (erenumab) (Diener et al., 2020).
- Monoclonal antibodies against CGRP (eptinezumab, fremanezumab, galcanezumab) (Diener et al., 2020).

1.2.4. Experimental models of migraine

Our knowledge on the neurobiology of migraine headache has largely improved as a result of basic science research utilizing animal models of migraine-related pain. Today, there are several well-validated animal models that are relevant to study migraine, all of which relies on the activation and sensitization of the meningeal nociceptors and the trigeminal neurons.

In vitro application of inflammatory mediators to dissociated meningeal afferents

Administration of inflammatory substances like CGRP, SP, prostaglandins and nitric oxide, is usually combined with electrophysiological tools that provide information on specific changes of meningeal afferent excitability, ion channel modulation, and afferent responses to migraine therapeutic targets (Harriott & Gold, 2009; Harriott et al., 2012).

Results from this model support the inflammatory mediator-induced sensitization of trigeminovascular nerve terminals, furthermore, provide evidence for the efficacy of sumatriptan, a 5-$HT_{1B/1D}$ receptor agonist and migraine abortive drug. Importantly, results from this model also revealed sex differences, where a greater proportion of the dural afferents were sensitized in response to the inflammatory mediator in female compared to male rats. There were also sex differences in active electrophysiological properties of the action potential (AP) in females as compared to males following inflammatory mediator exposure. This suggests sex-dependent inflammation-induced modulation of voltage gated ion channels (Vaughn & Gold, 2010; Scheff & Gold, 2011; Harriott et al., 2012).

Nevertheless, despite these significant findings, a number of limitations of this model should be carefully taken into account. Acute dissociation of trigeminal ganglion neurons may result

in changes in neuronal excitability and mild nerve damage. Due to the isolated nature of this model, studying the interactions with neuronal and non-neuronal populations, such as sympathetic and parasympathetic neurons and ganglionic satellite glial cells, is also impossible. Moreover, recruitment of *in vitro* methods to investigate the long-term, repeated administration of inflammatory agents is challenging. As a result, this model cannot be used to study migraines' recurrent nature (Kilkenny et al., 2010).

In vivo direct electrical stimulation of trigeminal neurons

Stereotaxtic bipolar electrodes inserted into anesthetized animals can be used to stimulate the TRG electrically. Compared to *in vitro* models, this model has the advantage of allowing a more direct examination of tissue-specific alterations in the meninges, central neuron activation, and the response of these changes to drug therapy. TRG stimulation in this model has been shown to induce CGRP release from perivascular afferent terminals that innervate the meninges and to activate neurons in the trigeminal nucleus caudalis (Knyihar-Csillik et al., 1995). The fact that sumatriptan administration did not affect this activation suggests that the drug has a peripheral mechanism of action (Knyihar-Csillik et al., 1997). Such studies opened new avenues in field to identify specific migraine-related pain processing nuclei throughout the brain.

Although *in vivo* electrical stimulation models as compared to *in vitro* models are more suitable for studying the biological complexity of disease, the invasive nature of craniotomy and tissue exposure limit their applicability in chronic migraine research. Additionally, upstream processes that result in trigeminal activation are circumvented and the stimulation parameters need to be carefully regulated to avoid supramaximal stimulation, which might not accurately represent a physiological state (Akerman et al., 2013). Considering that animals in this model are anesthetized, the response to pain cannot be assessed with suitable behavioral tests.

In vivo administration of inflammatory substances to the meninges

This model relies on the application of a single or a combination of inflammatory substances (inflammatory soup) to the dura. Commonly used substances include histamine, 5-HT, bradykinin, prostaglandin E2, cytokines and complete Freund’s adjuvant (Zhang et al., 2012; Lukács et al., 2017; Avona et al., 2019). Trigeminovascular meningeal afferents have been shown to be reliably activated and sensitized *in vivo* by meningeal exposure to the inflammatory substances listed above. Outcomes of this model showed activation and sensitization of the

spinal trigeminal nucleus (Lukács et al., 2017), furthermore, the repeated administration of inflammatory soup into the dura induces a chronic periorbital hypersensitivity to tactile stimuli, suggestive of a model of chronic migraine (Oshinsky & Gomonchareonsiri, 2007).

This model provides alternative delivery methods, requiring less invasive procedures that are now amenable to behavioral testing (Burgos-Vega et al., 2019). When selecting this model, the researcher must consider some limitations. For instance, upstream events leading to trigeminal activation are bypassed and the inflammatory substances utilized require careful control to prevent supramaximal stimulation. Moreover, mast cell degranulation around the catheter insertion site could be a consequence of such surgical procedures.

***In vivo* exogenous administration of algogenic substances**

Algogenic substances that are used in animal model of migraine includes nitroglycerin (NTG), CGRP, and PACAP. Recent preclinical studies have identified several pain-related and non-pain phenotypes following their administration and their utility is further enhanced by the ability to study both acute administration and a more chronic regime, considered relevant to migraine chronification (Ernstsen et al., 2022; Sureda-Gibert et al., 2022). The selection of a specific algogenic agent is dependent on the individual study requirements.

This model has several advantages as well as important limitations to consider. Exogenous algogenic substances are not restricted to specific peripheral or CNS sites and as such, have the potential to act more generally in migraine-relevant structures. This has clear advantages for disease modelling with the induction of premonitory symptoms in patients (Maniyar et al., 2014; Wattiez et al., 2019). Such model also has the potential to explore both acute and a more chronic migraine-like state in rodents (Pradhan et al., 2014). However, with this model events leading to trigeminal activation are bypassed and specific dosing regimens need to be adopted to allow more thorough comparison between studies.

Notably, all above mentioned animal models of migraine were shown to involve CGRP and its receptor in some way, highlighting its potential role in the neurobiology of migraine (**Figure 5.**).

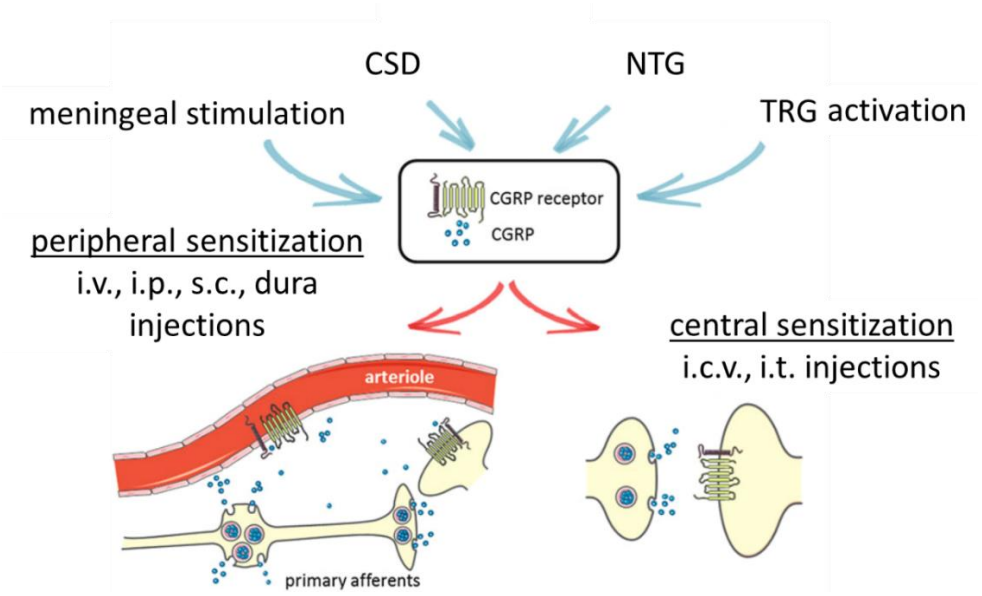

Figure 5. Calcitonin gene-related-peptide (CGRP) in animal models of migraine. Animal models of migraine induced by activation of the trigeminal ganglia (TRG), meningeal stimulation, infusion of nitroglycerin (NTG), or cortical spreading depression (CSD) have been shown to involve CGRP and its receptor. A schematic of the calcitonin-like receptor and receptor activity-modifying protein 1 (RAMP1) complex is shown on vessels and neurons. Not shown are CGRP receptors on other cells, including mast cells and glia. While the exact sites and actions of CGRP that are important for migraine are not known, evidence from animal models suggests that there are both peripheral and central sensitization mechanisms. Likewise, administration of CGRP by peripheral and central routes is believed to induce migraine-like phenotypes through these sensitization mechanisms. Peripheral delivery routes include intravenous (i.v.), intraperitoneal (i.p.), subcutaneous (s.c.), and direct administration onto the dura. Central delivery includes intracerebroventricular (i.c.v.) and intrathecal (i.t.) routes. Genetic models involving loss or gain of CGRP and/or receptor subunits can also modulate peripheral and central CGRP actions (Wattiez et al., 2019).

1.2.5. Possible role of EWcp in migraine

The involvement of the CRH-related neuropeptide, UCN1-containing division of the EWcp in acute pain was shown. It is known that the EWcp is activated and expresses more *Ucn1* mRNA in acute pain (Kozicz et al., 2001; Rouwette et al., 2011). Moreover, EWcp sends multiple projections to various pain-sensitive centers in the brain, implicated in the pathophysiology of migraine, including the DRN, STN and lateral hypothalamus (lH) (Zuniga & Ryabinin, 2020) (**Figure 2.**). Although, many resting-state functional connectivity studies have mapped the functional connectivity profile of numerous migraine-related centres in the brain, none of these studies investigated the functional connectivity profile of the EW nucleus (Skorobogatykh et al., 2019).

Among EWcp's projection areas the DRN plays a crucial role in the pathophysiology of migraine by regulating central 5-HT levels (Rattanawong et al., 2022; Shibata et al., 2022). 5-HT contribute to the pathomechanism of migraine possibly by regulating CGRP levels and by its direct vascular action (Puledda et al., 2023). Variations in the gene responsible for the production of the rate-limiting enzyme in 5-HT synthesis, known as tryptophan hydroxylase 2 (TPH2), could potentially increase individuals' susceptibility to migraine (Marziniak et al., 2009; Jung et al., 2010). The DRN expresses both CRH1R and CRH2R, with a relatively high CRH2R expression compared to other brain regions (Chalmers et al., 1995). As UCN1 is an endogenous ligand of these receptors, the presence of CRH receptors in migraine-related brain areas suggests potential regulatory role of EWcp in migraine.

This hypothesis is supported by prior studies demonstrating the presence of several migraine-related neurotransmitters, neuromodulators, and receptors in the EWcp, including PACAP and its specific receptor (PAC1) (Markovics et al., 2012; Fehér et al., 2023; Priest et al., 2023). Additionally, neuronal nitric oxide synthase (nNOS), substance P, TRPA1 ion channel (Kormos et al., 2022) and CGRP-immunoreactive nerve fibers have been identified in the EWcp (Maciewicz et al., 1983; Smith et al., 1994; Spina et al., 2004).

There is a large body of literature data on the role of peripheral TRPA1 ion channel in migraine pathogenesis (Souza Monteiro de Araujo et al., 2020; Shibata et al., 2021; Iannone et al., 2022a, 2022b; Spekker et al., 2022; Fila et al., 2023; Masood et al., 2023). Several substances identified as TRPA1 agonists, including cigarette smoke, ammonium chloride, formaldehyde, chlorine, garlic, and others (Bautista et al., 2005; McNamara et al., 2007; Andrè et al., 2008; Bessac et al., 2008; Fujita et al., 2008) are known triggering factors of migraine attacks (Courteau et al., 1994; Peatfield et al., 1995; Wantke et al., 2000; Irlbacher & Meyer, 2002; Kelman et al., 2007). Benemei and colleagues demonstrated that acrolein, a component of cigarette smoke, causes ipsilateral meningeal vasodilatation in rats through a CGRP and TRPA1-dependent mechanism after intranasal administration to the mucosa, providing a possible explanation for the correlation between exposure to cigarette smoke and the appearance or worsening of migraine attacks (Benemei et al., 2013). Additionally, it has been reported that activation of TRPA1 ion channels in Schwann cells contribute to ethanol-evoked periorbital mechanical allodynia in mice (Landini et al., 2023). Numerous studies have examined TRPA1-desensitizing compounds, such as parthenolide from the feverfew herb (Materazzi et al., 2013) and isopetasin from butterbur (Benemei et al., 2017), for their ability to desensitize meningeal nociceptors, potentially explaining their efficacy in the treatment of migraine. These studies have shown that natural-product modulators of TRPA1 lead to functional desensitization of both the channel and

the nerve ending expressing the channel. This results in a reduced response of nociceptive nerve endings to stimulation and, in the case of migraine, could lead to a decrease in nociceptive input from the meninges. Collectively, these studies indicate that compounds capable of desensitizing TRPA1 and TRPA1-expressing nerve endings may be considered as new therapeutic targets in the treatment of migraine (Benemei & Dussor, 2019). Our recent finding, that the peptidergic EWcp cells exhibit high *Trpa1* mRNA expression while in other brain areas the expression was relatively low, suggests that the investigation of the possible role of EWcp/TRPA1 in migraine is relevant.

In line with this idea, the EWcp also plays a role in stress adaptation (Kormos & Gaszner, 2013) is influenced by circadian rhythm (Gaszner et al., 2009) and ovarian hormones changes (Derks et al., 2007, 2010), which are known triggers of migraine attacks.

Based on all these, we decided to examine the potential role for EWcp in the neurobiology of migraine.

1.3. Alcohol addiction

Ethanol is a toxic and psychoactive chemical with strong addictive and dependence-producing properties (World Health Organization 2022). Misuse of alcohol is an important public health problem as well as a significant risk factor for disability and death worldwide (Ferraguti et al., 2015), as it is associated with more than 200 kinds of diseases (Ilhan & Yapar, 2020; Shield et al., 2013). Alcohol use disorders are responsible for 3 million deaths worldwide each year, accounting for 5.3% of all deaths. Adverse consequences of addiction include mental and behavioral changes, mood disorders, and depression, highlighting the importance of this research topic.

1.3.1. Role of EWcp in alcohol consumption

Many research groups have provided evidence on the role of EWcp UCN1 and CART neuropeptides in actions of alcohol and other addictive drugs (Ong & McNally, 2020; Zuniga & Ryabinin, 2020).

Several genetic studies have indicated that higher alcohol preference in various strains of mice and rats was associated with increased UCN1 levels (Turek et al., 2005; Bachtell et al., 2003; Fonareva et al., 2009). Additionally, lesions of the rodent EW nucleus significantly reduces ethanol preference (Bachtell et al., 2004; Ryabinin & Weitemier, 2006). UCN1/CART positive neurons exhibit a strong FOS (marker of acute neuronal activity) response, when exposed to

both passive and self-administered ethanol acutely, as demonstrated in several studies (Bachtell et al., 1999; Ryabinin et al., 2001; Weitemier et al., 2001; Zuniga & Ryabinin, 2020). The increased neuronal activity was positively correlated to the amount of consumed alcohol, suggesting a dose-dependent response (Sharpe et al., 2005; Giardino et al., 2017). Similarly, previous studies reported increased FOSB activity (marker of chronic neuronal activation) of EWcp UCN1/CART-expressing neurons in response to chronic alcohol exposure in mice (Bachtell et al., 1999; Ozburn et al., 2012).

While numerous studies have explored the significance of CART in addiction (Bakhtazad et al., 2016; Kuhar et al., 2016), there is a limited body of research concerning the involvement of EWcp/CART in the regulation of alcohol consumption. For instance, CART knockout (KO) mice exhibited significantly lower alcohol preference compared to WT mice in a free choice alcohol consumption model (Salinas et al., 2014). Another study reported that in low alcohol preference DBA/2J mice there is a decrease in CART expression at both the mRNA and peptide levels within the EWcp when compared to high alcohol-preferring C57BL6J mice (Giardino et al., 2017). The full co-localization of UCN1 and CART within the EWcp, along with their elevated peptide and mRNA levels in mice with higher alcohol preference, implies a shared and significant role in controlling alcohol consumption and associated behaviors.

The EWcp UCN1 and CART co-expressing neurons project to several addiction- and reward-related-, moreover CRH receptor-expressing brain areas, among which I would like to highlight the VTA and DRN (Schreiber & Gilpin, 2018; Zuniga & Ryabinin, 2020) (**Figure 2.**).

The DRN contains approximately one third of all serotonergic neurons in the brain (Huang et al., 2019). The brain's serotonergic system plays a crucial role in controlling reinforcement. 5-HT is known to be involved in the regulation of emotional response to reward (Ren et al., 2018; Liu et al., 2020).

The VTA is a part of the mesocorticolimbic pathway, regulating reward and addiction behaviors through mediating dopamine release (Cai et al., 2022).

1.3.2. Possible role of TRPA1 ion channel in alcohol addiction

The peripheral role of TRPA1 in nociception and inflammatory responses has been well established (Kádková et al., 2017, Jannis et al., 2019). In contrast, only limited knowledge has accumulated on its central role and to the best of our knowledge it has not been studied in

relation to alcohol addiction. Some articles described the relationship between alcohol, and TRPA1, but it was studied exclusively in context of pain.

Komatsu and colleagues (2012) found that ethanol activates TRPA1, as measured by calcium imaging in human embryonic kidney-derived 293 (HEK293) cells expressing human TRPA1.

Alcohol is metabolized by alcohol dehydrogenase into the reactive and toxic intermediate product acetaldehyde, which is rapidly converted into acetic acid (Cederbaum et al., 2012). Acetaldehyde is considered as the major contributor of the detrimental effects by acute and chronic alcohol consumption including flushing, headache, cirrhosis, and cancer (Eriksson et al., 2001).

Bang and colleagues (2007) found in pain models that human and mouse TRPA1 are activated by acetaldehyde, in the HEK293T cell heterologous expression system and in cultured mouse trigeminal neurons. Acetaldehyde failed to activate other temperature sensitive transient receptor potential ion channels (TRP) expressed in sensory neurons. TRPA1 antagonists, camphor, gadolinium, and a general TRP blocker ruthenium red inhibited the TRPA1 activation by acetaldehyde. Another research group showed that Schwann cells express TRPA1 that orchestrates ethanol-evoked neuropathic pain in mice (De Logu et al. 2019). Most recently Landini (2023) found that acetaldehyde *via* CGRP receptor and TRPA1 in Schwann cells mediates ethanol-evoked periorbital mechanical allodynia in mice.

Wang's research group (2011) found that the final metabolite of alcohol, acetic acid also can activate the TRPA1 in trigeminal neurons based on patch clamp recordings and Ca^{2+} microfluorometry.

As we most recently showed that urocortinergic neurons in EWcp uniquely express significant amount of TRPA1 in the mouse CNS (Kormos et al. 2022) **(Figure 3.)** and because a) the CRH system, more particularly UCN1 is involved in acute and chronic alcohol consumption (Schreiber & Gilpin, 2018; Zuniga & Ryabinin, 2020), moreover, b) alcohol and all the above-described metabolites efficiently pass through the blood brain barrier, the question arises if they directly act on TRPA1 receptors in the EWcp. The activation of TRPA1 leads to calcium influx which triggers several intracellular pathways, which may contribute to the regulation of UCN1 and/or CART peptide release.

Based on this, we decided to examine the role of TRPA1 in the UCN1 and CART co-expressing EWcp neurons response to acute alcohol exposure in mice.

2. Aims and hypothesis

2.1. Investigation of EWcp in migraine

We aimed to investigate the involvement of EWcp urocortinergic neurons in the neurobiology of migraine. We hypothesized that EWcp urocortinergic neurons may be involved in the regulation of migraine induction or in the endogenous response to migraine through direct neuroanatomical connection with migraine-related brain areas.

I. Neuroanatomical and qualitative morphological examination of migraine-related targets

To support our hypothesis on the involvement of EWcp urocortinergic neurons in the neurobiology of migraine, we aimed to investigate the expression of CGRP receptor components in mouse and human EWcp and DRN, as well as mouse STN. We also aimed to examine a possible urocortinergic projection from EWcp to *Crhr1* and *Crhr2* positive neurons in the STN. Here, we anticipated that the migraine-related targets express the CGRP receptor components and that the EWcp/UCN1 neurons may influence the function of *Crhr1*- and *Crhr2*-expressing cells in the STN *via* a direct urocortinergic projection.

II. Investigation of the EWcp in a nitroglycerin-induced migraine mouse model

Our goal was here to assess the functional and morphological changes in the EWcp in the NTG-induced migraine model. In this study, we hypothesized that NTG may modulate the EWcp function by inducing a migraine-like state.

III. Investigation of the EWcp and its migraine-related projection areas in a CGRP-induced migraine model

In this project we aimed at investigating the functional-morphological changes in the urocotinergic EWcp and its in migraine-related projection areas (such as DRN and STN) in the CGRP-induced migraine-like state. Here, our expectation was that CGRP influences the function of EWcp, DRN and STN.

IV. Targeted ablation of the EWcp urocortinergic neurons with leptin-conjugated saporin in mice

To confirm the role of EWcp/UCN1 neurons in migraine, upon selective ablation of EWcp/UCN1 neurons we examined the migraine-related behaviors in response to CGRP

treatment. Our hypothesis was that the selective ablation of EWcp/UCN1 neurons will influence the migraine-related behaviors induced by CGRP.

V. Mapping of human EW's functional connectivity by fMRI

To provide human data supporting our hypothesis that EW can influence the function of migraine-related areas through a direct anatomical connection, we aimed to examine the functional connectivity matrix of EW in control humans, with a special focus on the STN and DRN. Then, to compare it with interictal migraineurs' functional connectivity matrix. Finally, we also aimed to examine the association between migraine frequency and the functional connectivity of the EW. In this study, we anticipated that there is a positive functional connectivity between the EW nucleus and the STN as well as the DRN.

2.2. Examination of EWcp/TRPA1 in acute alcohol exposure model

In this project we aimed to investigate the involvement of EWcp/TRPA1 in a mouse model of acute alcohol exposure. We hypothesized that alcohol and its metabolites, may influence the function of EWcp urocortinergic neurons by activating TRPA1 ion channels.

I. Investigation of the functional activity of TRPA1 in the mouse EWcp

Because we did not have evidence for the occurrence of TRPA1 at protein level due to the lack of reliable antibodies, our first aim in this project was to provide evidence for the functional activity of the TRPA1 in acute mouse EWcp slices by electrophysiology. Here we expected that TRPA1 in the EWcp is functionally active.

II. Examination of the expression of *TRPA1* mRNA in human EWcp

To support the translational relevance of our previous findings and due to the lack of literature data on the expression of TRPA1 ion channel in human EW, our objective was to examine the expression of *TRPA1* mRNA in human EWcp urocortinergic neurons. In this experiment we hypothesized that, like the mouse EWcp/UCN1 neurons, human EWcp/UCN1 neurons also expresses *TRPA1* mRNA.

III. Investigation of the *Trpa1*-expressing EWcp in a mouse model of acute alcohol exposure

Here, we aimed to test weather TRPA1 ion channels may contribute to the recruitment of EWcp urocortinergic neurons in response to acute alcohol exposure involving *Trpa1* KO mice. Here, our hypothesis was that alcohol may regulate UCN1 and/or CART peptide levels in the EWcp by modulating the function of TRPA1 ion channel.

3. Materials and methods

3.1. Experimental design of animal studies

3.1.1. Investigation of EWcp in migraine

3.1.1.1. Neuroanatomical and qualitative morphological examination of migraine-related targets

Naïve C57Bl6/J mice (n=6) were used to examine the expression of AMY1 and CGRP receptor components in the EWcp, DRN and STN as well as *Crhr1*, *Crhr2* mRNA in the STN.

Immunofluorescence targeting CLR and RNAscope *in situ* hybridization (ISH) targeting *Ramp1*, *Calcr* and *Crcp* mRNA was combined with a) UCN1 immunofluorescence in the EWcp to assess the co-localization with urocortinergic neurons; b) TPH2 or 5-HT immunostaining in the DRN as a marker of the serotonergic neurons; c) a neuronal nuclear marker (NeuN) immunofluorescence in the STN to visualize the dorsal horn neurons.

To examine the possible urocortinergic connection between the EWcp and STN, the mouse EWcp (n=6) was injected with an anterograde tracer, adeno-associated virus serotype 8 (AAV8) containing enhanced green fluorescent protein gene (EGFP) (AAV8 Syn EGFP). For the mouse STN, the dorsal horn of the C1 spinal segment (n=6) was injected by a retrograde tracer, cholera toxin subunit B (CTB). To validate the anatomical localization of the site of injections, CTB and green fluorescent protein (GFP) immunofluorescence was performed in the C1 segment of spinal cord and in the EWcp, respectively. For anterograde tracing, UCN1 and GFP double immunostaining was applied on C1 spinal cord sections. For the retrograde tracing, UCN1 and CTB double immunofluorescence was performed on EWcp slices.

Finally, we investigated the expression of the receptor targets of UCN1, *Crhr1* and *Crhr2* in the I-III laminae of the STN. For this purpose, RNAscope ISH targeting *Crhr1*, *Crhr2* and *NeuN* as a neuronal marker, was combined with UCN1 immunofluorescence in the STN. Our goal was here to identify urocortinergic afferentation innervating *Crhr1*- and *Crhr2*-positive neurons in the STN.

3.1.1.2. Investigation of the EWcp in NTG-induced migraine model

C57Bl6/J mice (n=6/group) were assigned into three experimental groups: NTG as treatment group, vehicle and saline as control groups. Mice were intraperitoneally injected by NTG (10 mg/kg) or by the vehicle (saline-based solution containing 6% ethanol and 16% propylene glycol) or by saline, respectively. Mice were euthanized 4 hours after the treatment for the

morphological studies. Immunohistochemistry (IHC) for the acute neuronal marker (FOS) with diaminobenzidine (DAB) was performed in the EWcp slices.

3.1.1.3. Investigation of the EWcp and its migraine-related projection areas in a CGRP-induced migraine model

C57Bl6/J mice (n=11-15/group) were handled for two weeks and assigned into two experimental groups: saline as control and CGRP-treated groups. Upon i.p. injection of 0.1 mg/kg CGRP (α-CGRP mouse, rat (CRB), Cat. No.: crb1000889) or saline, light aversion was measured 30 minutes after the injection using light-dark box (LDB) test to assess photophobia associated with migraine-like state. Another cohort of mice (n=13) was used to assess periorbital hyperalgesia using von Frey filaments in the same model, 30 minutes after the treatment.

Because the EWcp is known to be sensitive to various stressors (Gaszner et al., 2004, 2012), we had to avoid the acute stress-related changes in the EWcp caused by LDB or von Frey tests. Therefore, we used an independent cohort of mice for the functional-morphological studies. Two experimental groups were created: saline (n=6) as a control and CGRP-treated (n=6) groups. After two weeks handling and habituation to i.p. injections, mice were treated with 0.1 mg/kg CGRP or saline, respectively. Mice were euthanized 4 hours after the treatment. Immunohistochemistry for the neuronal activation marker FOS was performed in the EWcp, lateral periaqueductal gray matter (lPAG) and laminae I-III of STN. Additionally, we performed immunofluorescence for the alternative neuronal activity marker phosphorylated cAMP-responsive element binding protein (P-CREB) (Priest et al., 2021) in the STN. Immunohistochemistry for FOS with DAB was performed in the EWcp, lPAG and STN. Whole mount FOS immunofluorescence was applied in the TRGs to assess the acute neuronal activation in response to CGRP treatment. UCN1 and FOS immunofluorescent staining was applied to prove that the activated neurons in the EWcp were urocortinergic. *Ucn1* RNAscope ISH was combined with UCN1 immunofluorescence to assess the mRNA's and peptide's density in the EWcp. 5-HT and TPH2 double staining was performed to assess 5-HT and TPH2 signal density in the DRN.

3.1.1.4. Targeted ablation of the EWcp urocortinergic neurons

We performed stereotactic surgery to induce selective UCN1 neuron ablation using leptin-conjugated saporin (ribosome-inactivating protein) in C57Bl6/J mice (n=13). Saporin is a

neurotoxin that enters neurons only if it is conjugated to a substance that is internalized by receptor-mediated endocytosis and irreversibly inhibits the cells' protein synthesis (Wiley et al., 2000). Given that in the EWcp only UCN1 immunoreactive neurons express leptin receptor, leptin-conjugated saporin injection provides a reliable tool to perform selective UCN1 neuron ablation (Ujvári et al., 2022, Xu et al., 2022). Periorbital hyperalgesia in response to intraperitoneal injection of 0.1 mg/kg CGRP or saline were assessed before and 2 weeks after the surgery. EWcp/UCN1 positive cells were counted to evaluate the saporin-induced urocortinergic neuronal loss using DAB immunohistochemistry for UCN1.

3.1.2. Examination of EWcp/TRPA1 in acute alcohol exposure model

3.1.2.1. Examination of the functional activity of TRPA1 in the mouse EWcp

We performed patch clamp electrophysiological examinations to test the functional activity of the TRPA1 in acute mouse EWcp slices by electrophysiology, using JT010, a selective and potent TRPA1 agonist.

3.1.2.2. Investigation of the TRPA1-expressing EWcp in a mouse model of acute alcohol exposure

9-12 weeks-old male *Trpa1* KO mice and their WT counterparts were assigned to four experimental groups (n=6-8/group): *Trpa1* KO and WT mice received i.p. injection of 6% ethanol (D=1g/Kg), another set of *Trpa1* KO and WT mice received i.p. injection of equivalent volume of physiological saline as control. Mice were euthanized 2 hours after the treatment for the morphological studies, where we examined the FOS, UCN1 and CART peptide immunoreactivities, moreover *Trpa1*, *Ucn1* and *Cart* mRNA expression.

3.2. Experimental design of human studies

3.2.1. Qualitative morphological studies

To examine the expression of *TRPA1* mRNA in the EWcp, AMY1 and CGRP receptor components in the EWcp and DRN, we used human EW and DRN samples from subjects who died suddenly from extracranial disease and did not show any brain neuropathologies. RNAscope ISH targeting *TRPA1* mRNA was combined with UCN1 immunofluorescence in the EWcp to assess the co-localization with urocortinergic neurons. Immunofluorescence targeting CLR and RNAscope ISH targeting *Ramp1*, *Calcr* and *Crcp* mRNA was combined with a) UCN1 immunofluorescence in the EWcp to assess the co-localization with urocortinergic neurons; b) TPH2 or 5-HT immunostaining in the DRN as a marker of the serotonergic neurons.

3.2.2. Mapping of human EW's functional connectivity profile

We analysed the functional connectivity matrix of EW in control humans with a special focus on the STN and DRN. Then, we compared it with the functional connectivity matrix of interictal migraineurs. Finally, we examined the association between migraine frequency and the functional connectivity of EW.

3.3. Animals

Animals (C57Bl6/J, *Trpa1* wild-type and KO mice) were housed in a temperature and humidity controlled 12h light-dark cycle environment (lights on at 6 am) in standard polycarbonate cages (365 mm × 207 mm × 144 mm) in four to six mice *per* cage groups, at the animal facility of the Department of Pharmacology and Pharmacotherapy, University of Pécs. Mice were provided *ad libitum* with standard rodent chow and tap water. All procedures were approved by the Animal Welfare Committee at Pécs University, National Scientific Ethical Committee on Animal Experimentation in Hungary (BA02/2000-57/2022 and BA02/2000-25/2021) in agreement with the directive of the European Communities Council in 1986, and with the Law of XXCIII, in 1998, on Animal Care and Use in Hungary.

The original breeding pairs of *Trpa1* KO mice were obtained from Prof. P. Geppetti, University of Florence, Italy. *Trpa1* KO mice were bred on C57Bl6/J background and crossed back after 10 generations. WT and KO mice were selected from different litters. Offspring were genotyped for *Trpa1* gene by polymerase chain reaction (PCR) (sequences of primers: ASM2: ATC ACC TAC CAG TAA GTT CAT; ASP2: AGC TGC ATG TGT GAA TTA AAT) (Kormos et al., 2022).

3.4. Electrophysiology

3.4.1. Acute brain slice preparation for electrophysiology

Electrophysiology experiments were performed in acute coronal EWcp slices (from Bregma -2.92 to -4.04 according to (Paxinos and Franklin, 2001) taken from C57Bl6/J mice. Under deep isoflurane anaesthesia, mice were decapitated and 300 µm thick coronal slices were cut in ice-cold external solution containing (in mM): 93 NMDG, 2.5 KCl, 25 Glucose, 20 HEPES, 1.2 $NaH2PO_4$, 10 $MgSO_4$, 0.5 $CaCl_2$, 30 $NaHCO_3$, 5 L-ascorbate, 3 Na-pyruvate, 2 thiourea bubbled with 95% O_2 and 5% CO_2. Slices were transferred to artificial cerebrospinal fluid containing (in mM) 2.5 KCl, 10 glucose, 126 NaCl, 1.25 $NaH2PO_4$, 2 $MgCl_2$, 2 $CaCl_2$, 26 $NaHCO_3$ bubbled with 95% O_2 and 5% CO_2. After an incubation period of 10 min at 34 °C in the first solution, the slices were maintained at 20–22 °C in ACSF until use. After recordings,

the sections were immersed into fixative (4% paraformaldehyde (PFA) with 0.1% picric acid in 0.01 M phosphate buffer saline (PBS)) for overnight fixation, then 50 µm thick coronal slices were re-sectioned using Leica VT1000S vibratome (Leica Biosystems, Wetzlar, Germany) for further immunostaining.

3.4.2. *In vitro* electrophysiological recordings

Patch pipettes were pulled from borosilicate glass capillaries with filament (1.5 mm outer diameter and 1.1 mm inner diameter; Sutter Instruments, Novato, CA, USA) with a resistance of 2–3 MΩ. The pipette recording solution contained (in mM) 5 KCl, 135 K-gluconate, 1.8 NaCl, 0.2 EGTA, 10 HEPES, 2 Na-ATP and 0.2% Biocytin, pH 7.3 adjusted with KOH; 290–300 mOsm. Whole-cell recordings were made with Axopatch 700B amplifier (Molecular Devices, San José, CA, USA) using an upright microscope (Eclipse FN1, Nikon) with 40× (NA: 0.8) water immersion objective lens equipped with differential interference contrast (DIC) optics. DIC images were captured with an Andor Zyla 5.5 s CMOS camera (Oxford Instruments, Abingdon, UK). All recordings were performed at 32 °C, in ACSF bubbled with 95% O2 and 5% CO2. Cells with lower than 20 MΩ access resistance (continuously monitored) were accepted for analysis. Signals were low-pass filtered at 5 kHz and digitized at 20 kHz (Digidata 1550B, Molecular Devices). When it is indicated 5 µM JT010, 10 µM CNQX (Sigma) and 1 µM Gabazine (Sigma) were applied to the bath solution. In these experiments membrane potential was manually adjusted (max. −50 pA) to keep the neuron just below the threshold for action potential firing. This method allowed us the easily monitor the effect of TRPA1 activation since ~5 mV depolarization already induced AP firing.

3.5. Stereotaxic surgery

Animals were anesthetized with i.p. ketamine-xylazine solution (16.6 mg/ml ketamine and 0.6 mg/ml xylazine-hydrochloride in 0.9% saline, 10 ml/kg) and fixed in a stereotaxic apparatus (David Kopf Instruments, Tujunga, CA, USA). For retrograde tracing, after a midline incision in the scalp and the nuchal skin, the muscles were detached from the occipital bone and reflected. Then, the posterior atlanto-occipital membrane was dissected and partially removed to visualize the spinal cord C1 segment that contains the STN. Under visual control using a surgical microscope, the glass capillary used for injection was moved 750 µm lateral to the posterior median sulcus in the midlevel of the space between the superior rim of the posterior arch of atlas and the inferior border of the occipital bone. Here, the tip of the capillary was

perpendicularly introduced 100 µm deep into the laminae II-III of the STN. 2x20 nL of CTB (Cat. No.: #104, List Biological Laboratories) was injected in two steps with an automated injector. After 2 min, the needle was slowly removed. Finally, the muscles and the skin were sutured.

For anterograde tracing, AAV8 Syn EGFP (Addgene, UK, Cat. No.: 50465-AAV8; containing EGFP) was microinjected (2x10 nL) into EWcp. Here we used the following stereotaxic coordinates from Bregma: posterior: -3.26mm; ventral: 3.35mm; lateral: 0. The injection was performed as described above for the STN, except that 1 min after the injection we lifted the needle by 0.5mm and upon additional 1 min it was slowly retracted from the brain and the skin were sutured. Fourteen days after surgery, both STN and EWcp-injected animals were euthanized and transcardially perfused as described below.

3.6. Targeted toxin-induced lesion of EWcp/UCN1 neurons in mice

For the selective UCN1 neuron ablation (Ujvári et al., 2022, Xu et al., 2022), 50 nl leptin-conjugated saporin (n=13) (#KIT-47, ATS INC, Carlsbad, CA, USA) was microinjected into the rostral (Bregma: posterior: -3.25mm; ventral: 3.75mm; lateral: 0) and caudal (Bregma: posterior: -3.75; ventral: 3.25; lateral: 0) part of the EWcp area. The injection was performed as described above for the anterograde tracer. Two weeks post-injection, mice were intraperitoneally injected with 0.1 mg/kg of either saline or CGRP, then subjected to the von Frey assay. Mice were later perfused as described below. The neuronal loss was assessed and verified by UCN1 immunostaining. Two mice were excluded from this experiment because the histological assessment revealed that the injection path missed the EWcp area.

3.7. Light-dark box test

The light-aversive behavior was assessed using LDB test in the time period between 30 to 60 min after the CGRP injection based on Mason at al. (2017). Mice were individually tested in the LDB device, consisting of two compartments connected by a small opening. The one chamber is brightly lit (1000 lux), while the other one is dark. Mice typically move in and out of the dark due to their curiosity to explore the novel environment, however, upon CGRP treatment, they prefer the dark compartment, in case of headache-like pain and photophobia (Mason et al., 2017). The time spent in the dark compartment was measured over 30 minutes to assess possible photophobia associated with migraine-like state.

3.8. Von Frey assay

Calibrated von Frey filaments were used to test periorbital hyperalgesia 30 min after 0.1 mg/kg i.p. injection of saline or CGRP. Each mouse was placed into a 10 cm long restraining plastic cylinder and allowed to poke out their heads and forepaws, but the restrainer prevented them from turning around (Farkas et al., 2016). Mice were allowed to habituate for 5 min. The filament was applied to the periorbital region of the face (the midline of the forehead at the level of the eyes) in an ascending manner starting from the 0.04 g filament. Briefly, if an animal did not respond, increasing filament forces were applied until the 0.6 g filament was reached or until a response was observed (Avona et al., 2020). A positive response was defined as a sharp withdrawal of the head upon stimulation. Each filament was applied five times for 1-2 s with a 10 s interval. The periorbital withdrawal threshold was defined as the force at which the positive response occurred in three of five stimuli (Tang et al., 2020).

3.9. Perfusion and tissue collection

Mice were euthanized by i.p. urethane (2.4 g/kg), then transcardially perfused with 20 ml of ice-cold 0.1 M PBS (pH 7.4) followed by 150 ml of 4% PFA solution in Millonig buffer (pH 7.4). Brain samples were dissected and postfixed in PFA solution for 72 hours at 4 °C. The brains were coronally sectioned using a Leica VT1000S vibratome (Leica Biosystems, Wetzlar, Germany). Four series of 30 µm sections were collected and stored in PBS containing sodium azide (0.01%) at 4°C, then for long-term storage in an anti-freeze solution.

Four representative sections of the EWcp, lPAG (from Bregma -2.92 mm to -4.04 mm), DRN (from Bregma −5.8 mm to −8.8 mm) and STN (spinal cord C1 segment) *per* animal were selected for each staining according to (Paxinos, 2001). The TRGs were collected and stored in a 4% PFA solution.

3.10. Urine alcohol concentration measurement

The ethanol content of the urine samples was examined by headspace gas chromatography with flame-ionization detection (Agilent 7890A GC system, G1888 Network Headspace Sampler). 50 µl of sample was added to 500 µl of internal standard solution (tert-butanol solution with a concentration of 0.05 g/l) previously introduced into a 20-mL headspace vial. The vial was crimp sealed and thermostated at 75 ± 0.1 °C. After the equilibrium was established (15 min), 2 µL of vapor was injected directly into the chromatographic columns (DB-ALC1, Agilent J&W Scientific, 30 m × 0.32-mm i.d., 1.8-µm film thickness and DB-ALC2, Agilent J&W Scientific,

30 m × 0.32-mm i.d., 1.2-µm film thickness). The HS loop and transfer line temperatures were set at 75 °C and 85 °C, respectively. The injection port temperature was held at 150 °C and used in split mode with a split ratio of 5:1. The flame ionization detector temperature was maintained at 260 °C. Nitrogen was used as carrier gas. The GC oven temperature was kept at 35 °C during the run time (4 min). The analytical method was validated for system suitability, selectivity, accuracy, linearity, repeatability, and intermediate precision in accordance with the current ICH guidelines (https://www.ema.europa.eu/en/documents/scientific-guideline/ich-guideline-q2r2-validation-analytical-procedures-step-2b_en.pdf (accessed August 17, 2022)). Detector response was linear over the range of 0.025-2.5 g/L for both acetaldehyde and ethanol. The detection limit and quantitation limit values of both compounds were found to be 0.015 g/L and 0.025 g/L, respectively.

3.11. RNAscope ISH

The pretreatment procedure was optimized for 30 µm-thick PFA-fixed sections (Kormos et al., 2022). Further steps (probe hybridization, signal amplification and channel development) were performed according to RNAscope Multiplex Fluorescent Reagent Kit v2 user manual (ACD, Hayward, CA, United States) to visualize the various targets (**Table 1.**). Mouse (ACD; Cat. No.: 320881) and human triplex positive (ACD; Cat. No.: 320861) control probes and triplex negative (ACD; Cat. No.: 320871) control probes were tested on the samples. The triplex positive control probes gave well-detectable signal, while the negative control probes did not give any recognizable fluorescence in the preparations (images not shown).

Target	Probes	Fluorophores
Crcp mRNA	*Crcp*-C3 (Cat. No.: 810161-C3, ACD)	Cyanine3 1:750
Ramp1 mRNA	*Ramp1*-C1 (Cat. No. 532681, ACD)	Cyanine3 1:750
Ctr mRNA	*Calcr*-C2 (Cat. No. 494071-C2, ACD)	Cyanine5 1:750
Crh1r mRNA	*Crh1r*-C1 (Cat. No.: 418011, ACD)	Cyanine3 1:750
Crh2r mRNA	*Crh2r*-C2 (Cat. No.: 413201-C2, ACD)	Cyanine3 1:750
NeuN mRNA	*Neun*-C3 (Cat. No.: 313311-C3, ACD)	Cyanine5 1:750
Ucn1 mRNA	*Ucn1*-C1 (Cat. No.: 466261, ACD)	Fluorescein 1:3000

Table 1. RNAscope *in situ* hybridization mRNA targets, respective probes and fluorophores. *Crcp*: calcitonin gene-related peptide receptor component, *Ramp1*: receptor activity-modifying protein 1, *Ctr*: calcitonin receptor, *Crh1r*: corticotropin-releasing hormone receptor 1, *Crh2r*: corticotropin-releasing hormone receptor 2, *NeuN*: neuronal nuclear marker, *Ucn1*: urocortin 1.

3.12. Fluorescent immunostaining

After washes, sections were treated with 0.5% Triton X-100 (Sigma Chemical, Zwijndrecht, The Netherlands) in PBS for 30 minutes and nonspecific binding sites were blocked with 2% normal donkey serum in PBS. Sections were incubated with the primary antibody/antibodies (**Table 3.**) for 24 hours. The secondary antibody/antibodies treatment (**Table 2.**) was applied for 3 hours at room temperature. Sections were counterstained with 4′,6-diamidino-2-phenylindole (DAPI) (ACD) and mounted on gelatin-coated glass slides, air-dried and cover-slipped with glycerol-PBS (1:1).

For the acute brain slices used for electrophysiological recordings, biocytin was visualized using Alexa 488-conjugated Streptavidin (Cat. No: 016-540-084 Jackson Immunoresearch Europe Ltd., Cambridgeshire, United Kingdom) diluted to 1:2.000.

Target	Primary antibodies	Secondary antibodies
CART	Rabbit anti-CART (Cat. No.: H-003-62 (55–102), Phoenix) 1: 10.000	Cy3-conjugated donkey anti-rabbit (Cat. No.: 711-165-152 Jackson) 1: 500
GFP	Chicken anti-GFP (Cat. No.: A10262, Life Technologies) 1:1000	Alexa 488-conjugated donkey anti-chicken (Cat. No.: 703-546-155, Jackson) 1:500
CTB	Goat anti-CTB (Cat. No.: #703, List Biological Laboratories) 1:5000	Alexa 488-conjugated donkey anti-goat (Cat. No.: 705-545-003, Jackson) 1:500
UCN1	Rabbit anti-UCN1 (Cat. No.: ab283503, Abcam) 1:5000	Alexa 488-conjugated donkey anti-rabbit (Cat. No.: 711-545-152, Jackson) 1:500 or Cy3-conjugated donkey anti-rabbit (Cat. No.: 711-165-152, Jackson) 1:500
UCN1	Goat anti-UCN1 (Cat. No.: SC1825, Santa Cruz)1:250	Alexa 488-conjugated donkey anti-goat (Cat. No.: 705-545-003, Jackson) 1:500
GFAP	Mouse anti-GFAP (Cat. No.: NCLLGFAP-GA5, Novocastra) 1:1000	Cy3-conjugated donkey anti-mouse (Cat. No.: 715-165-150, Jackson) 1:500
P-CREB	Rabbit anti-P-CREB (Cat. No.: #9191, Cell Signaling) 1:500	Cy3-conjugated donkey anti-rabbit (Cat. No.: 711-165-152, Jackson) 1:500
CALCRL	Rabbit anti-CALCRL (Cat. No.: 703811, Invitrogen) 1:250	Cy3-conjugated donkey anti-rabbit (Cat. No.: 711-165-152, Jackson) 1:500
NeuN	Mouse anti-NeuN (Cat. No.: MAB377, Sigma-Aldrich) 1:1000	Cy3-conjugated donkey anti-mouse (Cat. No.: 715-165-150, Jackson) 1:500 or Alexa 488-conjugated donkey anti-mouse (Cat. No.: 715-545-150, Jackson) 1:500
5-HT	Goat anti-5HT (Cat. No.: ab66047, Abcam) 1:2000	Alexa 488-conjugated donkey anti-goat (Cat. No.: 705-545-003, Jackson) 1:500
TPH2	Rabbit anti-TPH2 (Cat. No.: 348003, Synaptic Systems GmbH) 1:500	Alexa 647-conjugated donkey anti-rabbit (Cat. No.: 711-605-152, Jackson) 1:500 or Alexa 488-conjugated donkey anti-rabbit (Cat. No.: 711-545-152, Jackson) 1:500
FOS	Rabbit anti-cFOS (Cat. No.: 226 003, Synaptic Systems GmbH) 1:2000	Cy3-conjugated donkey anti-rabbit (Cat. No.: 711-165-152, Jackson) 1:500
FOS	Guinea pig anti-cFOS (Cat. No.: 226 005, Synaptic Systems GmbH) 1:1000	Alexa 488-conjugated donkey anti-guinea pig (Cat. No.: 706-545-148, Jackson) 1:500

Table 2. Antibodies used for immunostainings. CART**:** Cocaine and amphetamine-regulated transcript**,** GFP: green fluorescent protein, CTB: cholera toxin beta subunit, UCN1: urocortin 1, GFAP: glial fibrillary acidic protein, P-CREB: phosphorylated product of c-AMP-responsive element binding protein, CALCRL: calcitonin receptor-like, NeuN: neuronal nuclear marker, 5-HT: 5-hydoxtryptamine, TPH2: tryptophan hydroxylase 2, FOS: marker of acute neuronal activity, Cy3: Cyanine 3.

4.13. RNAscope ISH combined with immunofluorescence.

After the RNAscope procedure (see above), slides were treated with the primary antibody (**Table 2.**) for 24 hours. After washes, slides were incubated with secondary antibody (**Table 2.**) for 3 hours at room temperature in dark, and then counterstained with DAPI (ACD), air-dried and cover-slipped with glycerol-PBS (1:1).

3.14. Whole mount FOS immunostaining

After 3 days of postfixation in 4% PFA, TRGs were washed with PBS for 24 hours, incubated with 0.5% Triton X-100 for 6 hours (Sigma Chemical, Zwijndrecht, The Netherlands) in PBS to enhance the permeability. Nonspecific binding sites were blocked using 2% normal donkey serum in PBS for 2 hours. Then, TRGs were incubated with FOS primary antibody (**Table 2.**) for 48 hours. After washes (4×15 min) in PBS, samples were incubated with the secondary antibody (**Table 2.**) for 24 hours, followed by 4 ×15 min PBS washes.

3.15. Immunohistochemistry with diaminobenzidine

To assess the neuronal activity in EWcp, lPAG and STN, we used FOS immunohistochemistry. The neuronal loss upon EWcp/UCN1 neuron ablation was quantified by UCN1 immunohistochemistry.

Sections were washed three times with PBS, then treated with 1% H_2O_2 (Sigma Chemical, Zwijndrecht, The Netherlands) to quench the endogenous peroxidase activity of the tissue. After 3×10 min washes with PBS, sections were treated with 0.5% Triton X-100 (Sigma Chemical, Zwijndrecht, The Netherlands) in PBS to enhance their permeability. Then, nonspecific binding sites were blocked using 2% normal goat serum in PBS. Subsequently, sections were incubated with FOS antibody (anti-c-FOS polyclonal antibody produced in rabbit, Synaptic Systems GmbH, *Cat. No.: 226 003*) in a 1:2000 dilution or with UCN1 antibody (rabbit anti-UCN1, *Cat. No.: ab283503,* Abcam 1:5000) overnight at room temperature. After 3×10 min washes with PBS, sections were incubated with biotinylated anti-rabbit gamma globulin for 1 hour (VECTASTAIN® Elite ABC-HRP Kit, Peroxidase Rabbit IgG Vector Laboratories *Cat. No.: PK-6101*, produced in goat). After 3×10 min PBS washes, sections were then incubated in avidin-biotin complex solution for 1 hour. After washes, the labelling was developed with 0.05% DAB in Tris buffer with 0.06% H_2O_2 (Sigma Chemical, Zwijndrecht, The Netherlands). The reaction was controlled under a stereomicroscope and stopped with Tris buffer. After 3×10 min washes with PBS, sections were mounted on gelatin-coated slides, air-dried, treated with xylene (Merck, Leicester, UK), and cover-slipped with DPX mounting medium (Merck, Leicester, UK).

3.16. Microscopy, digital imaging and morphometry

The DAB-labelled sections were studied and digitalized using a Nikon Microphot FXA microscope with a Spot RT camera (Nikon, Tokyo, Japan). The number of FOS-positive nuclei

was determined by manual cell counting on the whole cross section surface area of the EWcp, lPAG and STN on four sections *per* animal. The average of these four values represented the FOS activity of one mouse in the given brain area.
For the targeted ablation, the number of UCN1-positive neurons was determined by manual cell counting on the whole cross section surface area of the EWcp on all sections *per* animal. The sum of these values represented the number of UCN1 neurons of one mouse in the EWcp.

Fluorescent-labelled sections were digitalized by an Olympus FluoView 1000 confocal microscope (Olympus, Europa, Hamburg, Germany) in sequential scanning in analogue mode. We used 3.5 µm optical thickness, 1024×1024-pixel resolution, and a 40x or 60x objective for scanning. The excitation and emission spectra for the respective fluorophores were selected using built-in settings of the FluoView software (FV10-ASW; Version 0102, Olympus, Europa, Hamburg, Germany). DAPI was excited at 405 nm, Fluorescein and Alexa Fluor 488 at 488 nm, Cy3 at 550 nm, Cy5 and Alexa Fluor 647 at 650 nm. Sections were scanned for the respective wavelengths of all channels. Digital images of the channels, depicting the same area, were automatically superimposed and merged.

The UCN1, CART, TPH2 and 5-HT immunofluorescence as well as the confluent or cluster-like *Ucn1* and *Cart* RNAscope signal was measured by Image J software (version 1.42., NIH, Bethesda, MD) in 5-20 cell bodies using four non-edited images of the corresponding channel. The regions of interest were manually determined at cytoplasmic areas of neurons. The signal density was corrected for the background signal. The average of the specific signal density (SSD) of 5-20 neurons was determined in four sections *per* animal. In case of low copy signals (i.e. *Trpa1)* where the individual signal dots did not overlap and remained distinguishable, we performed a manual signal dot counting and determined the number of mRNA copies *per* cell. We averaged the numbers of transcripts *per* cell as described above for the SSD values, in four sections. The average of these four values represented the SSD or mRNA transcript *per* cell count value of one mouse. The SSD was expressed in arbitrary units (a.u.).

In human samples, autofluorescence caused by lipofuscin accumulation disturbed the imaging. Because the lipofuscin accumulation is characteristic for the cytoplasm, but not for the karyoplasm, we show high magnification images including the cross-section profiles of neuronal nuclei. With this strategy, nuclear mRNA signal dots get well-distinguishable from cytoplasmic lipofuscin-related autofluorescence that appears in all channels.

3.17. Human brain samples for histology

Subjects (n=3) studied in this project died suddenly from extracranial disease and did not show any brain neuropathologies (**Table 3.**). The removal of brains was performed within a time window of 2 to 5 hours *post mortem*, after perfusion *via* cannula placed into the internal carotid and vertebral arteries. Perfusion was commenced with 1.5 Liter of 0.33% heparin containing physiological saline for 30 minutes, then with 4-5 Liters of a Zamboni fixative solution containing 4% paraformaldehyde and 15% picric acid in phosphate buffer (pH 7.4) over a duration of 1.5-2 hours.

The study received ethical approval from the Regional and Institutional Committee of Science and Research Ethics of the Scientific Council of Health (ETT TUKEB 15032/2019/EKU) and was conducted in adherence to the principles of the Declaration of Helsinki.

Tissue samples of the mesencephalic ventral periaqueductal gray matter (PAG) were microdissected. The EWcp and DRN area was identified according to the Allen human brain atlas (Ding et al., 2016), and post-fixed in the Zamboni solution without glutaraldehyde overnight (Szekeres-Paraczky et al., 2022). The brain samples were sectioned for 30 μm thickness using a Leica VT1000S vibratome (Leica Biosystems, Wetzlar, Germany), then, the sections were collected and stored in PBS, containing sodium azide (0.01%) at 4 °C. For long-term storage at -20 °C, they were transferred into anti-freeze solution.

Case code	Gender	Age	*Post mortem* time (min)
SKO27	Female	76 Years	195
SKO28	Female	93 Years	224
SKO29	Female	69 Years	212

Table 3. Characteristics of human brain samples used for histology

3.18. Human fMRI study

3.18.1. fMRI study participants

In the functional connectivity analysis, 35 migraine patients (27 females and 8 males, mean age ± SD=25.24 ± 4.35 years) with diagnosis of episodic migraine without aura (third edition of the International Classification of Headache Disorders (ICHD-III)) (Olesen, 2018) and 41 healthy control volunteers (25 females and 16 males, mean age ± SD=26.00 ± 4.59 years) were

included. All participants were screened by headache specialists, free from any serious medical, neurologic (except migraine without aura) or psychiatric disorders, have not taken any daily medications (except oral contraceptives) and they were right-handed. The functional magnetic imaging (fMRI) experiment was carried out in the interictal period of migraine patients, they were free from migraine attack 48 hours before and 24 hours after the fMRI session. Their average migraine frequency was 3.36 ± 3.11 attacks *per* month.

3.18.2. Functional magnetic imaging acquisition and seed region definition

The fMRI session started with the acquisition of a high-resolution structural data using T1-weighted 3D turbo field echo (TFE) sequence and 1 × 1 × 1 mm3 resolution in a 3 T MRI scanner (Achieva 3 T, Philips Medical System). The resting-state fMRI session lasted 6 minutes when the participants were instructed to close their eyes but remain awake. The imaging dataset acquisition parameters of T2*-weighted echo-planar (EPI) pulse-sequence were the following: repetition time (TR)=2.500 ms, echo time (TE)=30 ms, field of view (FOV)=240 × 240 mm^2; with 3 × 3 × 3 mm^3 resolution. The state-of-the-art preprocessing pipeline was applied on raw data based on previous analysis of the research group (Gecse et al., 2022).

After the preprocessing steps, seed-to-voxel analysis was conducted with the EW [Montreal Neurological Institute (MNI) coordinates: x=0; y=-23; z=-7, radius: 2 mm]. The seed definition was carried out based on literature data (You & Park, 2023) and confirmed by the visual check of expert scientists. The spherical mask of the region was created using fslmaths command of FSL, the extraction of time-series data and subsequent computations of voxel-wise connectivity analysis the NiBabel and NumPy modules were used. The seed-based connectivity map for each participant, established through voxel-wise Pearson correlation with the averaged seed region data, underwent transformation into Z-scores *via* Fisher transformation. These Z-score maps for each individual were subsequently employed in both within-group and between-group comparisons using the Statistical Parametric Mapping (SPM12) software package (Wellcome Department of Imaging Neuroscience, Institute of Neurology, London, UK). Given the fact that the EW is lying under the PAG, we examined the extent to which we could differentiate its connectivity from those of the PAG using previously applied PAG seeds (Gecse et al., 2022).

3.18.3. Functional connectivity analysis

The functional connectivity of EW was determined in whole group analysis using one sample t-test. After, two sample t-test was conducted to compare the EW connectivity between migraine

and control groups. A correlation analysis was used to investigate the relationship between migraine frequency and EW connectivity in migraine patients. In order to confirm the connection identified in animal experiments between EW with STN (MNI coordinates: left STN x=-6, y=-42, z=-48; right STN x=6, y=-42, z=-48; radius: 4 mm), DRN (from Harvard Ascending Arousal Network Atlas) (Brian L. Edlow 2012), and hypothalamus (MNI coordinates: x=0, y=-16, z=-10, radius: 4 mm), region-of-interest analysis was conducted with these three regions.

All analysis was corrected for sex, age, and motion by adding them as covariates of no interest. An initial threshold of $p<0.001$ uncorrected for multiple comparison and at least twenty contiguous voxels was used in the whole brain analyses. All reported results survived family-wise error correction at a cluster-level threshold of $p_{FWE}<0.05$. In the region of interest (ROI) analysis, the initial threshold of $p<0.001$ uncorrected for multiple comparison was used, and the reported results survived family-wise error correction at peak-level threshold of $p_{FWE}<0.05$.

For data visualization, statistical maps of significant clusters were used as overlay on MNI 152 template brain in MRIcroGL (Rorden & Brett, 2000).

3.19. Statistical analysis

Data were expressed as mean ± standard error of the mean for each experimental group. Data sets were tested for normality (Shapiro-Wilk test; Shapiro & Wilk, 1965) and homogeneity (Bartlett's Chi-square test; Snedecor and Cochran, 1989). Outlier data beyond the two-sigma range were excluded from the analysis.

Statistical analyses of electrophysiological data were performed using Clampfit v. 10.7 (Molecular Devices) and OriginPro v. 8.6. Data were evaluated by Tukey's *post hoc* test upon one-way analysis of variance (ANOVA).

Data sets obtained from the functional and morphological changes in the CGRP mouse model of migraine and the *Trpa1* expression following acute alcohol exposure were evaluated using Student's *t test.*

One-way ANOVA was used to evaluate data sets obtained from the NTG mouse model of migraine and two-way ANOVA for data sets obtained from the mouse model of acute alcohol exposure. Tukey's *post hoc* tests were performed based on first or second order effects in ANOVA tests.

Datasets obtained in the experiment of targeted UCN1 neuron ablation were evaluated by repeated measures ANOVA to assess the effect of CGRP treatment before and after EWcp/UCN1 ablation (as within subject factor) on the pain threshold values, obtained in the von Frey test. Tukey's *post hoc* comparisons were used. The analyses were performed with the software Statistica 8.0 (StatSoft, Tulsa, OK) (α=5%).

4. Results

4.1. Investigation of EWcp in migraine

4.1.1. Neuroanatomical and qualitative morphological examination of migraine-related targets

4.1.1.1. Expression of the CGRP receptor target components in the EWcp, DRN and STN

To prove that central CGRP may directly affect the urocortinergic EWcp neurons, we performed RNAscope ISH for *Calcr*, *Ramp1* and *Crcp* mRNA moreover immunofluorescence for CLR and UCN1. We proved that *Ramp1* and *Calcr* mRNAs coding for AMY1 components are co-expressed both in mouse and human EWcp neurons (**Figure 6.**). Notably, the expression pattern of *Calcr* mRNA in the EWcp suggests a substantial co-localization with UCN1 immunoreactive neurons. Moreover, almost all EWcp/UCN1 neurons were found to contain CLR (**Figure 7.**) and *Crcp* (**Figure 8.**) both in mice and humans.

In the DRN, RNAscope ISH in combination with immunofluorescence for *Calcr, Ramp1* (**Figure 6.**) and CLR (**Figure 7.**) as well as *Crcp* mRNAs (**Figure 8.**) were found to be expressed in TPH2-immunoreactive serotonergic and non-serotonergic neurons.

We detected *Calcr, Ramp1* (**Figure 6.**) and *Crcp* mRNAs (**Figure 8.**) in both neuronal and glial cells in the mouse STN laminae I-III. Additionally, in line with an earlier study, the expression of CGRP receptor component CLR was confirmed in both neurons (Miller et al., 2016) and astrocytes (**Figure 9.**).

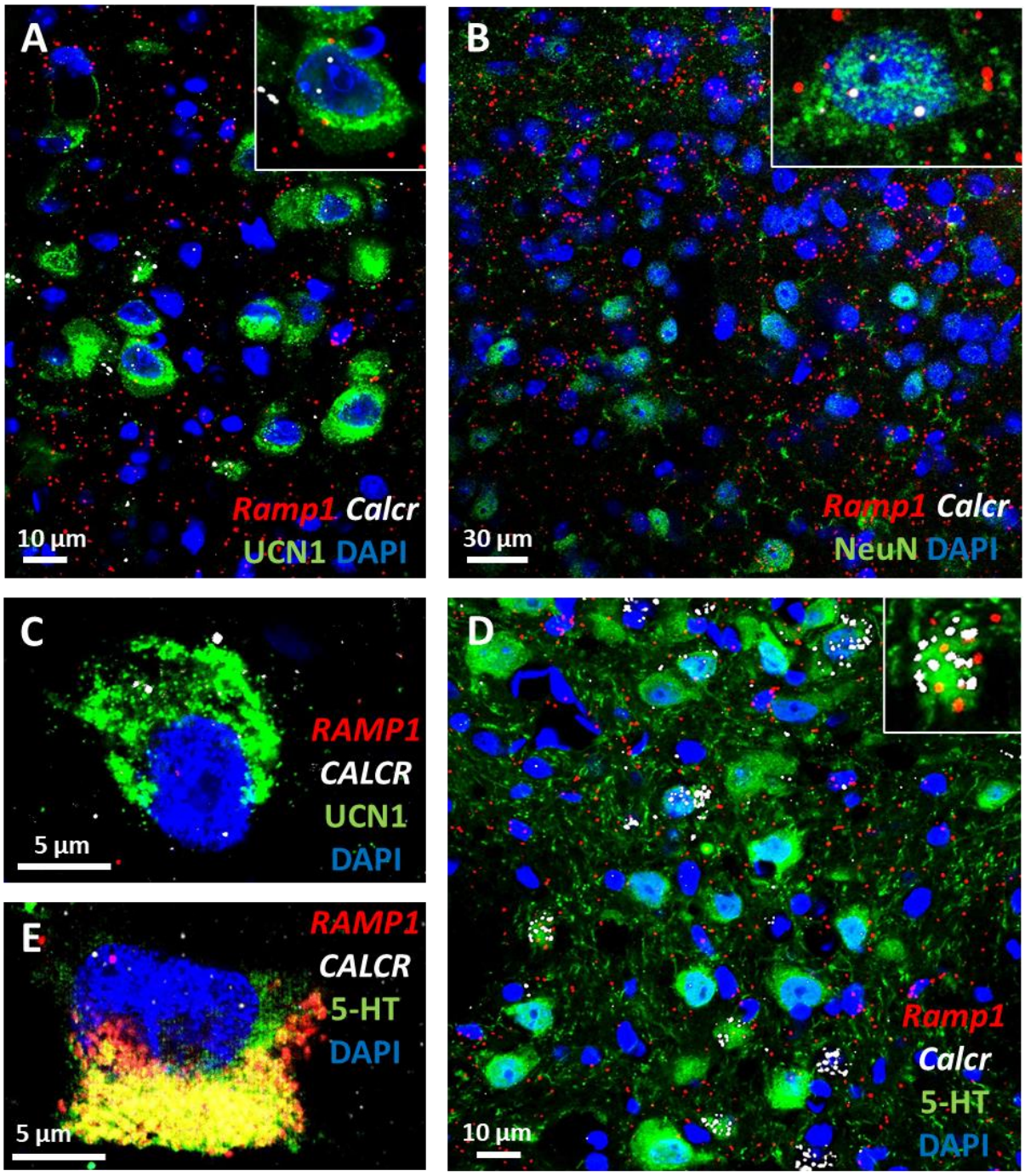

Figure 6. Calcitonin receptor (*Calcr*) and receptor activity-modifying protein 1 (*Ramp1*) mRNA expression. (A) Representative fluorescence images showing the *Calcr* (white) and *Ramp1* (red) mRNA transcripts co-expressed with urocortin 1 peptide (UCN1, green) in the mouse centrally projecting Edinger-Westphal nucleus (EWcp). (B) Neurons (neuronal marker NeuN, green) of the mouse spinal trigeminal nucleus express both of *Calcr* (white) and *Ramp1* (red) mRNA. (C) Representative fluorescence images showing the *CALCR* (white) and *RAMP1* (red) mRNA transcripts co-expressed with UCN1 (green) in the human EWcp. (D) In the mouse dorsal raphe nucleus (DRN), the serotonin (5-HT, green) immunoreactive cells also contained *Calcr* (white) and *Ramp1* (red) mRNA transcripts. (E) In the human DRN, the 5-HT (green) immunoreactive cells also contained *CALCR* (white) and *RAMP1* (red) mRNA transcripts. The yellow cytoplasmic area in E corresponds to lipofuscin autofluorescence. Nuclear counterstaining was performed with 4′,6- diamidino-2-phenylindole (DAPI, blue).

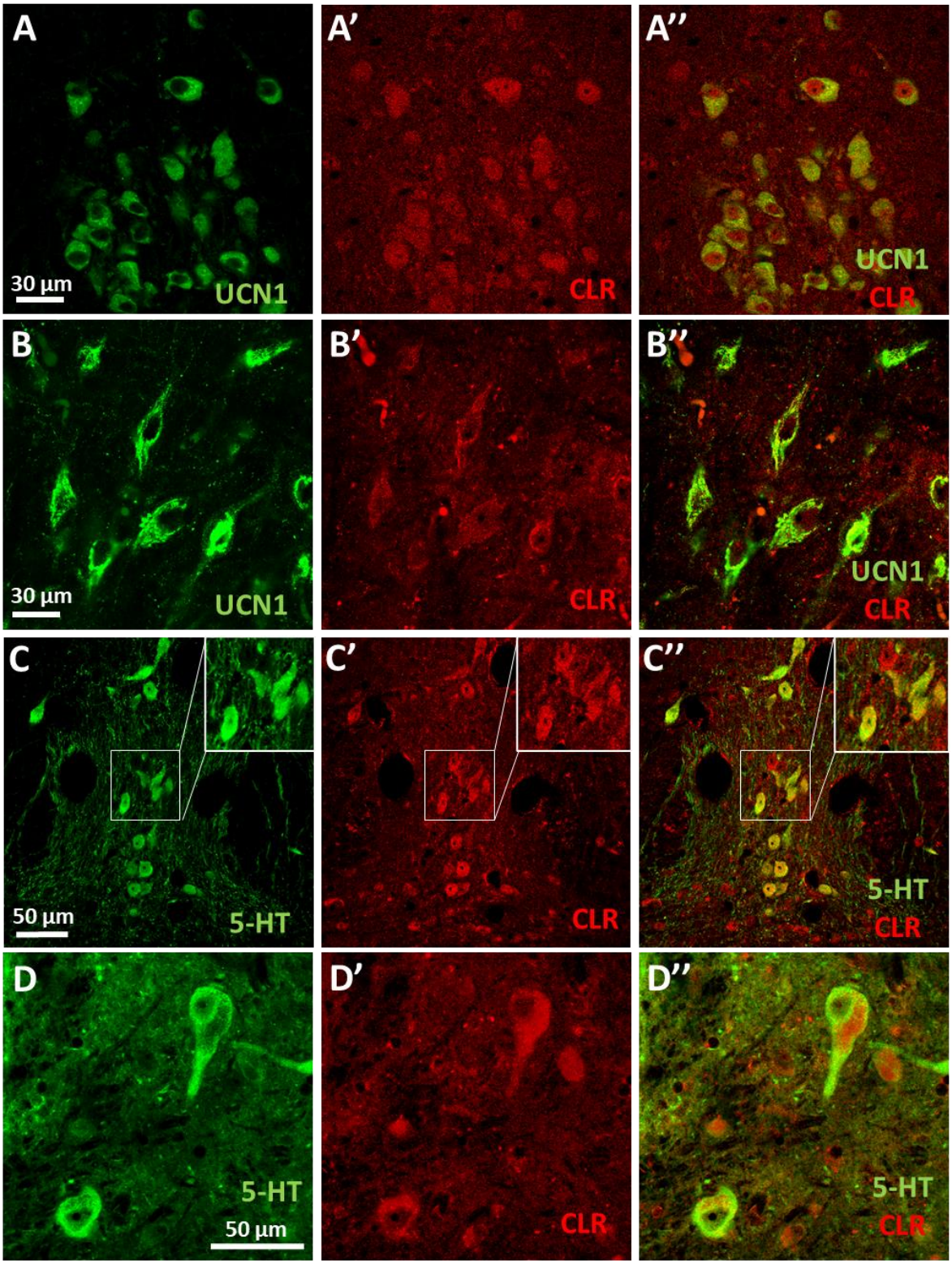

Figure 7. Calcitonin-like receptor (CLR) expression. (A-A'') Representative immunofluorescence images showing the CLR (red) co-expressed with urocortin 1 peptide (UCN1, green) in the mouse centrally projecting Edinger-Westphal nucleus (EWcp). (B-B'') Representative immunofluorescence images showing the CLR (red) co-expressed with urocortin 1 peptide (UCN1, green) in the human EWcp. (C-C'') In the mouse dorsal raphe nucleus (DRN), the serotonin (5-HT, green) immunoreactive cells also contained CLR (red). (D-D'') In the human DRN, the 5-HT (green) immunoreactive cells co-expressed CLR (red).

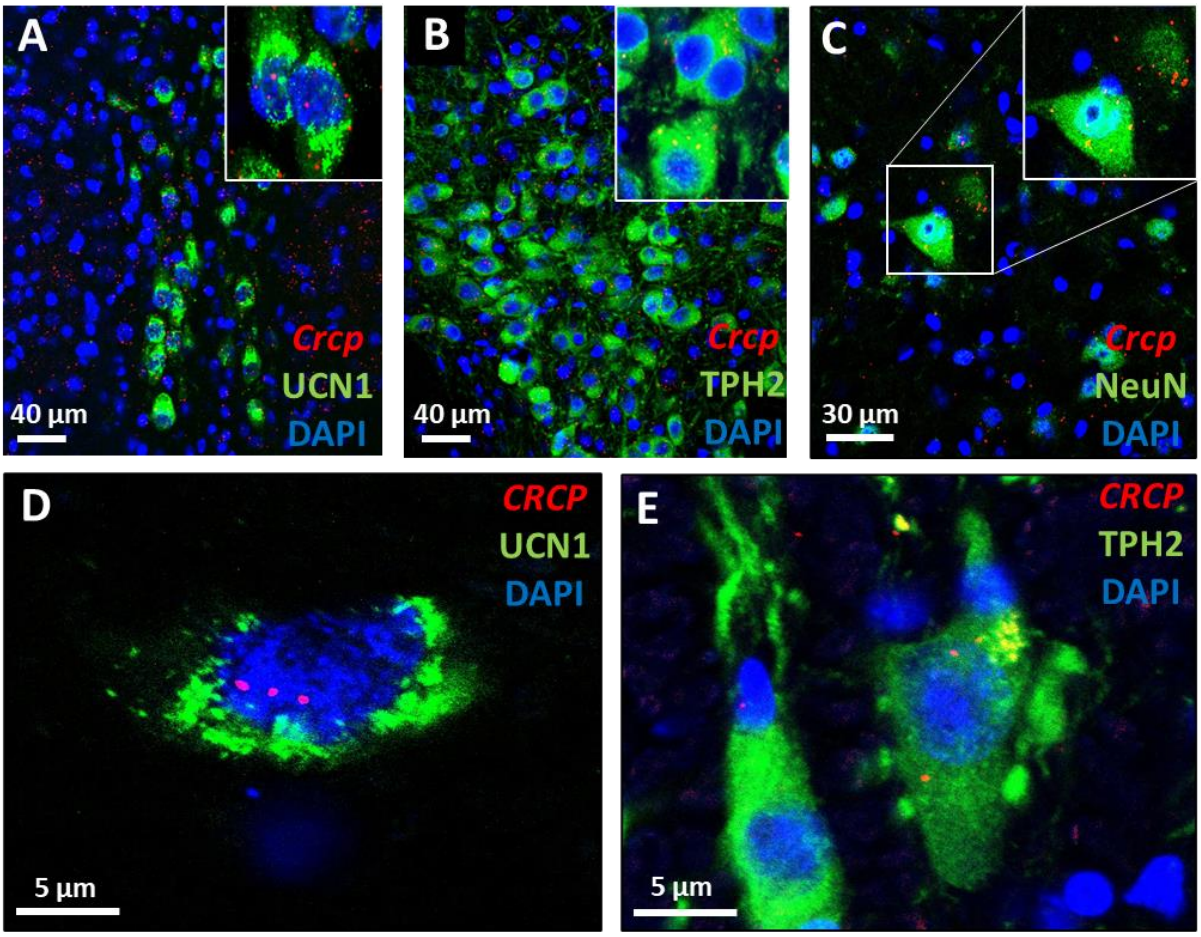

Figure 8. Calcitonin gene-related peptide receptor component (*Crcp*) mRNA expression. Representative fluorescence images showing the *Crcp* mRNA transcripts (red) co-expressed with urocortin1 peptide (UCN1, green) in the mouse (A) and human (D) centrally projecting Edinger-Westphal nucleus. In the mouse (B) and human (E) dorsal raphe nucleus the tryptophan hydroxylase 2 (TPH2, green) immunoreactive cells also contained *Crcp* mRNA transcripts (red). Neurons (neuronal marker NeuN, green) of the mouse spinal trigeminal nucleus (C) express also *Crcp* mRNA (red). Nuclear counterstaining was performed with 4′,6- diamidino-2-phenylindole (DAPI, blue).

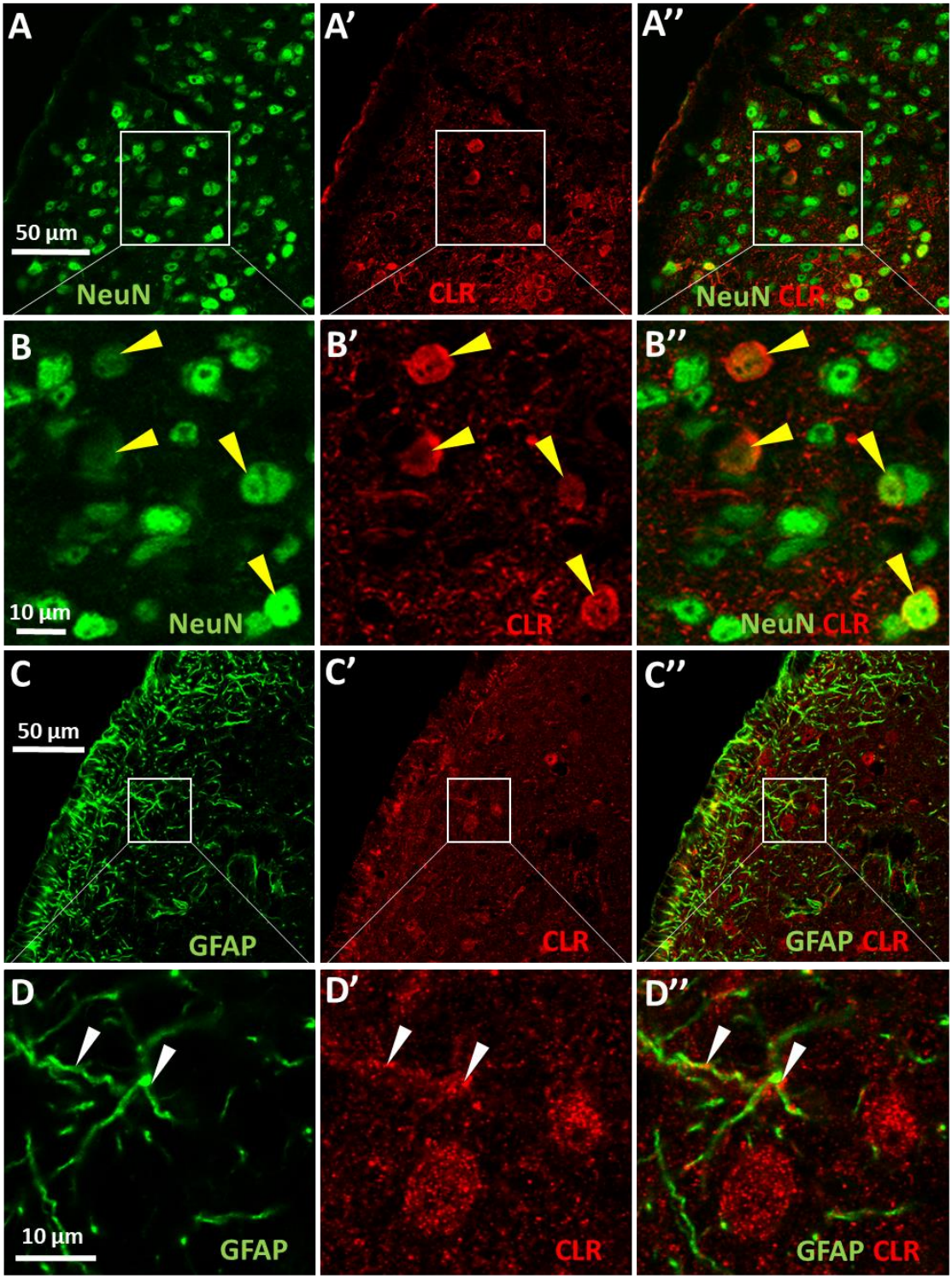

Figure 9. Calcitonin receptor-like receptor protein (CLR) expression in mouse spinal trigeminal nucleus (STN). (A-B) The NeuN (green) labelling combined with CLR staining (red) revealed that a part of the STN neurons show also CLR immunoreactivity. See the yellow arrowheads in the higher magnification images (B) depicting the boxed areas in A. (C-D) Glial fibrillary acidic protein (GFAP)-CLR double labelling demonstrates that the GFAP (green)-immunoreactive astrocytes show also some CLR (red) immunopositivity. See the white arrowheads in the high magnification images in panel D, demonstrating the marked areas in C. The overlay images (A''-D'') in the right column demonstrate the co-localization of the labelled antigens.

4.1.1.2. Urocortinergic afferentation of the *Crh1r* and *Crh2r*-expressing neurons in the mouse STN

Anterograde and retrograde tracing studies were performed to investigate a possible urocortinergic projection from the EWcp to the STN. The accurate anatomical position of the injection site was approved by CTB and GFP immunostaining on C1 spinal cord (**Figure 10A**) and EWcp (**Figure 10B**) sections, respectively. CTB and UCN1 double positive neurons were detected in EWcp after a CTB injection into the STN (**Figure 10C**). Moreover, GFP and UCN1 double positive fibers were observed in the STN in samples of mice injected with AAV8-EGFP injection into the EWcp (**Figure 10D**).

Next, we examined the expression of UCN1 receptor targets, *Crhr1* and *Crhr2*, in the I-III lamina of the STN and we tested whether they are approached by UCN1-immunoreactive fibers. RNAscope ISH for *Crh1r, Crh2r* and *NeuN* mRNAs was combined with UCN1 immunofluorescence. In laminae I-III of the STN, the neurons were seen to express both *Crhr1* (**Figure 10E**) and *Crhr2* (**Figure 10F**) mRNAs and they received urocortinergic fibers.

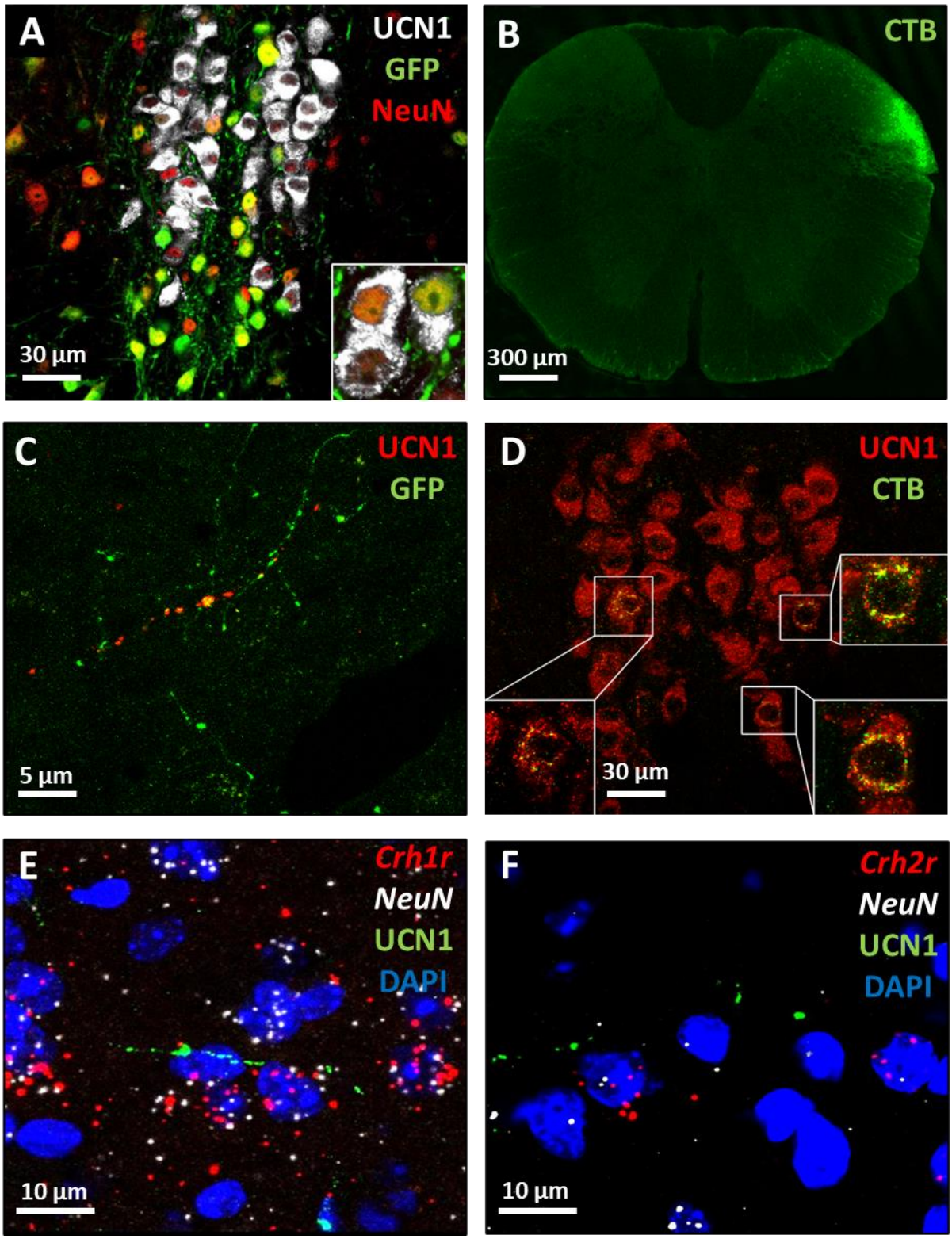

Figure 10. Urocortinergic afferentation from the centrally projecting Edinger-Westphal nucleus (EWcp) to the spinal trigeminal nucleus (STN). (A) Representative images showing the injection site of AAV8 Syn EGFP by green fluorescent protein (GFP, green) immunofluorescence in the EWcp urocortinergic (UCN1, white) neurons. All of the virus-infected cells are neurons (neuronal marker: NeuN, red), note the UCN1 and NeuN co-localization (yellow). (B) Fluorescence labelling for cholera toxin subunit B (CTB) in the dorsal horn of STN. (C) The co-localization of UCN1 (red) with GFP (green) in a nerve fiber in the

STN and (D) the co-localization of UCN1 (red) with CTB (green) in the EWcp neurons. (E) Cells co-expressing neuronal marker mRNA (*NeuN*, white) and corticotropin-releasing hormone receptor 1 mRNA (*Crhr1*, red) as well as (F) corticotropin-releasing hormone receptor 2 (*Crhr2*, red), receiving a UCN1 (green) positive afferentation in the STN. Nuclear counterstaining was performed by 4′,6- diamidino-2-phenylindole (DAPI, blue).

4.1.2. Investigation of the EWcp in a nitroglycerin-induced migraine mouse model

To examine the neuronal activity in the EWcp, we performed FOS immunohistochemistry with DAB. Both the vehicle and NTG treatment significantly increased the number of FOS positive neurons in the EWcp with a strong main effect of the treatment in one-way ANOVA ($p=0.02$), compared to saline (Tukey's *post hoc* test, $p_{veh}=0.02$; $p_{NTG}=0.01$). However, there was no significant difference between the vehicle- and NTG-treated groups ($p=0.7$) (**Figure 11**).

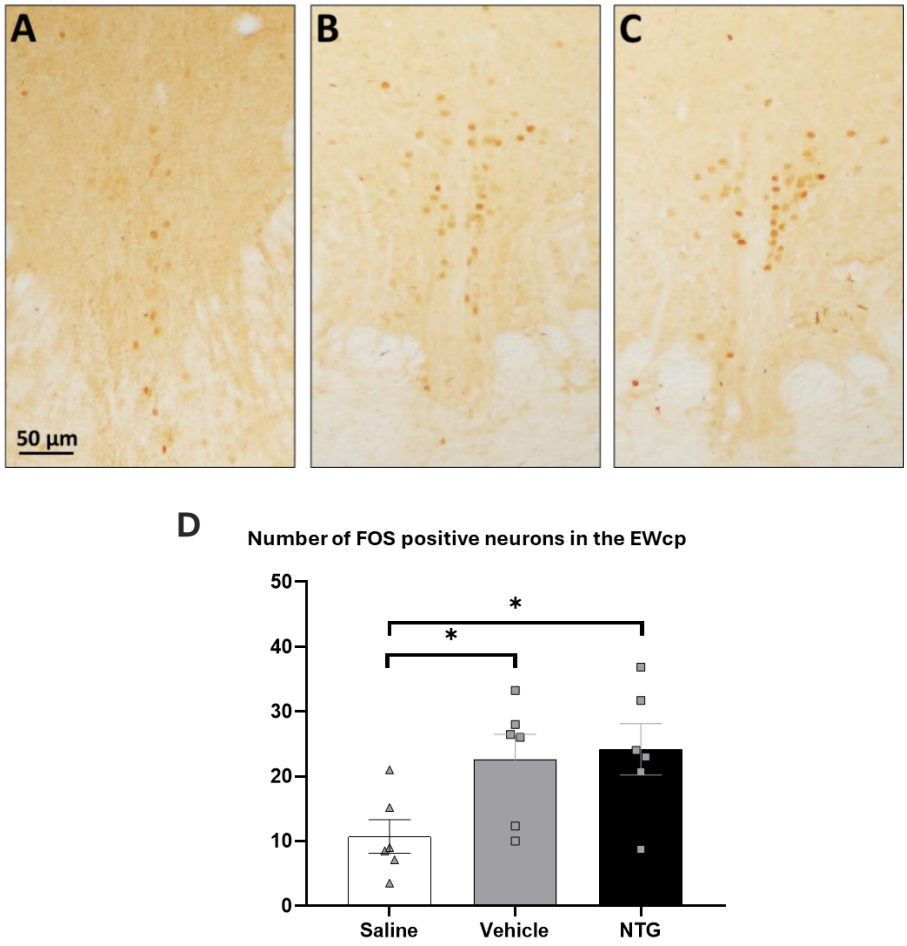

Figure 11. **FOS immunoreactivity in the centrally projecting Edinger-Westphal nucleus (EWcp).** Representative images showing the nuclei (brown dots) of activated FOS positive neurons, in the EWcp 2 h after i.p. injection of 10 mg/kg saline (control; A), vehicle (saline-based solution containing 6% alcohol and 16% propylene glycol; B) and nitroglycerin (NTG; C). Columns show means ± SEM of the number of FOS positive neurons in the EWcp after i.p. injection of saline (white), vehicle (gray) and NTG (black) (n=6; *p<0.05; one-way ANOVA with Tukey's *post hoc* test) (D).

4.1.3. Investigation of the EWcp and its migraine-related projection areas in a CGRP-induced migraine model

4.1.3.1. Model validation

To assess photophobia associated with migraine-like headache, we performed LDB test. CGRP-treated mice spent significantly increased ratio of time in the dark compartment compared to the controls (Student's t-test, p=0.02) (**Figure 12A**).

Von Frey test was performed to assess periorbital pain associated with migraine-like headache. CGRP treatment significantly reduced the periorbital withdrawal threshold compared to the saline (Student's t-test, $p=8.25x10^{-13}$) (**Figure 12B**).

FOS immunofluorescent labelling was performed to assess the activation of the TRG neurons in the trigeminovascular nociceptive pathway. CGRP treatment resulted in significantly increased number of FOS positive neurons in the TRG, compared to the controls (Student's t-test, p=0.0004) (**Figure 12C**).

In the STN, although CGRP treatment did not affect the FOS positive neuron count (Student's t-test, p=0.18; data not shown), it increased the number of P-CREB (Student's t-test, p=0.003) in laminae I-III (**Figure 12D**).

FOS immunohistochemistry was performed in the lPAG to assess the activation of the antinociceptive pathway in a migraine-like state. We found about two-fold increase in the number of activated lPAG nuclei in the CGRP-treated group, compared to the control (Student's t test, p=0.002) (**Figure 12E**).

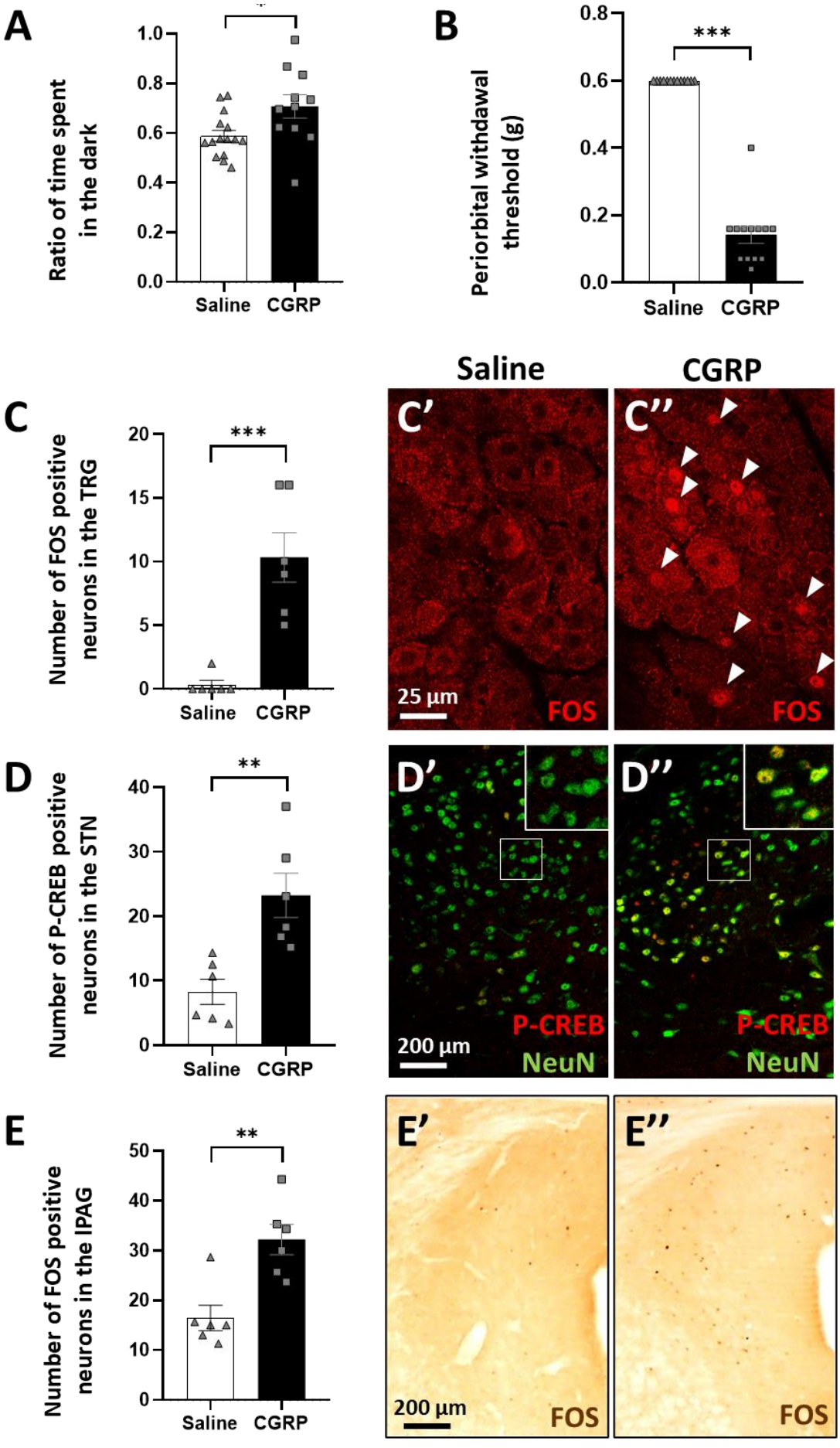
A
Ratio of time spent in the dark
1.0
0.8
0.6
0.4
0.2
0.0
Saline
CGRP
B
Periorbital withdawal threshold (g)
0.8
0.6
0.4
0.2
0.0
***
Saline
CGRP
Saline
CGRP
C
Number of FOS positive neurons in the TRG
20
15
10
5
0
***
Saline
CGRP
C'
C''
25 µm
FOS
FOS
D
Number of P-CREB positive neurons in the STN
40
30
20
10
0
**
Saline
CGRP
D'
D''
200 µm
P-CREB
NeuN
P-CREB
NeuN
E
Number of FOS positive neurons in the IPAG
50
40
30
20
10
0
**
Saline
CGRP
E'
E''
200 µm
FOS
FOS

Figure 12. Model validation. (A) Columns show the ratio of time spent in the dark compartment of the light-dark box device, 30 min after saline (control) or calcitonin gene-related peptide (CGRP) injection (n=11-15, *p=0.02; Student's t-test). (B) Columns show the facial withdrawal threshold (g) in von Frey test, 30 min after saline (control) or CGRP injection (n=13, ***p=$8.25x10^{-13}$; Student's t-test). (C) Columns show the number of FOS-positive neurons in the trigeminal ganglia (TRG), 4 hours after saline (control) or CGRP injection (n=6; ***p=0.0004; Student's t test). (C'-C") Representative fluorescence images showing the expression of FOS, as a marker of early neural activation in the TRG, 4 h after saline (control) and CGRP injection. Nuclei of FOS positive activated neurons (red) are highlighted by the white arrowheads. (D) Columns show the number of P-CREB positive neurons in the spinal trigeminal nucleus (STN) 4 h after saline (control) and CGRP injection (n=6; **p=0.003; Student's t test). (D'-D") Representative fluorescence images showing the expression of P-CREB, as a marker of neural activation in the STN, 4 h after saline (control) and CGRP injection. Nuclei of P-CREB positive activated neurons (red) are co-localized (yellow) with the neuronal marker (NeuN, green). (E) Columns show the number of FOS positive neurons in the lateral periaqueductal gray matter (lPAG), 4 h after saline (control) and CGRP injection (n=6; **p=0.002; Student's t test). (E'-E") Representative images showing the nuclei (brown dots) of activated FOS positive neurons in the lPAG in control and CGRP-treated mice.

4.1.3.2. Functional and morphological changes of the EWcp in the CGRP model

FOS immunohistochemistry was performed to assess the acute neuronal activity of the EWcp. CGRP treatment resulted in an approximately two-fold rise in the number of FOS positive neurons, compared to the control (Student's t-test, p=0.03) (**Figure 13A**).

Using a double-label immunofluorescence, we found that most of the FOS-immunoreactive nuclei were localized to UCN1 neurons (91.79%) suggesting that the urocortinergic EWcp was activated (**Figure 13B**).

To assess the effect of CGRP treatment on *Ucn1* mRNA expression and UCN1 peptide content in the EWcp neurons, RNAscope ISH was performed, combined with immunofluorescence. In CGRP-treated animals, significantly higher *Ucn1* mRNA expression (Student's t-test, p=0.0004) (**Figure 13C**) and UCN1 peptide immunosignal (Student's t-test, p=0.0007) (**Figure 13D**) was found in the EWcp neurons, compared to the controls.

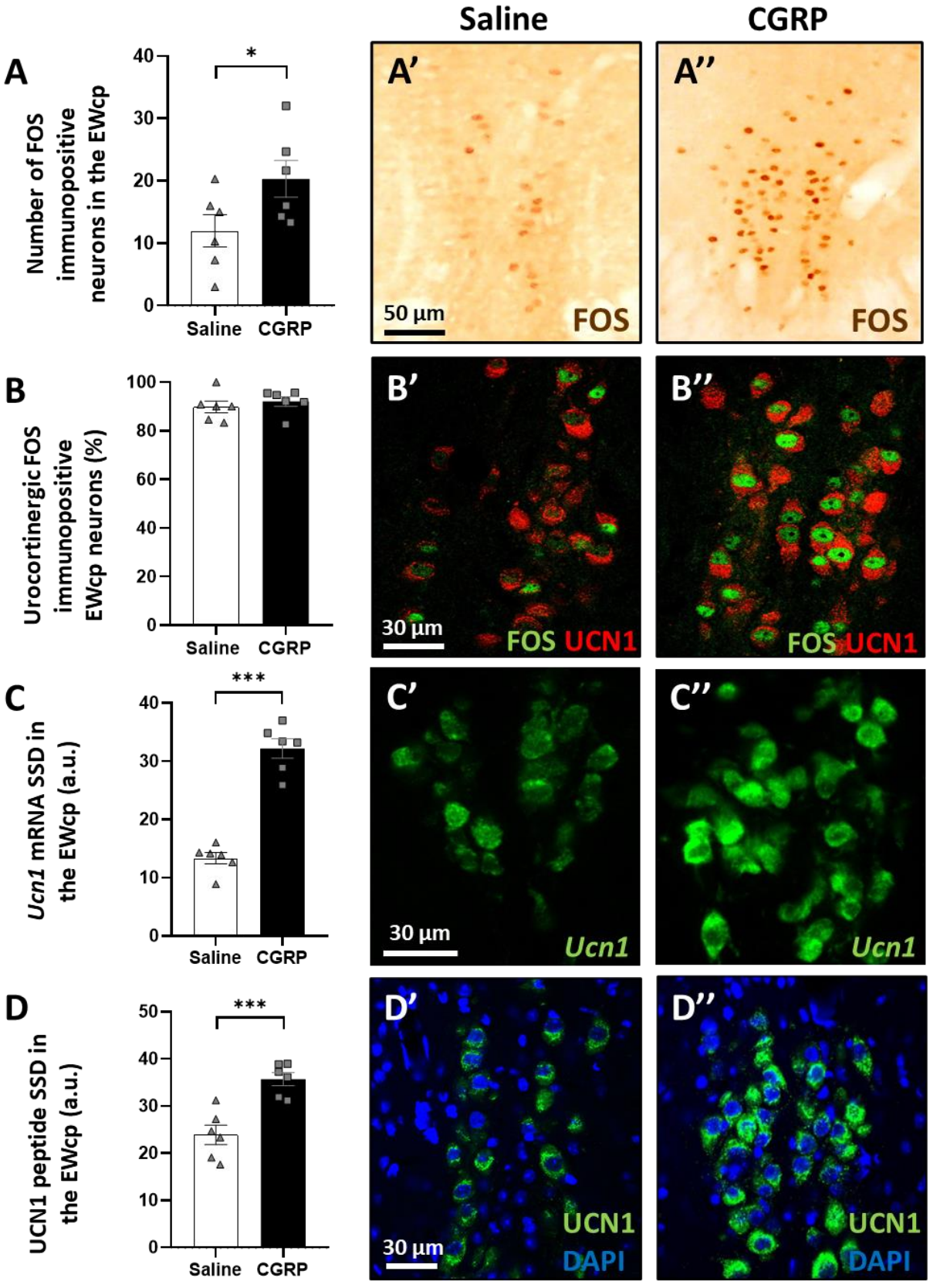

Figure 13. Response of the mouse centrally projecting Edinger-Westphal nucleus (EWcp) to calcitonin gene-related peptide (CGRP) treatment. (A) Columns show the number of FOS-immunoreactive neurons in the EWcp, 4 h after saline (control) or CGRP injection (n=6; *p=0.03; Student's t test). (A'-A") Representative images showing the nuclei of the neurons positive (brown dots) for the early neural activation marker (FOS) in the EWcp, 4 h after saline

(control) or CGRP injection. (B) Quantitative evaluation of the ratio of UCN1/FOS double-labelled neurons from all FOS-immunoreactive neurons in the EWcp revealed the urocortinergic identity of activated (FOS-immunoreactive) neurons, 4 h after saline (control) and CGRP injection. (B'-B") Representative fluorescence images showing the co-localization of urocortin 1 (UCN1, red) and FOS (green) in the EWcp of control and CGRP-injected mice. (C) Quantitative evaluation of *Ucn1* mRNA specific signal density (SSD) in the EWcp, 4 h after saline (control) or CGRP injection (n=6; ***p=0.00045; Student's t test). (C'-C") Representative fluorescence images showing the expression of *Ucn1* mRNA (green) in the EWcp in control and CGRP-treated mice. (D) Quantitative evaluation of UCN1 peptide SSD in the EWcp, 4 h after saline (control) or CGRP injection (n=6; ***p=0.0007; Student's t test). (D'-D") Representative images illustrate UCN1 peptide (green) immunoreactivity in the EWcp in control and CGRP-injected mice. For nuclear counterstaining, 4′,6- diamidino-2-phenylindole (DAPI, blue) was used.

In order to assess how migraine-like state affects the number of *Trpa1* mRNA transcripts in the EWcp/UCN1 cells, we performed RNAscope ISH to detect *Trpa1* mRNA combined with UCN1 immunostaining. Semi-quantification of the staining showed that CGRP treatment increased nearly two-fold the number of *Trpa1* transcripts in UCN1 neurons (p=0.0003) (**Figure 14**).

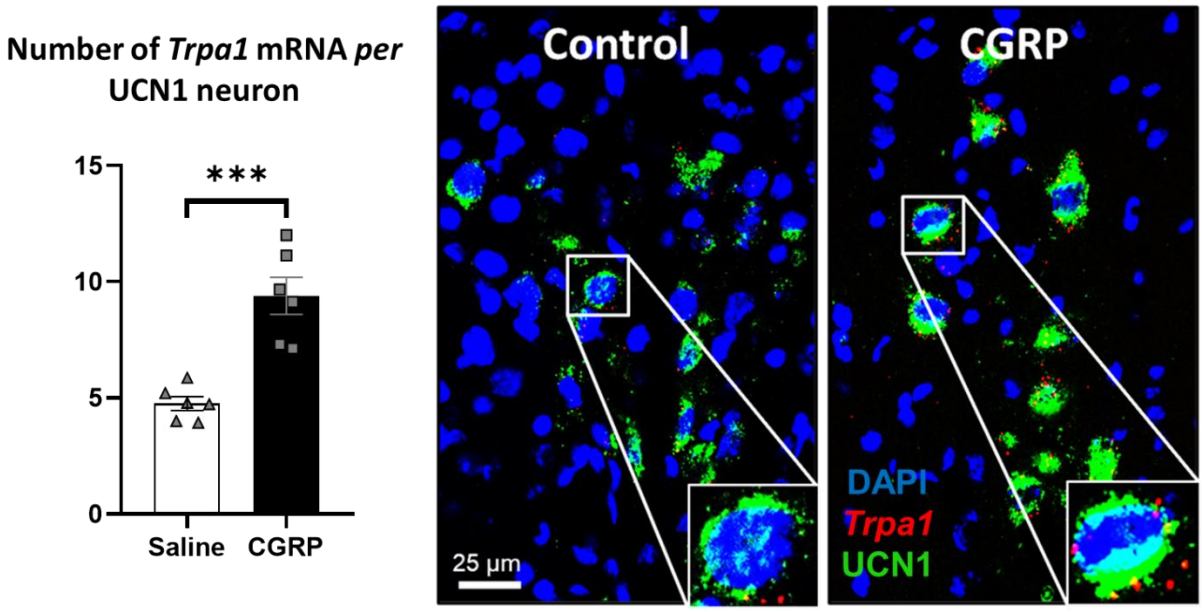

Figure 14. *Trpa1* mRNA expression in the centrally projecting Edinger-Westphal nucleus (EWcp) upon calcitonin gene-related peptide (CGRP) treatment. Columns show the number of *Trpa1* mRNA transcripts *per* urocortinergic neurons in the EWcp, 4 h after saline (control) and CGRP injection (n=6; *p=0.0003; Student's t test). Representative fluorescence images showing the expression of *Trpa1* mRNA (red) and its co-localization with the urocortin 1 (UCN1) peptide (green) in the EWcp 4 h after saline (control) and CGRP injection. Nuclear counterstaining was performed with 4′,6- diamidino-2-phenylindole (DAPI, blue).

4.1.3.3. Morphological changes of the DRN in the CGRP model

In the DRN, double immunostaining targeting 5-HT and TPH2 was performed. Both 5-HT (Student's t-test, p=0.03) (**Figure 15A**) and TPH2 (Student's t-test, p=0.01) (**Figure 15B**) content of the serotonergic neurons were significantly decreased in response to CGRP treatment in the DRN.

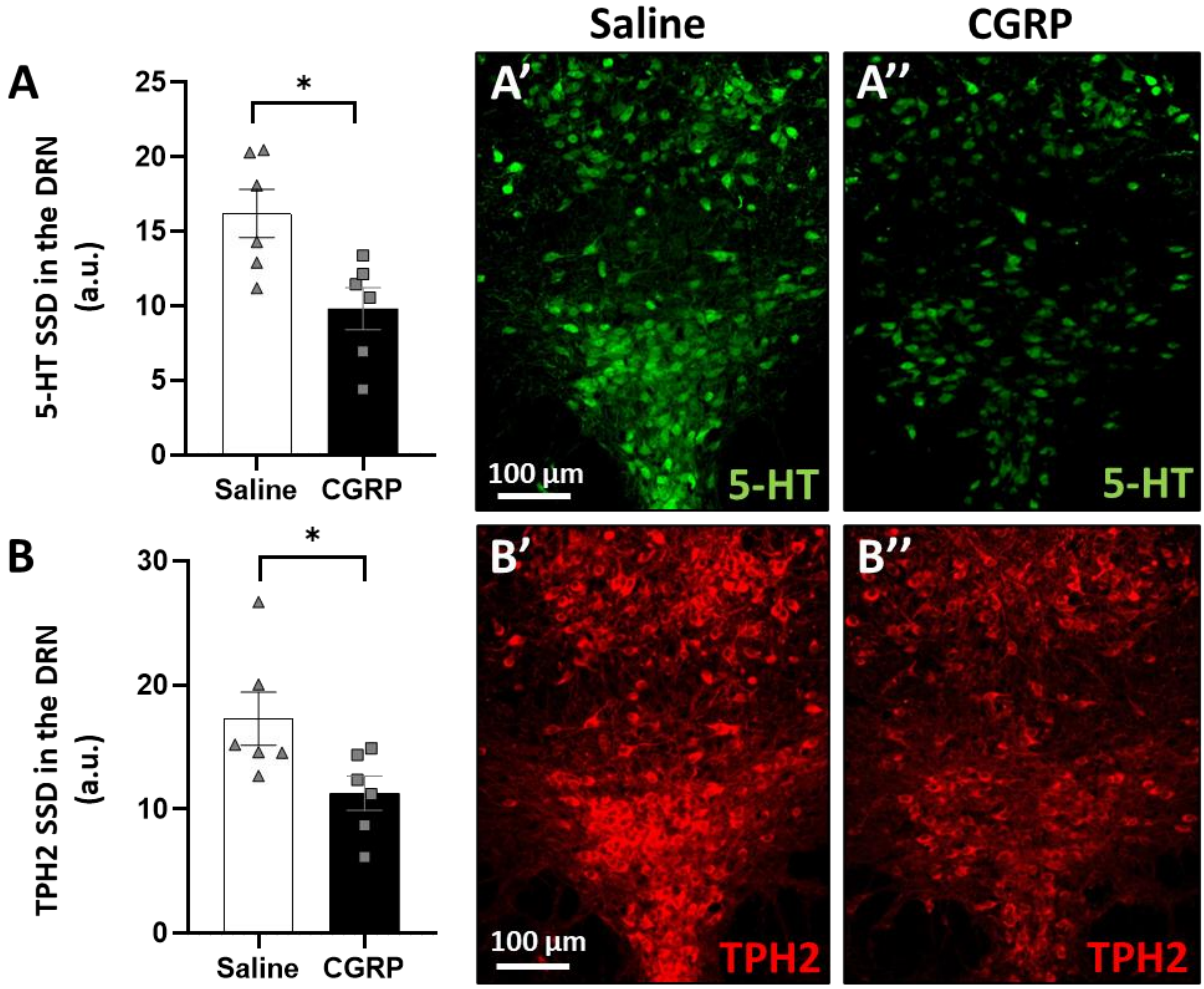

Figure 15. Serotonin (5-HT) and tryptophan hydroxylase 2 (TPH2) immunoreactivity in the dorsal raphe nucleus (DRN). (A) Specific signal density (SSD) of 5-HT in the DRN, 4 h after saline (control) and calcitonin gene-related peptide (CGRP) injection (n=6; *p=0.03; Student's t test). (A'-A") Representative fluorescence images showing the 5-HT (green) immunoreactivity in the DRN, 4 h after saline (control) and CGRP injection. (B) TPH2 SSD in the DRN, 4 h after saline (control) and CGRP injection (n=6; *p=0.01; Student's t test). (B'-B") Representative fluorescence images illustrate TPH2 (red) immunosignal in the DRN, 4 h after saline (control) and CGRP injection.

4.1.4. Targeted ablation of the EWcp urocortinergic neurons with leptin-conjugated saporin in mice

UCN1 immunohistochemistry was performed to confirm EWcp/UCN1 neuron loss. Leptin-conjugated saporin treatment significantly reduced the number of UCN1 immunoreactive neurons in the EWcp compared to the naïve mice (p=0.0002) (**Figure 16A**). Von Frey test was performed to assess periorbital pain associated with migraine-like headache. Before the ablation of EWcp/UCN1 neurons CGRP treatment significantly reduced the periorbital withdrawal threshold compared to saline (p=0.0001). Interestingly, after the ablation of EWcp/UCN1 neurons, the saline treatment significantly reduced periorbital withdrawal threshold compared to non-ablated controls (p=0.0001), and CGRP treatment did not change it further (**Figure 16B**).

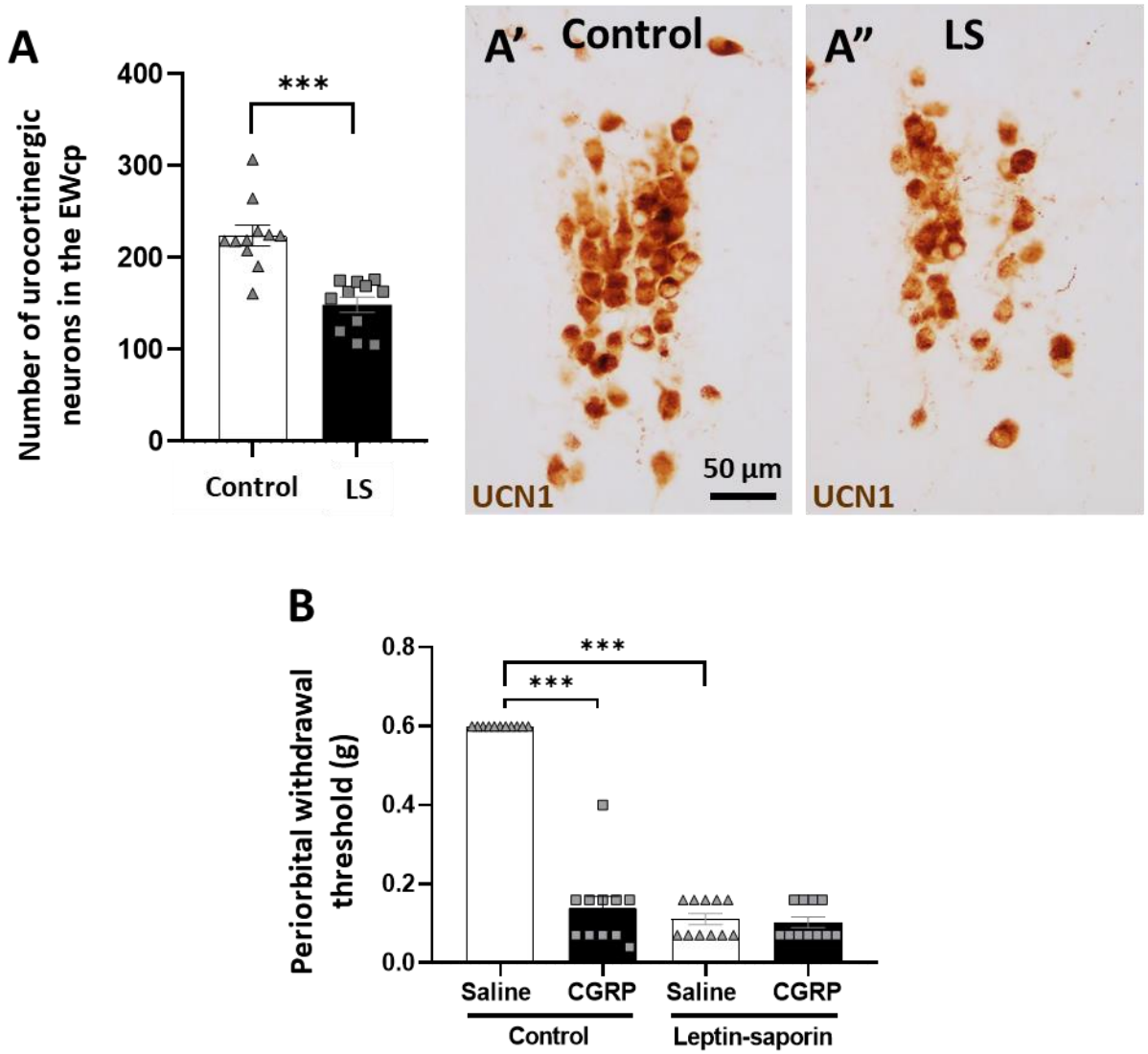

Figure 16. Ablation of urocortinergic (UCN1) neurons in the centrally projecting Edinger-Westphal nucleus (EWcp) by leptin-saporin (LS). (A) Columns show the number of UCN1 neurons in the EWcp in controls and LS-injected groups (n=11; ***p=0.0002; Student's t test). (A'-A") Representative images showing the UCN1 neurons (brown) in the EWcp, in control

and LS-injected mice. (B) Columns show the facial withdrawal threshold (g) in von Frey test, 30 min after saline or calcitonin gene-related peptide (CGRP) injection in control and LS-injected mice (n=11, ***p=0.0001; Tukey's *post hoc* test upon repeated measures ANOVA).

4.2. Human fMRI study

An fMRI study was performed to investigate the functional connectivity matrix of the EWcp in humans.

4.2.1. Functional connectivity of the human Edinger-Westphal nucleus

Extensive positive functional connectivity of the EW nucleus with frontal and temporal gyri, cerebellum, caudate and midbrain were identified in the whole population (**Figure 18. and Table 4.**). In accordance, significant positive functional connectivity was found between the EW and DRN (Peak pFWE=0.004; Peak Z-value=3.51, Peak MNI coordinates: x=0, y=-28, z=-14) as well as STN (Peak pFWE=0.007; Peak Z-value=3.10, Peak MNI coordinates: x=4, y=-40, z=-44) in whole group analysis. No significant negative connections were detected.

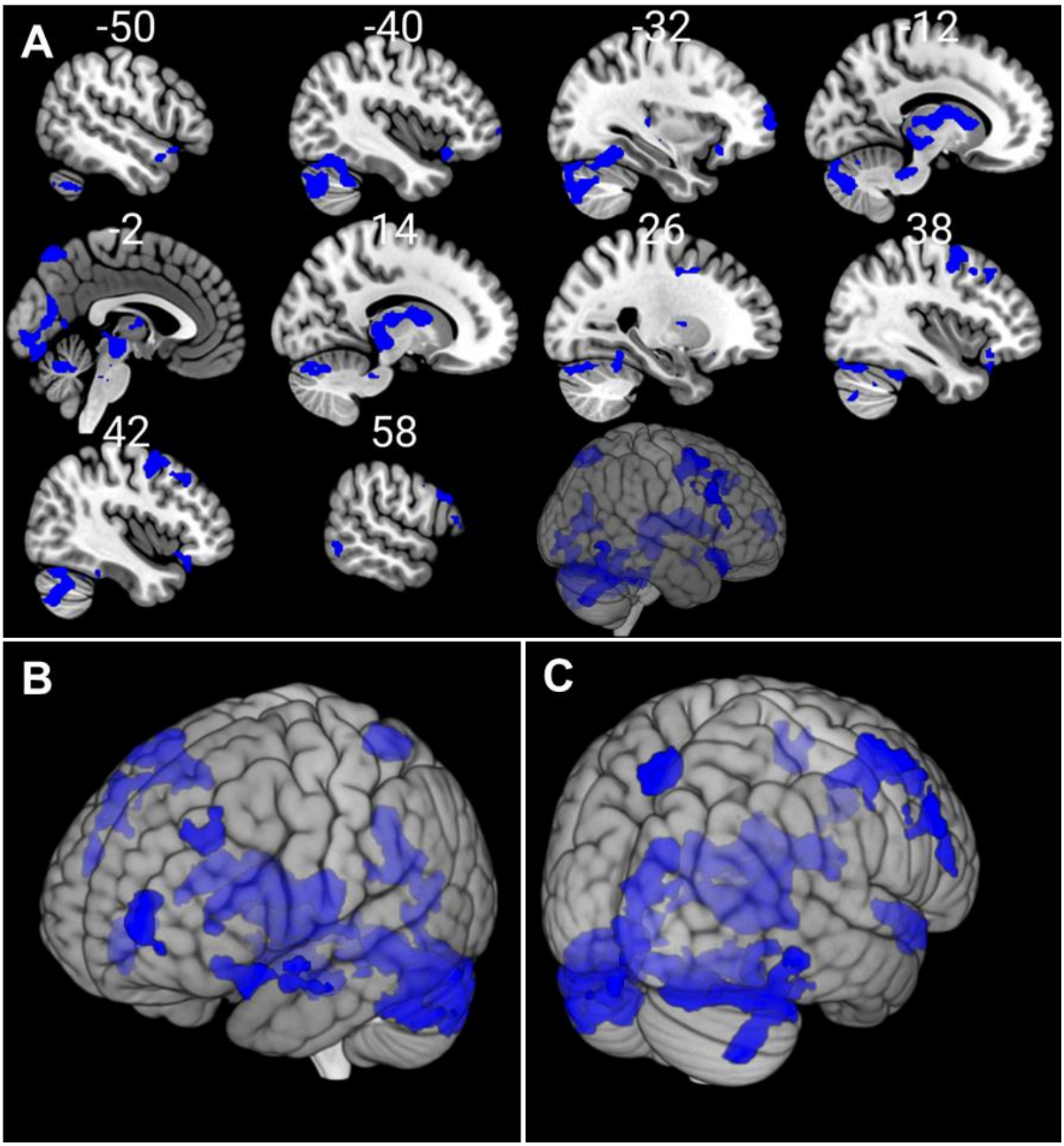

Figure 18. Functional connectivity matrix of Edinger-Westphal nucleus. Blue color represents functional connectivity of Edinger-Westphal nucleus with other brain areas. Significance threshold was cluster-level p(FWE)<0.05 including at least 10 contiguous voxels. Results are corrected for age and sex. Statistical maps were visualized on the MNI 152 template brain provided in MRIcroGL (http://www.mccauslandcenter.sc.edu/mricrogl/).

Cluster size (voxel)	Region	Peak coordinates			Peak
		x	y	z	T-value
5518	L Thalamus	-2	-24	-8	17.99
	R Lingual gyrus	12	-24	-6	5.882
	R Caudate	14	-2	14	5.474
	L Caudate	-10	10	6	4.91
	R Thalamus	10	-20	10	4.69
	R Pallidum	22	0	6	4.62
221	R Precuneus	2	-72	56	5.410
319	L Posterior cingulate cortex	-10	-34	-30	5.084
	R Cerebellum III	12	-30	-30	4.672
1524	R Cerebellum VI	36	-40	-28	5.027
	R Cerebellum Crus 2	42	-70	-44	4.660
278	R Orbital part of inferior frontal gyrus	32	26	-14	4.973
596	R Middle frontal gyrus	50	14	52	4.906
	R Precentral gyrus	36	0	48	4.700
247	L Superior temporal pole	-42	20	-16	4.905
173	L Middle frontal gyrus	-24	28	34	4.534
196	R Triangular part of inferior frontal gyrus	54	28	14	4.364
	R Opercular part of inferior frontal gyrus	56	20	38	3.952
132	L Middle temporal gyrus	-68	-30	-6	4.349
342	R Medial part of superior frontal gyrus	2	56	34	4.331
	L Medial part of superior frontal gyrus	0	52	46	3.898
230	L Middle frontal gyrus	-30	60	8	4.159
	L Orbital part of middle frontal gyrus	-38	56	-2	3.468

Table 4. Significant positive functional connectivity of Edinger-Westphal nucleus. Reported results are significant at cluster-level $p_{FWE}<0.05$. Coordinates are in Montreal Neurological Institute (MNI) space. R: right hemisphere, L: left hemisphere.

Since the EW nucleus is located within the borders of the PAG, we also identified the functional connectivity matrix of PAG (**Table 5.**). Moreover, we summarized the similarities and differences in functional connectivity matrix of EW and PAG (**Figure 19.**).

cluster size (voxel)	Region	Peak coordinates			peak
		x	y	z	T-value
2855	Midbrain	4	-28	-6	16.100
	Midbrain	18	-22	-8	5.677
	Midbrain	-24	-22	-6	4.810
222	L Superior frontal gyrus	-26	62	10	5.328
	L Middle frontal gyrus	-24	50	16	4.097
1468	R Vermis_7	2	-74	-26	4.66
	R Cerebelum_IX	12	-54	-34	4.62
	L Cerebelum_VI	-26	-60	-36	4.499
171	L Cerebelum_Crus1	-40	-46	-36	4.506
170	R Anterior cingulate cortex	12	50	8	4.318
	L Anterior cingulate cortex	-2	48	12	3.593
318	L Calcarine	-2	-68	22	4.313
	L Precuneus	-2	-72	32	3.849
	R Precuneus	8	-66	30	3.601
173	L Superior frontal gyrus	-12	28	36	4.111
	L Middle frontal gyrus	-24	36	40	3.659
192	L Cerebelum_Crus1	-46	-58	-38	4.111
	L Cerebelum_Crus2	-40	-74	-46	4.015

Table 5. Significant positive functional connectivity of periaqueductal gray matter. Reported results are significant at cluster-level $p_{FWE}<0.05$. Coordinates are in Montreal Neurological Institute (MNI) space. R: right hemisphere, L: left hemisphere.

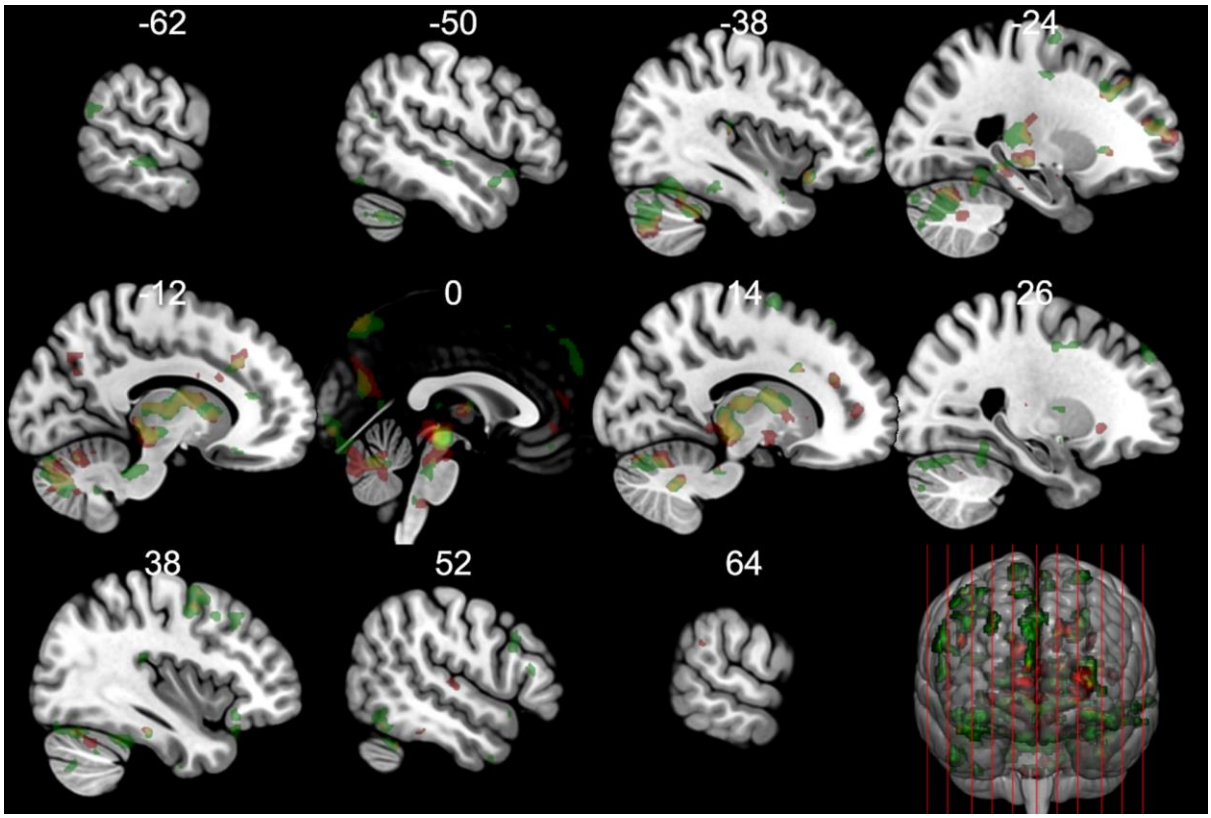

Figure 19. Similarities and differences in functional connectivity of Edinger-Westphal nucleus and periaqueductal gray matter. Green color represents the functional connectivity of Edinger-Westphal nucleus; red color represents the functional connectivity of periaqueductal gray matter; yellow color represents the overlapping connectivity. Initial threshold of $p<0.001$ uncorrected for multiple comparison and at least twenty contiguous voxels was used in the analysis. All connections were positive.

4.2.2. Comparison of Edinger-Westphal nucleus functional connectivity between interictal migrainours and control groups

There was no significant difference between interictal migraine patients and healthy controls in the functional connectivity of EW nucleus after correction for multiple testing.

4.2.3. Association between migraine frequency and functional connectivity of Edinger-Westphal nucleus

We identified a positive correlation between migraine frequency and the functional connectivity of EW nucleus with two clusters. One cluster (cluster size=123 voxel, pFWE=0.045) contained the angular gyrus (Peak T-value=4.211, Peak MNI coordinates: x=54, y=-52, z=26) and superior temporal gyrus (Peak T-value=3.961, Peak MNI coordinates: x=58, y=-40, z=22), while the other cluster (cluster size=166 voxel, pFWE=0.011) contained the middle frontal

(Peak T-value=3.994, Peak MNI coordinates: x=54, y=34, z=22), and triangular part of inferior frontal gyri (Peak T-value=4.189, Peak MNI coordinates: x=48, y=30, z=14) (**Figure 20.**).

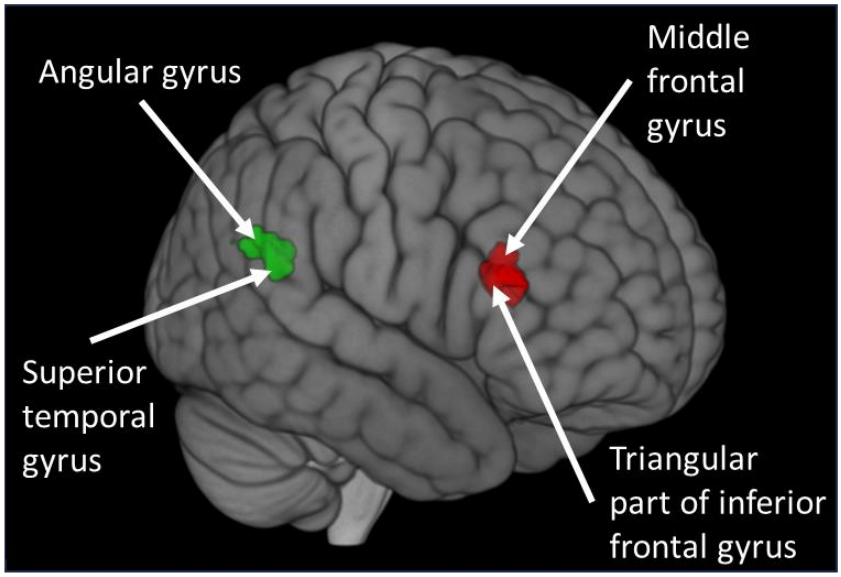

Figure 20. Brain clusters where functional connectivity of Edinger-Westphal nucleus was positively correlated to migraine frequency. The green area represents the first cluster containing the angular gyrus and superior temporal gyrus, while red area is the other cluster containing the middle frontal and triangular part of inferior frontal gyri. Significance threshold was cluster-level p(FWE)<0.05 including at least 10 contiguous voxels. Results are corrected for age and sex. Statistical maps were visualized on the MNI 152 template brain provided in MRIcroGL (http://www.mccauslandcenter.sc.edu/mricrogl/).

4.3. Examination of EWcp/TRPA1 in acute alcohol exposure model

4.3.1. Investigation of the functional activity of TRPA1 in mouse EWcp

As we aimed to examine the importance on TRPA1 in EWcp/UCN1 neurons, we first wanted to see whether our mRNA studies would be confirmed by a functional tool. This was important for us, because the lack of reliable TRPA1 antibody precluded the opportunity to provide evidence at protein level.

To test the functional activity of TRPA1 ion channel in the urocortinergic neurons of EWcp, we performed patch clamp experiment in whole cell configuration on acute brain slices. All patched neurons were filled with biocytin and tested for UCN1 immunoreactivity *post hoc* (**Figure 21A-C**). Only UCN1-immunoreactive cells were used in the statistical analysis. UCN1-immunoreactive neurons were tonically active at resting membrane potential as it was shown previously (Topilko et al., 2022). We used JT010, a potent and selective, covalently binding agonist (Takaya et al., 2015) to activate the TRPA1. Since recording of a relatively small

transmembrane current in neurons can be challenging, we decided to monitor membrane potential changes in current clamp mode upon application of JT010. Resting membrane potential of recorded cells were adjusted *via* the amplifier to keep the cells just below the threshold for AP firing (few AP still occurred). This strategy prevented spontaneous firing, however even a moderate membrane potential depolarization -by the activation of TRPA1- resulted in high frequency firing. Firing frequency was significantly increased during JT010 application in UCN1-immunoreactive neurons **(Figure 21E-F)**. AP frequency was 0.14 ±0.07 Hz at baseline, 0.87 ± 0.17 Hz during drug application and 0.22 ± 0.07 Hz after washing out the drug (n=9/4 mice) **(Figure 21F)**. Notably UCN1-immunonegative neurons in the EW region showed no change in firing frequency or in membrane potential upon the application of JT010 **(Figure 22.)**.

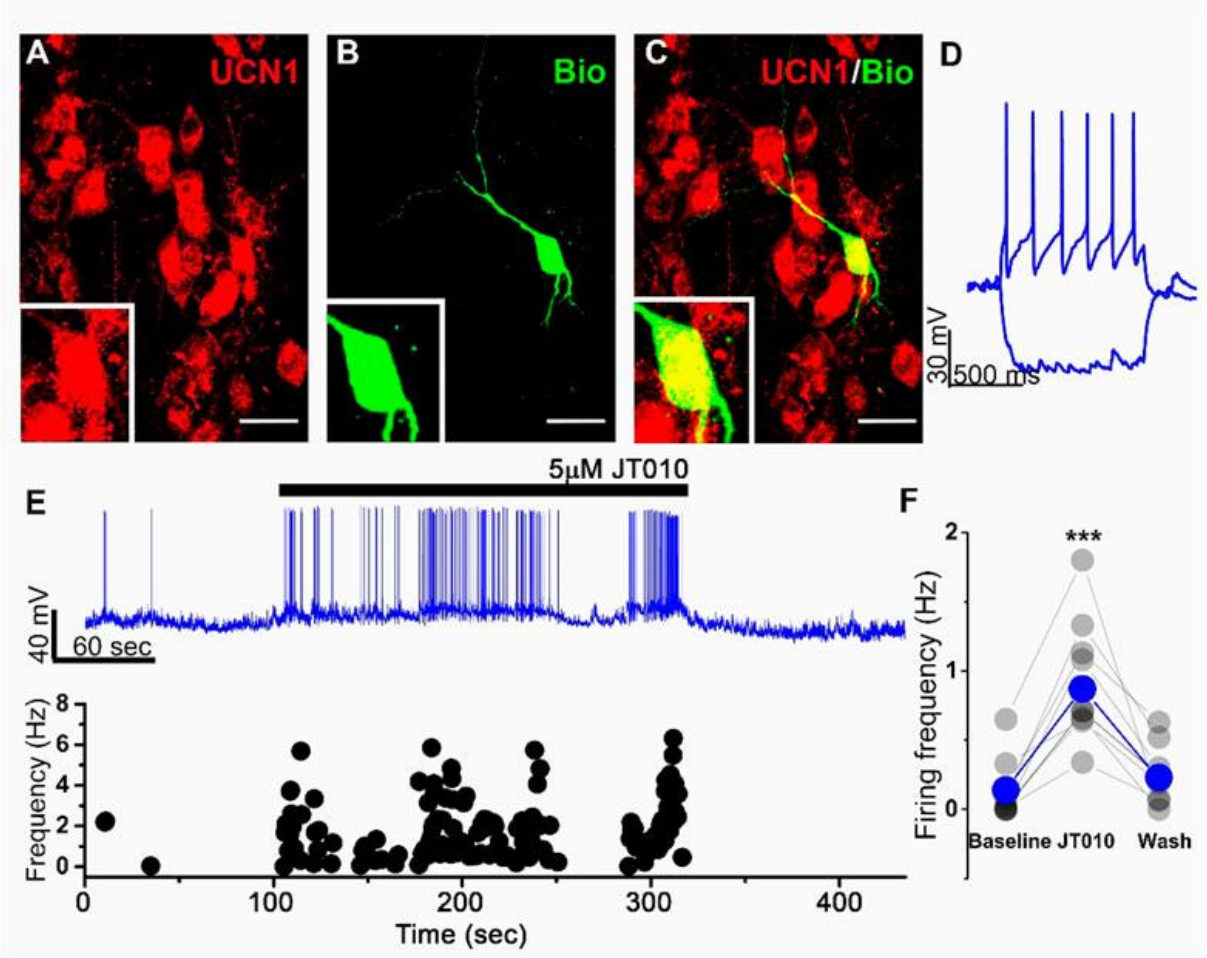

Figure 21. The TRPA1 agonist JT010 increases spontaneous firing frequency of urocortin 1 (UCN1)-immunoreactive neurons in the centrally projecting Edinger-Westphal nucleus. Representative confocal images of UCN1-immunoreactive (red) cells (A), a biocytin (Bio, green) filled patched neuron (B) and the merged image (C). Insets shows the magnified soma of the patched neuron. Scale bars: 40 µm. Response of the recorded cell (D) to 1 s current injection (−100 and +100 pA). Representative current clamp recordings (E, upper panel) showing the spontaneous activity of UCN1-immunoreactive neuron. Black bar represents

JT010 application (5 µM). Instantaneous firing frequency (E) (lower panel) of each action potential in the upper recording is plotted. Statistics (F) showing the firing frequency at baseline (2 min before drug application) during JT010 application and after washing out the drug (n=9 from 4 mice). ***p<0.001; Tukey's *post hoc* test upon one-way ANOVA.

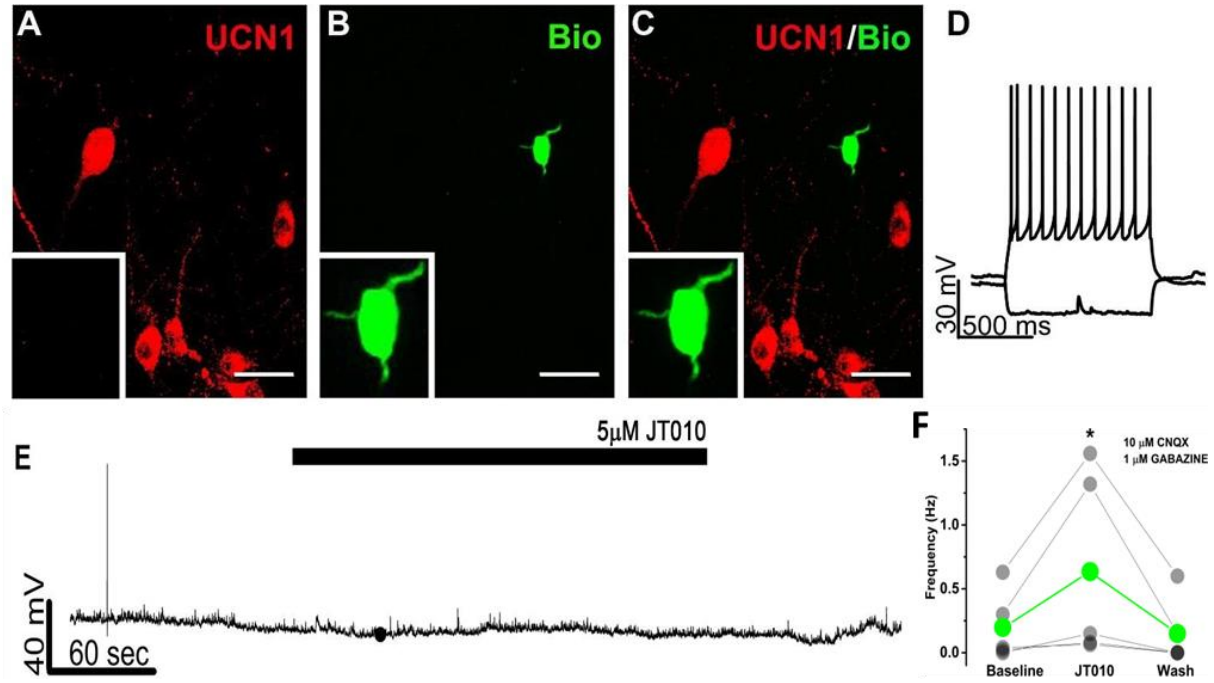

Figure 22. JT010 does not alter spontaneous activity of urocortin 1 (UCN1)-immunonegative neurons in the Edinger-Westphal nucleus. Representative confocal images of UCN1 immunostaining (A, red), biocytin (B, Bio, green) filled patched neuron and the merged image (C) respectively. Insets show the magnified soma of the patched neuron. Note that the recorded neuron is UCN1-immunonegative. Scale bars: 40 µm. Respond of the recorded cell (D) to 1s current injection (-100 and +150 pA). Representative current clamp recordings (E) showing the spontaneous activity of the UCN1-immunonegative neuron. Black bar represents JT010 application (5 µM). Statistics showing the firing frequency at baseline (2 min before drug application), during JT010 application and after washing out the drug in the presence of cyanquixaline (CNQX, a competitive AMPA/kainate receptor antagonist) and Gabazine (antagonist at $GABA_A$ receptors) (n=5 from 2 mice). *p<0.05; paired Student t test (F).

4.3.2. Examination of *TRPA1* mRNA expression in the human EWcp

To confirm the expression of *TRPA1* mRNA in human EWcp urocortinergic neurons also, RNAscope ISH targeting *TRPA1* mRNA was combined with UCN1 immunofluorescence. UCN1 positive neurons in human EWcp were found to co-express *TRPA1* mRNA (**Figure 23.**).

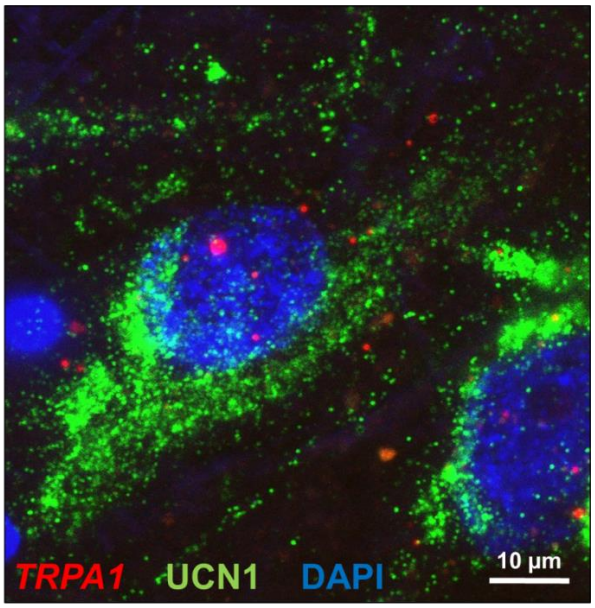

Figure 23. *TRPA1* expression in human centrally projecting Edinger-Westphal nucleus (EWcp). Representative fluorescence images showing *TRPA1* mRNA transcripts (red) co-expressed with urocortin 1 peptide (UCN1, green) in human EWcp. Nuclear counterstaining was performed with 4′,6- diamidino-2-phenylindole (DAPI, blue).

4.3.3. Investigation of the *Trpa1*-expressing EWcp in a mouse model of acute alcohol exposure

4.3.3.1. UAC measurement

To confirm the absorption of i.p. administered ethanol, the urine alcohol concentration (UAC) was measured using headspace gas chromatography. As expected, in the saline-treated groups no ethanol was detected in the urine. We detected similar ethanol concentration in the urine of both alcohol-treated WT and *Trpa1* KO animals (ANOVA, main effect of treatment: $F_{1,24}=37.030$; $p<10^{-6}$; main effect of genotype $F_{1,24}=0.09$; $p=0.76$) (**Figure 24.**).

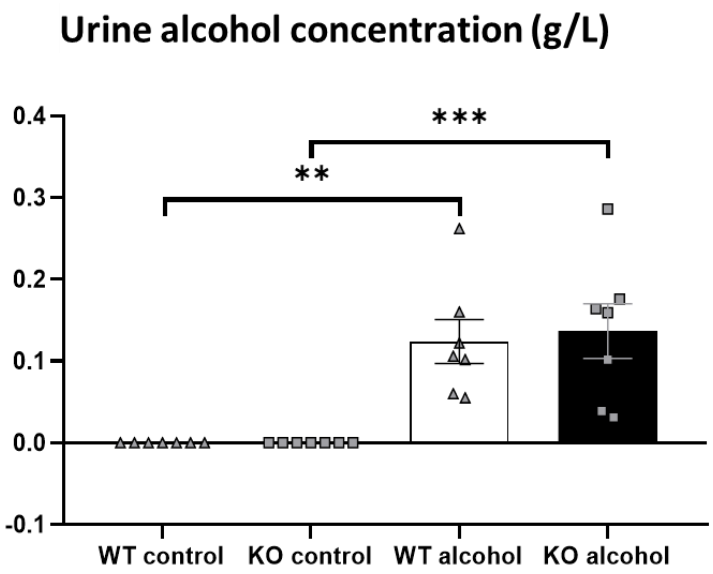

Figure 24 Urine alcohol concentration. Quantitative evaluation of alcohol concentration in the urine of wild-type (WT) and *Trpa1* knockout (KO) mice, 2 h after i.p. saline (control) or 1 g/kg ethanol injection. Columns show means ± SEM of alcohol concentration (g/L) (n=6-7; **p=0.002; ***p=0.0009; Tukey's *post hoc* test upon two-way ANOVA).

4.3.3.2. FOS immunohistochemistry

FOS immunohistochemistry was performed to assess the acute neuronal activity in EWcp. Alcohol treatment significantly increased the number of FOS-positive neurons in the EWcp of both WT and *Trpa1* KO mice, compared to the respective controls (ANOVA, main effect of treatment: $F_{1,25}$=183.33; $p<10^{-6}$) without the main effect of genotype (**Figure 25.**).

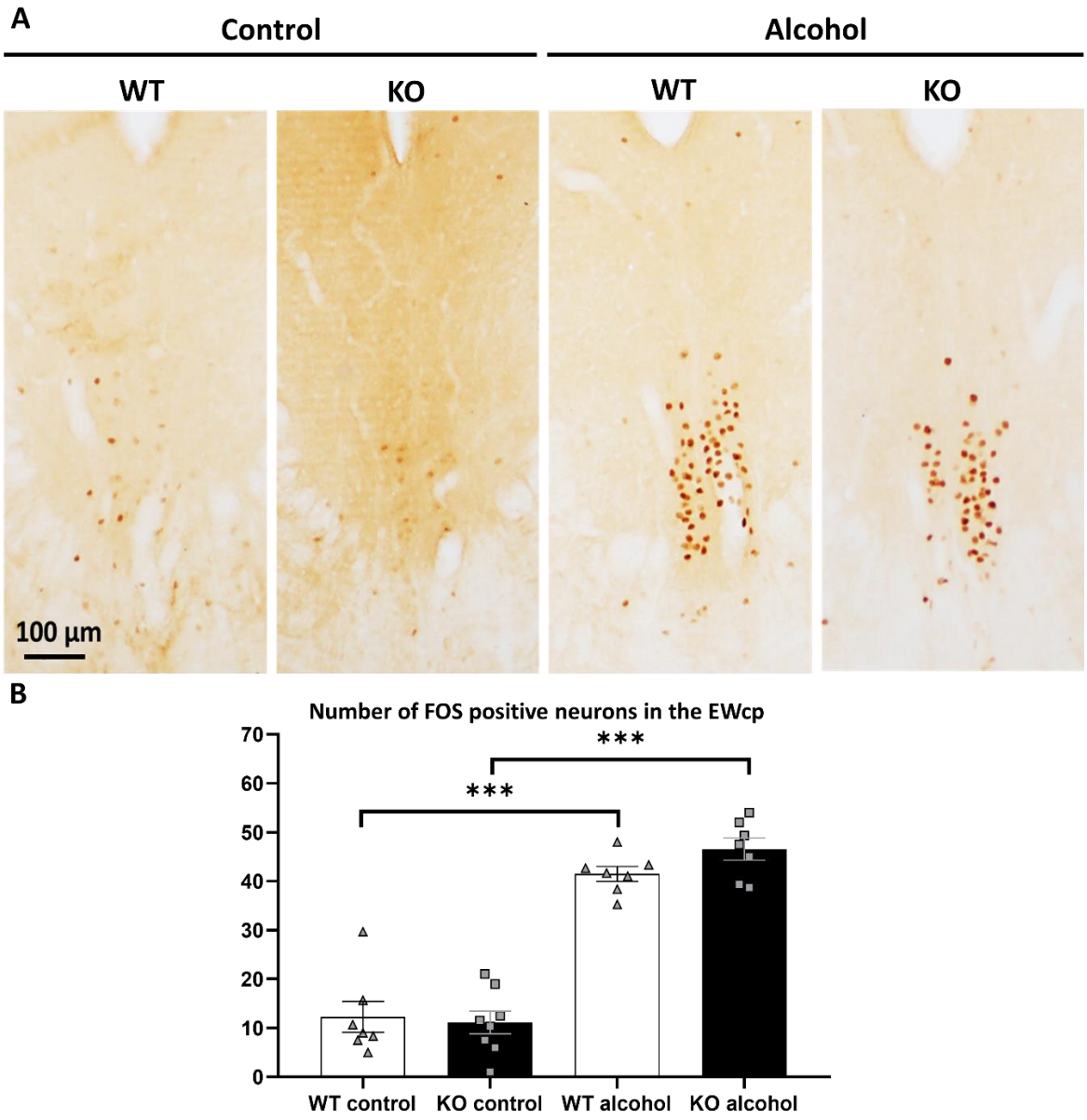

Figure 25. FOS immunoreactivity in the centrally projecting Edinger-Westphal nucleus (EWcp) upon alcohol treatment. (A) Representative immunohistochemical images showing the expression of FOS, as a marker of early neural activation, in the EWcp of wild-type (WT) and *Trpa1* knockout (KO) mice, 2 h after i.p. saline (control) and 1 g/kg ethanol injection. Neuronal activation is represented by brown-colored nuclei. **(B)** Quantitative evaluation of FOS immunostaining in the EWcp of WT and *Trpa1* KO mice, 2 h after i.p. saline (control) and 1 g/kg ethanol injection. Columns show means ± SEM of FOS positive neurons in the EWcp (n=6-8; ***p=0.0001; Tukey's *post hoc* test upon two-way ANOVA).

4.3.3.3. *Trpa1* RNAscope *in situ* hybridization

RNAscope ISH was performed to examine the effect of ethanol on the number of *Trpa1* mRNA transcripts in the EWcp/UCN1 neurons of WT animals. *Trpa1* mRNA showed a full co-localization with the UCN1 peptide immunosignal in the EWcp (**Figure 26A**). Ethanol treatment significantly decreased the number of *Trpa1* transcripts compared to the control (p=0.0001) (**Figure 26B**).

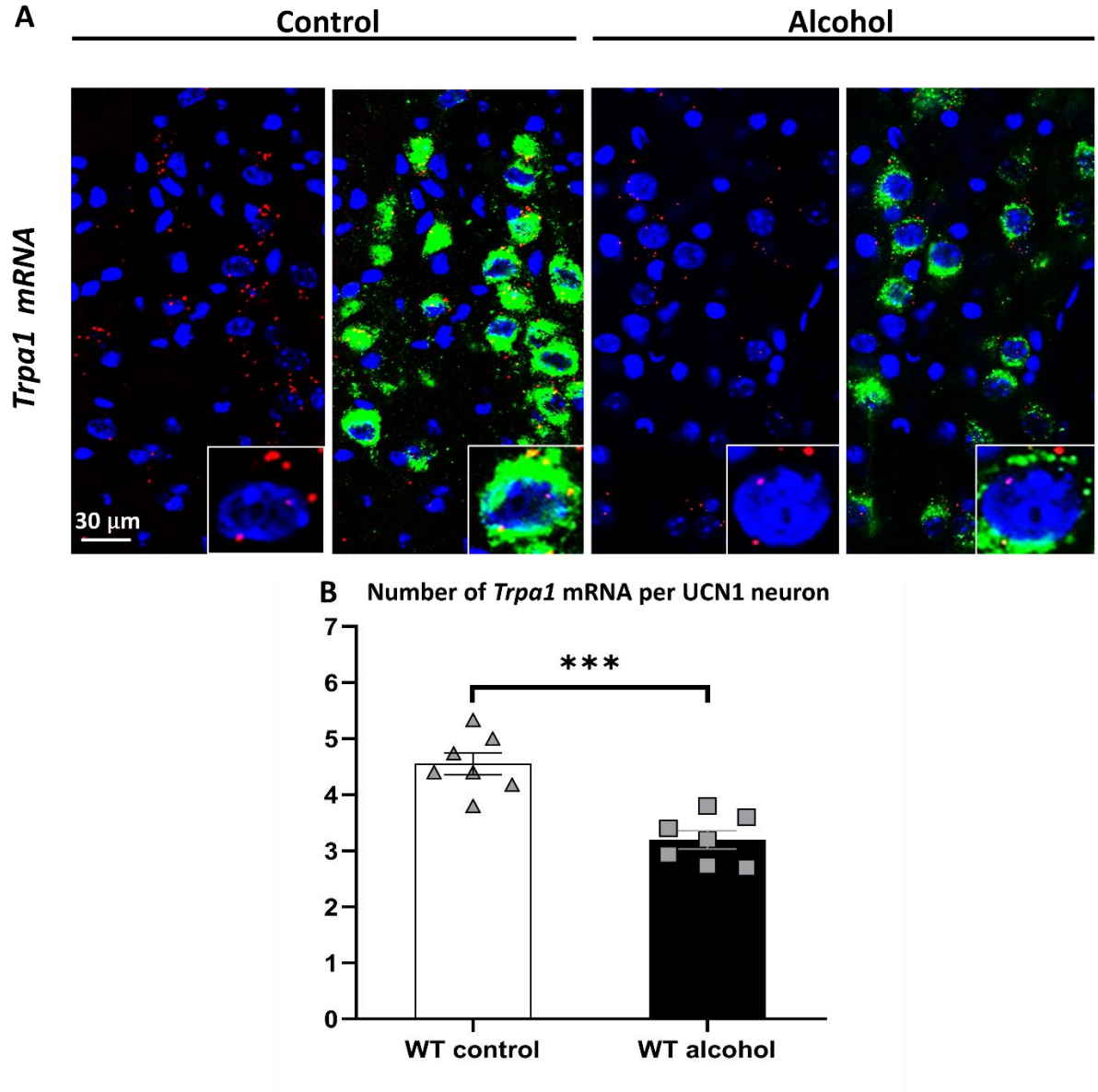

Figure 26. *Trpa1* mRNA expression in the centrally projecting Edinger-Westphal nucleus (EWcp) of control and alcohol-treated mice. (A) Representative fluorescence images showing the expression of *Trpa1* mRNA (red) by RNAscope *in situ* hybridization and its co-localization with the urocortin 1 (UCN1) peptide (green) by immunofluorescence in the EWcp of *Trpa1* wild-type (WT) mice, 2 h after i.p. saline (control) and 1 g/kg ethanol injection. For nuclei, the sections were counterstained with 4′,6-diamidino-2-phenylindole (DAPI) (blue). **(B)** Quantitative evaluation of *Trpa1* mRNA expression in the EWcp of WT mice, 2 h after i.p.

saline (control) and 1 g/kg ethanol injection. Columns show means ± SEM of *Trpa1* mRNA transcripts in the EWcp (n=6-8; ***p=0.0001; Student's t-test).

4.3.3.4. Dynamics of UCN1 mRNA and peptide upon alcohol treatment

To examine the *Ucn1* mRNA expression and UCN1 peptide content in the EWcp neurons in response to alcohol treatment, RNAscope ISH and immunofluorescence were performed, respectively. We detected a main effect of the genotype (ANOVA: $F_{1,23}$=6.758; p=0.016) on *Ucn1* mRNA expression. In control groups, no difference was detected, however a lower *Ucn1* mRNA expression was observed in KO animals upon alcohol treatment (p=0.030) (**Figures 27A, C**).

We also observed a strong effect of genotype × treatment interaction on UCN1 at peptide level (ANOVA: $F_{1,22}$=51.816; $p<10^{-6}$). The basal UCN1 content of the EWcp neurons was significantly lower in *Trpa1* KO mice compared to WTs ($p<10^{-4}$). Moreover, alcohol treatment differentially regulated the UCN1 peptide content in the EWcp. The UCN1 peptide content of EWcp was significantly decreased in WT mice ($p<10^{-3}$) and significantly increased in KO mice (p=0.002), in response to alcohol treatment (**Figures 27B, D**).

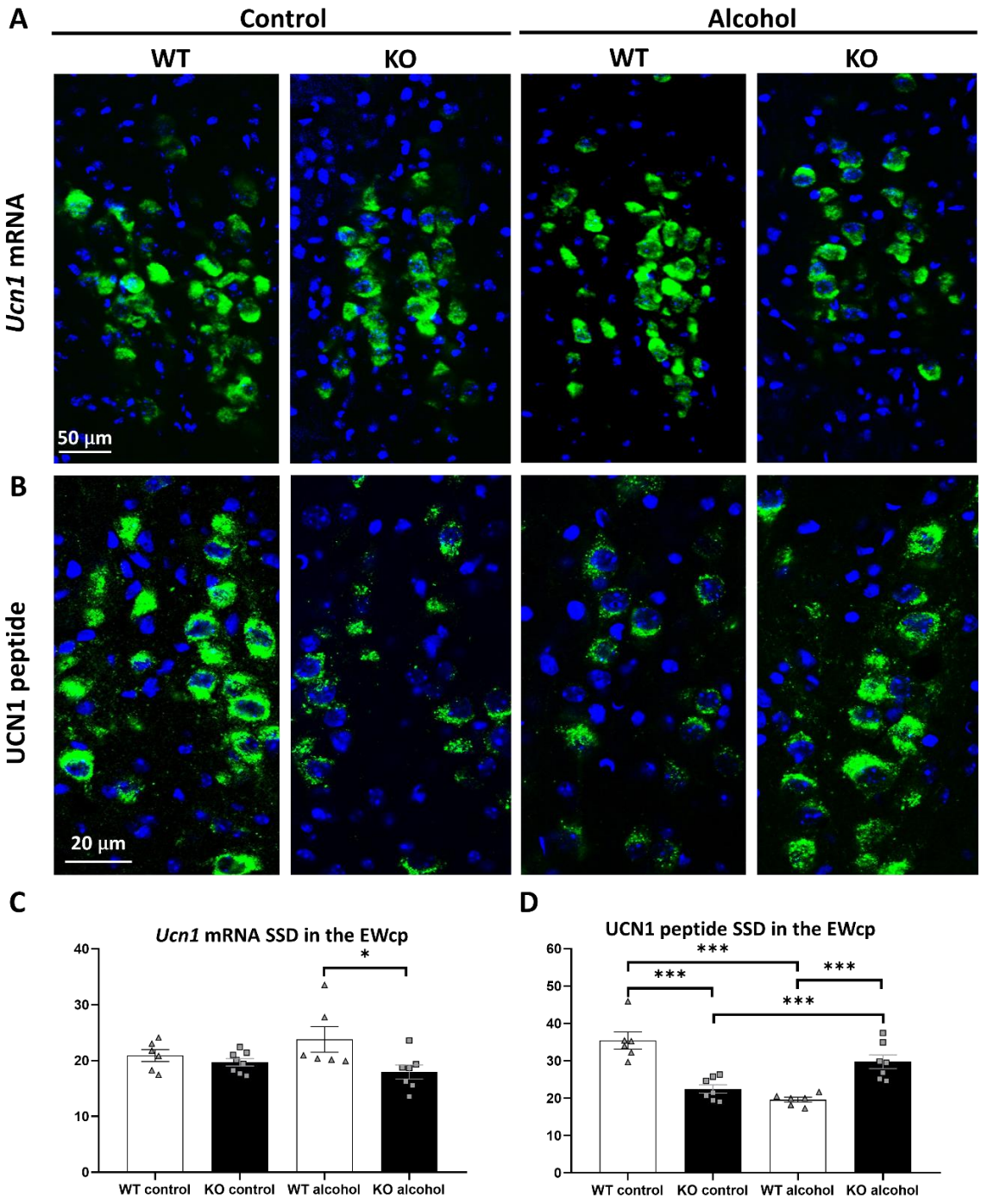

Figure 27. UCN1 mRNA and peptide content of the centrally projecting Edinger-Westphal nucleus (EWcp) of control and alcohol-treated mice. Representative fluorescence images showing the expression of urocortin 1 (*Ucn1*) mRNA (green) by RNAscope *in situ* hybridization **(A)** and the UCN1 peptide (green) by immunofluorescence **(B)**, in the EWcp of wild-type (WT) and *Trpa1* knockout (KO) mice, 2 h after i.p. saline (control) and 1 g/kg ethanol injection. For nuclei, the sections were counterstained with 4′,6-diamidino-2-phenylindole (DAPI) (blue). Quantitative evaluation of *Ucn1* mRNA **(C)** and UCN1 peptide **(D)** specific signal density (SSD) in the EWcp of *Trpa1* WT and *Trpa1* KO mice, 2 h after i.p. saline (control) and 1 g/kg ethanol injection. Columns show means ± SEM of *Ucn1* mRNA **(C)** and UCN1 peptide **(D)** SSD in the EWcp (n=6-8; *p=0.03; ***p=0.0001; Tukey's *post hoc* test upon two-way ANOVA).

4.3.3.5. Dynamics of CART mRNA and peptide upon alcohol treatment

To examine the *Cart* mRNA expression and CART peptide content in the EWcp neurons in response to alcohol treatment, we performed RNAscope ISH and immunofluorescence, respectively.

We observed a main effect of the genotype on *Cart* mRNA expression (ANOVA: $F_{1,21}$=10.37; p=0.004). A lower expression of *Cart* was observed in *Trpa1* KO mice regardless the treatment condition (**Figures 28A, C**). There was no main effect of alcohol treatment nor that of genotype on CART peptide content (**Figures 28B, D**).

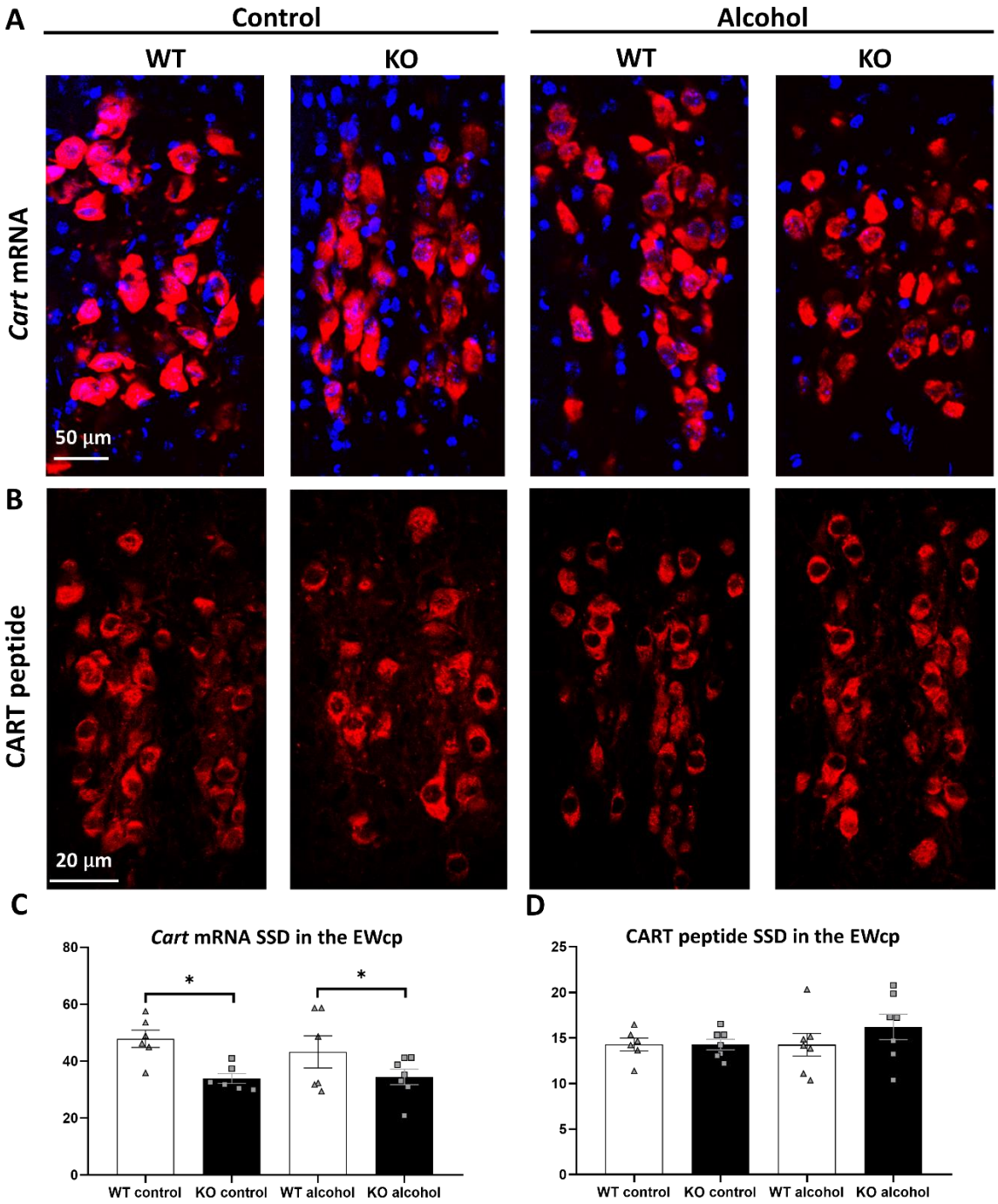

Figure 28. CART mRNA and peptide content of the centrally projecting Edinger-Westphal nucleus (EWcp) of control and alcohol-treated mice. Representative fluorescence images showing the expression of cocaine- and amphetamine-regulated transcript (*Cart*) mRNA (red) by RNAscope *in situ* hybridization **(A)** and the CART peptide (red) by immunofluorescence **(B)** in the EWcp of wild-type (WT) and *Trpa1* knockout (KO) mice, 2 h after i.p. saline (control) and 1 g/kg ethanol injection. For nuclei, the sections were counterstained with 4′,6-diamidino-2-phenylindole (DAPI) (blue). Quantitative evaluation of *Cart* mRNA **(C)** and CART peptide **(D)** specific signal density (SSD) in the EWcp of WT and *Trpa1* KO mice, 2 h after i.p. saline (control) and 1 g/kg ethanol injection. Columns show means ± SEM of *Cart* mRNA **(C)** and CART peptide **(D)** SSD in the EWcp (n=6-8; *p=0.05; two-way ANOVA and Tukey's *post hoc* test).

5. Discussion

5.1. Investigation of EWcp in migraine

CGRP plays a key role in migraine, however, the central distribution of CGRP and its receptor components has been described in rat, mouse and human brain (Ma et al., 2003; Edvinsson et al., 2020; Huang et al., 2021) using immunohistochemistry, CGRP receptor expression in the EWcp has not been studied yet. As we hypothesized that EWcp urocortinergic neurons may be involved in migraine, first we aimed to investigate the expression of CGRP receptor components in mouse and human EWcp and DRN, as well as mouse STN. Here we have confirmed the expression of *Ramp1*, *Calcr* and *Crcp* mRNA as well as CLR protein in EWcp/UCN1 neurons using the highly sensitive and specific RNAscope ISH technique (Wang et al., 2012) combined with immunofluorescence in both mice and humans, which supports the translational relevance of our animal data. Moreover, because AMY1 and CGRP receptor components were also detected in the migraine-related EWcp projection areas such as DRN and STN, we assume that the CGRP may activate the DRN and STN directly or indirectly *via* AMY1 and CGRP receptor-expressing EWcp/UCN1 neurons.

As RNAscope ISH revealed *Crh1r* and *Crh2r* mRNA in the STN neurons and in their close proximity UCN1 fibers were detected, we assumed that a direct, descending urocortinergic EWcp projection innervates the STN neurons in the I-III laminas. Our neuroanatomical studies proved the direct urocortinergic projection from the EWcp to the STN, both by anterograde and retrograde tracing. This suggests that UCN1 released from EWcp-derived fibers may modulate the function of STN neurons *via* CRH1R and CRH2R.

Having supported the anatomical basis of our hypothesis, we next investigated how does the EWcp respond in a migraine model. Several well-validated *in vivo* animal migraine models were described, including direct electrical stimulation of trigeminal neurons, administration of inflammatory substances to the meninges and administration of algogenic substances (Harriott et al., 2019). Importantly, the recruitment of CGRP signaling was approved in all these models (Wattiez et al., 2019). Migraine models applying direct electrical stimulation of trigeminal neurons and administration of inflammatory substances to the meninges are limited by their invasive nature. Considering the acute pain sensitivity of EWcp (Kozicz et al., 2001; Rouwette et al., 2011) these models were not suitable to examine the recruitment of EWcp in migraine. Algogenic substances that are used in animal models of migraine include NTG and CGRP. Intraperitoneal administration of NTG and CGRP successfully resembled many aspects of

migraine in rodents. Moreover, symptoms of NTG- and CGRP-induced migraine like-states were alleviated by anti-migraine drugs like sumatriptan (Bates et al., 2010; Farkas et al., 2016; Mason et al., 2017; Rea et al., 2018; Wattiez et al., 2019). In addition, repetitive administration of algogenic substances allows studying chronic migraine (Kim et al., 2018; Harriott et al., 2019).

In our preliminary pilot study, the NTG administration did not cause significant activation in the EWcp in comparison to the vehicle control. In the view that the vehicle injection elicited a strong neuronal activation in comparison to the saline control, we concluded that the ethanol content of the NTG preparation caused the activation and not the NTG effect proper. Indeed, the EWcp was shown to be very sensitive to ethanol (Zuniga & Ryabinin, 2020; Al-Omari et al., 2023) and because all available NTG preparations contain high concentrations of alcohol as vehicle (Bates et al., 2010; Farkas et al., 2016; Kim et al., 2018), we decided to use the intraperitoneal injection of CGRP as a model of migraine according to Mason et al. (2017).

Several migraine-related symptoms have been observed following central and peripheral CGRP administration in humans and rodents (Lassen et al., 2002.; Kaiser, 2014; Mason et al., 2017), suggesting both peripheral and central site of action. This is further supported by the wide distribution of CGRP and its receptors in the CNS and the periphery (Iyengar et al., 2017; Edvinsson et al., 2020). The TRG neurons express CGRP outside the BBB and provide anatomical connection between peripheral and CNS. Activation of CGRP receptors in trigeminal neurons stimulate CGRP release from a) the peripheral nerve endings of afferent terminals which innervate meninges, b) the cell bodies in TRG and c) the terminals of central processes in the STN (Durham et al., 2016). CGRP release from the central process terminals of TRG neurons can activate the CGRP receptors of the second-order nociceptive nerve cells in the STN promoting the development of central sensitization (Durham et al., 2016; Iyengar et al., 2019), which may ultimately lead to further central CGRP release from CGRP-expressing neurons in the brain. This is one suggested mechanism for central sensitization mediated by peripheral action of CGRP. However, there are several other suggested mechanisms that can lead to central sensitization (Mason et al., 2017; Iyengar et al., 2017, 2019).

In our present study we have used i.p. injection of CGRP as a mouse model of migraine (Mason et al., 2017). For model validation, we examined the periorbital hyperalgesia and the light aversion behavior using von Frey and LDB test respectively, acute FOS neuronal activation in the TRGs (part of the trigeminovascular system) and lPAG (part of the antinociceptive system)

as well as P-CREB and FOS expression in the STN. Assessment of von Frey test results revealed a significantly decreased periorbital withdrawal threshold following CGRP treatment suggesting periorbital hyperalgesia associated with migraine (Farkas et al., 2016; Avona et al., 2020; Tang et al., 2020). Light aversion behavior observed in response to CGRP treatment revealed photophobia, suggesting the development of a migraine-like state in our mice. According to Mason et al. (2017), CGRP treatment did not induce anxiety in mice as revealed by open field test, suggesting that the observed light aversion behavior in response to CGRP is specific to photophobia, associated with migraine-like state. The CGRP-induced light aversion was still observed even with normalized blood pressure, suggesting that CGRP may contribute to light aversion behavior through non-vasomotor mechanisms (Mason et al., 2020). Increased TRG/FOS and STN/P-CREB immunosignals in response to CGRP treatment suggest acute activation of these key players in migraine pathogenesis, which in this setup also proves the validity of our model (Markovics et al., 2012; Farkas et al., 2016). Moreover, increased FOS immunosignal in the lPAG of CGRP-treated mice suggests the activation of the descending antinociceptive pathway. This further reinforces that a migraine-like headache has occurred (Vila-Pueyo et al., 2019). The above-described arguments unequivocally prove the validity of our migraine model.

Several studies have reported a neuromodulatory role of PAG in migraine (Napadow et al., 2019; Vila-Pueyo et al., 2019). However, to the best of our knowledge, no studies have pointed out any possible roles of EWcp in the neurobiology of migraine, even though the EWcp is located within the boundaries of PAG. We propose that peripherally administered CGRP may influence the EWcp/UCN1 neurons' activity directly by the CGRP released centrally or by indirect manner as a consequence of the central sensitization. Here we have reported a two-fold increase in the number of FOS positive EWcp/UCN1 neurons upon CGRP treatment. We also confirmed the urocortinergic identity of the activated, FOS immunoreactive EWcp cells. The acute neuronal activation as shown by immediate early gene expression suggests that the cells' response requires the adaptation at the level of gene expression (Al-Omari et al., 2023; Gaszner et al., 2012). This idea is supported by increased *Ucn1* mRNA and UCN1 peptide content of EWcp/UCN1 positive neurons in response to CGRP administration. Increased *Ucn1* mRNA in association with higher UCN1 peptide content in EWcp/UCN1 neurons suggests that the UCN1 peptide is released in a higher rate. In the present study, we have demonstrated a direct anatomical link between the EWcp and STN and we also detected CRH receptor mRNA expression in STN neurons. Therefore, the presumably increased UCN1 release from EWcp

neurons may directly influence the function of the STN *via* CRH1R and CRH2Rs, as supported by increased P-CREB immunosignal in the STN. In line with earlier studies (Bhatt et al., 2014, 2015), no FOS activation was observed in the STN upon CGRP treatment.

As the *Trpa1* mRNA is expressed at the highest level in the EWcp in mouse brain (Kormos et al., 2022), moreover, literature has linked TRPA1 to migraine (Souza Monteiro de Araujo et al., 2020; Shibata et al., 2021; Iannone et al., 2022a, 2022b; Spekker et al., 2022; Fila et al., 2023; Masood et al., 2023), we aimed to examine the *Trpa1* mRNA expression of EWcp in our migraine model. Using RNAscope ISH we showed that urocorinergic neurons in the EWcp of the CGRP-treated group exhibited significantly higher number of *Trpa1* mRNA transcripts compared to the control. We assume, that the upregulation of *Trpa1*, a cation channel may lead to higher influx of calcium, hence causing an increase in the release of UCN1. This expectation is supported by our findings suggesting increased urocortinergic activity, although this awaits experimental confirmation.

Beyond the STN, the serotonergic DRN is also a brain area known to be activated in migraine (Shibata et al., 2022). The EWcp urocortinergic neurons innervate the serotonergic cells of the DRN (Dos Santos Júnior et al., 2015; van der Doelen et al., 2017; Zuniga & Ryabinin et, 2020), where both CRH receptors are expressed (Chalmers et al., 1995; Ma et al., 2003; Valentino et al., 2010; van der Doelen et al., 2017). It has been reported that the activation of CRH1R in DRN serotonergic neurons reduces 5-HT release, whereas the activation of CRH2R has opposite effect (Lukkes et al., 2011; Fox & Lowry, 2013). In our study, we observed a decreased 5-HT content in the serotonergic DRN neurons of CGRP-treated mice, suggesting the release of 5-HT in response to CGRP administration. Supporting our results, several studies indicate raised 5-HT levels in the CNS during migraine attack (Drummond & Drummond, 2006; Sakai et al., 2008; Deen et al., 2018; Razeghi et al., 2019). Here we conclude that the CGRP induced elevation of UCN1 release from nerve terminals in the DRN. This may activate CRH2Rs in the serotonergic DRN neurons that ultimately results in elevated 5-HT release. Nevertheless, we cannot exclude the direct effect of CGRP on serotonergic neurons as they also express the CGRP receptor (Ma et al., 2003).

TPH2 is the rate-limiting enzyme of the 5-HT synthesis in the brain (Walther et al., 2003) and its gene polymorphisms have been linked to the migraine (Marziniak et al., 2009; Jung et al., 2010). Our study reported decreased TPH2 enzyme level in DRN serotonergic neurons upon CGRP treatment. Only one study reported that the UCN1 may interact with the TPH2 level.

Donner et al. (2020) observed that chronic central UCN1 microinjection elevated the *Tph2* mRNA expression in the caudal and dorsal subdivision of the DRN. In contrast, UCN1 decreased *Tph2* expression in the ventrolateral part of DRN serotonergic neurons (Donner et al., 2020). This finding contrasts with our results as we saw that the CGRP treatment caused a rise in the UCN1 levels but decreased the TPH2 protein content. This may be explained on one hand by the fact that in our study we examined the TPH2 not the mRNA, but at protein level. On the other hand, we applied a single CGRP treatment, which elevated the UCN1 level in our model, in contrast to the work of Donner et al. (2020) where a chronic UCN1 administration was applied. Third, the CRH2R expression pattern differs in the subdivisions of DRN too. The caudal part of the DRN expresses higher levels of CRH2R, compared to the ventrolateral part (Lukkes et al., 2011). Under basal conditions, CRH1R is localized mainly in the plasma membrane in contrast to CRH2R which is more prominent in the cytoplasm. Stress result in trafficking of the CRH receptor subtypes in opposing directions such that CRH1R tends to move to the cytoplasm while the CRH2R is transported to the plasma membrane (Waselus et al., 2009). The complex action of UCN1 on DRN serotonergic neurons reflects the proclaimed abnormalities in central 5-HT turnover in migraine (Drummond & Drummond, 2006.; Razeghi et al., 2019).

As further evidence for the role of EW in migraine, we performed selective UCN1 neuron ablation using leptin-conjugated saporin (ribosome-inactivating protein) in mice. Saporin is a neurotoxin that enters neurons only if it is conjugated to a substance that is internalized by receptor-mediated endocytosis and irreversibly inhibits the cells' protein synthesis (Wiley et al., 2000). Given that in the EWcp only UCN1-immunoreactive neurons expresses leptin receptor, leptin-conjugated saporin injection provides a reliable tool to perform selective UCN1 neuron ablation (Ujvári et al., 2022, Xu et al., 2022). Periorbital hyperalgesia in response to CGRP or saline were assessed before and 2 weeks after the surgery. Given that the CART and UCN1 show full co-localization in the EWcp (Zuniga & Ryabinin, 2020; Priest et al., 2023), decreased periorbital withdrawal threshold following EWcp/UCN1 ablation aligns with earlier study result where the increased activity of EWcp/CART resulted in increased paw withdrawal threshold, suggesting that these neurons modulate pain (Priest et al., 2021).

The ability of EWcp to influence migraine-related areas through direct neuroanatomical connection was further supported here by the significant positive functional connectivity between EW and the DRN and STN in human fMRI study. To the best of our knowledge this is the first study to describe the functional connectivity of EW. Moreover, our fMRI study revealed

a strong positive correlation between the frequency of migraine attacks and the functional connectivity of EW with brain areas that are known to be part of the affective pain pathway including angular gyrus, superior temporal gyrus, middle frontal and the triangular part of inferior frontal gyri (Jia & Yu, 2017; Ong et al., 2019; Wang et al., 2019), supporting previous finding that changes in these brain areas may predispose a person to pain conditions including migraine (Jia & Yu, 2017).

5.2. Examination of EWcp/TRPA1 in acute alcohol exposure model

Ethanol and its metabolites efficiently pass through the BBB and they are the activators of TRPA1 ion channels (Bang et al., 2007; Wang et al., 2011; Komatsu et al., 2012; De Logu et al. 2019; Landini et al., 2023;). As UCN1 is involved in acute and chronic alcohol consumption (Schreiber & Gilpin, 2018; Zuniga & Ryabinin, 2020), moreover, urocortinergic neurons in EWcp uniquely express significant amount of TRPA1 in the mouse CNS (Kormos et al. 2022), we hypothesized that ethanol and its metabolites may influence the function of EWcp urocortinergic neurons *via* TRPA1. The activation of TRPA1 leads to calcium influx which triggers several intracellular pathways. This may contribute to the regulation of UCN1 and/or CART peptide release in the EWcp. Our aim was to examine this ion channel in the UCN1 and CART co-expressing EWcp neurons response to acute alcohol exposure in mice.

In our earlier studies (Kormos et al., 2022) we had to face the criticism of reviewers and peers in scientific discussions that we do not show the existence of TRPA1 in the EWcp at protein level. Because there is no reliable antibody available against TRPA1, we cannot directly prove the presence of this ion channel at protein level in the EWcp. Nevertheless, as our preliminary tests strongly suggested the recruitment of *Trpa1* mRNA on the alcohol model, we decided to apply electrophysiological tools to prove that TPRA1 is functional in the EWcp neurons. Therefore, we applied the patch clamp method in whole cell configuration on acute EW slices and proved the functional activity of TRPA1 channel. The EWcp urocortinergic neurons are spontaneously active and fire APs at resting membrane potential. Here we hypothesized that the activation of TRPA1 in these neurons will result in Ca^{2+} influx and subsequent membrane potential depolarization which in turn will increase the frequency of spontaneous firing. Indeed, the application of a selective and potent TRPA1 agonist (JT010), significantly increased the spontaneous firing frequency of UCN1-immunoreactive neurons while it was ineffective in neighbouring non-urocortinergic neurons lacking TRPA1. To the best of our knowledge, our

study is the first to provide evidence for the functional role of TRPA1 in neurons of the mouse brain.

In order to support the human translational value of our findings, we previously proved the expression of the *TRPA1* mRNA in human EW by TaqMan PCR method (Kormos et al., 2022). However, the PCR technique does not provide morphological context, because in a homogenized tissue sample the detected mRNA may originate from any cells of the sample. Hence with this approach we cannot distinguish mRNAs of the urocortinergic neurons, from those that are from other types of cells in homogenized human EW tissue samples. Therefore, we applied the highly sensitive RNAscope ISH method on perfused human EW samples by which we proved the urocortinergic identity of the TRPA1 positive neurons in the EWcp.

Taking into account the alcohol sensitivity of EWcp and supported by our data (in the NTG model), we decided to investigate the role of EWcp/CART/UCN1/*Trpa1* neurons on the effect of acute alcohol administration, using *Trpa1* KO and WT mice. In our model for acute alcohol exposure, the UAC measurement proved the reliability of the model as the absorption of ethanol was identical in WT and *Trpa1* KO mice.

Increased FOS expression upon alcohol treatment is consistent with the previous studies result (Bachtell et al., 1999; Ryabinin et al., 2001; Weitemier et al., 2001; Zuniga & Ryabinin, 2020), and further supports the ability of alcohol and its metabolites to activate the EWcp urocortinergic neurons. Increased FOS activation in the EWcp of *Trpa1* KO mice in response to alcohol treatment implies that, in addition to TRPA1 other receptors and ion channels may also contribute to the alcohol-induced activation of urocortinergic cells. In line with this assumption, a previous study suggested that the alcohol-induced FOS response in EWcp is mediated by signaling *via* GABA-A receptors, modified by α2A/D-adrenoceptors and dopamine receptors (Bachtell et al., 2002). An alternative explanation is that the alcohol-induced FOS activation in the EWcp is at least in part coordinated *via* a TRPA1 independent mechanisms by another alcohol-responsive brain area that innervates the urocortinergic cells of the EWcp (Ryabinin et al., 1997; da Silva et al., 2013).

While our FOS data do not unequivocally suggest the involvement of TRPA1 in the EWcp, decreased expression of *Trpa1* mRNA in WT mice following ethanol treatment offers additional support for this hypothesis. Indeed, it is widely accepted that an agonist can lead to the downregulation of its target (Finch et al., 2009). The fact that the expression of *Trpa1* mRNA was restricted to the UCN1-immunoreactive neurons in both groups, on one hand reaffirms our

previous finding that within the EWcp, exclusively urocortinergic neurons express the *Trpa1* (Kormos et al., 2022), on the other hand it proves that acute alcohol treatment does not induce the transcription of *Trpa1* mRNA in non-urocortinergic EWcp neurons.

The UCN1 peptide levels in the EWcp varied between the two genotypes following saline treatment, suggesting a basal genotypic difference. The WT mice exhibited significantly higher UCN1 content compared to *Trpa1* KO mice. The comparison of alterations in UCN1 peptide content in the EWcp following acute alcohol treatment unveiled contrasting trends, with a decrease in WT mice and an increase in *Trpa1* KO mice. This suggests that in WT mice, alcohol triggers the release of UCN1 from EWcp/UCN1 neurons, whereas, in *Trpa1* KO mice, the elevated UCN1 peptide content suggests an accumulation of the peptide, possibly due to diminished release. This was partially supported by RNAscope ISH results, which revealed a lower *Ucn1* mRNA expression in alcohol-treated *Trpa1* KO mice compared to their WT counterpart mice. This suggests that the accumulation of the UCN1 peptide was associated with reduced mRNA production as a consequence of a slower turnover (Gaszner et al., 2009). Our observations collectively suggest a potential role of TRPA1 signaling in both the storage and release of UCN1 peptide from EWcp/UCN1 neurons. Our earlier study also demonstrated that the absence of a functionally active TRPA1 had an impact on UCN1 content in the EWcp in mouse models of depression (Kormos et al., 2022) and posttraumatic stress disorder (Konkoly et al., 2022).

Both control and alcohol-treated *Trpa1* KO mice exhibited a lower *Cart* mRNA expression compared to the WTs. Since decreased *Cart* mRNA expression is associated with a lower alcohol preference (Giardino et al., 2017), we aimed to test if this pattern is a characteristic feature of *Trpa1* KO mice. Neither the *Cart* mRNA expression nor the CART peptide content of EWcp/UCN1 neurons showed any alteration following acute alcohol treatment across both genotypes. This suggests that acute alcohol exposure does not have a significant impact on EWcp/CART. However, considering the established role of CART in addiction (Vicentic & Jones, 2007; Ong & McNally, 2020; Zuniga & Ryabinin, 2020), we anticipate that a chronic alcohol exposure model could demonstrate its involvement in alcohol abuse.

Stimulation of TRPA1 on the membrane triggers calcium influx, leading to the activation of various intracellular pathways (Song et al., 2019). Our electrophysiological experiments confirmed that TRPA1 activation enhances the excitability and spontaneous firing rate of UCN1-expressing neurons, consequently elevating calcium levels. The elevated intracellular

calcium levels may induce the exocytosis of vesicles containing the neuropeptide. Additional investigations using pharmacological and electrophysiological tools are needed to ascertain the precise mechanism by which TRPA1 signaling influences the content and release of the UCN1 peptide. Given that the lack of TRPA1 influenced only the UCN1 and not CART content of EWcp neurons, despite their co-localization (Kozicz et al, 2003; Priest et al., 2023; Li & Ryabinin, 2022) which we also confirmed in our current study (Al-Omari et al., 2023), it becomes crucial to explore the mechanism underlying the UCN1-specific regulatory role of the TRPA1 channel.

Taking the involvement of EWcp/UCN1 in chronic alcohol consumption and addiction in consideration (Schreiber & Gilpin, 2018; Zuniga & Ryabinin, 2020), in our ongoing research, we are investigating the recruitment of EWcp/TRPA1/UCN1/CART neurons in mouse models of chronic alcohol abuse.

Limitations

When assessing our present results, some limitations have to be considered. None of the models for migraine can reliably mimic all aspects of human disease and the CGRP model is also not an exception. Although migraine is more prevalent in females (Rossi et al., 2022), we utilized male mice because a) EWcp/UCN1 neurons express estrogen receptor beta and estrous cycle-related hormonal fluctuations modulate UCN1 levels (Derks et al., 2007, 2010) and b) 0.1 mg/kg CGRP induced migraine-like symptoms in both male and female mice (Mason et al., 2017; Rea et al., 2018). Our fMRI study recruited male and female migraineurs only during the interictal period, thus the results do not reflect the brain status during the active headache episodes. This may explain the lack of significant difference in the functional connectivity of EW between the study groups. EW seed has not been described earlier (Skorobogatykh et al., 2019). In this study EW seed definition was carried out based on recent literature data (You & Park, 2023) and confirmed by the visual check of expert scientists.

Because, at the moment, no reliable TRPA1 receptor antibody is available, we are unable to support our morphological findings at protein level. In the acute alcohol administration study, because the functional TRPA1 receptor was deleted both in the periphery and the CNS in our global knockout mouse strain, we cannot exclude the possibility that peripheral or central compensatory mechanisms contributed to the alterations of the examined variables, observed in present study. The *in vivo* pharmacological manipulation on the TRPA1 receptor was also not possible due to the lack of information on the safety and pharmacokinetic profile of selective

TRPA1 agonists and antagonists. We did not examine alcohol-treated mice in our electrophysiological experiments, because we assume, that the effect of the alcohol is not TRPA1-selective (Pozos & Oakes, 1987; Crews et al., 1996).

6. Conclusions

In summary **(Figure 29.)**, we identified a direct urocortinergic projection arising from the EWcp to the STN. We also provided evidence on the expression of CGRP receptors in the EWcp and the activation of EWcp in a CGRP mouse model of migraine. Moreover, EWcp activation was associated with an increase in UCN1 peptide content and *Ucn1*, as well as *Trpa1* mRNA expression. The STN and DRN, recipients of the urocortinergic projection from EWcp, express CGRP receptors, as well as *Crh1r* and *Crh2r* mRNAs. Consequently, we propose that augmented central CGRP levels and increased release of UCN1 from EWcp urocortinergic neurons in response to CGRP may directly influence the function of the STN and DRN. Aligned with these findings, we also unveiled a significant positive functional connectivity between EW and STN as well as DRN in human subjects. As a conclusion, our findings strongly suggest a regulatory role of EWcp/UCN1 neurons in migraine with high translational value.

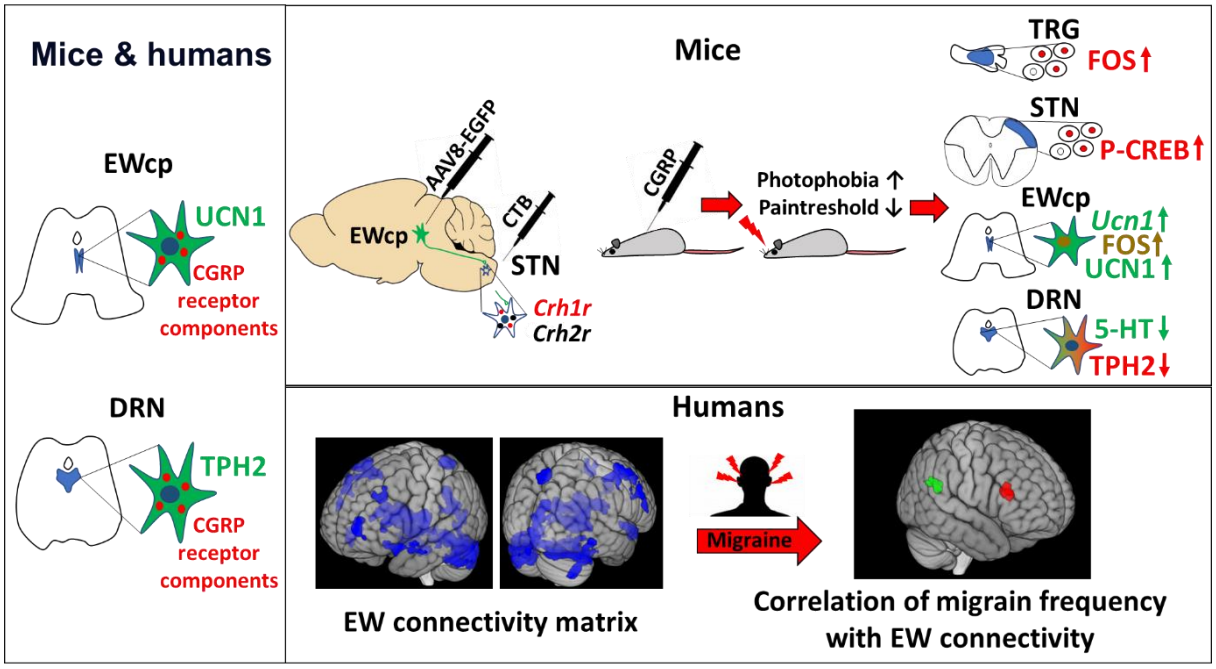

Figure 29. Graphical summary of our finding in the migraine studies.

In our second project on acute alcohol exposure **(Figure 30.)**, we proved the presence of *TRPA1* mRNA in human EWcp/UCN1 neurons, highlighting the translational relevance of our findings. We also proved the functional activity of TRPA1 ion channel in the EWcp of mice. We have shown that the EWcp urocortinergic neurons were activated in a mouse model of acute alcohol exposure, this activation was associated with reduced *Trpa1* mRNA expression and decreased UCN1 peptide content, suggesting the involvement of TRPA1 ion channels in the regulation of UCN1 storage and release, which could influence the alcohol consumption.

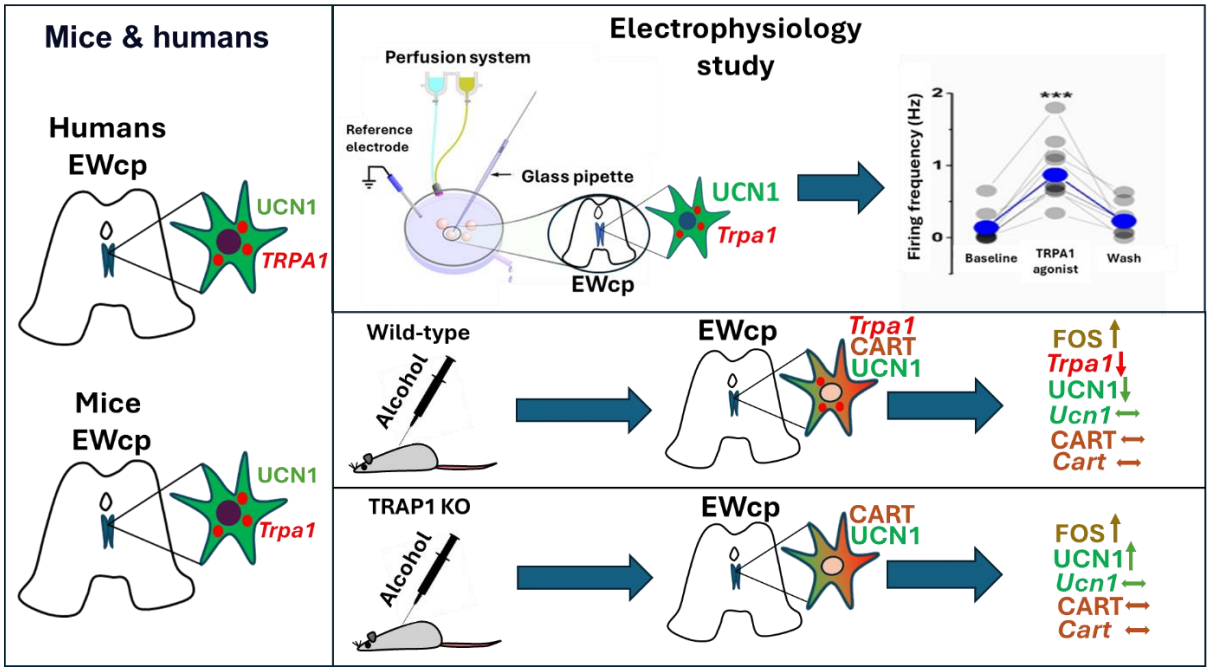

Figure 30. Graphical summary of our findings obtained in the studies on the contribution of TRPA1 to the response of EWcp peptidergic cells upon acute alcohol exposure.

7. Future plans

Considering the regulatory role of EWcp/UCN1 neurons in migraine, we aim to investigate the ability of antimigraine agents including monoclonal antibodies targeting circulating CGRP and its receptor elements, to reverse CGRP-induced behavioral and morphological changes in mouse EWcp.

Given the regulatory role of TRPA1 in the storage and release of UCN1 in the EWcp and taking into account our preliminary result suggesting a significant upregulation of *Trpa1* mRNA in response to CGRP treatment, we also plan to examine *Trpa1* KO mice in our CGRP mouse model of migraine to investigate the potential role of EWcp/TRPA1 ion channels in the neurobiology of migraine.

Since our experiments utilized global *Trpa1* KO mice, where the gene encoding TRPA1 is deleted since conception in all tissues, we plan to recruit conditional *Trpa1* KO mice, where the gene encoding TRPA1 is deleted specifically in the EWcp.

Given that the EWcp/UCN1/TRPA1 neurons were activated in mouse models of acute alcohol exposure and CGRP-induced migraine-like status moreover considering that alcohol and its metabolites to activate TRPA1, we plan to investigate the possible connection between hangover and migraine-induced headaches.

Finally, we also plan to investigate involvement of EWcp/TRPA1/UCN1/CART neurons in a mouse model of chronic alcohol consumption.

8. Summary of the new findings

- We proved the expression of CGRP receptor targets in the EWcp and DRN in mice and humans.
- We identified a direct urocortinergic projection arising from the EWcp to the STN.
- We demonstrated the expression of UCN1 receptors (CRH1R and CRH2R) in the I-III laminae of the STN dorsal horn.
- We showed behavioral and morphological evidences to support the validity of the CGRP mouse model of migraine.
- We proved the activation of the EWcp/UCN1 expressing neurons in the mouse CGRP model of migraine, with inceased UCN1 peptide content and *Ucn1*, as well as *Trpa1* mRNA expression in the EWcp, moreover, decreased 5-HT and TPH2 content in the DRN.
- We showed that the selective ablation of the EWcp/UCN1 neurons reduces the periorbital pain threshold.
- We provided evidence on a positive functional connectivity between the EWcp and the STN as well as the DRN in humans by fMRI.
- We proved the functional activity of TRPA1 ion channel in the mouse EWcp/UCN1 neurons by electrophysiological tools.
- We demonstrated the expression of *TRPA1* mRNA in human EWcp/UCN1 neurons.
- We showed the activation of EWcp/UCN1 expressing neurons in a mouse model of acute alcohol exposure with decreased *Trpa1* mRNA expression and UCN1 peptide content.

9. List of references

1. Akerman, S., Holland, P. R., & Hoffmann, J. (2013). Pearls and pitfalls in experimental in vivo models of migraine: Dural trigeminovascular nociception. *Cephalalgia*, *33*(8), 577–592. https://doi.org/10.1177/0333102412472071
2. Almeida, T. F., Roizenblatt, S., & Tufik, S. (2004). Afferent pain pathways: a neuroanatomical review. *Brain research*, *1000*(1-2), 40–56. https://doi.org/10.1016/j.brainres.2003.10.073
3. Al-Omari A, Kecskés M, Gaszner B, Biró-Sütő T, Fazekas B, Berta G, Kuzma M, Pintér E, Kormos V. Functionally active TRPA1 ion channel is downregulated in peptidergic neurons of the Edinger-Westphal nucleus upon acute alcohol exposure. Front Cell Dev Biol 2023;10:1046559.
4. And, I., & Biol, C. (2002). *The Role of Corticotropin-Releasing Factor Receptors in Stress and Anxiety 1* (Vol. 42). https://academic.oup.com/icb/article/42/3/552/723955
5. Andrè, E., Campi, B., Materazzi, S., Trevisani, M., Amadesi, S., Massi, D., Creminon, C., Vaksman, N., Nassini, R., Civelli, M., Baraldi, P. G., Poole, D. P., Bunnett, N. W., Geppetti, P., & Patacchini, R. (2008). Cigarette smoke–induced neurogenic inflammation is mediated by α,β-unsaturated aldehydes and the TRPA1 receptor in rodents. *Journal of Clinical Investigation*. https://doi.org/10.1172/JCI34886
6. Andrade R, Haj-Dahmane S. Serotonin neuron diversity in the dorsal raphe. ACS Chem Neurosci. 2013 Jan 16;4(1):22-5. doi: 10.1021/cn300224n. PMID: 23336040; PMCID: PMC3547477.
7. Asghar MS, Hansen AE, Amin FM, van der Geest RJ, Koning P van der, Larsson HBW, Olesen J, Ashina M. Evidence for a vascular factor in migraine. Ann Neurol 2011;69:635–645.
8. Ashina H, Schytz HW, Ashina M. CGRP in human models of migraine. Handbook of Experimental Pharmacology. Springer New York LLC, 2019, Vol. 255. pp. 109–120.
9. Ashina M, Hansen JM, á Dunga BO, Olesen J. Human models of migraine — short-term pain for long-term gain. Nat Rev Neurol 2017;13:713–724.
10. Ashina, Messoud, Zaza Katsarava, Thien Phu Do, Dawn C. Buse, Patricia Pozo-Rosich, Aynur Özge, Abouch v Krymchantowski, Elena R. Lebedeva, Krishnamurthy Ravishankar, Shengyuan Yu, Simona Sacco, Sait Ashina, Samaira Younis, Timothy J. Steiner, and Richard B. Lipton. 2021. "Migraine: Epidemiology and Systems of Care." *The Lancet* 397(10283):1485–95. doi: 10.1016/S0140-6736(20)32160-7.
11. Ashina, Messoud, Jakob Møller Hansen, Thien Phu Do, Agustin Melo-Carrillo, Rami Burstein, and Michael A. Moskowitz. 2019. "Migraine and the Trigeminovascular System—40 Years and Counting." *The Lancet Neurology* 18(8):795–804.
12. Avona, A., Burgos-Ega, C., Burton, M. D., Akopian, A. N., Price, T. J., & Dussor, G. (2019). Dural calcitonin gene-related peptide produces female-specific responses in rodent migraine models. *Journal of Neuroscience*, *39*(22), 4323–4331. https://doi.org/10.1523/JNEUROSCI.0364-19.2019
13. Avona, A., Mason, B. N., Lackovic, J., Wajahat, N., Motina, M., Quigley, L., Burgos-Vega, C., Moldovan Loomis, C., Garcia-Martinez, L. F., Akopian, A. N., Price, T. J., & Dussor, G. (2020). Repetitive stress in mice causes migraine-like behaviors and calcitonin gene-

related peptide-dependent hyperalgesic priming to a migraine trigger. Pain, 161(11), 2539–2550. https://doi.org/10.1097/j.pain.0000000000001953
14. Bachtell, R. K., Wang, Y.-M., Freeman, P., Risinger, F. O., & Ryabinin, A. E. (1999). Alcohol drinking produces brain region-selective changes in expression of inducible transcription factors. In Brain Research (Vol. 847). www.elsevier.comrlocaterbres
15. Bachtell RK, Tsivkovskaia NO, Ryabinin AE. Strain differences in urocortin expression in the Edinger-Westphal nucleus and its relation to alcohol-induced hypothermia. Neuroscience. 2002;113(2):421-34. doi: 10.1016/s0306-4522(02)00174-4. PMID: 12127099.
16. Bachtell, R. K., Weitemier, A. Z., Galvan-Rosas, A., Tsivkovskaia, N. O., Risinger, F. O., Phillips, T. J., Grahame, N. J., & Ryabinin, A. E. (2003). The Edinger-Westphal-Lateral Septum Urocortin Pathway and Its Relationship to Alcohol Consumption.
17. Bachtell, R. K., Weitemier, A. Z., & Ryabinin, A. E. (2004). Lesions of the Edinger-Westphal nucleus in C57BL/6J mice disrupt ethanol-induced hypothermia and ethanol consumption. European Journal of Neuroscience, 20(6), 1613–1623. https://doi.org/10.1111/j.1460-9568.2004.03594.x
18. Bakhtazad, A., Vousooghi, N., Garmabi, B., & Zarrindast, M. R. (2016). CART peptide and opioid addiction: Expression changes in male rat brain. *Neuroscience*, *325*, 63–73. https://doi.org/10.1016/j.neuroscience.2016.02.071
19. Bale TL, Picetti R, Contarino A, Koob GF, Vale WW, Lee K-F. Mice Deficient for Both Corticotropin-Releasing Factor Receptor 1 (CRFR1) and CRFR2 Have an Impaired Stress Response and Display Sexually Dichotomous Anxiety-Like Behavior. J Neurosci. 2002;22(1):193-199.
20. Bang, S., Kim, K. Y., Yoo, S., Kim, Y. G., & Hwang, S. W. (2007). Transient receptor potential A1 mediates acetaldehyde-evoked pain sensation. European Journal of Neuroscience, 26(9), 2516–2523. https://doi.org/10.1111/j.1460-9568.2007.05882.x
21. Bartsch T. Increased responses in trigeminocervical nociceptive neurons to cervical input after stimulation of the dura mater. Brain 2003;126:1801–1813.
22. Bates EA, Nikai T, Brennan KC, Fu YH, Charles AC, Basbaum AI, Ptáček LJ, Ahn AH. Sumatriptan alleviates nitroglycerin-induced mechanical and thermal allodynia in mice. Cephalalgia 2010;30:170–178.
23. Bautista, D. M., Movahed, P., Hinman, A., Axelsson, H. E., Sterner, O., Högestätt, E. D., Julius, D., Jordt, S.-E., & Zygmunt, P. M. (2005). Pungent products from garlic activate the sensory ion channel TRPA1. *Proceedings of the National Academy of Sciences*, *102*(34), 12248–12252. https://doi.org/10.1073/pnas.0505356102
24. Benemei, Silvia, and Greg Dussor. 2019. "TRP Channels and Migraine: Recent Developments and New Therapeutic Opportunities." *Pharmaceuticals (Basel, Switzerland)* 12(2):54. doi: 10.3390/ph12020054.
25. Benemei, S., de Cesaris, F., Fusi, C., Rossi, E., Lupi, C., & Geppetti, P. (2013). TRPA1 and other TRP channels in migraine. *The Journal of Headache and Pain*, *14*(1), 71. https://doi.org/10.1186/1129-2377-14-71
26. Benemei S, De Logu F, Li Puma S, Marone IM, Coppi E, Ugolini F, Liedtke W, Pollastro F, Appendino G, Geppetti P, Materazzi S, Nassini R. The anti-migraine component of butterbur extracts, isopetasin, desensitizes peptidergic nociceptors by acting on TRPA1 cation channel. Br J Pharmacol 2017;174:2897–2911.

27. Bessac, B. F., Sivula, M., von Hehn, C. A., Escalera, J., Cohn, L., & Jordt, S.-E. (2008). TRPA1 is a major oxidant sensor in murine airway sensory neurons. *Journal of Clinical Investigation*, *118*(5), 1899–1910. https://doi.org/10.1172/JCI34192
28. Bhatt DK, Gupta S, Ploug KB, Jansen-Olesen I, Olesen J. MRNA distribution of CGRP and its receptor components in the trigeminovascular system and other pain related structures in rat brain, and effect of intracerebroventricular administration of CGRP on Fos expression in the TNC. Neurosci Lett 2014;559:99–104.
29. Bhatt DK, Ramachandran R, Christensen SL, Gupta S, Jansen-Olesen I, Olesen J. CGRP infusion in unanesthetized rats increases expression of c-Fos in the nucleus tractus solitarius and caudal ventrolateral medulla, but not in the trigeminal nucleus caudalis. Cephalalgia 2015;35:220–233.
30. Brain SD, Grant AD. Vascular Actions of Calcitonin Gene-Related Peptide and Adrenomedullin. Physiol Rev 2004;84:903–934.
31. Burch, R. (2019). Antidepressants for Preventive Treatment of Migraine. In *Current Treatment Options in Neurology* (Vol. 21, Issue 4). Current Science Inc. https://doi.org/10.1007/s11940-019-0557-2
32. Burgos-Vega, C. C., Quigley, L. D., Trevisan dos Santos, G., Yan, F., Asiedu, M., Jacobs, B., Motina, M., Safdar, N., Yousuf, H., Avona, A., Price, T. J., & Dussor, G. (2019). Non-invasive dural stimulation in mice: A novel preclinical model of migraine. *Cephalalgia*, *39*(1), 123–134. https://doi.org/10.1177/0333102418779557
33. Cahill, C. Majella, and Kieran C. Murphy. 2004. "Migraine: Another Headache for Psychiatrists?" *British Journal of Psychiatry* 185(SEPT.):191–93.
34. Cai J, Tong Q. Anatomy and Function of Ventral Tegmental Area Glutamate Neurons. Front Neural Circuits. 2022 May 20;16:867053. doi: 10.3389/fncir.2022.867053. PMID: 35669454; PMCID: PMC9164627.
35. Cederbaum, A. I. (2012). Alcohol Metabolism. In Clinics in Liver Disease (Vol. 16, Issue 4, pp. 667–685). https://doi.org/10.1016/j.cld.2012.08.002
36. Cernuda-Morollon, E., Larrosa, D., Ramon, C., Vega, J., Martinez-Camblor, P., & Pascual, J. (2013). Interictal increase of CGRP levels in peripheral blood as a biomarker for chronic migraine. *Neurology*, *81*(14), 1191–1196. https://doi.org/10.1212/WNL.0b013e3182a6cb72
37. Chalmers, D. T., Lovenberg, T. W., & De Souza, E. B. (1995). Localization of novel corticotropin-releasing factor receptor (CRF2) mRNA expression to specific subcortical nuclei in rat brain: comparison with CRF1 receptor mRNA expression. The Journal of neuroscience : the official journal of the Society for Neuroscience, 15(10), 6340–6350.
38. Courteau, J. P., Cushman, R., Bouchard, F., Quevillon, M., Chartrand, A., & Bherer, L. (1994). Survey of construction workers repeatedly exposed to chlorine over a three to six month period in a pulpmill: I. Exposure and symptomatology. *Occupational and Environmental Medicine*, *51*(4), 219–224. https://doi.org/10.1136/oem.51.4.219
39. Crews, F. T., Morrow, A. L., Criswell, H., and Breese, G. (1996). Effects of ethanol on ion channels. Int. Rev. Neurobiol. 39, 283–367. PMID: 8894851. doi:10.1016/s0074-7742(08)60670-4
40. Cutrer, Michael F., and Jerry W. Swanson. 2022. "Pathophysiology, Clinical Manifestations, and Diagnosis of Migraine in Adults." in *UpToDate*.

41. da Silva, A. V. et al. (2013) 'The Edinger-Westphal nucleus II: Hypothalamic afferents in the rat', Journal of Chemical Neuroanatomy, 54, pp. 5–19. doi: 10.1016/j.jchemneu.2013.04.001.
42. Danesh, A., & Gottschalk, P. C. H. (2019). Beta-Blockers for Migraine Prevention: a Review Article. In *Current Treatment Options in Neurology* (Vol. 21, Issue 4). Current Science Inc. https://doi.org/10.1007/s11940-019-0556-3
43. de Vries T, MaassenVanDenBrink A. CGRP-targeted antibodies in difficult-to-treat migraine. Nat Rev Neurol 2019;15:688–689.
44. De Logu, F., Puma, S. L., Landini, L., Portelli, F., Innocenti, A., De Araujo, D. S. M., Janal, M. N., Patacchini, R., Bunnett, N. W., Geppetti, P., & Nassini, R. (2019). Schwann cells expressing nociceptive channel TRPA1 orchestrate ethanol-evoked neuropathic pain in mice. *Journal of Clinical Investigation*, *129*(12), 5424–5441. https://doi.org/10.1172/JCI128022
45. De Souza EB, Insel TR, Perrin MH, Rivier J, Vale WW, And Q, Kuhar MJ. Corticotropin-releasing Factor Receptors Are Widely Distributed within the Rat Central Nervous System: an autoradiographic study. J Neurosci. 1985;5(12):3189-3203.
46. Deen M, Hansen HD, Hougaard A, Nørgaard M, Eiberg H, Lehel S, Ashina M, Knudsen GM. High brain serotonin levels in migraine between attacks: A 5-HT4 receptor binding PET study. Neuroimage Clin 2018;18:97–102.
47. Derks, N. M., Gaszner, B., Roubos, E. W., & Kozicz, L. T. (2010). Sex differences in urocortin 1 dynamics in the non-preganglionic Edinger-Westphal nucleus of the rat. Neuroscience Research, 66(1), 117–123. https://doi.org/10.1016/j.neures.2009.10.003
48. Derks NM, Roubos EW, Kozicz T. Presence of estrogen receptor β in urocortin 1-neurons in the mouse non-preganglionic Edinger-Westphal nucleus. Gen Comp Endocrinol 2007;153:228–234.
49. Dickerson IM. Role of CGRP-receptor component protein (RCP) in CLR/RAMP function. Curr Protein Pept Sci. 2013;14(5):407-415. doi:10.2174/13892037113149990057
50. Diener, H. C., Förderreuther, S., Gaul, C., Giese, F., Hamann, T., Holle-Lee, D., Jürgens, T. P., Kamm, K., Kraya, T., Lampl, C., May, A., Reuter, U., Scheffler, A., & Tfelt-Hansen, P. (2020). Prevention of migraine with monoclonal antibodies against CGRP or the CGRP receptor. In *Neurological Research and Practice* (Vol. 2, Issue 1). BioMed Central Ltd. https://doi.org/10.1186/s42466-020-00057-1
51. Diener, H. C., Tassorelli, C., Dodick, D. W., Silberstein, S. D., Lipton, R. B., Ashina, M., Becker, W. J., Ferrari, M. D., Goadsby, P. J., Pozo-Rosich, P., Wang, S. J., & Mandrekar, J. (2019). Guidelines of the International Headache Society for controlled trials of acute treatment of migraine attacks in adults: Fourth edition. *Cephalalgia*, *39*(6), 687–710. https://doi.org/10.1177/0333102419828967
52. Ding SL, Royall JJ, Sunkin SM, Ng L, Facer BAC, Lesnar P, Guillozet-Bongaarts A, McMurray B, Szafer A, Dolbeare TA, Stevens A, Tirrell L, Benner T, Caldejon S, Dalley RA, Dee N, Lau C, Nyhus J, Reding M, Riley ZL, Sandman D, Shen E, van der Kouwe A, Varjabedian A, Write M, Zollei L, Dang C, Knowles JA, Koch C, Phillips JW, Sestan N, Wohnoutka P, Zielke HR, Hohmann JG, Jones AR, Bernard A, Hawrylycz MJ, Hof PR, Fischl B, Lein ES. Comprehensive cellular-resolution atlas of the adult human brain. Journal of Comparative Neurology 2016;524:3127–3481.

53. Donner NC, Mani S, Fitz SD, Kienzle DM, Shekhar A, Lowry CA. Crh receptor priming in the bed nucleus of the stria terminalis induces tph2 gene expression in the dorsomedial dorsal raphe nucleus and chronic anxiety HHS Public Access. Prog Neuropsychopharmacol Biol Psychiatry 2020;96:109730.
54. Dos Santos Júnior ED, Da Silva A V., Da Silva KRT, Haemmerle CAS, Batagello DS, Da Silva JM, Lima LB, Da Silva RJ, Diniz GB, Sita L V., Elias CF, Bittencourt JC. The centrally projecting Edinger-Westphal nucleus-I: Efferents in the rat brain. J Chem Neuroanat 2015;68:22–38.
55. Drummond PD. Tryptophan depletion increases nausea, headache and photophobia in migraine sufferers. Cephalalgia. 2006;26(10):1225-1233.
56. Dubowchik, G. M., Conway, C. M., & Xin, A. W. (2020). Blocking the CGRP Pathway for Acute and Preventive Treatment of Migraine: The Evolution of Success. *Journal of Medicinal Chemistry*, *63*(13), 6600–6623. https://doi.org/10.1021/acs.jmedchem.9b01810
57. Durham PL. Diverse Physiological Roles of Calcitonin Gene-Related Peptide in Migraine Pathology: Modulation of Neuronal-Glial-Immune Cells to Promote Peripheral and Central Sensitization. Curr Pain Headache Rep. 2016;20(8):48.
58. Edlow BL, Takahashi E, Wu O, Benner T, Dai G, Bu L, Grant PE, Greer DM, Greenberg SM, Kinney HC, Folkerth RD. Neuroanatomic connectivity of the human ascending arousal system critical to consciousness and its disorders. J Neuropathol Exp Neurol 2012;71:531–546.
59. Edvinsson, J. C. A., Viganò, A., Alekseeva, A., Alieva, E., Arruda, R., De Luca, C., D'Ettore, N., Frattale, I., Kurnukhina, M., Macerola, N., Malenkova, E., Maiorova, M., Novikova, A., Řehulka, P., Rapaccini, V., Roshchina, O., Vanderschueren, G., Zvaune, L., Andreou, A. P., Haanes, K. A., … European Headache Federation School of Advanced Studies (EHF-SAS) (2020). The fifth cranial nerve in headaches. *The journal of headache and pain*, *21*(1), 65. https://doi.org/10.1186/s10194-020-01134-1
60. Edvinsson, L., Nilsson, E., & Jansen-Olesen, I. (2007). Inhibitory effect of BIBN4096BS, CGRP $_{8-37}$, a CGRP antibody and an RNA-Spiegelmer on CGRP induced vasodilatation in the perfused and non-perfused rat middle cerebral artery. *British Journal of Pharmacology*, *150*(5), 633–640. https://doi.org/10.1038/sj.bjp.0707134
61. Edvinsson L. CGRP receptor antagonists and antibodies against CGRP and its receptor in migraine treatment. Br J Clin Pharmacol 2015;80:193–199.
62. Edvinsson L, Grell AS, Warfvinge K. Expression of the CGRP Family of Neuropeptides and their Receptors in the Trigeminal Ganglion. Journal of Molecular Neuroscience 2020;70:930–944.
63. Elias, C. F., Lee, C. E., Kelly, J. F., Ahima, R. S., Kuhar, M., Saper, C. B., & Elmquist, J. K. (2001). Characterization of CART Neurons in the Rat and Human Hypothalamus THE JOURNAL OF COMPARATIVE NEUROLOGY 432:1-19 (2001). In J. Comp. Neurol (Vol. 432).
64. Eriksson CJ. The role of acetaldehyde in the actions of alcohol (update 2000). Alcohol Clin Exp Res. 2001 May;25(5 Suppl ISBRA):15S-32S. doi: 10.1097/00000374-200105051-00005. PMID: 11391045.Farzi, A. et al. (2018) 'Arcuate nucleus and lateral hypothalamic cart neurons in the mouse brain exert opposing effects on energy expenditure', eLife, 7, pp. 1–27. doi: 10.7554/eLife.36494.

65. Ernstsen, C., Christensen, S. L., Rasmussen, R. H., Nielsen, B. S., Jansen-Olesen, I., Olesen, J., & Kristensen, D. M. (2022). The PACAP pathway is independent of CGRP in mouse models of migraine: Possible new drug target? *Brain*, *145*(7), 2450–2460. https://doi.org/10.1093/brain/awac040
66. Farkas S, Bölcskei K, Markovics A, Varga A, Kis-Varga Á, Kormos V, Gaszner B, Horváth C, Tuka B, Tajti J, Helyes Z. Utility of different outcome measures for the nitroglycerin model of migraine in mice. J Pharmacol Toxicol Methods 2016;77:33–44.
67. Fehér M, Márton Z, Szabó Á, Kocsa J, Kormos V, Hunyady Á, Kovács LÁ, Ujvári B, Berta G, Farkas J, Füredi N, Gaszner T, Pytel B, Reglődi D, Gaszner B. Downregulation of PACAP and the PAC1 Receptor in the Basal Ganglia, Substantia Nigra and Centrally Projecting Edinger–Westphal Nucleus in the Rotenone model of Parkinson's Disease. Int J Mol Sci 2023;24 (14), 11843.
68. Fekete ÉM, Inoue K, Zhao Y, Rivier JE, Vale WW, Szücs A, Koob GF, Zorrilla EP. Delayed satiety-like actions and altered feeding microstructure by a selective type 2 corticotropin-releasing factor agonist in rats: Intra-hypothalamic urocortin 3 administration reduces food intake by prolonging the post-meal interval. Neuropsychopharmacology 2007;32:1052–1068.
69. Ferraguti G, Pascale E, Lucarelli M. Alcohol addiction: a molecular biology perspective. Curr Med Chem. 2015;22(6):670-84. doi:10.2174/0929867321666141229103158. PMID: 25544474.
70. Fila M, Pawlowska E, Szczepanska J, Blasiak J. Epigenetic Connections of the TRPA1 Ion Channel in Pain Transmission and Neurogenic Inflammation - a Therapeutic Perspective in Migraine? Mol Neurobiol. 2023 Oct;60(10):5578-5591. doi: 10.1007/s12035-023-03428-2. Epub 2023 Jun 16. PMID: 37326902; PMCID: PMC10471718.
71. Finch, A. R. et al. (2009) 'Agonist-induced internalization and downregulation of gonadotropin- releasing hormone receptors', American Journal of Physiology - Cell Physiology, 297(3), pp. 591–601. doi: 10.1152/ajpcell.00166.2009.
72. Fonareva, I., Spangler, E., Cannella, N., Sabino, V., Cottone, P., Ciccocioppo, R., Zorrilla, E. P., & Ryabinin, A. E. (2009). Increased perioculomotor urocortin 1 immunoreactivity in genetically selected alcohol preferring rats. Alcoholism: Clinical and Experimental Research, 33(11), 1956–1965. https://doi.org/10.1111/j.1530-0277.2009.01033.x
73. Fox JH, Lowry CA. Corticotropin-releasing factor-related peptides, serotonergic systems, and emotional behavior. Front Neurosci. 2013;7:169.
74. Fujita, F., Uchida, K., Moriyama, T., Shima, A., Shibasaki, K., Inada, H., Sokabe, T., & Tominaga, M. (2008). Intracellular alkalization causes pain sensation through activation of TRPA1 in mice. *Journal of Clinical Investigation*, *118*(12), 4049–4057. https://doi.org/10.1172/JCI35957
75. Gaszner, B., Csernus, V., & Kozicz, T. (2004). Urocortinergic neurons respond in a differentiated manner to various acute stressors in the Edinger-Westphal nucleus in the rat. Journal of Comparative Neurology, 480(2), 170–179. https://doi.org/10.1002/cne.20343
76. Gaszner, B., Kormos, V., Kozicz, T., Hashimoto, H., Reglodi, D., & Helyes, Z. (2012). The behavioral phenotype of pituitary adenylate-cyclase activating polypeptide-deficient mice in anxiety and depression tests is accompanied by blunted c-Fos expression in the bed

nucleus of the stria terminalis, central projecting Edinger-Westphal nucleu. Neuroscience, 202, 283–299. https://doi.org/10.1016/j.neuroscience.2011.11.046
77. Gaszner, B., van Wijk, D. C. W. A., Korosi, A., Józsa, R., Roubos, E. W., & Kozicz, T. (2009). Diurnal expression of period 2 and urocortin 1 in neurones of the non-preganglionic Edinger-Westphal nucleus in the rat. Stress, 12(2), 115–124. https://doi.org/10.1080/10253890802057221
78. Gecse K, Dobos D, Aranyi CS, Galambos A, Baksa D, Kocsel N, Szabó E, Pap D, Virág D, Ludányi K, Kökönyei G, Emri M, Bagdy G, Juhasz G. Association of plasma tryptophan concentration with periaqueductal gray matter functional connectivity in migraine patients. Sci Rep 2022;12(1), 739.
79. Giardino, W. J., Rodriguez, E. D., Smith, M. L., Ford, M. M., Galili, D., Mitchell, S. H., Chen, A., & Ryabinin, A. E. (2017). Control of chronic excessive alcohol drinking by genetic manipulation of the Edinger-Westphal nucleus urocortin-1 neuropeptide system. Translational Psychiatry, 7(1). https://doi.org/10.1038/tp.2016.293
80. Goadsby, Peter J. 2018. "Migraine and Other Primary Headache Disorders." in *Harrison's Principles of Internal Medicine, 20e*, edited by J. L. Jameson, A. S. Fauci, D. L. Kasper, S. L. Hauser, D. L. Longo, and J. Loscalzo. New York, NY: McGraw-Hill Education
81. Goadsby PJ, Edvinsson L. The trigeminovascular system and migraine: Studies characterizing cerebrovascular and neuropeptide changes seen in humans and cats. Ann Neurol 1993;33:48–56.
82. Goadsby PJ, Edvinsson L, Ekman R. Vasoactive peptide release in the extracerebral circulation of humans during migraine headache. Ann Neurol 1990;28:183–187.
83. Haanes, Kristian Agmund, and Lars Edvinsson. 2019. "Pathophysiological Mechanisms in Migraine and the Identification of New Therapeutic Targets." *CNS Drugs* 33(6):525–37. doi: 10.1007/s40263-019-00630-6.
84. Hargreaves, R., & Olesen, J. (2019). Calcitonin Gene-Related Peptide Modulators – The History and Renaissance of a New Migraine Drug Class. *Headache: The Journal of Head and Face Pain*, *59*(6), 951–970. https://doi.org/10.1111/head.13510
85. Harriott, A. M., & Gold, M. S. (2009). Electrophysiological properties of dural afferents in the absence and presence of inflammatory mediators. *Journal of Neurophysiology*, *101*(6), 3126–3134. https://doi.org/10.1152/jn.91339.2008
86. Harriott, A. M., Scheff, N. N., & Gold, M. S. (2012). The complex actions of sumatriptan on rat dural afferents. *Cephalalgia*, *32*(10), 738–749. https://doi.org/10.1177/0333102412451356
87. Harriott, A. M., Takizawa, T., Chung, D. Y., & Chen, S. P. (2019). Spreading depression as a preclinical model of migraine. In *Journal of Headache and Pain* (Vol. 20, Issue 1). BioMed Central Ltd. https://doi.org/10.1186/s10194-019-1001-4
88. Harriott AM, Strother LC, Vila-Pueyo M, Holland PR. Animal models of migraine and experimental techniques used to examine trigeminal sensory processing. Journal of Headache and Pain 2019;20(1):91.
89. Henson B, Hollingsworth H, Nevois E, Herndon C. Calcitonin Gene-Related Peptide (CGRP) Antagonists and Their Use in Migraines. J Pain Palliat Care Pharmacother 2020;34:22–31.

90. Huang D, Grady FS, Peltekian L, Laing JJ, Geerling JC. Efferent projections of CGRP/Calca-expressing parabrachial neurons in mice. Journal of Comparative Neurology 2021;529:2911–2957.
91. Huang KW, Ochandarena NE, Philson AC, Hyun M, Birnbaum JE, Cicconet M, Sabatini BL. Molecular and anatomical organization of the dorsal raphe nucleus. Elife. 2019 Aug 14;8:e46464. doi: 10.7554/eLife.46464. PMID: 31411560; PMCID: PMC6726424.
92. Iannone LF, Nassini R, Patacchini R, Geppetti P, De Logu F. Neuronal and non-neuronal TRPA1 as therapeutic targets for pain and headache relief. Temperature (Austin). 2022 May 29;10(1):50-66. doi: 10.1080/23328940.2022.2075218. PMID: 37187829; PMCID: PMC10177743.
93. Iannone LF, De Logu F, Geppetti P, De Cesaris F. The role of TRP ion channels in migraine and headache. Neurosci Lett. 2022 Jan 18;768:136380. doi: 10.1016/j.neulet.2021.136380. Epub 2021 Nov 30. PMID: 34861342.
94. Ilhan MN, Yapar D. Alcohol consumption and alcohol policy. Turk J Med Sci. 2020 Aug 26;50(5):1197-1202. doi: 10.3906/sag-2002-237. PMID: 32421277; PMCID: PMC7491269.
95. Im E. Multi-facets of corticotropin-releasing factor in modulating inflammation and angiogenesis. J Neurogastroenterol Motil 2015;21:25–32.
96. Irlbacher, K., & Meyer, B. (2002). Nasally triggered headache. *Neurology*, *58*(2), 294–294. https://doi.org/10.1212/WNL.58.2.294
97. Iyengar S, Johnson KW, Ossipov MH, Aurora SK. CGRP and the Trigeminal System in Migraine. Headache 2019;59:659–681.
98. Iyengar S, Ossipov MH, Johnson KW. The role of calcitonin gene-related peptide in peripheral and central pain mechanisms including migraine. Pain 2017;158:543–559.
99. Jannis, X., Meents, E., Ciotu, C. I., Michael, X., & Fischer, J. M. (2019). TRPA1: a molecular view. REVIEW Cellular and Molecular Properties of Neurons J Neurophysiol, 121, 427–443. https://doi.org/10.1152/jn.00524.2018.
100. Jia Z, Yu S. Grey matter alterations in migraine: A systematic review and meta-analysis. Neuroimage Clin 2017;14:130–140.
101. Jiang, Liwen, Dongqing Ma, Blair D. Grubb, and Minyan Wang. 2019. "ROS/TRPA1/CGRP Signaling Mediates Cortical Spreading Depression." *The Journal of Headache and Pain* 20(1):25. doi: 10.1186/s10194-019-0978-z.
102. Juhasz G, Zsombok T, Jakab B, Nemeth J, Szolcsanyi J, Bagdy G. Sumatriptan Causes Parallel Decrease in Plasma Calcitonin Gene-Related Peptide (CGRP) Concentration and Migraine Headache During Nitroglycerin Induced Migraine Attack. Cephalalgia 2005;25:179–183.
103. Julius, D. (2013). TRP channels and pain. *Annual review of cell and developmental biology*, *29*, 355-384.
104. Jung A, Huge A, Kuhlenbäumer G, Kempt S, Seehafer T, Evers S, Berger K, Marziniak M. Genetic TPH2 variants and the susceptibility for migraine: Association of a TPH2 haplotype with migraine without aura. J Neural Transm 2010;117:1253–1260.
105. Kaiser EA, Kuburas A, Recober A, Russo AF. Modulation of CGRP-induced light aversion in wild-type mice by a 5-HT1B/D agonist. Journal of Neuroscience 2012;32:15439–15449.

106. Kádková, A., Synytsya, V., Krusek, J., Zímová, L., & Vlachová, V. (2017). Molecular basis of TRPA1 regulation in nociceptive neurons. A review. In Physiological Research (Vol. 66, Issue 3, pp. 425–439). Czech Academy of Sciences. https://doi.org/10.33549/physiolres.933553
107. Kelman, L. (2007). The Triggers or Precipitants of the Acute Migraine Attack. *Cephalalgia*, *27*(5), 394–402. https://doi.org/10.1111/j.1468-2982.2007.01303.x
108. Kikkeri Shankar, Nidhi, and Shivaraj Nagalli. 2022. *Migraine with Aura*. Treasure Island (FL): StatPearls Publishing.
109. Kilkenny, C., Browne, W., Cuthill, I. C., Emerson, M., & Altman, D. G. (2010). Animal research: Reporting in vivo experiments: The ARRIVE guidelines. In *British Journal of Pharmacology* (Vol. 160, Issue 7, pp. 1577–1579). https://doi.org/10.1111/j.1476-5381.2010.00872.x
110. Kim S-J, Yeo J-H, Yoon S-Y, Kwon S-G, Lee J-H, Beitz AJ, Roh D-H. Differential Development of Facial and Hind Paw Allodynia in a Nitroglycerin-Induced Mouse Model of Chronic Migraine: Role of Capsaicin Sensitive Primary Afferents. Biological & pharmaceutical bulletin 2018; 41(2), 172–181.
111. Komatsu, T., Uchida, K., Fujita, F., Zhou, Y., & Tominaga, M. (2012). Primary alcohols activate human TRPA1 channel in a carbon chain length-dependent manner. Pflugers Archiv European Journal of Physiology, 463(4), 549–559. https://doi.org/10.1007/s00424-011-1069-4
112. Konkoly, J., Kormos, V., Gaszner, B., Correia, P., Berta, G., Biró-Sütő, T., Zelena, D., & Pintér, E. (2022). Transient receptor potential ankyrin 1 ion channel expressed by the Edinger-Westphal nucleus contributes to stress adaptation in murine model of posttraumatic stress disorder. *Frontiers in Cell and Developmental Biology*, *10*. https://doi.org/10.3389/fcell.2022.1059073
113. Kormos, V., & Gaszner, B. (2013). Role of neuropeptides in anxiety, stress, and depression: From animals to humans. In Neuropeptides (Vol. 47, Issue 6, pp. 401–419). https://doi.org/10.1016/j.npep.2013.10.014
114. Kormos, V., Kecskés, A., Farkas, J., Gaszner, T., Csernus, V., Alomari, A., Hegedüs, D., Renner, É., Palkovits, M., Zelena, D., Helyes, Z., Pintér, E., & Gaszner, B. (2022). Peptidergic neurons of the Edinger-Westphal nucleus express TRPA1 ion channel that is downregulated both upon chronic variable mild stress in male mice and in humans who died by suicide. Journal of Psychiatry & Neuroscience : JPN, 47(3), E162–E175. https://doi.org/10.1503/jpn.210187
115. Kozicz, T. (2003). Neurons colocalizing urocortin and cocaine and amphetamine-regulated transcript immunoreactivities are induced by acute lipopolysaccharide stress in the Edinger-Westphal nucleus in the rat. Neuroscience, 116(2), 315–320. https://doi.org/10.1016/S0306-4522(02)00772-8
116. Kozicz T. On the role of urocortin 1 in the non-preganglionic Edinger-Westphal nucleus in stress adaptation. Gen Comp Endocrinol 2007;153:235–240.
117. Kozicz, T., Bittencourt, J. C., May, P. J., Reiner, A., Gamlin, P. D. R., Palkovits, M., Horn, A. K. E., Toledo, C. A. B., & Ryabinin, A. E. (2011). The Edinger-Westphal nucleus: A historical, structural, and functional perspective on a dichotomous terminology. In Journal of Comparative Neurology (Vol. 519, Issue 8, pp. 1413–1434). https://doi.org/10.1002/cne.22580

118. Kozicz T, Li M, Arimura A. The activation of urocortin immunoreactive neurons in the Edinger-Westphal nucleus following acute pain stress in rats. Stress 2001;4:85–90.
119. Kristensen, P., Judge, M. E., Thim, L., Ribel, U., Christjansen, K. N., Wulff, B. S., Clausen, J. T., Jensen, P. B., Madsen, O. D., Vrang, N., Larsen, P. J., & Hastrup, S. (1998). Hypothalamic CART is a new anorectic peptide regulated by leptin. Nature 1998 393:6680, 393(6680), 72–76. https://doi.org/10.1038/29993.
120. Knyihar-Csillik, E., Tajti, J., Mohtasham, S., Sari, G., & Vecsei, L. (1995). NIUNH [Electrical stimulation of the Gasserian ganglion induces structural alterations of calcitonin gene-related peptide-immunoreactive perivascular sensory nerve terminals in the rat cerebral dura mater: a possible model of migraine headache. In *ELS EVHER Neuroscience Letters* (Vol. 184).
121. Knyihár-Csillik, E., Tajti, J., Samsam, M., Sáry, G., Slezák, S., & Vécsei, L. (1997). Effect of a serotonin agonist (sumatriptan) on the peptidergic innervation of the rat cerebral dura mater and on the expression of c-fos in the caudal trigeminal nucleus in an experimental migraine model. *Journal of neuroscience research*, *48*(5), 449–464.
122. Kuburas, A., & Russo, A. F. (2023). Shared and independent roles of CGRP and PACAP in migraine pathophysiology. In *Journal of Headache and Pain* (Vol. 24, Issue 1). BioMed Central Ltd. https://doi.org/10.1186/s10194-023-01569-2
123. Kuhar, M. J. (2016). CART peptides and drugs of abuse: A review of recent progress. In *Journal of Drug and Alcohol Research* (Vol. 2016, Issue 5). Ashdin Publishing. https://doi.org/10.4303/jdar/235984
124. Landini, L., Souza Monteiro de Araujo, D., Chieca, M., De Siena, G., Bellantoni, E., Geppetti, P., Nassini, R., & De Logu, F. (2023). Acetaldehyde via CGRP receptor and TRPA1 in Schwann cells mediates ethanol-evoked periorbital mechanical allodynia in mice: relevance for migraine. *Journal of Biomedical Science*, *30*(1). https://doi.org/10.1186/s12929-023-00922-6
125. Lassen LH, Haderslev PA, Jacobsen VB, Iversen HK, Sperling B, Olesen J. CGRP may play a causative role in migraine. Cephalalgia. 2002;22(1):54-61.
126. Lau, J. et al. (2018) 'CART neurons in the arcuate nucleus and lateral hypothalamic area exert differential controls on energy homeostasis', Molecular Metabolism, 7(November 2017), pp. 102–118. doi: 10.1016/j.molmet.2017.10.015.
127. Li, J., & Ryabinin, A. E. (2022). Oxytocin Receptors in the Mouse Centrally-projecting Edinger-Westphal Nucleus and their Potential Functional Significance for Thermoregulation. Neuroscience, 498, 93–104. https://doi.org/10.1016/J.NEUROSCIENCE.2022.07.002.
128. Li YQ, Takada M, Matsuzaki S, Shinonaga Y, Mizuno N. Identification of periaqueductal gray and dorsal raphe nucleus neurons projecting to both the trigeminal sensory complex and forebrain structures: a fluorescent retrograde double-labeling study in the rat. Brain Res. 1993 Oct 1;623(2):267-77. doi: 10.1016/0006-8993(93)91437-w. PMID: 8221108.
129. Lipton, Richard B., and Marcelo E. Bigal. 2005. "Migraine: Epidemiology, Impact, and Risk Factors for Progression." *Headache* 45(SUPPL. 1).
130. Liu, Z., Lin, R., & Luo, M. (2020). Reward Contributions to Serotonergic Functions. *Annual review of neuroscience*, *43*, 141–162. https://doi.org/10.1146/annurev-neuro-093019-112252

131. Lukács, M., Warfvinge, K., Tajti, J., Fülöp, F., Toldi, J., Vécsei, L., & Edvinsson, L. (2017). Topical dura mater application of CFA induces enhanced expression of c-fos and glutamate in rat trigeminal nucleus caudalis: attenuated by KYNA derivate (SZR72). *Journal of Headache and Pain*, *18*(1). https://doi.org/10.1186/s10194-017-0746-x
132. Lukkes JL, Staub DR, Dietrich A, Truitt W, Neufeld-Cohen A, Chen A, Johnson PL, Shekhar A, Lowry CA. Topographical distribution of corticotropin-releasing factor type 2 receptor-like immunoreactivity in the rat dorsal raphe nucleus: Co-localization with tryptophan hydroxylase. Neuroscience 2011;183:47–63.
133. Ma W, Chabot JG, Powell KJ, Jhamandas K, Dickerson IM, Quirion R. Localization and modulation of calcitonin gene-related peptide-receptor component protein-immunoreactive cells in the rat central and peripheral nervous systems. Neuroscience 2003;120:677–694.
134. Maciewicz R, Phipps BS, Foote WE, Aronin N, DiFiglia M. The distribution of substance P-containing neurons in the cat Edinger-Westphal nucleus: relationship to efferent projection systems. Brain Res. 1983;270(2):217-230.
135. Maniyar, F. H., Sprenger, T., Monteith, T., Schankin, C., & Goadsby, P. J. (2014). Brain activations in the premonitory phase of nitroglycerin-triggered migraine attacks. *Brain*, *137*(1), 232–241. https://doi.org/10.1093/brain/awt320
136. Markovics A, Kormos V, Gaszner B, Lashgarara A, Szoke E, Sandor K, Szabadfi K, Tuka B, Tajti J, Szolcsanyi J, Pinter E, Hashimoto H, Kun J, Reglodi D, Helyes Z. Pituitary adenylate cyclase-activating polypeptide plays a key role in nitroglycerol-induced trigeminovascular activation in mice. Neurobiol Dis 2012;45:633–644.
137. Marziniak M, Kienzler C, Kuhlenbäumer G, Sommer C, Mössner R. Functional gene variants of the serotonin-synthesizing enzyme tryptophan hydroxylase 2 in migraine. J Neural Transm 2009;116:815–819.
138. Mason BN, Kaiser EA, Kuburas A, Loomis MCM, Latham JA, Garcia-Martinez LF, Russo AF. Induction of migraine-like photophobic behavior in mice by both peripheral and central CGRP mechanisms. Journal of Neuroscience 2017;37:204–216.
139. Mason BN, Wattiez AS, Balcziak LK, Kuburas A, Kutschke WJ, Russo AF. Vascular actions of peripheral CGRP in migraine-like photophobia in mice. Cephalalgia 2020;40:1585–1604.
140. Masood T, Lakatos S, Rosta J. Modification of the TRP Channel TRPA1 as a Relevant Factor in Migraine-Related Intracranial Hypersensitivity. Int J Mol Sci. 2023 Mar 11;24(6):5375. doi: 10.3390/ijms24065375. PMID: 36982450; PMCID: PMC10049246.
141. Materazzi, S., Benemei, S., Fusi, C., Gualdani, R., de Siena, G., Vastani, N., Andersson, D. A., Trevisan, G., Moncelli, M. R., Wei, X., Dussor, G., Pollastro, F., Patacchini, R., Appendino, G., Geppetti, P., & Nassini, R. (2013). Parthenolide inhibits nociception and neurogenic vasodilatation in the trigeminovascular system by targeting the TRPA1 channel. *Pain*, *154*(12), 2750–2758. https://doi.org/10.1016/j.pain.2013.08.002
142. McLatchie, L. M., Fraser, N. J., Main, M. J., Wise, A., Brown, J., Thompson, N., Solari, R., Lee, M. G., & Foord, S. M. (1998). RAMPs regulate the transport and ligand specificity of the calcitonin-receptor-like receptor. *Nature*, *393*(6683), 333–339. https://doi.org/10.1038/30666
143. McNamara, C. R., Mandel-Brehm, J., Bautista, D. M., Siemens, J., Deranian, K. L., Zhao, M., Hayward, N. J., Chong, J. A., Julius, D., Moran, M. M., & Fanger, C. M. (2007).

TRPA1 mediates formalin-induced pain. *Proceedings of the National Academy of Sciences*, *104*(33), 13525–13530. https://doi.org/10.1073/pnas.0705924104

144. Miller, S., Liu, H., Warfvinge, K., Shi, L., Dovlatyan, M., Xu, C., & Edvinsson, L. (2016). Immunohistochemical localization of the calcitonin gene-related peptide binding site in the primate trigeminovascular system using functional antagonist antibodies. Neuroscience, 328, 165–183. https://doi.org/10.1016/j.neuroscience.2016.04.046
145. Napadow V, Sclocco R, Henderson LA. Brainstem neuroimaging of nociception and pain circuitries. Pain Rep. 2019;4(4):e745.
146. Negro, A., & Martelletti, P. (2019). Gepants for the treatment of migraine. *Expert Opinion on Investigational Drugs*, *28*(6), 555–567. https://doi.org/10.1080/13543784.2019.1618830
147. Olesen J, Diener H-C, Husstedt IW, Goadsby PJ, Hall D, Meier U, Pollentier S, Lesko LM. Calcitonin Gene–Related Peptide Receptor Antagonist BIBN 4096 BS for the Acute Treatment of Migraine. New England Journal of Medicine 2004;350:1104–1110.
148. Olesen J. Headache Classification Committee of the International Headache Society (IHS) The International Classification of Headache Disorders, 3rd edition. Cephalalgia 2018;38:1–211.
149. Ong WY, Stohler CS, Herr DR. Role of the Prefrontal Cortex in Pain Processing. Mol Neurobiol 2019;56:1137–1166.
150. Ong, Z. Y. and McNally, G. P. (2020) 'CART in energy balance and drug addiction: Current insights and mechanisms', Brain research, 1740(April), p. 146852. doi: 10.1016/j.brainres.2020.146852.
151. Oshinsky, M. L., & Gomonchareonsiri, S. (2007). Episodic dural stimulation in awake rats: A model for recurrent headache. *Headache*, *47*(7), 1026–1036. https://doi.org/10.1111/j.1526-4610.2007.00871.x
152. Ozburn, A. R., Larson, E. B., Self, D. W., & McClung, C. A. (2012). Cocaine self-administration behaviors in ClockΔ19 mice. Psychopharmacology, 223(2), 169–177. https://doi.org/10.1007/s00213-012-2704-2
153. Pardutz, A., & Schoenen, J. (2010). NSAIDs in the acute treatment of migraine: A review of clinical and experimental data. In *Pharmaceuticals* (Vol. 3, Issue 6, pp. 1966–1987). MDPI AG. https://doi.org/10.3390/ph3061966
154. Parikh, S. K., & Silberstein, S. D. (2019). Current Status of Antiepileptic Drugs as Preventive Migraine Therapy. In *Current Treatment Options in Neurology* (Vol. 21, Issue 4). Current Science Inc. https://doi.org/10.1007/s11940-019-0558-1
155. Patel NM, Jozsa F, M Das J. Neuroanatomy, Spinal Trigeminal Nucleus. 2022 Oct 18. In: StatPearls [Internet]. Treasure Island (FL): StatPearls Publishing; 2024 Jan–. PMID: 30969551.
156. Paxinos G. The mouse brain in stereotaxic coordinates /. 2nd ed. San Diego : Academic Press, 2001 pg: 105-120.
157. Peatfield, R. C. (1995). Relationships Between Food, Wine, and Beer-Precipitated Migrainous Headaches. *Headache: The Journal of Head and Face Pain*, *35*(6), 355–357. https://doi.org/10.1111/j.1526-4610.1995.hed3506355.x
158. Pozos, R. S., and Oakes, S. G. (1987). The effects of ethanol on the electrophysiology of calcium channels. Recent Dev. Alcohol 5, 327–345. PMID: 2436259. doi:10.1007/978-1- 4899-1684-6_13

159. Pradhan, A. A., Smith, M. L., McGuire, B., Tarash, I., Evans, C. J., & Charles, A. (2014). Characterization of a novel model of chronic migraine. *Pain*, *155*(2), 269–274. https://doi.org/10.1016/j.pain.2013.10.004
160. Priest MF, Freda SN, Rieth IJ, Badong D, Dumrongprechachan V, Kozorovitskiy Y. Peptidergic and functional delineation of the Edinger-Westphal nucleus. Cell Rep. 2023 Aug 29;42(8):112992. doi: 10.1016/j.celrep.2023.112992. Epub 2023 Aug 17. PMID: 37594894; PMCID: PMC10512657.
161. Priest MF, Freda SN, Rieth IJ, Badong D, Dumrongprechachan V, Kozorovitskiy Y. Peptidergic and functional delineation of the Edinger-Westphal nucleus. (2021). Peptidergic modulation of fear responses by the Edinger-Westphal nucleus. bioRxiv preprint doi: https://doi.org/10.1101/2021.08.05.455317
162. Puledda F, Silva EM, Suwanlaong K, Goadsby PJ. Migraine: from pathophysiology to treatment. J Neurol. 2023 Jul;270(7):3654-3666. doi: 10.1007/s00415-023-11706-1. Epub 2023 Apr 8. PMID: 37029836; PMCID: PMC10267278.
163. Raddant AC, Russo AF. Calcitonin gene-related peptide in migraine: intersection of peripheral inflammation and central modulation. Expert Rev Mol Med. 2011;13:e36.
164. Rattanawong W, Rapoport A, Srikiatkhachorn A. Neurobiology of migraine progression. Neurobiol Pain. 2022 Jun 9;12:100094. doi: 10.1016/j.ynpai.2022.100094. PMID: 35720639; PMCID: PMC9204797.
165. Razeghi Jahromi S, Togha M, Ghorbani Z, Hekmatdoost A, Khorsha F, Rafiee P, Shirani P, Nourmohammadi M, Ansari H. The association between dietary tryptophan intake and migraine. Neurological Sciences 2019;40:2349–2355.
166. Rea BJ, Wattiez AS, Waite JS, Castonguay WC, Schmidt CM, Fairbanks AM, Robertson BR, Brown CJ, Mason BN, Moldovan-Loomis MC, Garcia-Martinez LF, Poolman P, Ledolter J, Kardon RH, Sowers LP, Russo AF. Peripherally administered calcitonin gene-related peptide induces spontaneous pain in mice: Implications for migraine. Pain 2018;159:2306–2317.
167. Ren J, Friedmann D, Xiong J, Liu CD, Ferguson BR, Weerakkody T, DeLoach KE, Ran C, Pun A, Sun Y, Weissbourd B, Neve RL, Huguenard J, Horowitz MA, Luo L. Anatomically Defined and Functionally Distinct Dorsal Raphe Serotonin Sub-systems. Cell. 2018 Oct 4;175(2):472-487.e20. doi: 10.1016/j.cell.2018.07.043. Epub 2018 Aug 23. PMID: 30146164; PMCID: PMC6173627.
168. Rissardo, J. P., & Caprara, A. L. F. (2022). Gepants for Acute and Preventive Migraine Treatment: A Narrative Review. In *Brain Sciences* (Vol. 12, Issue 12). MDPI. https://doi.org/10.3390/brainsci12121612
169. Rorden C, Brett M. Stereotaxic display of brain lesions. Behav Neurol. 2000;12(4):191-200.
170. Rossi MF, Tumminello A, Marconi M, Gualano MR, Santoro PE, Malorni W, Moscato U. Sex and gender differences in migraines: a narrative review. Neurological Sciences 2022;43:5729–5734.
171. Rouwette, T., Klemann, K., Gaszner, B., Scheffer, G. J., Roubos, E. W., Scheenen, W. J. J. M., Vissers, K., & Kozicz, T. (2011). Differential responses of corticotropin-releasing factor and urocortin 1 to acute pain stress in the rat brain. Neuroscience, 183, 15–24. https://doi.org/10.1016/j.neuroscience.2011.03.054

172. Ryabinin, A. E. et al. (1997) ‘Differential sensitivity of c-Fos expression in hippocampus and other brain regions to moderate and low doses of alcohol’, Molecular Psychiatry, 2(1), pp. 32–43. doi: 10.1038/sj.mp.4000206.
173. Ryabinin, A. E., Bachtell, R. K., Freeman, P., & Risinger, F. O. (2001). ITF expression in mouse brain during acquisition of alcohol self-administration. In Brain Research (Vol. 890). www.elsevier.com/locate/bres
174. Ryabinin, A. E., & Weitemier, A. Z. (2006). The urocortin 1 neurocircuit: Ethanol-sensitivity and potential involvement in alcohol consumption. In Brain Research Reviews (Vol. 52, Issue 2, pp. 368–380). https://doi.org/10.1016/j.brainresrev.2006.04.007
175. Sakai Y, Dobson C, Diksic M, Aubé M, Hamel E. Sumatriptan normalizes the migraine attack-related increase in brain serotonin synthesis. Neurology. 2008;70(6):431-439.
176. Salinas, A. G. et al. (2014) ‘Reduced ethanol consumption and preference in cocaine- and amphetamine-regulated transcript (CART) knockout mice’, Addiction Biology, 19(2), pp. 175–184. doi: 10.1111/j.1369-1600.2012.00475.x.
177. Salvatore, C. A., Mallee, J. J., Bell, I. M., Zartman, C. B., Williams, T. M., Koblan, K. S., & Kane, S. A. (2006). Identification and pharmacological characterization of domains involved in binding of CGRP receptor antagonists to the calcitonin-like receptor. Biochemistry, 45(6), 1881–1887. https://doi.org/10.1021/bi052044w
178. Scheff, N. N., & Gold, M. S. (2011). Sex differences in the inflammatory mediator-induced sensitization of dural afferents. *J Neurophysiol*, *106*, 1662–1668. https://doi.org/10.1152/jn.00196.2011.-Ap
179. Schiano di Cola, F., Bolchini, M., Ceccardi, G., Caratozzolo, S., Liberini, P., Rao, R., & Padovani, A. (2023). An observational study on monoclonal antibodies against calcitonin-gene-related peptide and its receptor. *European Journal of Neurology*, *30*(6), 1764–1773. https://doi.org/10.1111/ene.15761
180. Schreiber, A. L., & Gilpin, N. W. (2018). Corticotropin-Releasing Factor (CRF) Neurocircuitry and Neuropharmacology in Alcohol Drinking. In Handbook of Experimental Pharmacology (Vol. 248, pp. 435–471). Springer New York LLC. https://doi.org/10.1007/164_2017_86
181. Shapiro SS, Wilk MB. An Analysis of Variance Test for Normality (Complete Samples). Biometrika 1965;52:591.
182. Sharpe, A. L., Tsivkovskaia, N. O., & Ryabinin, A. E. (2005). Ataxia and c-Fos expression in mice drinking ethanol in a limited access session. Alcoholism: Clinical and Experimental Research, 29(8), 1419–1426. https://doi.org/10.1097/01.alc.0000174746.64499.83
183. Shibata M, Tang C. Implications of Transient Receptor Potential Cation Channels in Migraine Pathophysiology. Neurosci Bull. 2021 Jan;37(1):103-116. doi: 10.1007/s12264-020-00569-5. Epub 2020 Sep 1. PMID: 32870468; PMCID: PMC7811976.
184. Shibata Y. Migraine Pathophysiology Revisited: Proposal of a New Molecular Theory of Migraine Pathophysiology and Headache Diagnostic Criteria. Int J Mol Sci 2022;23(21):13002.
185. Shield KD, Parry C, Rehm J. Chronic diseases and conditions related to alcohol use. Alcohol Res. 2013;35(2):155-73. PMID: 24881324; PMCID: PMC3908707.

186. Skorobogatykh K, Van Hoogstraten WS, Degan D, Prischepa A, Savitskaya A, Ileen BM, Bentivegna E, Skiba I, D'Acunto L, Ferri L, Sacco S, Hansen JM, Amin FM. Functional connectivity studies in migraine: What have we learned? Journal of Headache and Pain 2019;20(1):108.
187. Smith GST, Savery D, Marden C, Costa JJL, Averill S, Priestley J V., Rattray M. Distribution of messenger RNAs encoding enkephalin, substance P, somatostatin, galanin, vasoactive intestinal polypeptide, neuropeptide Y, and calcitonin gene-related peptide in the midbrain periaqueductal grey in the rat. Journal of Comparative Neurology 1994;350:23–40.
188. Snedecor GW, Cochran WG. Statistical Methods. Iowa State University Press 1989.
189. Song F, Guo J. [Progress on structural biology of voltage-gated ion channels]. Zhejiang Da Xue Xue Bao Yi Xue Ban. 2019 May 25;48(1):25-33. Chinese. PMID: 31102354.
190. Souza Monteiro de Araujo D, Nassini R, Geppetti P, De Logu F. TRPA1 as a therapeutic target for nociceptive pain. Expert Opin Ther Targets. 2020 Oct;24(10):997-1008. doi: 10.1080/14728222.2020.1815191. Epub 2020 Sep 11. PMID: 32838583; PMCID: PMC7610834.
191. Spekker E, Körtési T, Vécsei L. TRP Channels: Recent Development in Translational Research and Potential Therapeutic Targets in Migraine. Int J Mol Sci. 2022 Dec 31;24(1):700. doi: 10.3390/ijms24010700. PMID: 36614146; PMCID: PMC9820749.
192. Spekker, E.; Nagy-Grócz, G.; Vécsei, L. Ion Channel Disturbances in Migraine Headache: Exploring the Potential Role of the Kynurenine System in the Context of the Trigeminovascular System. *Int. J. Mol. Sci.* 2023, *24*, 16574. https://doi.org/10.3390/ijms242316574
193. Spina MG, Langnaese K, Orlando GF, Horn TFW, Rivier J, Vale WW, Wolf G, Engelmann M. Colocalization of Urocortin and neuronal nitric oxide synthase in the hypothalamus and Edinger-Westphal nucleus of the rat. Journal of Comparative Neurology 2004;479:271–286.
194. Stovner, L. J., Nichols, E., Steiner, T. J., Abd-Allah, F., Abdelalim, A., Al-Raddadi, R. M., Ansha, M. G., Barac, A., Bensenor, I. M., Doan, L. P., Edessa, D., Endres, M., Foreman, K. J., Gankpe, F. G., Gopalkrishna, G., Goulart, A. C., Gupta, R., Hankey, G. J., Hay, S. I., … Murray, C. J. L. (2018). Global, regional, and national burden of migraine and tension-type headache, 1990–2016: a systematic analysis for the Global Burden of Disease Study 2016. *The Lancet Neurology*, *17*(11), 954–976. https://doi.org/10.1016/S1474-4422(18)30322-3
195. Stranding S (Ed) Gray's Anatomy: The Anatomical Basis of Clinical Pracice 42nd Edition 2020, Elsevier ISBN: 0702077054, 9780702077050
196. Sureda-Gibert, P., Romero-Reyes, M., & Akerman, S. (2022). Nitroglycerin as a model of migraine: Clinical and preclinical review. In *Neurobiology of Pain* (Vol. 12). Elsevier B.V. https://doi.org/10.1016/j.ynpai.2022.100105
197. Szekeres-Paraczky C, Szocsics P, Erőss L, Fabó D, Mód L, Maglóczky Z. Reorganization of Parvalbumin Immunopositive Perisomatic Innervation of Principal Cells in Focal Cortical Dysplasia Type IIB in Human Epileptic Patients. Int J Mol Sci 2022;23(9):4746.

198. Talavera, K. et al. (2020) ‘Mammalian transient receptor potential TRPA1 channels: From structure to disease’, Physiological Reviews, 100(2 725), p. 803. doi: 10.1152/physrev.00005.2019.
199. Tang, Y., Liu, S., Shu, H., Yanagisawa, L., & Tao, F. (2020). Gut Microbiota Dysbiosis Enhances Migraine-Like Pain Via TNFα Upregulation. Molecular neurobiology, 57(1), 461–468. https://doi.org/10.1007/s12035-019-01721-7
200. Tepper SJ. Anti-Calcitonin Gene-Related Peptide (CGRP) Therapies: Update on a Previous Review After the American Headache Society 60th Scientific Meeting, San Francisco, June 2018. Headache: The Journal of Head and Face Pain 2018;58:276–290.
201. Turek, V. F., Tsivkovskaia, N. O., Hyytia, P., Harding, S., Lê, A. D., & Ryabinin, A. E. (2005). Urocortin 1 expression in five pairs of rat lines selectively bred for differences in alcohol drinking. Psychopharmacology, 181(3), 511–517. https://doi.org/10.1007/s00213-005-0011-x
202. Ujvári, B., Pytel, B., Márton, Z., Bognár, M., Kovács, L. Á., Farkas, J., Gaszner, T., Berta, G., Kecskés, A., Kormos, V., Farkas, B., Füredi, N., & Gaszner, B. (2022). Neurodegeneration in the centrally-projecting Edinger–Westphal nucleus contributes to the non-motor symptoms of Parkinson’s disease in the rat. Journal of Neuroinflammation, 19(1). https://doi.org/10.1186/s12974-022-02399-w
203. Valentino RJ, Lucki I, Van Bockstaele E. Corticotropin-releasing factor in the dorsal raphe nucleus: Linking stress coping and addiction. Brain Res 2010;1314:29–37
204. van der Doelen RHA, Robroch B, Arnoldussen IA, Schulpen M, Homberg JR, Kozicz T. Serotonin and urocortin 1 in the dorsal raphe and Edinger–Westphal nuclei after early life stress in serotonin transporter knockout rats. Neuroscience 2017;340:345–358.
205. Vaughn, A. H., & Gold, M. S. (2010). Ionic mechanisms underlying inflammatory mediator-induced sensitization of dural afferents. *Journal of Neuroscience*, *30*(23), 7878–7888. https://doi.org/10.1523/JNEUROSCI.6053-09.2010
206. Vaughan J, Donaldson C, Bittencourt J, Perrin MH, Lewis K, Sutton S, Chan R, Turnbull AV, Lovejoy D, Rivier C, et al. Urocortin, a mammalian neuropeptide related to fish urotensin I and to corticotropin-releasing factor. Nature. 1995 Nov 16;378(6554):287-92. doi: 10.1038/378287a0. PMID: 7477349.Vicentic, A., & Jones, D. C. (2007). The CART (Cocaine- and Amphetamine-Regulated Transcript) System in Appetite and Drug Addiction. Journal of Pharmacology and Experimental Therapeutics, 320(2), 499–506. https://doi.org/10.1124/JPET.105.091512.
207. Vicentic, A., & Jones, D. C. (2007). The CART (cocaine- and amphetamine-regulated transcript) system in appetite and drug addiction. In *Journal of Pharmacology and Experimental Therapeutics* (Vol. 320, Issue 2, pp. 499–506). https://doi.org/10.1124/jpet.105.091512
208. Vila-Pueyo, M., Page, | Keith, Murdock, P. R., Loraine, H. J., Woodrooffe, A. J., Kirk, |, Johnson, W., Peter, |, Goadsby, J., & Holland, P. R. (2021). *The selective 5-HT 1F receptor agonist lasmiditan inhibits trigeminal nociceptive processing: Implications for migraine and cluster headache*. https://doi.org/10.1111/bph.v179.3/issuetoc
209. Vila-Pueyo M, Hoffmann J, Romero-Reyes M, Akerman S. Brain structure and function related to headache: Brainstem structure and function in headache. Cephalalgia 2019;39:1635–1660.

210. Vos, T., Abajobir, A. A., Abbafati, C., Abbas, K. M., Abate, K. H., Abd-Allah, F., Abdulle, A. M., Abebo, T. A., Abera, S. F., Aboyans, V., Abu-Raddad, L. J., Ackerman, I. N., Adamu, A. A., Adetokunboh, O., Afarideh, M., Afshin, A., Agarwal, S. K., Aggarwal, R., Agrawal, A., … Murray, C. J. L. (2017). Global, regional, and national incidence, prevalence, and years lived with disability for 328 diseases and injuries for 195 countries, 1990-2016: A systematic analysis for the Global Burden of Disease Study 2016. *The Lancet*, *390*(10100), 1211–1259. https://doi.org/10.1016/S0140-6736(17)32154-2
211. Walther DJ, Peter JU, Bashammakh S, Hörtnagl H, Voits M, Fink H, Bader M. Synthesis of serotonin by a second tryptophan hydroxylase isoform. Science. 2003;299:76.
212. Wang F, Flanagan J, Su N, Wang LC, Bui S, Nielson A, Wu X, Vo HT, Ma XJ, Luo Y. RNAscope: A novel in situ RNA analysis platform for formalin-fixed, paraffin-embedded tissues. Journal of Molecular Diagnostics 2012;14:22–29.
213. Wang S, Wang H, Zhao D, Liu X, Yan W, Wang M, Zhao R. Grey matter changes in patients with vestibular migraine. Clin Radiol 2019;74:898.e1-898.e5.
214. Wang, Y. Y., Chang, R. B., Allgood, S. D., Silver, W. L., & Liman, E. R. (2011). A TRPA1-dependent mechanism for the pungent sensationof weak acids. Journal of General Physiology, 137(6), 493–505. https://doi.org/10.1085/jgp.201110615
215. Wantke, F., Focke, M., Hemmer, W., Bracun, R., Wolf-Abdolvahab, S., Götz, M., Jarisch, R., Götz, M., Tschabitscher, M., Gann, M., & Tappler, P. (2000). Exposure to formaldehyde and phenol during an anatomy dissecting course: sensitizing potency of formaldehyde in medical students. *Allergy*, *55*(1), 84–87. https://doi.org/10.1034/j.1398-9995.2000.00307.x
216. Waselus M, Nazzaro C, Valentino RJ, Van Bockstaele EJ. Stress-Induced Redistribution of Corticotropin-Releasing Factor Receptor Subtypes in the Dorsal Raphe Nucleus. Biol Psychiatry 2009;66:76–83.
217. Wattiez AS, Wang M, Russo AF. CGRP in animal models of migraine. Handbook of Experimental Pharmacology. Springer New York LLC, 2019, Vol. 255. pp. 85–107.
218. Weitemier, A. Z., Woerner, A., Bäckström, P., Hyytiä, P., & Ryabinin, A. E. (2001). Expression of c-Fos in Alko Alcohol Rats Responding for Ethanol in an Operant Paradigm.
219. Wiley RG, Kline IV RH. Neuronal lesioning with axonally transported toxins. J Neurosci Methods. 2000;103(1):73-82. doi:10.1016/s0165-0270(00)00297-1
220. World Health Organization. (2022, May 9 th). Alcohol. https://www.who.int/news-room/fact-sheets/detail/alcohol
221. Wood AJJ, Welch KMA. Drug Therapy of Migraine. New England Journal of Medicine 1993;329:1476–1483.
222. Xu, L., Füredi, N., Lutter, C., Geenen, B., Pétervári, E., Balaskó, M., Dénes, Á., Kovács, K. J., Gaszner, B., & Kozicz, T. (2022). Leptin coordinates efferent sympathetic outflow to the white adipose tissue through the midbrain centrally-projecting Edinger-Westphal nucleus in male rats. Neuropharmacology, 205. https://doi.org/10.1016/j.neuropharm.2021.108898
223. Yang, C. P., Liang, C. S., Chang, C. M., Yang, C. C., Shih, P. H., Yau, Y. C., Tang, K. T., & Wang, S. J. (2021). Comparison of New Pharmacologic Agents with Triptans for Treatment of Migraine: A Systematic Review and Meta-analysis. In *JAMA Network Open*. American Medical Association. https://doi.org/10.1001/jamanetworkopen.2021.28544

224. You Y, Park JS. A Novel Human Brainstem Map Based on True-Color Sectioned Images. J Korean Med Sci 2023;38(10):e76.
225. Zhang, X., Burstein, R., & Levy, D. (2012). Local action of the proinflammatory cytokines IL-1β and IL-6 on intracranial meningeal nociceptors. *Cephalalgia*, *32*(1), 66–72. https://doi.org/10.1177/0333102411430848
226. Zuniga, A., & Ryabinin, A. E. (2020). Involvement of centrally projecting edinger–westphal nucleus neuropeptides in actions of addictive drugs. Brain Sciences, 10(2), 1–14. https://doi.org/10.3390/brainsci10020067

10. List of abbreviations

5-HT: Serotonin

a.u.: arbitrary units

AAV8: Adeno-associated virus serotype 8

AAV8 Syn EGFP: Adeno-associated virus serotype 8 containing enhanced green fluorescent protein gene

ACC: anterior cingulate cortex

ANOVA: analysis of variance

AMY1: amylin receptor 1

AP: action potential

BBB: blood brain barrier

BNST: bed nucleus of the stria terminalis

CALCRL: calcitonin receptor-like

CART: cocaine- and amphetamine-regulated transcript

Cart: cocaine- and amphetamine-regulated transcript mRNA

CCK: cholecystokinin

CeA: central nucleus of the amygdala

CGRP: calcitonin gene-related peptide

CHAT: choline acetyltransferase

CLR: calcitonin-like receptor

Calcr: calcitonin receptor mRNA

CNS: central nervous system

CNQX: cyanquixaline

CRCP: calcitonin gene-related peptide receptor component protein

Crcp: calcitonin gene-related peptide receptor component mRNA

CRH: corticotropin-releasing hormone

CRH1R: corticotropin-releasing hormone receptor 1

Crh1r: corticotropin-releasing hormone receptor 1 mRNA

CRH2R: corticotropin-releasing hormone receptor 2

Crh2r: corticotropin-releasing hormone receptor 2 mRNA

CSD: cortical spreading depression

CTB: cholera toxin subunit B

CRT: calcitonin receptor

Ctr: calcitonin receptor mRNA

DAB: diaminobenzidine

DAPI: 4′,6-diamidino-2-phenylindole

DIC: differential interference contrast

DRN: dorsal raphe nucleus

EGFP: enhanced green fluorescent protein

EW: Edinger-Westphal nucleus

EWpg: preganglionic Edinger-Westphal nucleus

EWcp: centrally projecting Edinger-Westphal nucleus

fMRI: functional magnetic resonance imaging

FOS: acute neuronal activation marker, protein product of Finkel-Biskis-Jenkins mouse sarcoma virus-derived cellular oncogene (c-fos)

FOV: field of view

GFAP: glial fibrillary acidic protein

GFP: green fluorescent protein

HEK293: human embryonic kidney-derived 293 cells

i.c.v.: intracerebroventricular

i.p.: intraperitoneal

i.t.: intrathecal

i.v.: intravenous

ICHD-III: third edition of the International Classification of Headache Disorders

IHC: immunohistochemistry

ISH: *in situ* hybridization

KO: knockout

LDB: light-dark box test

lH: lateral hypothalamus

lPAG: lateral periaqueductal gray matter

lS: later septum

LS: leptin-saporin conjugate

MNI: Montreal Neurological Institute

mPFC: medial prefrontal cortex

NeuN: neuronal nuclear marker

nNOS: neuronal nitric oxide synthase

NTG: nitroglycerin

proCT: procalcitonin

P-CREB: phosphorylated product of c-AMP-responsive element binding protein

PAC1: pituitary adenylate cyclase-activating polypeptide receptor

PACAP: pituitary adenylate cyclase-activating polypeptide

PAG: periaqueductal gray matter

PBS: phosphate buffered saline

PCR: polymerase chain reaction

PFA: paraformaldehyde

POA: preoptic area

PVT: paraventricular nucleus of the thalamus

RAMP1: receptor activity-modifying protein 1

Ramp1: receptor activity-modifying protein 1 mRNA

ROI: region of interest

s.c.: subcutaneous

SC: spinal cord

SMP12: Statistical Parametric Mapping 12

SSD: specific signal density

SP: substance P

STN: spinal trigeminal nucleus

TE: echo time

TFE: turbo field echo

TH: tyrosine hydroxylase

TNF-α: tumour necrosis factor α

TPH2: tryptophan hydroxylase 2

Tph2: tryptophan hydroxylase 2 mRNA

TR: repetition time

TRG: trigeminal ganglion

TRP: transient receptor potential ion channel

TRPA1: transient receptor potential cation channel subfamily A member 1

Trpa1: transient receptor potential cation channel subfamily A member 1 mRNA in mice

TRPA1: transient receptor potential cation channel subfamily A member 1 mRNA in humans

UAC: urine alcohol concentration

UCN1: urocortin 1 peptide

Ucn1: urocortin 1 mRNA in mice

VTA: ventral tegmental area

WT: wild-type

11. Publications

The thesis is based on the following publications:

Al-Omari A, Kecskés M, Gaszner B, Biró-Sütő T, Fazekas B, Berta G, Kuzma M, Pintér E, Kormos V. Functionally active TRPA1 ion channel is downregulated in peptidergic neurons of the Edinger-Westphal nucleus upon acute alcohol exposure. **Frontiers in Cell and Developmental Biology** 2023 Jan 10;10:1046559. doi: 10.3389/fcell.2022.1046559. PMID: 36704197; PMCID: PMC9872022. **IF: 4.6; Q1**

Al-Omari A, Gaszner B, Zelena D, Gecse K, Berta G, Biró-Sütő T, Szocsics P, Maglóczky Z, Gombás P, Pintér E, Juhász G, Kormos V. Neuroanatomical evidence and a mouse calcitonin gene-related peptide model in line with human functional magnetic resonance imaging data support the involvement of peptidergic Edinger-Westphal nucleus in migraine. **Pain**. 2024 Jun 14. doi: 10.1097/j.pain.0000000000003294. Epub ahead of print. PMID: 38875125. **IF: 5.9; Q1; D1**

Other publications of the author:

Konkoly J, Kormos V, Gaszner B, Sándor Z, Kecskés A, **Al-Omari A**, Szilágyi A, Szilágyi B, Zelena D, Pintér E. The Role of TRPA1 Channels in the Central Processing of Odours Contributing to the Behavioral Responses of Mice. **Pharmaceuticals** (Basel). 2021 Dec 20;14(12):1336. doi: 10.3390/ph14121336. PMID: 34959735; PMCID: PMC8703823. **IF: 5,21; Q1**

Kormos V, Kecskés A, Farkas J, Gaszner T, Csernus V, **Al-Omari A**, Hegedüs D, Renner É, Palkovits M, Zelena D, Helyes Z, Pintér E, Gaszner B. Peptidergic neurons of the Edinger-Westphal nucleus express TRPA1 ion channel that is downregulated both upon chronic variable mild stress in male mice and in humans who died by suicide. **Journal of Psychiatry and Neuroscience** 2022 May 4;47(3):E162-E175. doi: 10.1503/jpn.210187. PMID: 35508327; PMCID: PMC9074809. **IF: 4.3; Q1**

Orján EM, Kormányos ES, Fűr GM, Dombi Á, Bálint ER, Balla Z, Balog BA, Dágó Á, Totonji A, Bátai ZI, Jurányi EP, Ditrói T, **Al-Omari A**, Pozsgai G, Kormos V, Nagy P, Pintér E, Rakonczay Z Jr, Kiss L. The anti-inflammatory effect of dimethyl trisulfide in experimental acute pancreatitis. **Scientific Reports** 2023 Oct 5;13(1):16813. doi: 10.1038/s41598-023-43692-9. PMID: 37798377; PMCID: PMC10556037. **IF: 3.8; Q1; D1**

Kormos V, Kriszta G, **Al-Omari A**, Kovács-Rozmer K, Konkoly J, Pozsgai G, Pintér E. TRP Channels as Therapeutic Targets. Chapter: TRP channels as potential target molecules for pharmacotherapy of neurological diseases. Elsevier, ISBN: 9780443186530 (accepted, in press)

Cumulative IF: 23.81
MTMT ID: 10082296

12. Conference attendences

Al-Omari Ammar, Balázs Gaszner, Zsuzsanna Helyes, Viktória Kormos
Transient *Receptor Potential Ankyrin 1 cation channel-expressing cells of the Edinger-Westphal nucleus are activated in a mouse migraine model.*
International Neuroscience Meeting, Budapest 2022 – IBRO Workshop

Al-Omari Ammar, Fazekas Balázs, Gaszner Balázs, Pintér Erika, Kormos Viktória
The role of Central Transient Receptor Potential Ankyrin 1 in a mouse model of acute alcohol exposure.
Hungarian Society of Experimental and Clinical Pharmacology, MFT Conference (2022)
.

Al-Omari Ammar, Gaszner Balázs, Pintér Erika, Kormos Viktória
Transient Receptor Potential Ankyrin 1 cation channel-expressing cells of the Edinger-Westphal nucleus are activated in a mouse migraine model.
3rd Regional Congress of Physiological Societies (2022)

Al-Omari Ammar, Gaszner Balázs, Pintér Erika, Kormos Viktória
Involvement of the centrally projecting Edinger-Westphal nucleus in a mouse model of migraine.
6th Hungarian Neuroscience Doctoral Conference (2023)

Al-Omari Ammar, Gaszner Balázs, Pintér Erika, Kormos Viktória
Involvement of the centrally projecting Edinger-Westphal nucleus in a mouse model of migraine.
Medical Conference for PhD Students and Experts of Clinical Sciences **(**MedPECS2023)

Al-Omari Ammar, Balázs Gaszner, Dóra Zelena, Gabriella Juhász, Viktória Kormos
Functional and Neuroanatomical evidence in line with a mouse CGRP model support the involvement of peptidergic Edinger-Westphal nucleus in migraine
International Translation Medicine Congress of Students and Young Physicans (OSCON 2024)

Ammar Al-Omari, Balázs Gaszner, Dóra Zelena, Kinga Gecse, Gergely Berta, Tünde Biró-Sütő, Péter Szocsics, Zsófia Maglóczky, Péter Gombás, Erika Pintér, Gabriella Juhász, Viktória Kormos.
Neuroanatomical evidence and a mouse CGRP model in line with human fMRI data support the recruitment of peptidergic Edinger-Westphal nucleus in migraine
International Neuroscience Conference (INC 2024)

Ammar Al-Omari, Balázs Gaszner, Dóra Zelena, Kinga Gecse, Gergely Berta, Tünde Biró-Sütő, Péter Szocsics, Zsófia Maglóczky, Péter Gombás, Erika Pintér, Gabriella Juhász, Viktória Kormos.
Involvement of peptidergic Edinger-Westphal nucleus in the neurobiology of migraine
Federation of European Neuroscience Societies Forum (FENS 2024)

13. Acknowledgements

First and foremost, I express my deepest gratitude to my supervisor, Dr. Gasznerné Dr. Kormos Viktória, whose expertise, patience, mentorship and limitless support have been indispensable. Her insightful feedback and constructive criticism have shaped my academic progress. I am fortunate to have had the opportunity to work under her guidance.

I am grateful to Prof. Dr. Erika Pintér, Head of the Doctoral School and Head of our Institute, for her scientific advice and support throughout my studies. I extend my deepest appreciation to Dr. Balázs Gaszner for his exceptional contributions and profound insights that have greatly enriched every facet of this project. This work would have not been possible without their contribution.

I extend my sincere appreciation to my thesis committee members, for their insightful feedback, constructive criticism, and scholarly guidance. Your collective wisdom and expertise have significantly enriched the quality of this thesis.

I would like to thank Tünde Biró-Sütő for her substantial dedication and assistance in the laboratory work, Dóra Zelena for performing the stereotaxic surgery, Miklós Kecskés for the electrophysiological experiments, Zsófia Maglóczky, Péter Gombás and Péter Szocsics for providing us with the human brain samples, Gabriella Juhász and Kinga Gecse for performing the fMRI study, Gergely Berta for helping with the confocal microscopy, Mónika Kuzuma for conducting the urine alcohol concentration measurement and Balázs Fazekas for his TDK work. I am grateful for the staff and resources at the University of Pécs, Medical School, Department of Pharmacology and Pharmacotherapy who have facilitated a conducive research environment.

I would like to express my heartfelt gratitude and appreciation to my family for their unwavering love, steadfast support, and enduring encouragement, illuminating even the darkest moments though out this journey.

Finally, I acknowledge the countless individuals, friends, and colleagues who have supported me through any acts of kindness. Your contributions, no matter how small, have not gone unnoticed and are deeply appreciated.

This thesis is a testament to the collective efforts of all those mentioned above, and I am profoundly grateful for the role each one of you.

Research Paper

PAIN 00 (2024) 1–20

PAIN®

OPEN

Neuroanatomical evidence and a mouse calcitonin gene–related peptide model in line with human functional magnetic resonance imaging data support the involvement of peptidergic Edinger–Westphal nucleus in migraine

Ammar Al-Omari[a], Balázs Gaszner[b], Dóra Zelena[c], Kinga Gecse[d,e], Gergely Berta[f], Tünde Biró-Sütő[a], Péter Szocsics[g,h], Zsófia Maglóczky[g,h], Péter Gombás[i], Erika Pintér[a], Gabriella Juhász[d,e], Viktória Kormos[a,*]

Abstract

The urocortin 1 (UCN1)–expressing centrally projecting Edinger–Westphal (EWcp) nucleus is influenced by circadian rhythms, hormones, stress, and pain, all known migraine triggers. Our study investigated EWcp's potential involvement in migraine. Using RNAscope in situ hybridization and immunostaining, we examined the expression of calcitonin gene–related peptide (CGRP) receptor components in both mouse and human EWcp and dorsal raphe nucleus (DRN). Tracing study examined connection between EWcp and the spinal trigeminal nucleus (STN). The intraperitoneal CGRP injection model of migraine was applied and validated by light–dark box, and von Frey assays in mice, in situ hybridization combined with immunostaining, were used to assess the functional–morphological changes. The functional connectivity matrix of EW was examined using functional magnetic resonance imaging in control humans and interictal migraineurs. We proved the expression of CGRP receptor components in both murine and human DRN and EWcp. We identified a direct urocortinergic projection from EWcp to the STN. Photophobic behavior, periorbital hyperalgesia, increased c-fos gene–encoded protein immunoreactivity in the lateral periaqueductal gray matter and trigeminal ganglia, and phosphorylated c-AMP–responsive element binding protein in the STN supported the efficacy of CGRP-induced migraine-like state. Calcitonin gene–related peptide administration also increased c-fos gene–encoded protein expression, *Ucn1* mRNA, and peptide content in EWcp/UCN1 neurons while reducing serotonin and tryptophan hydroxylase-2 levels in the DRN. Targeted ablation of EWcp/UCN1 neurons induced hyperalgesia. A positive functional connectivity between EW and STN as well as DRN has been identified by functional magnetic resonance imaging. The presented data strongly suggest the regulatory role of EWcp/UCN1 neurons in migraine through the STN and DRN with high translational value.

Keywords: Migraine model, Centrally projecting Edinger–Westphal nucleus, Urocortin 1, Calcitonin gene–related peptide, Serotonin, Nucleus raphe dorsalis, Spinal trigeminal nucleus, fMRI

1. Introduction

Migraine is a neurovascular disorder[47,49] that appears in the neurological practice as one of the most common complaints.[62] Migraine attacks can last hours or days associated with headache, nausea, vomiting, photophobia, and phonophobia.[106] The condition is attributed to activation and sensitization of the trigeminovascular system.[4] Furthermore, a primary dysregulation of sensory processing may result in a constellation of neurological symptoms.[10] The underlying mechanisms of migraine are not fully understood, and its therapy is not entirely resolved, highlighting the importance of further research.

Sponsorships or competing interests that may be relevant to content are disclosed at the end of this article.

[a] *Department of Pharmacology and Pharmacotherapy, Medical School, University of Pécs, Pécs, Hungary,* [b] *Department of Anatomy, Medical School and Research Group for Mood Disorders, Centre for Neuroscience, University of Pécs, Pécs, Hungary,* [c] *Institute of Physiology, Medical School, University of Pécs, Pécs, Hungary,* [d] *Department of Pharmacodynamics, Faculty of Pharmaceutical Sciences, Semmelweis University, Budapest, Hungary,* [e] *NAP3.0-SE Neuropsychopharmacology Research Group, Hungarian Brain Research Program, Semmelweis University, Budapest, Hungary,* [f] *Department of Medical Biology, Medical School, University of Pécs, Hungary,* [g] *Human Brain Research Laboratory, HUN-REN Institute of Experimental Medicine, Budapest, Hungary,* [h] *Szentágothai János Doctoral School of Neuroscience, Semmelweis University, Budapest, Hungary,* [i] *Department of Pathology, St. Borbála Hospital, Tatabánya, Hungary*

**Corresponding author. Address: Department of Pharmacology and Pharmacotherapy, Medical School, University of Pecs, Szigeti ut 12., Pecs 7624, Hungary. Tel.: +3672536001/Ext.: 38202. E-mail address: viktoria.kormos@aok.pte.hu (V. Kormos).*

Supplemental digital content is available for this article. Direct URL citations appear in the printed text and are provided in the HTML and PDF versions of this article on the journal's Web site (www.painjournalonline.com).

http://dx.doi.org/10.1097/j.pain.0000000000003294

The Edinger–Westphal (EW) nucleus includes a cholinergic preganglionic parasympathetic division that controls pupil constriction and lens accommodation, moreover, a peptidergic, centrally projecting division (centrally projecting EW [EWcp]).[57] Interestingly, the latter is affected by stress,[54] circadian rhythm,[35] and ovarian hormones[18,19] that are triggering factors of migraine attacks. The EWcp is the main source of central urocortin 1 (UCN1),[58,61,78,98,109] a corticotropin-releasing hormone (CRH)–related neuropeptide that binds to both CRH receptors (CRH receptor 1 [CRH1R] and CRH receptor 2 [CRH2R]).[6,7,44,59] Urocortin 1 has been implicated in control of food intake, energy homeostasis, stress response, mood level, and in response to acute pain.[32,53,57,84,109] Centrally projecting EW projections include migraine-related centers, the spinal trigeminal (spinal trigeminal nucleus [STN]) and dorsal raphe nucleus (DRN),[109] that express CRHRs,[14,15] suggesting the possible ment of EWcp/UCN1 in migraine.

In the EWcp, several migraine-related neurotransmitters, neuromodulators, and receptors were found (eg, pituitary adenylate cyclase-activating polypeptide, pituitary adenylate cyclase-activating polypeptide type I receptor,[31,66,78] neuronal nitric oxide synthase,[91] substance P[65]), including calcitonin gene–related peptide (CGRP) fibers.[90]

Calcitonin gene–related peptide is a sensory neuropeptide with potent cerebral vasodilative activity,[13] expressed abundantly in nociceptive trigeminal ganglion (TRG) neurons. Calcitonin gene–related peptide binds with equal affinity to calcitonin-like receptor (CLR) and calcitonin receptor (encoded by *Calcr* gene) when coexpressed with receptor activity-modifying protein 1 (RAMP1). The CLR/RAMP1 complex forms CGRP receptor and calcitonin receptor/RAMP1 complex forms amylin receptor1 (AMY1).[86] Calcitonin gene–related peptide receptor component protein is not necessary for the receptor's activity, but it enhances the efficacy of CGRP.[20]

The CGRP, released by central nerve endings, stimulates the CGRP receptor on second-order neurons in the caudal division of STN, contributing to central sensitization.[8,46] The trigeminal activation during migraine attacks elevates CGRP level.[39] Human studies have reported migraine-like attacks following intravenous CGRP infusion.[40,60] Serotonin (5-HT) receptor agonists (sumatriptan, dihydroergotamine) restore baseline CGRP level[38,85] concurrent with pain relief.[50]

In spite that CGRP cannot pass the blood–brain barrier,[70] intravenous CGRP administration can cause attacks in migraineurs,[2] which can be reversed by CGRP receptor antagonist olcegepant infusion.[74] Anti-CGRP and anti-CGRP receptor antibodies were effective in attack prevention,[16,94] further suggesting a peripheral site of action.[3,28]

Other mouse studies demonstrated that CGRP may act both in the central nervous system (CNS) and periphery.[52,68,81] Potential targets may be meningeal nociceptors leading to vasodilatation,[79] the trigeminal system, cerebral blood vessels, and dura mater,[42] but peripheral CGRP may alter the trigeminovascular microenvironment, leading to central sensitization.[25,29,45,46,68,81]

Here, we aimed to show neuroanatomical evidence that the EWcp/UCN1 may contribute to migraine. In a CGRP mouse model of migraine, we examined the EWcp and its migraine-related projection areas. Human functional magnetic resonance imaging (fMRI) studies were conducted to support the translational value of animal studies.

2. Materials and methods

2.1. Animals

Twelve-week-old male C57BL6/J mice were used and housed in a temperature and humidity controlled 12-hour light–dark cycle environment (lights on at 6 AM) in standard polycarbonate cages (365 × 207 × 144 mm) in 4 to 6 mice per cage groups, at the animal facility of the Department of Pharmacology and Pharmacotherapy, University of Pécs. Mice were provided ad libitum with standard rodent chow and tap water. All procedures were approved by the Animal Welfare Committee at Pécs University, National Scientific Ethical Committee on Animal Experimentation in Hungary (BA02/2000-57/2022) in agreement with the directive of the European Communities Council in 1986, and with the Law of XXCIII, in 1998, on Animal Care and Use in Hungary.

2.2. Experimental design

2.2.1. Neuroanatomical qualitative studies

Naive mice (n = 6) were used to examine the expression of AMY1 and CGRP receptor components in the EWcp, DRN, and STN as well as *Crhr1* and *Crhr2* mRNA in the STN.

Immunofluorescence targeting CLR and RNAscope in situ hybridization (ISH) targeting *Ramp1*, *Calcr*, and *Crcp* mRNA was combined with (1) UCN1 immunofluorescence in the EWcp to assess the colocalization with urocortinergic neurons in mice and in control human samples; (2) tryptophan hydroxylase-2 (TPH2) or 5-HT immunostaining in the DRN as a marker of the serotonergic neurons in mice, as TPH2 is the rate-limiting enzyme of the 5-HT synthesis; and (3) a neuronal marker (NeuN) immunofluorescence in the STN to visualize the dorsal horn neurons in mice.

To prove the connection between the urocortinergic EWcp neurons and STN, the EWcp of 6 naive mice was injected with an anterograde tracer adenoassociated virus serotype 8 (containing the green fluorescent protein [GFP] gene: AAV8 Syn enhanced GFP [EGFP]). Six animals received the injection of the retrograde tracer, cholera toxin subunit B (CTB), into their STN. To validate the anatomical localization of injections, CTB and GFP immunofluorescence was performed in the C1 segment of spinal cord and EWcp, respectively. For the retrograde tracing, UCN1 and CTB double immunofluorescence was performed on EWcp sections. For anterograde tracing, UCN1 and GFP double immunostaining was applied on C1 spinal cord sections.

Next, we investigated the expression of *Crhr1* and *Crhr2*, the receptor targets of UCN1, in the I-III laminae of the STN. For this purpose, RNAscope ISH for *Crhr1*, *Crhr2*, and *NeuN* was combined with UCN1 immunofluorescence in the STN. Our goal was to identify urocortinergic afferentation from EWcp to *Crhr1* and *Crhr2* positive neurons in the STN.

2.2.2. Semiquantitative functional–morphological examination of the centrally projecting Edinger–Westphal in the calcitonin gene–related peptide model

Based on our neuroanatomical results, we aimed to prove the involvement of EWcp in a CGRP mouse model of migraine. Mice were handled for 2 weeks and assigned to saline-injected control (n = 11) and CGRP-treated (n = 15) groups. Upon intraperitoneal injection of 0.1 mg/kg CGRP or saline, light aversion was measured using light–dark box (LDB) test 30 minutes after the injection to assess photophobia associated with migraine-like state.

Another cohort of mice (n = 13) was used to assess periorbital hyperalgesia by the same model. Mice were subjected to the von Frey assay 30 minutes after the treatment.

The EWcp is known to be sensitive to various stressors.[34,36] To exclude the changes in the EWcp caused by acute stress of LDB

test, we used an independent cohort of mice for the functional–morphological studies. Two experimental groups were created: saline (n = 6) as a control group and CGRP-treated (n = 6) group. After 2 weeks of handling and habituation to intraperitoneal (i.p.) injections, mice were treated with 0.1 mg/kg of saline or CGRP (α-CGRP Mouse, Rat [CRB], Cat. No.: crb1000889), respectively. Mice were euthanized 4 hours after the treatment. Immunohistochemistry for the neuronal activity marker c-fos gene–encoded protein (FOS) was performed in the EWcp, lateral periaqueductal gray matter (lPAG), and laminae I to III of STN. In addition, we performed immunofluorescence for the alternative neuronal activity marker phosphorylated c-AMP–responsive element binding protein (P-CREB)[72] in the STN. A whole mount FOS immunofluorescence was applied in the TRG to assess the neuronal activation in response to CGRP treatment. Double-label immunofluorescence for UCN1 and FOS was applied to prove the urocortinergic identity of activated EWcp neurons. *Ucn1* RNAscope ISH was combined with UCN1 immunofluorescence to assess UCN1 mRNA and peptide density in the EWcp. Serotonin (5-HT) and TPH2 double staining was performed to assess 5-HT and TPH2 density in the DRN.

2.2.3. Targeted ablation of the centrally projecting Edinger–Westphal urocortinergic neurons

We performed stereotactic surgery to induce selective UCN1 neuron ablation using leptin-conjugated saporin in C57BL6/J mice (n = 13). Periorbital hyperalgesia in response to intraperitoneal injection of 0.1 mg/kg CGRP or saline was assessed before and 2 weeks after the surgery. Centrally projecting EW/UCN1 positive cells were counted to evaluate the saporin-induced urocortinergic neuronal loss using diaminobenzidine immunohistochemistry.

2.2.4. Functional magnetic resonance imaging study

First, we performed the functional connectivity matrix analysis of EW in control humans, especially focused on the STN and DRN. Then, we compared it with interictal migraineurs' functional connectivity matrix. Finally, we examined the association between migraine frequency and the functional connectivity of EW.

2.3. Stereotaxic surgery in mice

Animals were anesthetized with i.p. ketamine-xylazine solution (16.6 mg/mL ketamine and 0.6 mg/mL xylazine-hydrochloride in 0.9% saline, 10 mL/kg) and fixed in a stereotaxic apparatus (David Kopf Instruments, Tujunga, CA).

For retrograde tracing, after a midline incision in the scalp and the nuchal skin, the muscles were detached from the occipital bone and reflected. Then, the posterior atlanto-occipital membrane was dissected and partially removed to visualize the spinal cord C1 segment that contains the STN. Under visual control using a surgical microscope, the glass capillary used for injection was moved 750 μm lateral to the posterior median sulcus in the midlevel of the space between the superior rim of the posterior arch of atlas and the inferior border of the occipital bone. Here, the tip of the capillary was perpendicularly introduced 100-μm deep into the laminae 2 to 3 of the STN. 2 × 20 nL of CTB (Cat. No.: #104; List Biological Laboratories, Campbell, CA) was injected in 2 steps with an automated injector. After 2 minutes, the needle was slowly removed. Finally, the muscles and the skin were sutured.

For anterograde tracing, AAV8 Syn EGFP (Addgene, Watertown MA, Cat. No.: 50465-AAV8; containing EGFP) was microinjected (2 × 10 nL) into EWcp. Here, we used the following stereotaxic coordinates from Bregma: posterior: −3.26; ventral: 3.35; lateral: 0. The injection was performed as described above for the STN, except that 1 minute after the injection, we lifted the needle by 0.5 mm, and upon additional 1 minute, it was slowly retracted from the brain, and the skin were sutured. Fourteen days after the surgery, both STN- and EWcp-injected animals were euthanized and transcardially perfused as described below.

2.4. Targeted toxin-induced lesion of centrally projecting Edinger–Westphal/urocortin 1 neurons

Saporin is a neurotoxin that enters neurons only if it is conjugated to a substance that is internalized by receptor-mediated endocytosis and irreversibly inhibits the cells' protein synthesis.[105] Given that in the EWcp, only UCN1 immunoreactive neurons express leptin receptor, leptin-conjugated saporin injection provides a reliable tool to perform selective UCN1 neuron ablation.[95,107] Fifty-nanolitre leptin-conjugated saporin (n = 13) (#KIT-47; ATS, Inc, Carlsbad, CA) was microinjected into the rostral (Bregma: posterior: −3.25; ventral: 3.75; lateral: 0) and caudal (Bregma: posterior: −3.75; ventral: 3.25; lateral: 0) part of the EWcp area. The injection was performed as described above for the anterograde tracer. Two weeks postinjection, mice were intraperitoneally injected with 0.1 mg/kg of either saline or CGRP, then subjected the von Frey assay. Mice were later perfused as described below. The neuronal loss was assessed and verified by UCN1 immunostaining. Two mice were excluded from this experiment because the histological assessment revealed that the injection path missed the EWcp area.

2.5. Light–dark box test

The light-aversive behavior was assessed using LDB test in the period between 30 and 60 minutes after 0.1 mg/kg i.p. injection of saline or CGRP.[68] Mice were individually tested in the LDB device, consisting of 2 compartments connected by a small opening. The one chamber was brightly lit (1000 lux), whereas the other one was dark. Mice typically move in and out of the dark because of their curiosity to explore the novel environment; however, upon CGRP treatment, they prefer the dark compartment, in case of headache-like pain and photophobia.[68] The time spent in the dark compartment was measured over 30 minutes to assess possible photophobia associated with migraine-like state.

2.6. Von Frey assay

Calibrated von Frey filaments were used to test periorbital hyperalgesia 30 minutes after 0.1 mg/kg i.p. injection of saline or CGRP. Each mouse was placed into a 10-cm-long restraining glass cylinder and allowed to poke out their heads and forepaws, but the restrainer prevented them from turning around.[30] Mice were allowed to habituate for 5 minutes. The filament was applied to the periorbital region of the face (the midline of the forehead at the level of the eyes) in an ascending manner starting from the 0.04 g filament. Briefly, if an animal did not respond, increasing filament forces were applied until the 0.6-g filament was reached or until a response was observed.[5] A positive response was defined as a sharp withdrawal of the head upon stimulation. Each filament was applied 5 times for 1 to 2 seconds with a 10-second interval. The periorbital withdrawal threshold was defined as the force at which the positive response occurred in 3 of 5 stimuli.[93]

2.7. Perfusion and tissue collection

Mice were euthanized by i.p. urethane (2.4 g/kg), then transcardially perfused with 20 mL of ice-cold 0.1 M phosphate-buffered saline (PBS) (pH 7.4) followed by 150 mL of 4% paraformaldehyde (PFA) solution in Millonig buffer (pH 7.4). Brain samples were dissected and postfixed for 72 hours in 4°C PFA solution. The brains were coronally sectioned using a Leica VT1000S vibratome (Leica Biosystems, Wetzlar, Germany). Four series of 30-μm sections were collected and stored in PBS containing sodium azide (0.01%) at 4°C, then for long-term storage in an antifreeze solution.

Four representative sections of the EWcp and lPAG (from Bregma −2.92 to −4.04), DRN (from Bregma −5.8 to −8.8 mm), and STN (spinal cord C1 segment) per animal were selected for each staining according to Paxinos.[77] The trigeminal ganglion were collected and stored in a 4% PFA solution.

2.8. Human brain samples

Subjects (n = 3) studied in this project had no diagnosed neurological or psychiatric disorders or brain trauma, died from any non–brain-related cause and did not show any signs of brain neuropathologies (supplementary material Table 1, http://links.lww.com/PAIN/C72). After the removal of brains, perfusion through cannula placed into the internal carotid, and vertebral arteries was performed within a time window of 3 to 4 hours postmortem. Perfusion was commenced with 1.5 L of 0.33% heparin containing physiological saline for 30 minutes, then with 4 to 5 L of a Zamboni fixative solution containing 4% PFA and 0.2% picric acid in phosphate buffer (pH 7.4) over a duration of 1.5 to 2 hours.

The study received ethical approval from the Regional and Institutional Committee of Science and Research Ethics of the Scientific Council of Health (ETT TUKEB 15032/2019/EKU) and was conducted in adherence to the principles of the Declaration of Helsinki.

Tissue samples of the mesencephalic ventral periaqueductal gray matter were microdissected. The EWcp and DRN areas were identified according to the Allen human brain atlas[21] and post-fixed in the Zamboni solution overnight.[92] The brain samples were sectioned for 30-μm thickness using a Leica VT1000S vibratome (Leica Biosystems); then, the sections were collected and stored in PBS containing sodium azide (0.01%) at 4°C. For long-term storage at −20°C, they were transferred into antifreeze solution.

2.9. RNAscope in situ hybridization

The pretreatment procedure was optimized for 30 μm-thick PFA-fixed sections.[55] Further steps (probe hybridization, signal amplification, and channel development) were performed according to RNAscope Multiplex Fluorescent Reagent Kit v2 user manual (ACD, Hayward, CA) to visualize the targets described in **Table 1**. Mouse (ACD; Cat. No.: 320881) and human triplex positive (ACD; Cat. No.: 320861) control probes and triplex negative (ACD; Cat. No.: 320871) control probes were tested on the samples. The triplex positive control probes gave well-detectable signal, whereas the negative control probes did not give any recognizable fluorescence in the preparations (images not shown).

2.10. Immunofluorescence

After washes, sections were treated with 0.5% Triton X-100 (Sigma Chemical, Zwijndrecht, the Netherlands) in PBS for 30 minutes, and nonspecific binding sites were blocked with 2% normal donkey serum in PBS. Then, sections were incubated with the primary antibody (**Table 2**) for 24 hours. The secondary antibody treatment (**Table 2**) was applied for 3 hours at room temperature. Sections were counterstained with 4′,6-diamidino-2-phenylindole (ACD) and mounted on gelatin-coated glass slides, air-dried, and cover-slipped with glycerol-PBS (1:1).

Table 1

RNAscope in situ hybridization mRNA targets, respective probes and fluorophores.

Target	Probes	Fluorophores
Crcp mRNA	*Crcp*-C3 (Cat. No.: 810161-C3, ACD)	Cyanine3 1:750
Ramp1 mRNA	*Ramp1*-C1 (Cat. No.: 532681, ACD)	Cyanine3 1:750
Ctr mRNA	*Calcr*-C2 (Cat. No.: 494071-C2, ACD)	Cyanine5 1:750
Crh1r mRNA	*Crh1r*-C1 (Cat. No.: 418011, ACD)	Cyanine3 1:750
Crh2r mRNA	*Crh2r*-C2 (Cat. No.: 413201-C2, ACD)	Cyanine3 1:750
NeuN mRNA	*Neun*-C3 (Cat. No.: 313311-C3, ACD)	Cyanine5 1:750
Ucn1 mRNA	*Ucn1*-C1 (Cat. No.: 466261, ACD)	Fluorescein 1:3000

2.11. RNAscope in situ hybridization combined with immunofluorescence

After the RNAscope procedure (see above), slides were treated with the primary antibody (**Table 2**) for 24 hours. After washing, the slides were incubated with secondary antibody (**Table 2**) for 3 hours at room temperature in dark and then counterstained with 4′,6-diamidino-2-phenylindole (ACD), air-dried, and cover-slipped with glycerol-PBS (1:1).

2.12. Whole mount c-fos gene–encoded protein immunostaining

After 3 days of postfixation in 4% PFA, mouse TRGs were washed with PBS for 24 hours, incubated with 0.5% Triton X-100 for 6 hours (Sigma, Zwijndrecht, the Netherlands), and blocked using 2% normal donkey serum in PBS for 2 hours. Then, TRGs were incubated with FOS primary antibody (**Table 2**) for 48 hours. After washes (4 × 15 minutes) in PBS, samples were incubated with the Cy3-conjugated donkey antirabbit secondary antibody for 24 hours (**Table 2**), followed by 4 × 15 minutes PBS washes.

2.13. Immunohistochemistry with diaminobenzidine

The neuronal activity was assessed in EWcp, lPAG, and STN by FOS immunohistochemistry. The neuronal loss upon EWcp/UCN1 neuron ablation was quantified by UCN1 immunohistochemistry.

Sections were treated with 1% H_2O_2 (Sigma), permeabilized with 0.5% Triton X-100 (Sigma), and blocked with 2% normal goat serum in PBS. Subsequently, sections were incubated with rabbit anti-FOS or anti-UCN1 antibody (**Table 2**) overnight at room temperature. After washes, sections were incubated with biotinylated antirabbit gamma globulin for 1 hour (1:200 VECTASTAIN Elite ABC-HRP Kit; Peroxidase Rabbit IgG Vector Laboratories Inc. Newark, CA, *Cat. No.: PK-6101*, produced in goat). Then, sections were incubated in avidin–biotin complex solution for 1 hour. After washes, the labeling was developed with 0.05% diaminobenzidine (DAB) in Tris buffer with 0.06% H_2O_2 (Sigma). The reaction was controlled under a stereomicroscope and stopped with Tris buffer. After washes, sections were

Table 2

Antibodies used for immunostainings.

Target	Primary antibodies	Secondary antibodies
GFP	Chicken anti-GFP (Cat. No.: A10262, Life Technologies) 1:1000	Alexa 488-conjugated donkey antichicken (Cat. No.: 703-546-155, Jackson) 1:500
CTB	Goat anti-CTB (Cat. No.: #703, List Biological Laboratories) 1:5000	Alexa 488-conjugated donkey antigoat (Cat. No.: 705-545-003, Jackson) 1:500
UCN1	Rabbit anti-UCN1 (Cat. No.: ab283503, Abcam) 1: 5000	Alexa 488-conjugated donkey antirabbit (Cat. No.: 711-545-152, Jackson) 1:500 or Cy3-conjugated donkey antirabbit (Cat. No.: 711-165-152, Jackson) 1:500
UCN1	Goat anti-UCN1 (Cat. No.: SC1825, Santa Cruz)1: 250	Alexa 488-conjugated donkey antigoat (Cat. No.: 705-545-003, Jackson) 1:500
GFAP	Mouse anti-GFAP (Cat. No.: NCLLGFAP-GA5, Novocastra) 1:1000	Cy3-conjugated donkey antimouse (Cat. No.: 715-165-150, Jackson) 1:500
IBA1	Rabbit anti-IBA1 (Cat. No.: 019-19,741, Wako Ltd) 1:1000	Alexa 647-conjugated donkey antirabbit (Cat. No.: 711-605-152, Jackson) 1:500
P-CREB	Rabbit anti-P-CREB (Cat. No.: #9191, Cell Signaling) 1:500	Cy3-conjugated donkey antirabbit (Cat. No.: 711-165-152, Jackson) 1:500
CALCRL	Rabbit anti-CALCRL (Cat. No.: 703811, Invitrogen) 1:250	Cy3-conjugated donkey antirabbit (Cat. No.: 711-165-152, Jackson) 1:500
NeuN	Mouse anti-NeuN (Cat. No.: MAB377, Sigma-Aldrich) 1:1000	Cy3-conjugated donkey antimouse (Cat. No.: 715-165-150, Jackson) 1:500 or Alexa 488-conjugated donkey antimouse (Cat. No.: 715-545-150, Jackson) 1:500
5-HT	Goat anti-5HT (Cat. No.: ab66047, Abcam) 1:2000	Alexa 488-conjugated donkey antigoat (Cat. No.: 705-545-003, Jackson) 1:500
TPH2	Rabbit anti-TPH2 (Cat. No.: 348003, Synaptic Systems GmbH) 1:500	Alexa 647-conjugated donkey antirabbit (Cat. No.: 711-605-152, Jackson) 1:500 or Alexa 488-conjugated donkey antirabbit (Cat. No.: 711-545-152, Jackson) 1:500
FOS	Rabbit anti-cFOS (Cat. No.: 226 003, Synaptic Systems GmbH) 1:2000	Cy3-conjugated donkey antirabbit (Cat. No.: 711-165-152, Jackson) 1:500
FOS	Guinea pig anti-cFOS (Cat. No.: 226 005, Synaptic Systems GmbH) 1:1000	Alexa 488-conjugated donkey antiguinea pig (Cat. No.: 706-545-148, Jackson) 1:500

5-HT, serotonin; CTB, cholera toxin subunit B; FOS, c-fos gene–encoded protein; GFP, green fluorescent protein; P-CREB, phosphorylated c-AMP–responsive element binding protein; TPH2, tryptophan hydroxylase-2; UCN1, urocortin 1.

mounted on gelatin-coated slides, air-dried, treated with xylene (Merck, Leicester, United Kingdom), and cover-slipped with Depex mounting medium (Merck).

2.14. Double-label immunofluorescence for c-fos gene–encoded protein and urocortin 1

Urocortin 1 and FOS immunofluorescence was applied to prove the urocortinergic identity of activated EWcp neurons. Sections were washed with PBS, incubated with 0.5% Triton X-100 (Sigma) in PBS for 30 minutes and treated with 2% normal donkey serum in PBS. Anti-UCN1 rabbit antibody (**Table 2**) and anti-cFOS guinea pig (**Table 2**) antibody cocktail was applied overnight, at room temperature. After washes, sections were incubated with Cy3-conjugated donkey antirabbit and Alexa 488-conjugated donkey antiguinea pig antisera (**Table 2**) for 3 hours. After washes, sections were mounted on gelatin-coated glass slides, air-dried, and cover-slipped with glycerol-PBS (1:1).

2.15. Microscopy, digital imaging, and morphometry

The diaminobenzidine-labeled sections were studied and digitalized using a Nikon Microphot FXA microscope with a Spot RT camera (Nikon, Tokyo, Japan). The number of FOS-positive nuclei was determined by manual cell counting on the whole cross-section surface area of the EWcp, lPAG and STN on 4 sections per animal. The average of these 4 values represented the FOS activation of one mouse in the given brain area. For the targeted ablation, the number of UCN1-positive neurons was determined by manual cell counting on the whole cross-section surface area of the EWcp on all sections per animal. The sum of these values represented the number of UCN1 neurons of one mouse in the EWcp.

Fluorescent-labeled sections were digitalized by an Olympus FluoView 1000 confocal microscope (Olympus, Europa, Hamburg, Germany) by sequential scanning in analogue mode. We used 3.5-μm optical thickness, 1024 $\times$ 1024-pixel resolution for scanning. The excitation and emission spectra for the respective fluorophores were selected using built-in settings of the FluoView software (FV10-ASW; Version 0102, Olympus Europa). 4′,6-Diamidino-2-phenylindole was excited at 405 nm, Cy3 at 550 nm, Cy5 at 650 nm, Fluorescein and Alexa 488 at 488 nm. Sections were scanned for the respective wavelengths at 4 channels. Digital images of the individual channels, depicting the same area, were automatically superimposed and merged.

The UCN1, TPH2, and 5-HT immunofluorescence and the confluent or cluster-like *Ucn1* RNAscope signal was measured by Image J software (version 1.42.; NIH, Bethesda, MD) in 5 to 20 cell bodies using 4 nonedited images of the corresponding channel. The region of interest was manually determined at cytoplasmic areas of neurons. The signal density was corrected for the background signal. The average of the specific signal density (SSD) of 5 to 20 neurons was determined in 4 sections per animal. The average of these 4 values represented the SSD value of one mouse. The SSD was expressed in arbitrary units.

In human samples, autofluorescence caused by lipofuscin accumulation disturbed the imaging. Because the lipofuscin accumulation is characteristic for the cytoplasm, but not for the karyoplasm, we show high-magnification images including the cross-section profiles of neuronal nuclei. With this strategy, nuclear mRNA signal dots get well-distinguishable from cytoplasmic lipofuscin-related autofluorescence that appears in all channels.

2.16. Statistical analysis

Data were expressed as mean ± SEM for each experimental group. Data sets were tested for normality by Shapiro–Wilk test[87] and evaluated using Student *t* test (**Table 3**). Data sets obtained in the experiment of targeted UCN1 neuron ablation were tested for homogeneity of variance and for normal distribution. Repeated-measures analysis of variance test was conducted to assess the effect of CGRP treatment before and after EWcp/UCN1 ablation (as within subject factor) on the pain threshold values, obtained in the von Frey test. The post hoc comparisons were performed by Tukey post hoc test. Analyses were performed with the software Statistica 8.0 (StatSoft, Tulsa, OK) ($\alpha = 5\%$).

Table 3

Summary of statistical results by Student *t* test analyses.

Measured parameters	*P*
Light dark box test	**0.02**
Von Frey test	**8.25×10^{-13}**
FOS-positive neurons in the TRG	**0.0004**
FOS-positive neurons in the STN	0.18
FOS-positive neurons in the lPAG	**0.002**
P-CREB–positive neurons in the STN	**0.003**
FOS positive neurons in the EWcp	**0.03**
Urocortinergic FOS immunopositive neurons in the EWcp	0.44
Ucn1 mRNA SSD in the EWcp	**0.0004**
UCN1 peptide SSD in the EWcp	**0.0007**
5-HT peptide SSD in the DRN	**0.03**
TPH2 peptide SSD in the DRN	**0.01**
UCN1 immunoreactive neurons in the EWcp upon LS-targeted ablation	**0.0002**

5-HT, serotonin; DRN, dorsal raphe nucleus; EWcp, centrally projecting Edinger–Westphal nucleus; FOS, c-fos gene–encoded protein; lPAG, lateral periaqueductal gray matter; LS, leptin-saporin; P-CREB, phosphorylated c-AMP-responsive element binding protein; SSD, specific signal density; STN, spinal trigeminal nucleus; TPH2, tryptophan hydroxylase-2; TRG, trigeminal ganglion; UCN1, urocortin 1. Significant values are highlighted in bold.

2.17. Functional magnetic resonance imaging

2.17.1. Participants

In the functional connectivity analysis, 35 migraine patients according to International Classification of Headache Disorders third edition[75] diagnosis of episodic migraine without aura (27 women and 8 men, mean age ± SD = 25.24 ± 4.35 years) and 41 healthy controls volunteers (25 women and 16 men, mean age ± SD = 26.00 ± 4.59 years) were included. All participants were screened by headache specialists, free from any serious medical, neurological (except migraine without aura) or psychiatric disorders, have not taken any daily medications (except oral contraceptives), and they were right handed. The fMRI experiment was carried out in the interictal period of migraine patients, and they were free from migraine attack 48 hours before and 24 hours after the fMRI session. Their average migraine frequency was 3.36 ± 3.11 attacks per month.

The human fMRI study protocol was approved by the Scientific and Research Ethics Committee of the Medical Research Council (Hungary) (23609-1/2011-EKU [747/PI/11], 23421-1/2015/EKU [0178/15]). The entire study was conducted according to the Declaration of Helsinki and with the written informed consent of each participant.

2.17.2. Functional magnetic imaging acquisition and seed region definition

The fMRI session started with the acquisition of a high-resolution structural data using T1-weighted 3D turbo field echo sequence and $1 \times 1 \times 1$ mm^3 resolution in a 3 T MRI scanner (Achieva 3 T; Philips Medical System, Eindhoven, the Netherlands). The resting-state fMRI session lasted 6 minutes when the participants were instructed to close their eyes but remain awake. The imaging data set acquisition parameters of T2*-weighted echo-planar imaging pulse sequence were the following: repetition time = 2.500 ms, echo time = 30 ms, field of view = 240×240 mm^2; with $3 \times 3 \times 3$ mm^3 resolution. The state-of-the-art preprocessing pipeline was applied on raw data based on previous analysis of the research group.[37]

After the preprocessing steps, seed-to-voxel analysis was conducted with the EW (Montreal Neurological Institute [MNI] coordinates: x = 0; y = −23; z = −7, radius: 2 mm). The seed definition was carried out based on literature data[108] and confirmed by the visual check of expert scientists. The spherical mask of the region was created using fslmaths command of FSL (Functional MRI of the Brain Software Library), whereas for the extraction of time-series data and subsequent computations of voxel-wise connectivity analysis, the NiBabel and NumPy modules were used. The seed-based connectivity map for each participant, established through voxel-wise Pearson correlation with the averaged seed region data, underwent transformation into Z-scores through Fisher transformation. These Z-score maps for each individual were subsequently employed in both within-group and between-group comparisons using the Statistical Parametric Mapping software package (Wellcome Department of Imaging Neuroscience, Institute of Neurology, London, United Kingdom). Given the fact that the EW is lying within the periaqueductal grey matter (PAG), we examined the extent to which we could differentiate its connectivity from those of the PAG using previously applied PAG seeds.[39] Both similarities and differences were revealed in its connections, which are detailed in the supplementary material (Figure S1 and Table S2, http://links.lww.com/PAIN/C72).

2.17.3. Functional connectivity analysis

The functional connectivity of EW was determined in whole-group analysis using one sample *t* test. After, 2 sample *t* test was conducted to compare the EW connectivity between migraine and control groups. A correlation analysis was used to investigate the relationship between migraine frequency and EW connectivity in migraine patients. To confirm the connection identified in animal experiments between EW with STN (MNI coordinates: left STN x = −6, y = −42, z = −48; right STN x = 6, y = −42, z = −48; radius: 4 mm) and DRN (from Harvard Ascending Arousal Network Atlas),[26] region-of-interest analysis was conducted with these 3 regions.

All analysis was corrected for sex, age, and motion by adding them as covariates of no interest. An initial threshold of $P < 0.001$ uncorrected for multiple comparison and at least 20 contiguous voxels was used in the whole-brain analyses. All reported results survived family-wise error correction at a cluster-level threshold of $p_{FWE} < 0.05$. In the ROI analysis, the initial threshold of $P < 0.001$ uncorrected for multiple comparison was used, and the reported results survived family-wise error correction at peak-level threshold of $p_{FWE} < 0.05$.

For data visualization, statistical maps of significant clusters were used as overlay on MNI 152 template brain in MRIcroGL.[82]

3. Results

3.1. Neuroanatomical qualitative studies

3.1.1. Amylin receptor1 and calcitonin gene–related peptide receptor components are expressed in the centrally projecting Edinger–Westphal, dorsal raphe nucleus and spinal trigeminal nucleus

To confirm that elevated central CGRP levels may directly affect the urocortinergic EWcp neurons, we performed RNAscope ISH for *Calcr*, *Ramp1*, and *Crcp* mRNA moreover immunofluorescence for CLR and UCN1. We proved that *Ramp1* and *Calcr* mRNAs coding for AMY1 components are coexpressed both in mouse and in human EWcp neurons (**Fig. 1**). Notably, the expression pattern of *Calcr* mRNA in the

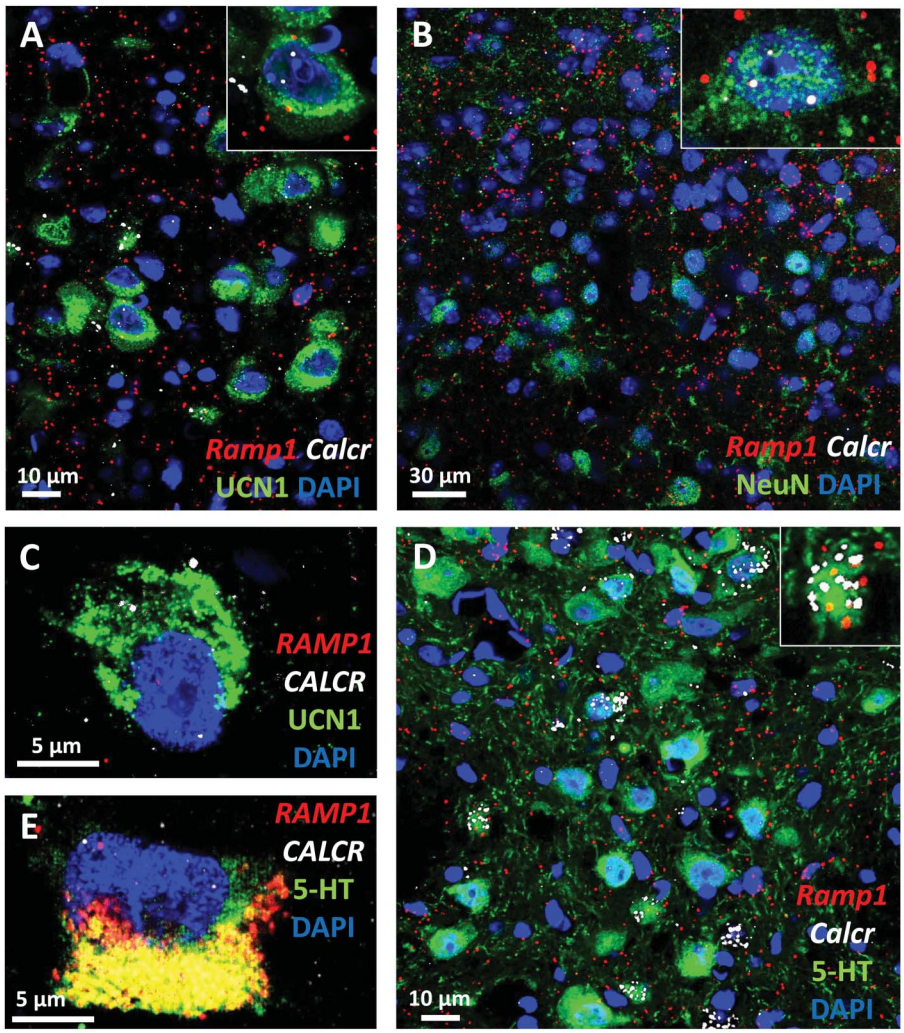

Figure 1. Calcitonin receptor (*Calcr*) and receptor activity–modifying protein 1 (*Ramp1*) mRNA expression. (A) Representative fluorescence images showing the *Calcr* (white) and *Ramp1* (red) mRNA transcripts coexpressed with urocortin 1 peptide (UCN1, green) in the mouse centrally projecting Edinger–Westphal (EWcp) nucleus. (B) Neurons (neuronal marker NeuN, green) of the mouse spinal trigeminal nucleus express both of *Calcr* (white) and *Ramp1* (red) mRNA. (C) Representative fluorescence images showing the *CALCR* (white) and *RAMP1* (red) mRNA transcripts coexpressed with UCN1 (green) in the human EWcp. (D) In the mouse dorsal raphe nucleus (DRN), the serotonin (5-HT, green) immunoreactive cells also contained *Calcr* (white) and *Ramp1* (red) mRNA transcripts. (E) In the human DRN, the 5-HT (green) immunoreactive cells also contained *CALCR* (white) and *RAMP1* (red) mRNA transcripts. The yellow cytoplasmic area in E corresponds to lipofuscin autofluorescence. Nuclear counterstaining was performed with 4′,6-diamidino-2-phenylindole (DAPI, blue).

EWcp suggests a substantial colocalization with UCN1 immunoreactive neurons. Moreover, almost all EWcp/UCN1 neurons were found to contain CLR (**Fig. 2**) and *Crcp* (**Fig. 3**) both in mice and humans.

In the DRN, RNAscope ISH in combination with immunofluorescence for *Calcr, Ramp1* (**Fig. 1**), and CLR (**Fig. 2**) as well as *Crcp* mRNAs (**Fig. 3**) were found to be expressed in TPH2-immunoreactive serotonergic and nonserotonergic neurons.

We detected *Calcr, Ramp1* (**Fig. 1**), and *Crcp* mRNAs (**Fig. 3**) in both neuronal and glial cells in the mouse STN laminae I to III. In addition, in line with an earlier study, the CGRP receptor component CLR was confirmed in both neurons[71] and astrocytes (**Fig. 4**).

3.1.2. Urocortinergic afferentation of the Crh1r- *and* Crh2r-*expressing spinal trigeminal nucleus neurons*

Anterograde and retrograde tracing studies were performed to investigate the possible urocortinergic projection from EWcp to STN. The accurate anatomical position of the injection site was

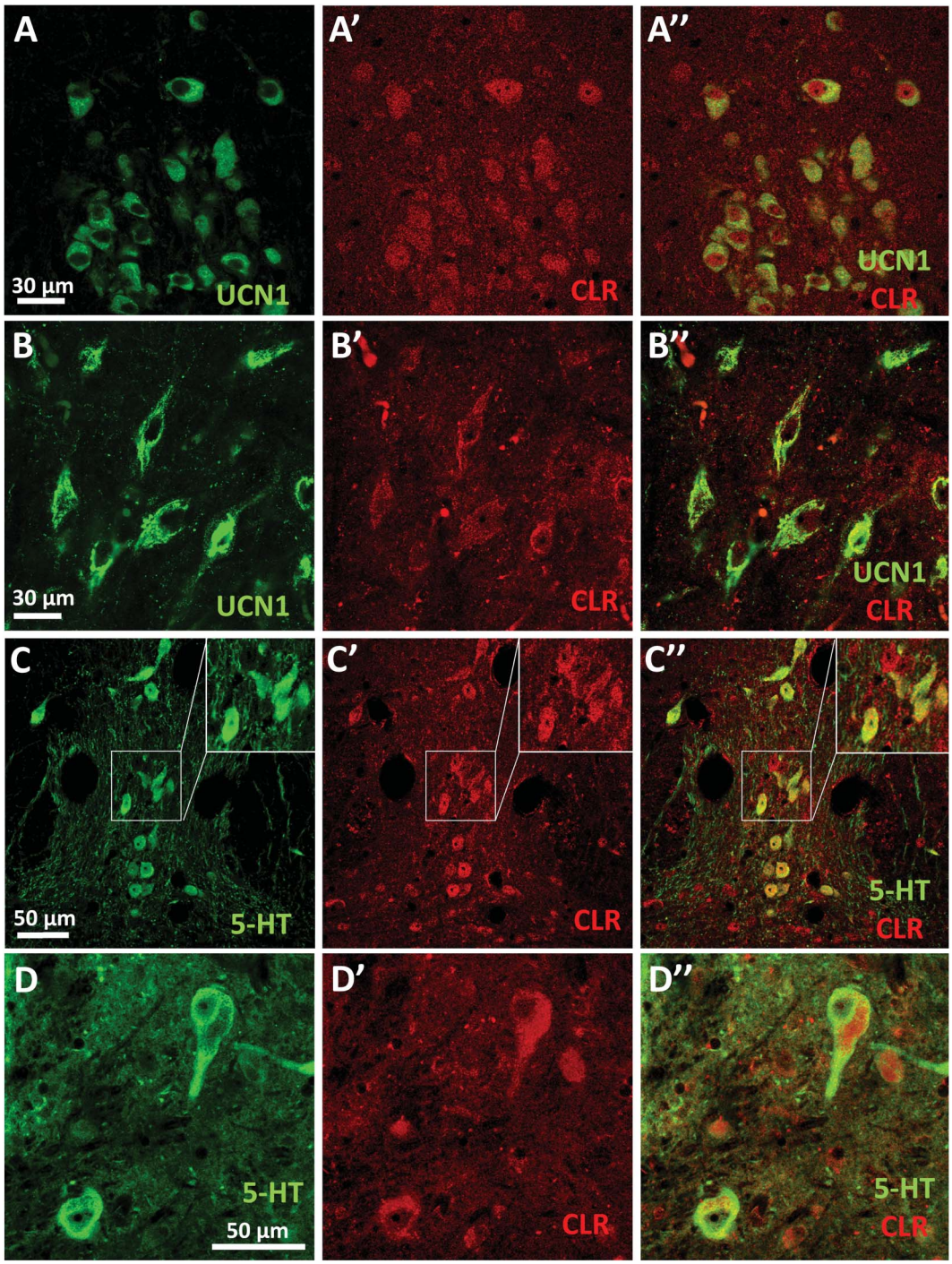

Figure 2. Calcitonin-like receptor (CLR) expression. (A–A″) Representative immunofluorescence images showing the CLR (red) coexpressed with urocortin 1 peptide (UCN1, green) in the mouse centrally projecting Edinger–Westphal (EWcp) nucleus. (B–B″) Representative immunofluorescence images showing the CLR (red) coexpressed with urocortin 1 peptide (UCN1, green) in the human EWcp. (C–C″) In the mouse dorsal raphe nucleus (DRN), the serotonin (5-HT, green) immunoreactive cells also contained CLR (red). (D–D″) In the human DRN, the 5-HT (green) immunoreactive cells coexpressed CLR (red).

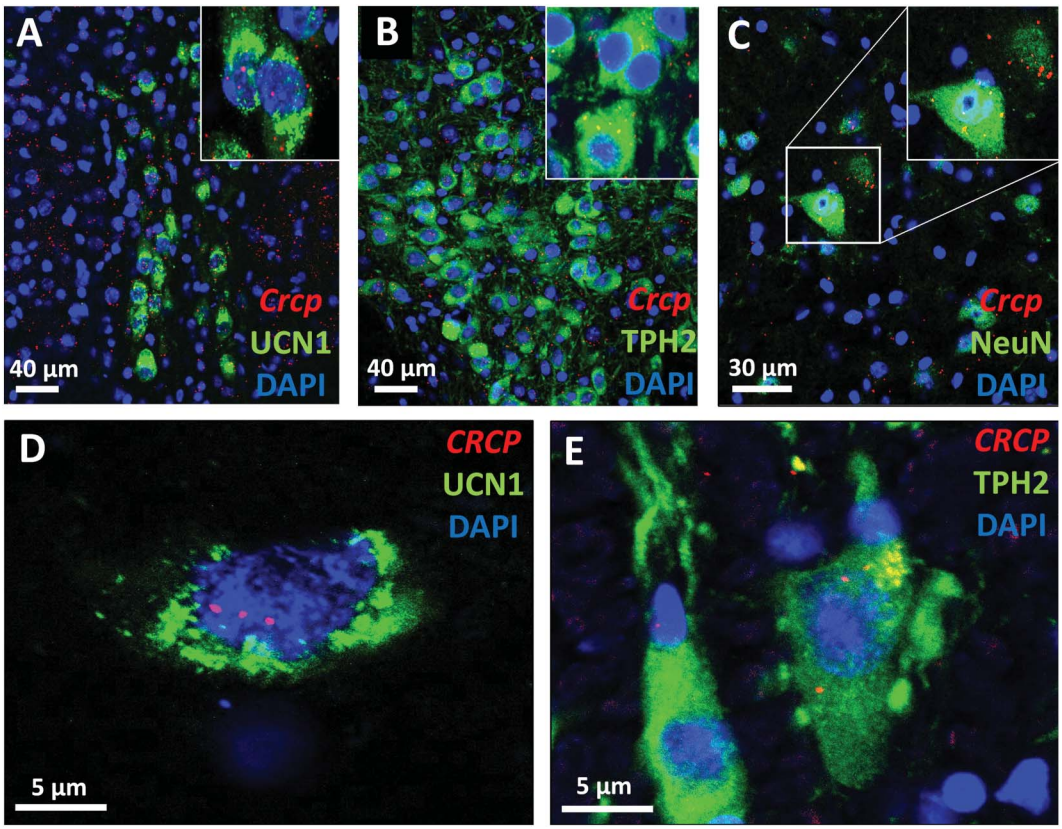

Figure 3. Calcitonin gene–related peptide receptor component (*Crcp*) mRNA expression. (A) Representative fluorescence images showing the *Crcp* mRNA transcripts (red) coexpressed with urocortin 1 peptide (UCN1, green) in the mouse centrally projecting Edinger–Westphal (EWcp) nucleus. (B) In the mouse dorsal raphe nucleus (DRN), the tryptophan hydroxylase-2 (TPH2, green) immunoreactive cells also contained *Crcp* mRNA transcripts (red). (C) Neurons (neuronal marker NeuN, green) of the mouse spinal trigeminal nucleus express also *Crcp* mRNA (red). (D) Representative fluorescence images showing the *CRCP* mRNA transcripts (red) coexpressed with UCN1 (green) in the human EWcp. (E) In the human DRN, the TPH2 (green) immunoreactive cells also contained *CRCP* mRNA transcripts (red). Nuclear counterstaining was performed with 4′,6-diamidino-2-phenylindole (DAPI, blue).

approved by GFP and CTB immunostaining in EWcp (**Fig. 5A**) and C1 spinal cord sections (**Fig. 5B**), respectively. Green fluorescent protein and UCN1 double-positive fibers were observed in the STN in samples of mice subjected to AAV8-GFP injection into the EWcp (**Fig. 5C**). Cholera toxin subunit B and UCN1 double-positive neurons were detected in EWcp after a CTB injection into the STN (**Fig. 5D**).

Next, we examined whether neurons in the laminae I to III of STN express *Crhr1* and *Crhr2*, and they are approached by UCN1-immunoreactive nerve fibres. RNAscope ISH for *Crh1r, Crh2r*, and *NeuN* mRNA was combined with UCN1 immunofluorescence. Neurons in STN laminae I to III expressed both *Crhr1* (**Fig. 5E**) and *Crhr2* (**Fig. 5F**) mRNAs, and they were juxtaposed by urocortinergic fibres.

3.2. Model validation

3.2.1. Light dark box test

Light–dark box test was performed to assess photophobia associated with migraine-like headache. Calcitonin gene–related peptide–treated mice spent significantly more time in the dark compared with the controls (Student *t* test, $P = 0.02$; **Fig. 6A**).

3.2.2. Von Frey test

Von Frey test was performed to assess periorbital pain behavior associated with migraine-like headache. Calcitonin gene–related peptide treatment significantly reduced the periorbital withdrawal threshold compared with saline (Student *t* test, $P = 8.25 \times 10^{-13}$; **Fig. 6B**).

3.2.3. Neuronal activation in the trigeminal ganglion, spinal trigeminal nucleus, and antinociceptive lateral periaqueductal gray matter

C-fos gene–encoded protein immunofluorescent labeling was performed to assess (1) the activation of the TRG neurons in the trigeminovascular nociceptive pathway and (2) the activation of the antinociceptive lPAG. To assess central sensitization and activation of STN neurons, immunofluorescence for FOS and P-CREB was performed.

Calcitonin gene–related peptide treatment resulted in a more than 10-fold increase in the number of FOS positive neurons in the TRG, compared with controls (Student *t* test, $P = 0.0004$) (**Fig. 6C**). In the STN, although CGRP treatment did not affect the FOS-positive neuron count (Student *t* test, $P = 0.18$), it increased the number of P-CREB (Student *t* test, $P = 0.003$) in laminae I to III (**Fig. 6D**). Calcitonin gene–related peptide treatment increased the FOS neuronal activation in the lPAG, compared with the control (Student *t* test, $P = 0.002$; **Fig. 6E**).

3.3. Activation of the centrally projecting Edinger–Westphal-circuit in the calcitonin gene–related peptide model

C-fos gene–encoded protein immunohistochemistry was performed to assess the neuronal activity of the EWcp.

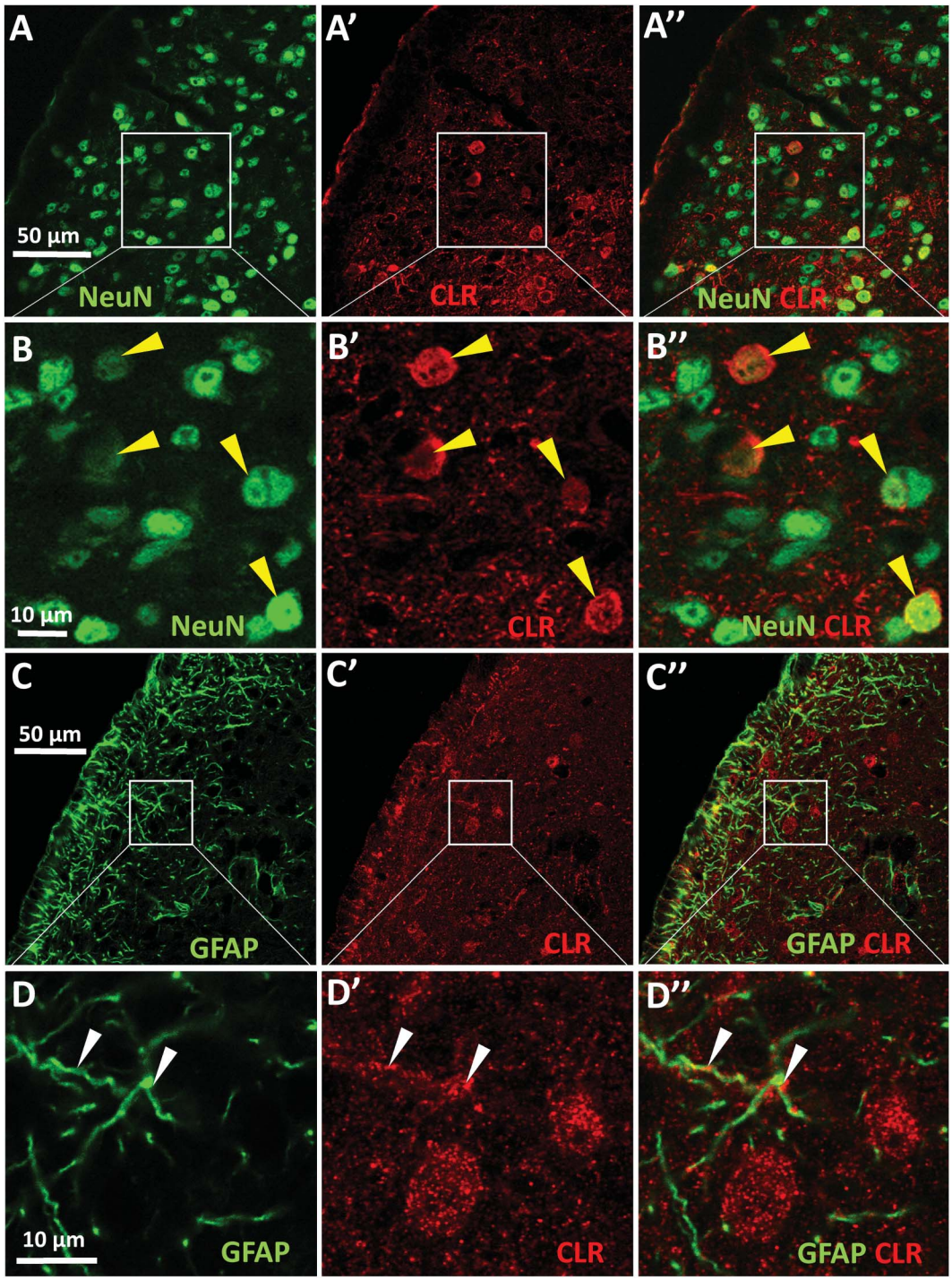

Figure 4. Calcitonin receptor-like receptor protein expression in mouse spinal trigeminal nucleus (STN). (A and B) The NeuN (green) labeling combined with CLR staining (red) revealed that a part of the STN neurons show also CLR immunoreactivity. Yellow arrowheads in the higher magnification images (B) depict the boxed areas in (A). (C and D) GFAP-CLR double labeling demonstrates that the GFAP (green)-immunoreactive astrocytes show also some CLR (red) immunopositivity. White arrowheads in the high magnification images in (D) demonstrating the marked areas in (C). The overlay images (A″–D″) in the right column demonstrate the colocalization of the labeled antigens. CLR, calcitonin-like receptor; GFAP, Glial fibrillary acidic protein.

Calcitonin gene–related peptide treatment resulted in an approximately 2-fold rise in the number of FOS-positive neurons, compared with the control (Student *t* test, $P = 0.03$; **Fig. 7A**).

By a double-label immunofluorescence, we found that most of the FOS immunoreactive nuclei were localized to UCN1 neurons (91.79%), suggesting that the urocortinergic EWcp cells were activated (**Fig. 7B**).

Indeed, combined RNAscope ISH and immunofluorescence analysis confirmed that in CGRP-treated animals, both the *Ucn1* mRNA (Student *t* test, $P = 0.0004$) expression (**Fig. 7C**) and UCN1 peptide immunosignal (Student's *t* test, $P = 0.0007$; **Fig. 7D**) was significantly higher than in controls.

In the DRN, CGRP treatment decreased both the 5-HT (Student *t* test, $P = 0.03$; **Fig. 8A**) and TPH2 (Student *t* test, $P = 0.01$; **Fig. 8B**) content of the serotonergic neurons.

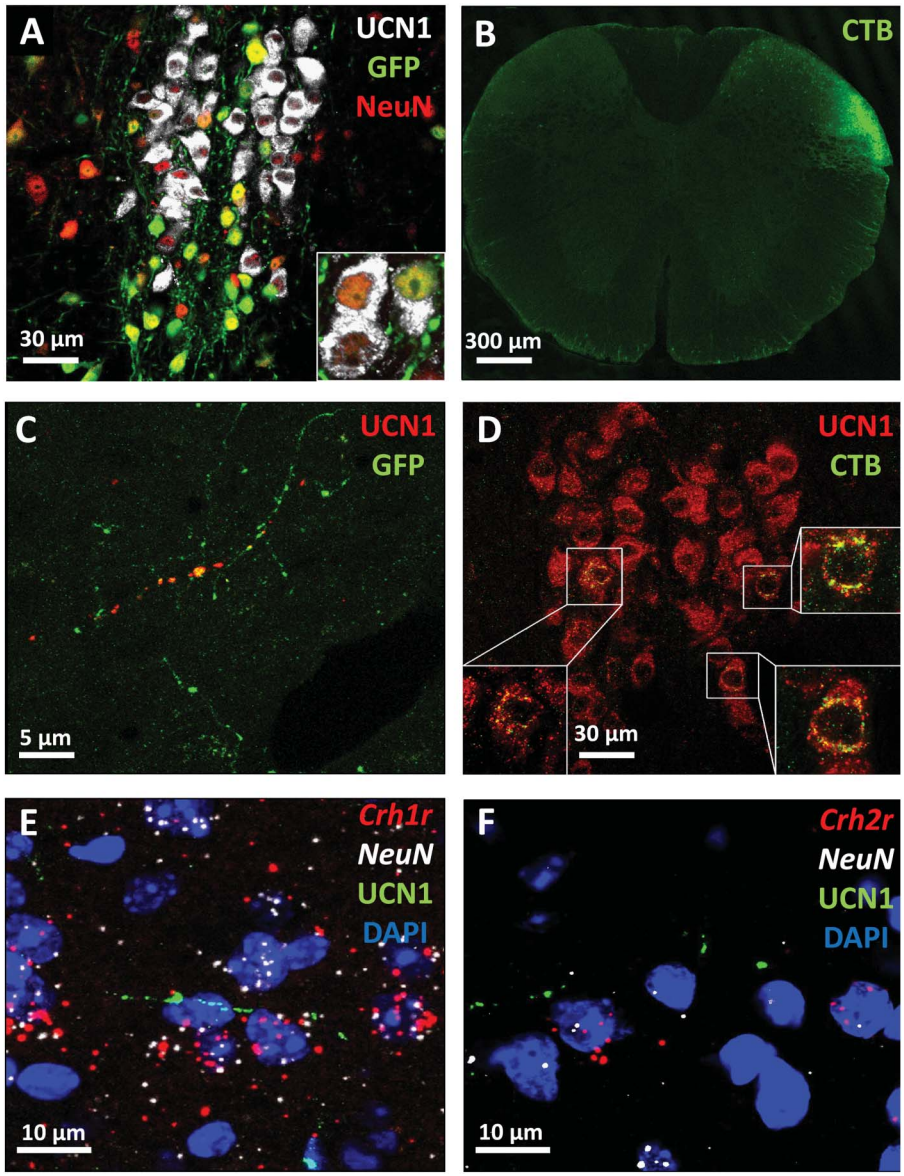

Figure 5. Urocortinergic afferentation from the centrally projecting Edinger–Westphal (EWcp) nucleus to the spinal trigeminal nucleus (STN). (A) Representative images showing the injection site of AAV8 Syn-enhanced green fluorescent protein (EGFP) by GFP (green) immunofluorescence in the EWcp urocortinergic (urocortin 1 [UCN1], white) neurons. All of the virus-infected cells are neurons (neuronal marker: NeuN, red), note the UCN1 and NeuN colocalization (yellow). (B) Fluorescence labeling for cholera toxin subunit B (CTB) in the dorsal horn of STN. (C) The colocalization of UCN1 (red) with GFP (green) in a nerve fiber in the STN and (D) the colocalization of UCN1 (red) with CTB (green) in the EWcp neurons. (E) Cells coexpressing neuronal marker mRNA (*NeuN*, white) and corticotropin-releasing hormone receptor 1 mRNA (*Crhr1*, red) as well as (F) corticotropin-releasing hormone receptor 2 (*Crhr2*, red) receiving a UCN1 (green)-positive afferentation in the STN. Nuclear counterstaining was performed with 4′,6-diamidino-2-phenylindole (DAPI, blue).

3.4. Ablation of centrally projecting Edinger–Westphal/ urocortin 1 neurons with leptin-conjugated saporin

Urocortin 1 immunohistochemistry was performed to confirm EWcp/UCN1 neuron loss. Leptin-conjugated saporin treatment significantly reduced the number of UCN1 immunoreactive neurons in the EWcp compared with the naive mice (P = 0.0002) (**Fig. 9A**). Von Frey test was performed to assess periorbital pain behavior associated with migraine-like headache. Before the ablation of EWcp/UCN1 neurons, CGRP treatment significantly reduced the periorbital withdrawal threshold compared with saline (P = 0.0001). Interestingly, after the ablation of EWcp/UCN1 neurons, the saline treatment significantly reduced periorbital withdrawal threshold compared with nonablated controls, (P = 0.0001), and CGRP treatment did not change it further (**Fig. 9B**).

3.5. Functional magnetic resonance imaging study

3.5.1. Functional connectivity of Edinger–Westphal nucleus

Extensive positive functional connectivity of the EW nucleus with frontal and temporal gyri, cerebellum, caudate, and midbrain were identified in the whole population (**Fig. 10** and **Table 4**). No significant negative connections were detected.

Extensive positive functional connectivity of the EW nucleus with frontal and temporal gyri, cerebellum, caudate, and midbrain were identified in the whole population (**Fig. 10** and **Table 4**). In accordance, significant positive functional connectivity was found between the EW and DRN (Peak pFWE = 0.004; Peak Z-value = 3.51, Peak MNI coordinates: x = 0, y = −28, z = −14) as well as STN (Peak pFWE = 0.007; Peak Z-value = 3.10, Peak MNI coordinates: x = 4, y = −40,

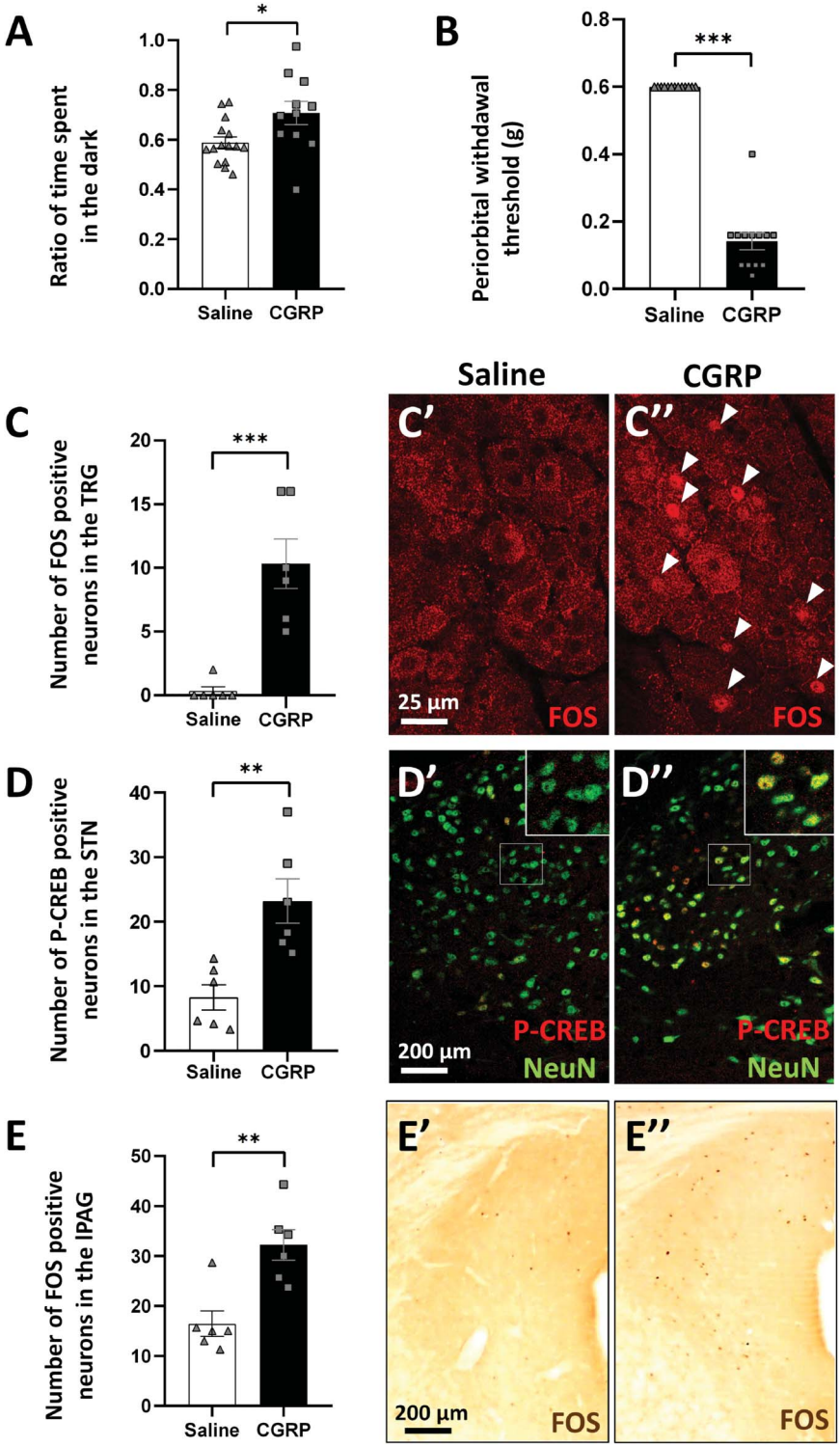

Figure 6. Model validation. (A) Columns show the ratio of time spent in the dark compartment of the light–dark box device, 30 minutes after saline (control) or calcitonin gene–related peptide (CGRP) injection (n = 11-15, $^{*}P = 0.02$; Student *t* test). (B) Columns show the facial withdrawal threshold (g) in von Frey test, 30 minutes after saline (control) or CGRP injection (n = 13, $^{***}P = 8.25531 \times 10^{-13}$; Student *t* test). (C) Columns show the number of FOS positive neurons in the TRG (n = 6; $^{***}P = 0.0004$; Student *t* test). (C′ and C″) Representative fluorescence images showing the expression of FOS, as a marker of early neural activation in the trigeminal ganglion (TRG), 4 hours after saline (control) and CGRP injection. Nuclei of FOS-positive activated neurons (red) are highlighted by the white arrowheads. (D) Columns show the number of phosphorylated c-AMP–responsive element binding protein (P-CREB) positive neurons in the spinal trigeminal nucleus (STN) (n = 6; $^{**}P = 0.003$; Student *t* test). (D′ and D″) Representative fluorescence images showing the expression of P-CREB, as a marker of neural activation in the STN, 4 hours after saline (control) and CGRP injection. Nuclei of P-CREB–positive activated neurons (red) are colocalized (yellow) with the neuronal marker (NeuN, green). (E) Columns show the number of FOS-positive neurons in the lateral periaqueductal gray matter (lPAG; n = 6; $^{**}P = 0.002$; Student *t* test). (E′ and E″) Representative images showing the nuclei (brown dots) of activated FOS-positive neurons in the lPAG in control and CGRP-treated mice. FOS, c-fos gen–encoded protein; STN, spinal trigeminal nucleus.

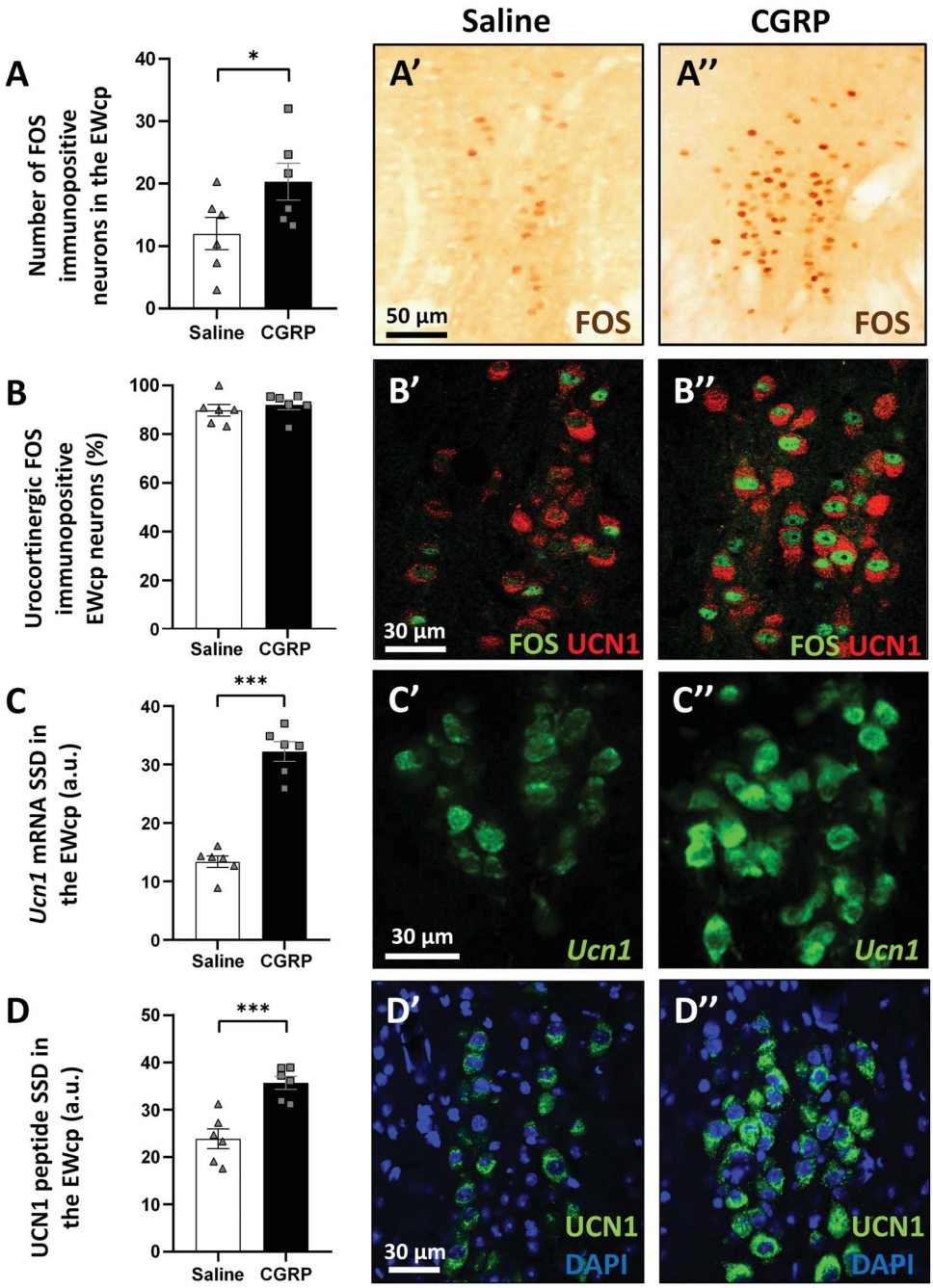

Figure 7. Response of the mouse centrally projecting Edinger–Westphal (EWcp) nucleus to calcitonin gene–related peptide (CGRP) treatment. (A) Columns show the number of FOS-immunoreactive neurons in the EWcp (n = 6; **P* = 0.03; Student *t* test). (A′ and A″) Representative images showing the nuclei of the neurons positive (brown dots) for the early neural activation marker (FOS) in the EWcp, 4 hours after saline (control) or CGRP injection. (B) Quantitative evaluation of the ratio of urocortin 1 (UCN1)/FOS double-labelled neurons from all FOS-immunoreactive neurons in the EWcp revealed the urocortinergic identity of activated (FOS-immunoreactive) neurons. (B′ and B″) Representative fluorescence images showing the colocalization of UCN1 (red) and FOS (green) in the EWcp of control and CGRP-injected mice. (C) Quantitative evaluation of *Ucn1* mRNA-specific signal density (SSD) in the EWcp (n = 6; ****P* = 0.00045; Student *t* test). (C′ and C″) Representative fluorescence images showing the expression of *Ucn1* mRNA (green) in the EWcp in control and CGRP-treated mice. (D) Quantitative evaluation of UCN1 peptide SSD in the EWcp (n = 6; ****P* = 0.0007; Student *t* test). (D′ and D″) Representative images illustrate UCN1 peptide (green) immunoreactivity in the EWcp in control and CGRP-injected mice. For nuclear counterstaining, 4′,6-diamidino-2-phenylindole (DAPI, blue) was used. a.u., arbitrary unit; FOS, c-fos gene–encoded protein.

z = −44) in whole group analysis. No significant negative connections were detected.

There was no significant difference between interictal migraine patients and healthy controls in the functional connectivity of EW nucleus after correction for multiple testing.

However, positive correlation was found between migraine frequency and functional connectivity of EW nucleus with 2 clusters. One cluster (cluster size = 123 voxel, pFWE = 0.045) contained the angular gyrus (Peak T-value = 4.211, Peak MNI coordinates: x = 54, y = −52, z = 26) and superior temporal gyrus (Peak T-value = 3.961, Peak MNI coordinates: x = 58, y = −40, z = 22), whereas the other cluster (cluster size = 166 voxel, pFWE = 0.011) contained the middle frontal (Peak T-value = 3.994, Peak MNI coordinates: x = 54, y = 34,

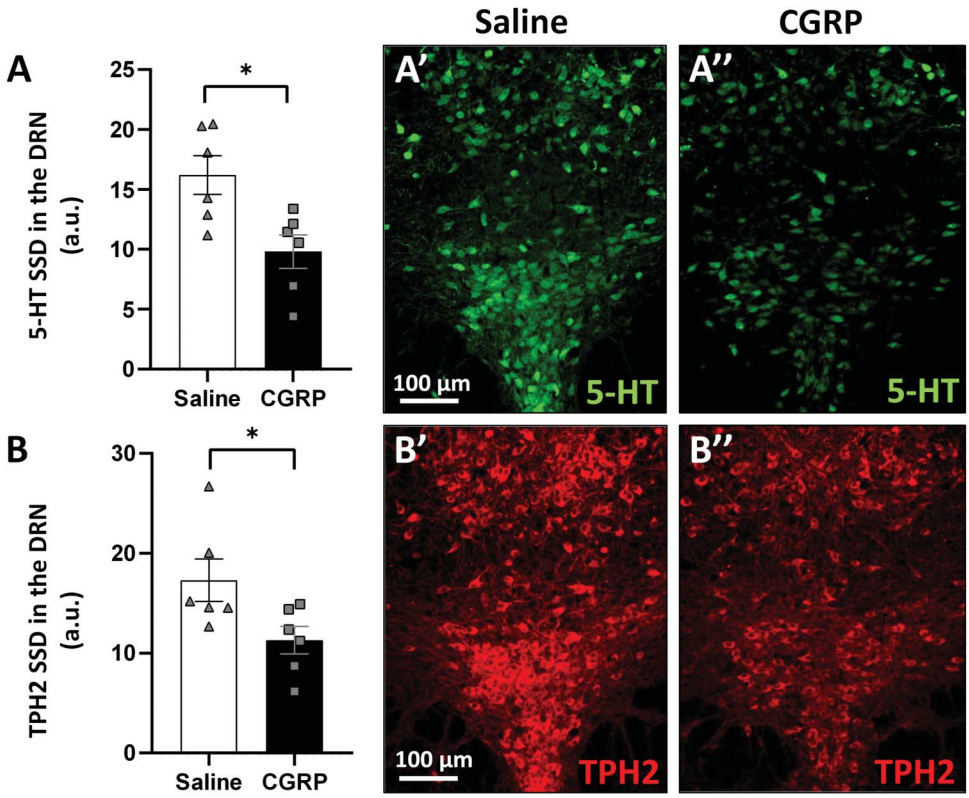

Figure 8. Serotonin (5-HT) and tryptophan hydroxylase-2 (TPH2) immunoreactivity in the dorsal raphe nucleus (DRN). (A) Specific signal density (SSD) of 5-HT in the DRN (n = 6; *P = 0.03; Student t test). (A′ and A″) Representative fluorescence images showing the 5-HT (green) immunoreactivity in the DRN, 4 hours after saline (control) and calcitonin gene–related peptide (CGRP) injection. (B) SSD of the TPH2 in the DRN (n = 6; *P = 0.01; Student t test). (B′ and B″) Representative fluorescence images illustrate TPH2 (red) immunosignal in the DRN. a.u., arbitrary unit.

z = 22) and triangular part of inferior frontal gyri (Peak T-value = 4.189, Peak MNI coordinates: x = 48, y = 30, z = 14; **Fig. 11**).

4. Discussion

The main goal of this study was to confirm the involvement of EWcp in migraine. The central distribution of CGRP and that of its receptor has been described at protein level in rats, mice, and humans.[27,43,64] However, CGRP receptors AMY1 and CGRP receptor components expression in EWcp has not been studied yet. Here, we have confirmed the expression of *Ramp1*, *Calcr*, and *Crcp* mRNA as well as CLR peptide in EWcp/UCN1 neurons using the highly sensitive and specific RNAscope ISH technique combined with immunofluorescence[101] in both mice and humans. This supports the translational relevance of our animal work and confirms findings of earlier mRNA studies.[27,64] Because AMY1 and CGRP receptor components were also detected in the migraine-related EWcp projection areas such as DRN and STN, we assume that the CGRP may activate the DRN and STN directly or indirectly through AMY1 and CGRP receptor-expressing EWcp/UCN1 neurons. Indeed, both our anterograde and retrograde tracing proved the direct projection from the EWcp to the STN. Because urocortinergic fibers were detected in the close proximity of STN neurons, which expressed *Crh1r* and *Crh2r* mRNAs, we provide neuroanatomical evidence for a direct urocortinergic EWcp projection to STN neurons with a possible functional significance.

Next, we investigated the response of EWcp in a migraine model. Several well-validated in vivo models were described, including direct electrical stimulation of trigeminal neurons, administration of inflammatory substances to the meninges, and the use of algogenic substances (eg, nitroglycerin, CGRP).[41] Importantly, the CGRP signaling is involved in all these models.[104] Electrical stimulation of TRG and meningeal administration of inflammatory substances are invasive, and considering the acute pain sensitivity of EWcp,[56,84] these models were not suitable. Intraperitoneal administration of nitroglycerin and CGRP successfully resembled many aspects of acute and chronic migraine[41,53] in rodents that were alleviated by antimigraine drugs like sumatriptan.[9,30,81,104] In our project, the use of nitroglycerin would have been unreliable because all available preparations contain ethanol as vehicle,[9,30,53] and the EWcp is highly alcohol sensitive.[1,109] Therefore, we decided to use the intraperitoneal CGRP treatment model of migraine described by Mason et al.[68] Several migraine-related symptoms have been observed upon central and peripheral CGRP administration in humans and rodents,[52,60,68] suggesting both peripheral and central site of action; this is in line with the wide distribution of CGRP and AMY1 receptors in the CNS and periphery.[27,45] TRG neurons express CGRP and its receptor, and TRG provide anatomical connection between peripheral and CNS. Activation of CGRP receptors in trigeminal neurons stimulate CGRP release from (1) peripheral nerve endings of afferent terminals, which innervate meninges, (2) TRG cell bodies, and (3) terminals of central processes in the STN.[25] Calcitonin gene–related peptide release from central terminals promote central sensitization through CGRP receptors on second-order nociceptive STN cells,[25,46] which may ultimately lead to further central CGRP release from CGRP-expressing brain areas. This is one mechanism for central sensitization mediated by peripheral action of CGRP, but several others may also contribute.[45,46,68]

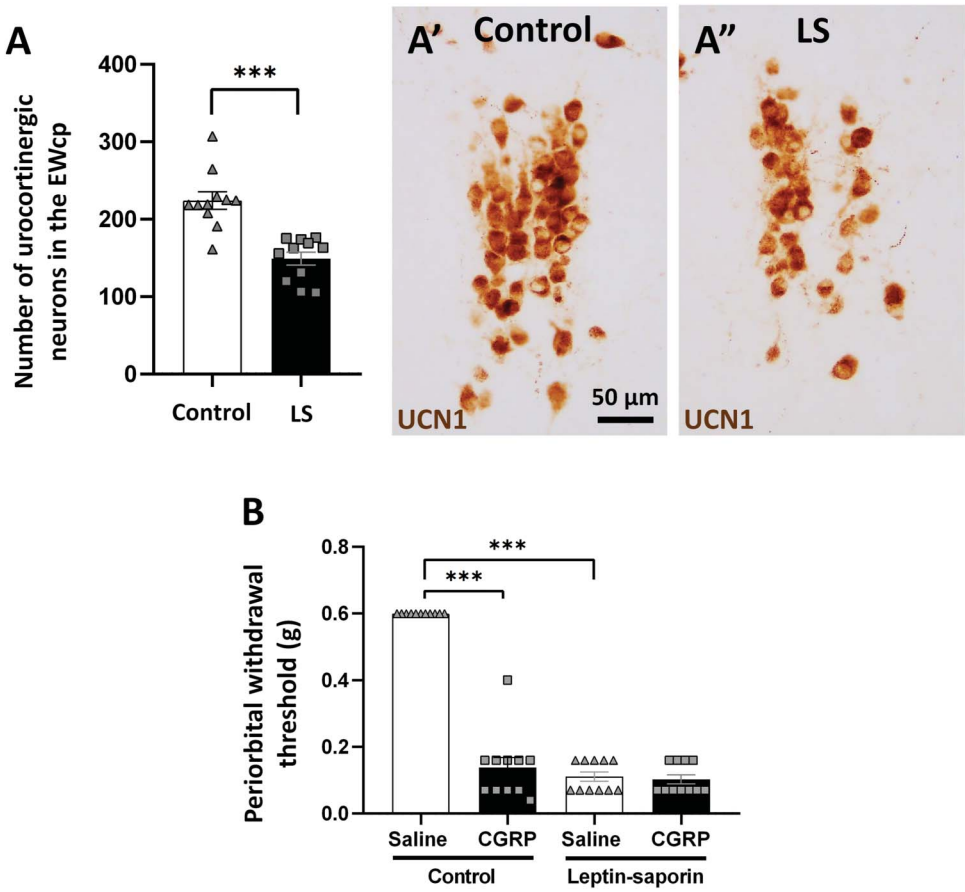

Figure 9. Ablation of urocortinergic (urocortin 1 [UCN1]) neurons in the centrally projecting Edinger–Westphal (EWcp) nucleus by leptin-saporin (LS). (A) Columns show the number of UCN1 neurons in the EWcp (n = 11; ***P = 0.0002; Student t test) in controls and LS-injected groups. (A′ and A″) Representative images showing the UCN1 neurons (brown) in the EWcp, in control and LS-injected mice. (B) Columns show the facial withdrawal threshold (g) in von Frey test, 30 minutes after saline or calcitonin gene–related peptide (CGRP) injection in control and LS-injected mice (n = 11, ***P = 0.0001; Tukey post hoc test upon repeated-measures ANOVA. ANOVA, analysis of variance.

The CGRP model[68] was validated by the periorbital hyperalgesia and light aversion behavior. According to Mason et al., calcitonin gene–related peptide treatment did not induce anxiety in mice; thus, the LDB behaviour can be considered as photophobia, referring to a migraine-like state. Furthermore, CGRP-induced light aversion did not correlate with the blood pressure excluding vasomotor mechanisms.[69]

The elevated TRG/FOS and STN/P-CREB immunosignals upon CGRP treatment refers to the activation of these key players in migraine pathogenesis.[29,46] Increased lPAG/FOS immunosignal in CGRP-treated mice suggests that the activation of the descending antinociceptive pathways further reinforce that a migraine-like headache has occurred.

The neuromodulatory role of PAG in migraine is well known,[73,99] but no studies have reported the contribution of EWcp to migraine, although it is located within the PAG. The twofold increase in the number of FOS-positive EWcp/UCN1 neurons upon CGRP treatment suggests increased neuronal activation that requires adaptation at the level of gene expression.[1,36] This was concomitant with an increased *Ucn1* mRNA and UCN1 peptide content in response to CGRP administration, suggesting higher UCN1 peptide release. We propose that peripherally administered CGRP may activate the EWcp/UCN1 neurons directly by centrally released CGRP or by indirect manner as a consequence of central sensitization. The presumably increased UCN1 release may directly influence the function of the STN through CRH1R and CRH2Rs, as supported by increased P-CREB immunosignal in the STN. In line with earlier studies,[11,12] no FOS activation was observed in the STN upon CGRP treatment.

Beyond the STN, the DRN is also a brain area known to be activated in migraine.[88] The EWcp/UCN1 neurons innervate the DRN,[23,97,109] where both CRH receptors are expressed.[14,64,96,97] Activation of CRH1R in DRN reduces 5-HT release, whereas CRH2R signaling has opposite effect.[33,63] The decreased DRN/5-HT content in our CGRP-treated mice suggests that 5-HT release upon CGRP administration. Supporting this, elevated CNS 5-HT levels were found during migraine attacks.[17,24,80,89] We propose that CGRP increased the UCN1 release in the DRN that through CRH2Rs of DRN/5-HT neurons ultimately elevated 5-HT release. Nevertheless, we cannot exclude a direct CGRP effect on serotonergic neurons as they also express CGRP receptors.[64]

Calcitonin gene–related peptide treatment decreased the TPH2 enzyme level in DRN. Tryptophan hydroxylase-2 is the rate-limiting enzyme of central 5-HT synthesis,[100] and its gene polymorphisms have been linked to migraine.[51,67] Chronic central UCN1 microinjection elevated the *Tph2* mRNA expression in the caudal and dorsal subdivision of the DRN, whereas an opposite effect was observed in the ventrolateral part.[22] This finding is in contrast with our results as we saw a rise in UCN1 levels but decreased the TPH2 protein content upon CGRP

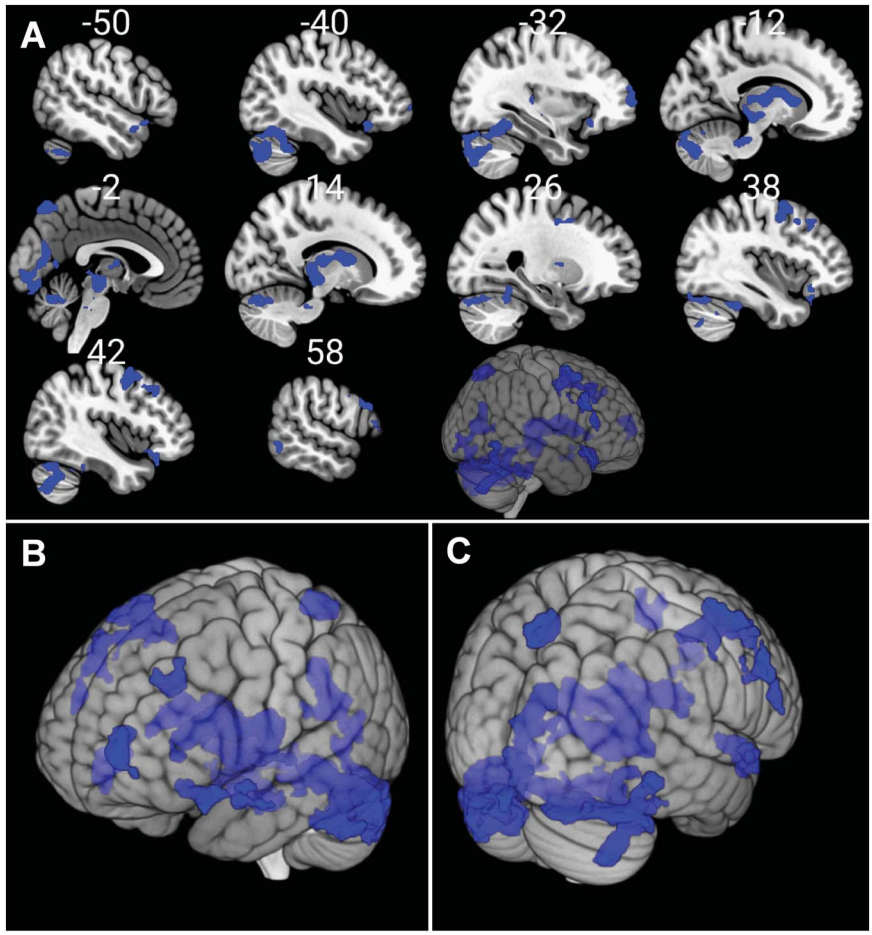

Figure 10. Functional connectivity matrix of Edinger–Westphal nucleus. Blue color represents functional connectivity of Edinger–Westphal nucleus with other brain areas: (A) sagittal reconstruction, lateral view; (B) left anterior aspect; (C) right posterior view. Significance threshold was cluster-level p(FWE) < 0.05 including at least 10 contiguous voxels. Results are corrected for age and sex. Statistical maps were visualized on the MNI 152 template brain provided in MRIcroGL (http://www.mccauslandcenter.sc.edu/mricrogl/). MNI, Montreal Neurological Institute.

treatment. This discrepancy may be explained by methodological differences as in our study, we examined the TPH2 at protein level. Conversely, we applied a single CGRP treatment, which elevated the UCN1 level, whereas Donner et al.[22] applied chronic UCN1 administration. Thirdly, a DRN subdivision-specific difference in CRH2R expression, moreover a stress exposure-dependent change in the CRH1R and CRH2R receptor trafficking and consequent ligand availability in the plasma membrane.[103] may explain the difference in the outcome of these studies. All in all, the complex action of UCN1 on DRN serotonergic neurons may reflect the proclaimed abnormalities in central 5-HT turnover in migraine.[24,80]

Given that the cocaine and amphetamine-regulated transcript and EWcp/UCN1 show full colocalization,[78,109] decreased periorbital withdrawal threshold following EWcp/UCN1 ablation aligns with earlier study result where increased the activity of EWcp/cocaine and amphetamine-regulated transcript resulted in increased paw withdrawal threshold, suggesting that these neurons modulates pain.[78]

The ability of EWcp to influence migraine-related areas through direct neuroanatomical connection was further supported by the significant positive functional connectivity between EW, DRN, and STN. To the best of our knowledge, this is the first study to describe the functional connectivity of EW in the human brain. Moreover, our fMRI study revealed a strong positive correlation between the frequency of migraine attacks and the functional connectivity of EW with brain areas that are known to be part of the affective pain pathway including angular gyrus, superior temporal gyrus, middle frontal and the triangular part of inferior frontal gyri,[48,76,102] supporting previous findings that changes in these brain areas may predispose a person to pain conditions including migraine.[48]

As to the limitations, none of the models for migraine can reliably mimic all aspects of human disease and the CGRP model is also not an exception. Although migraine is more prevalent in females,[83] we used male mice because (1) EWcp/UCN1 neurons express estrogen receptor beta and estrous cycle-related hormonal fluctuations modulate UCN1 levels[18,19] and (2) 0.1 mg/kg CGRP induced migraine-like symptoms in both male and female mice.[68,81] Our fMRI study recruited male and female migraineurs only during the interictal period; thus, the results do not reflect the brain status during the active headache episodes. This may explain the lack of significant difference in the functional connectivity of EW between the study groups. Edinger–Westphal seed has not been described earlier.[89] In this study EW seed definition was carried out based on recent literature data[108] and confirmed by the visual check of expert scientists.

With respect to the limitations above, we conclude that the EWcp was activated in the CGRP model of migraine associated with increased *Ucn1* mRNA expression and UCN1 peptide content in male mice. We found a direct EWcp-derived urocortinergic input to the STN and demonstrated that the STN

Table 4

Significant positive functional connectivity of Edinger–Westphal nucleus.

Cluster size (voxel)	Region	Peak coordinates			Peak
		x	y	z	T-value
5518	L thalamus	−2	−24	−8	17.99
	R lingual gyrus	12	−24	−6	5.882
	R caudate	14	−2	14	5.474
	L caudate	−10	10	6	4.91
	R thalamus	10	−20	10	4.69
	R pallidum	22	0	6	4.62
221	R precuneus	2	−72	56	5.410
319	L posterior cingulate cortex	−10	−34	−30	5.084
	R cerebellum III	12	−30	−30	4.672
1524	R cerebellum VI	36	−40	−28	5.027
	R cerebellum crus 2	42	−70	−44	4.660
278	R orbital part of inferior frontal gyrus	32	26	−14	4.973
596	R middle frontal gyrus	50	14	52	4.906
	R precentral gyrus	36	0	48	4.700
247	L superior temporal pole	−42	20	−16	4.905
173	L middle frontal gyrus	−24	28	34	4.534
196	R triangular part of inferior frontal gyrus	54	28	14	4.364
	R opercular part of inferior frontal gyrus	56	20	38	3.952
132	L middle temporal gyrus	−68	−30	−6	4.349
342	R medial part of superior frontal gyrus	2	56	34	4.331
	L medial part of superior frontal gyrus	0	52	46	3.898
230	L middle frontal gyrus	−30	60	8	4.159
	L orbital part of middle frontal gyrus	−38	56	−2	3.468

Reported results are significant at cluster-level $p_{FWE} < 0.05$. Coordinates are in Montreal Neurological Institute (MNI) space.
L, left hemisphere; R, right hemisphere.

and DRN neurons express *Crh1r* and *Crh2r* mRNAs. Hence, we propose that elevated central CGRP and increased UCN1 release from EWcp/UCN1 neurons in response to CGRP may directly modulate the function of STN and DRN. This suggests the role of EWcp in the endogenous response to migraine. In line with these, we have also revealed a significant positive functional connectivity between EW and STN as well as DRN by fMRI in humans. In our ongoing research, we are investigating the EWcp/UCN1 in antimigraine therapy too.

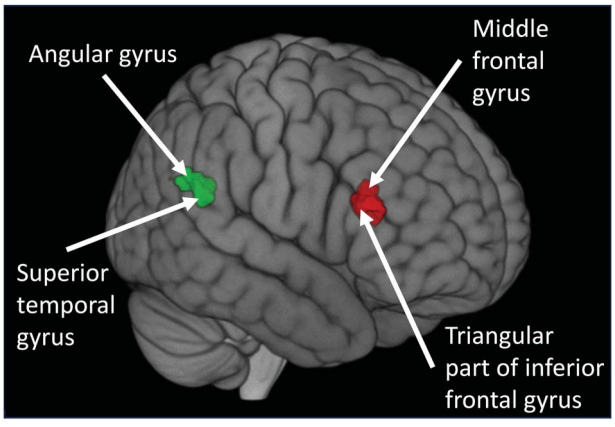

Figure 11. Brain clusters where functional connectivity of Edinger–Westphal nucleus positively correlated to migraine frequency. The green area represents the first cluster containing the angular gyrus and superior temporal gyrus, whereas red area is the other cluster containing the middle frontal and triangular part of inferior frontal gyri. Significance threshold was cluster-level p(FWE) < 0.05 including at least 10 contiguous voxels. Results are corrected for age and sex. Statistical maps were visualized on the MNI 152 template brain provided in MRIcroGL (http://www.mccauslandcenter.sc.edu/mricrogl/). MNI, Montreal Neurological Institute.

Conflict of interest statement

The authors declare that the research was conducted in the absence of any commercial or financial relationships that could be construed as a potential conflict of interest.

The datasets used and/or analyzed during the current study are available from the corresponding author on reasonable request.

All authors read and approved the final version of the manuscript.

Acknowledgements

The authors are grateful for the Reviewers and Editors of the Journal for their thorough work and valuable suggestions.

V.K. was supported by the János Bolyai Research Scholarship of the Hungarian Academy of Sciences (BO/00750/22/5), by the New National Excellence Program of the Ministry for Innovation and Technology from the source of the National Research, Development and Innovation Fund (ÚNKP-23-5-PTE-1991) and the Research grant of Medical School, University of Pécs (KA-2022-29). This project (TKP2021-EGA-16) has been implemented with the support provided from the National Research, Development and Innovation Fund of Hungary, financed under the TKP2021-EGA funding scheme and also under the 2020-4.1.1-TKP2020 funding scheme (Project No: TKP2020-IKA-08) and NKFI-146117 to B.G.

The fMRI study was supported by the Hungarian Brain Research Program (Grant: KTIA_NAP_13-2-2015-0001, 2017-1.2.1-NKP-2017-00002; NAP2022-I-4/2022); by project no. TKP2021-EGA-25 supported by the Ministry of Innovation and Technology of Hungary from the National Research, Development and Innovation Fund, under the TKP2021-EGA funding scheme; by the Hungarian National Research, Development, and Innovation Office (grant number: K 143391); and by the ÚNKP-22-3-II-SE-27, ÚNKP-23-4-I-SE-31 New National Excellence Program of the Ministry for Culture and Innovation from the source of the National Research, Development and Innovation Fund.

Author contributions: V.K. planned the study. D.Z. and B.G. performed the stereotaxic surgery. V.K. and A.A. accomplished the animal experiments. V.K., A.A., and B.S.T. performed the ISH, and the immunostaining. A.A. and V.K. contributed to the morphometry, cell counting and statistical evaluations. B.G. and G.B. helped with microscopy and digital images. A.A., V.K., and B.G. prepared the figures and wrote the manuscript. E.P. provided the C57BL6/J mice. Z.M., P.G., and P.S. were responsible for collection of the perfused human EW samples. K.G. and G.J. performed the human fMRI study. B.G. and D.Z. gave advice in the preparation of the manuscript. All authors have read and approved the final version of the manuscript.

Supplemental digital content

Supplemental digital content associated with this article can be found online at http://links.lww.com/PAIN/C72.

Article history:
Received 16 December 2023
Received in revised form 19 April 2024
Accepted 2 May 2024
Available online 14 June 2024

References

[1] Al-Omari A, Kecskés M, Gaszner B, Biró-Sütő T, Fazekas B, Berta G, Kuzma M, Pintér E, Kormos V. Functionally active TRPA1 ion channel is downregulated in peptidergic neurons of the Edinger-Westphal nucleus upon acute alcohol exposure. Front Cell Dev Biol 2023;10:1046559.
[2] Asghar MS, Hansen AE, Amin FM, van der Geest RJ, Koning Pvd, Larsson HBW, Olesen J, Ashina M. Evidence for a vascular factor in migraine. Ann Neurol 2011;69:635–45.
[3] Ashina M, Hansen JM, Á Dunga BO, Olesen J. Human models of migraine—short-term pain for long-term gain. Nat Rev Neurol 2017;13:713–24.
[4] Ashina H, Schytz HW, Ashina M. CGRP in human models of migraine. Handb Exp Pharmacol 2019;255:109–20.
[5] Avona A, Mason BN, Lackovic J, Wajahat N, Motina M, Quigley L, Burgos-Vega C, Moldovan Loomis C, Garcia-Martinez LF, Akopian AN, Price TJ, Dussor G. Repetitive stress in mice causes migraine-like behaviors and calcitonin gene-related peptide-dependent hyperalgesic priming to a migraine trigger. PAIN 2020;161:2539–50.
[6] Bale TL, Picetti R, Contarino A, Koob GF, Vale WW, Lee KF. Mice deficient for both corticotropin-releasing factor receptor 1 (CRFR1) and CRFR2 have an impaired stress response and display sexually dichotomous anxiety-like behavior. J Neurosci 2002;22:193–9.
[7] Bale TL, Lee KF, Vale WW. The role of corticotropin-releasing factor receptors in stress and anxiety. Integr Comp Biol 2002;42:552–5.
[8] Bartsch T, Goadsby PJ. Increased responses in trigeminocervical nociceptive neurons to cervical input after stimulation of the dura mater. Brain 2003;126:1801–13.
[9] Bates EA, Nikai T, Brennan KC, Fu YH, Charles AC, Basbaum AI, Ptáček LJ, Ahn AH. Sumatriptan alleviates nitroglycerin-induced mechanical and thermal allodynia in mice. Cephalalgia 2010;30:170–8.
[10] Benemei S, De Logu F, Li Puma S, Marone IM, Coppi E, Ugolini F, Liedtke W, Pollastro F, Appendino G, Geppetti P, Materazzi S, Nassini R. The anti-migraine component of butterbur extracts, isopetasin, desensitizes peptidergic nociceptors by acting on TRPA1 cation channel. Br J Pharmacol 2017;174:2897–911.
[11] Bhatt DK, Gupta S, Ploug KB, Jansen-Olesen I, Olesen J. MRNA distribution of CGRP and its receptor components in the trigeminovascular system and other pain related structures in rat brain, and effect of intracerebroventricular administration of CGRP on Fos expression in the TNC. Neurosci Lett 2014;559:99–104.
[12] Bhatt DK, Ramachandran R, Christensen SL, Gupta S, Jansen-Olesen I, Olesen J. CGRP infusion in unanesthetized rats increases expression of c-Fos in the nucleus tractus solitarius and caudal ventrolateral medulla, but not in the trigeminal nucleus caudalis. Cephalalgia 2015;35:220–33.
[13] Brain SD, Grant AD. Vascular actions of calcitonin gene-related peptide and adrenomedullin. Physiol Rev 2004;84:903–34.
[14] Chalmers DT, Lovenberg TW, De Souza EB. Localization of novel corticotropin-releasing factor receptor (CRF2) mRNA expression to specific subcortical nuclei in rat brain: comparison with CRF1 receptor mRNA expression. J Neurosci 1995;15:6340–50.
[15] De Souza EB, Insel TR, Perrin MH, Rivier J, Vale WW, Kuhar MJ. Corticotropin-releasing factor receptors are widely distributed within the rat central nervous system: an autoradiographic study. J Neurosci 1985;5:3189–203.
[16] de Vries T, MaassenVanDenBrink A. CGRP-targeted antibodies in difficult-to-treat migraine. Nat Rev Neurol 2019;15:688–9.
[17] Deen M, Hansen HD, Hougaard A, Nørgaard M, Eiberg H, Lehel S, Ashina M, Knudsen GM. High brain serotonin levels in migraine between attacks: a 5-HT4 receptor binding PET study. Neuroimage Clin 2018;18:97–102.
[18] Derks NM, Roubos EW, Kozicz T. Presence of estrogen receptor β in urocortin 1-neurons in the mouse non-preganglionic Edinger-Westphal nucleus. Gen Comp Endocrinol 2007;153:228–34.
[19] Derks NM, Gaszner B, Roubos EW, Kozicz LT. Sex differences in urocortin 1 dynamics in the non-preganglionic Edinger-Westphal nucleus of the rat. Neurosci Res 2010;66:117–23.
[20] Dickerson IM. Role of CGRP-receptor component protein (RCP) in CLR/RAMP function. Curr Protein Pept Sci 2013;14:407–15.
[21] Ding SL, Royall JJ, Sunkin SM, Ng L, Facer BAC, Lesnar P, Guillozet-Bongaarts A, McMurray B, Szafer A, Dolbeare TA, Stevens A, Tirrell L, Benner T, Caldejon S, Dalley RA, Dee N, Lau C, Nyhus J, Reding M, Riley ZL, Sandman D, Shen E, van der Kouwe A, Varjabedian A, Wright M, Zollei L, Dang C, Knowles JA, Koch C, Phillips JW, Sestan N, Wohnoutka P, Zielke HR, Hohmann JG, Jones AR, Bernard A, Hawrylycz MJ, Hof PR, Fischl B, Lein ES. Comprehensive cellular-resolution atlas of the adult human brain. J Comp Neurol 2016;524:3127–481.
[22] Donner NC, Davies SM, Fitz SD, Kienzle DM, Shekhar A, Lowry CA. Crh receptor priming in the bed nucleus of the stria terminalis (BNST) induces tph2 gene expression in the dorsomedial dorsal raphe nucleus and chronic anxiety. Prog Neuropsychopharmacol Biol Psychiatry 2020;96:109730.
[23] Dos Santos Júnior ED, Da Silva AV, Da Silva KRT, Haemmerle CAS, Batagello DS, Da Silva JM, Lima LB, Da Silva RJ, Diniz GB, Sita LV, Elias CF, Bittencourt JC. The centrally projecting Edinger-Westphal nucleus-I: efferents in the rat brain. J Chem Neuroanat 2015;68:22–38.
[24] Drummond PD. Tryptophan depletion increases nausea, headache and photophobia in migraine sufferers. Cephalalgia 2006;26:1225–33.
[25] Durham PL. Diverse physiological roles of calcitonin gene-related peptide in migraine pathology: modulation of neuronal-glial-immune cells to promote peripheral and central sensitization. Curr Pain Headache Rep 2016;20:48.
[26] Edlow BL, Takahashi E, Wu O, Benner T, Dai G, Bu L, Grant PE, Greer DM, Greenberg SM, Kinney HC, Folkerth RD. Neuroanatomic connectivity of the human ascending arousal system critical to consciousness and its disorders. J Neuropathol Exp Neurol 2012;71:531–46.
[27] Edvinsson L, Grell AS, Warfvinge K. Expression of the CGRP family of neuropeptides and their receptors in the trigeminal ganglion. J Mol Neurosci 2020;70:930–44.
[28] Edvinsson L. CGRP receptor antagonists and antibodies against CGRP and its receptor in migraine treatment. Br J Clin Pharmacol 2015;80:193–9.
[29] Edvinsson L. The trigeminovascular pathway: role of CGRP and CGRP receptors in migraine. Headache 2017;57(suppl 2):47–55.
[30] Farkas S, Bölcskei K, Markovics A, Varga A, Kis-Varga Á, Kormos V, Gaszner B, Horváth C, Tuka B, Tajti J, Helyes Z. Utility of different outcome measures for the nitroglycerin model of migraine in mice. J Pharmacol Toxicol Methods 2016;77:33–44.
[31] Fehér M, Márton Z, Szabó Á, Kocsa J, Kormos V, Hunyady Á, Kovács LÁ, Ujvári B, Berta G, Farkas J, Füredi N, Gaszner T, Pytel B, Reglődi D,

Gaszner B. Downregulation of PACAP and the PAC1 receptor in the basal ganglia, substantia nigra and centrally projecting Edinger–Westphal nucleus in the rotenone model of Parkinson's disease. Int J Mol Sci 2023;24:11843.
[32] Fekete ÉM, Inoue K, Zhao Y, Rivier JE, Vale WW, Szücs A, Koob GF, Zorrilla EP. Delayed satiety-like actions and altered feeding microstructure by a selective type 2 corticotropin-releasing factor agonist in rats: intra-hypothalamic urocortin 3 administration reduces food intake by prolonging the post-meal interval. Neuropsychopharmacology 2007;32:1052–68.
[33] Fox JH, Lowry CA. Corticotropin-releasing factor-related peptides, serotonergic systems, and emotional behavior. Front Neurosci 2013;7: 169.
[34] Gaszner B, Csernus V, Kozicz T. Urocortinergic neurons respond in a differentiated manner to various acute stressors in the Edinger-Westphal nucleus in the rat. J Comp Neurol 2004;480:170–9.
[35] Gaszner B, Van Wijk DCWA, Korosi A, Józsa R, Roubos EW, Kozicz T. Diurnal expression of period 2 and urocortin 1 in neurons of the non-preganglionic Edinger-Westphal nucleus in the rat. Stress 2009;12: 115–24.
[36] Gaszner B, Kormos V, Kozicz T, Hashimoto H, Reglodi D, Helyes Z. The behavioral phenotype of pituitary adenylate-cyclase activating polypeptide-deficient mice in anxiety and depression tests is accompanied by blunted c-Fos expression in the bed nucleus of the stria terminalis, central projecting Edinger-Westphal nucleus, ventral lateral septum, and dorsal raphe nucleus. Neuroscience 2012;202: 283–99.
[37] Gecse K, Dobos D, Aranyi CS, Galambos A, Baksa D, Kocsel N, Szabó E, Pap D, Virág D, Ludányi K, Kökönyei G, Emri M, Bagdy G, Juhasz G. Association of plasma tryptophan concentration with periaqueductal gray matter functional connectivity in migraine patients. Sci Rep 2022; 12:739.
[38] Goadsby PJ, Edvinsson L. The trigeminovascular system and migraine: studies characterizing cerebrovascular and neuropeptide changes seen in humans and cats. Ann Neurol 1993;33:48–56.
[39] Goadsby PJ, Edvinsson L, Ekman R. Vasoactive peptide release in the extracerebral circulation of humans during migraine headache. Ann Neurol 1990;28:183–7.
[40] Hansen JM, Hauge AW, Olesen J, Ashina M. Calcitonin gene-related peptide triggers migraine-like attacks in patients with migraine with aura. Cephalalgia 2010;30:1179–86.
[41] Harriott AM, Strother LC, Vila-Pueyo M, Holland PR. Animal models of migraine and experimental techniques used to examine trigeminal sensory processing. J Headache Pain 2019;20:91.
[42] Henson B, Hollingsworth H, Nevois E, Herndon C. Calcitonin gene-related peptide (CGRP) antagonists and their use in migraines. J Pain Palliat Care Pharmacother 2020;34:22–31.
[43] Huang D, Grady FS, Peltekian L, Laing JJ, Geerling JC. Efferent projections of CGRP/Calca-expressing parabrachial neurons in mice. J Comp Neurol 2021;529:2911–57.
[44] Im E. Multi-facets of corticotropin-releasing factor in modulating inflammation and angiogenesis. J Neurogastroenterol Motil 2015;21: 25–32.
[45] Iyengar S, Ossipov MH, Johnson KW. The role of calcitonin gene-related peptide in peripheral and central pain mechanisms including migraine. PAIN 2017;158:543–59.
[46] Iyengar S, Johnson KW, Ossipov MH, Aurora SK. CGRP and the trigeminal system in migraine. Headache 2019;59:659–81.
[47] Jacobs B, Dussor G. Neurovascular contributions to migraine: moving beyond vasodilation. Neuroscience 2016;338:130–44.
[48] Jia Z, Yu S. Grey matter alterations in migraine: a systematic review and meta-analysis. Neuroimage Clin 2017;14:130–40.
[49] Jiang W, Li Z, Wei N, Chang W, Chen W, Sui HJ. Effectiveness of physical therapy on the suboccipital area of patients with tension-type headache: a meta-analysis of randomized controlled trials. Medicine (Baltimore) 2019;98:e15487.
[50] Juhasz G, Zsombok T, Jakab B, Nemeth J, Szolcsanyi J, Bagdy G. Sumatriptan causes parallel decrease in plasma calcitonin gene-related peptide (CGRP) concentration and migraine headache during nitroglycerin induced migraine attack. Cephalalgia 2005;25: 179–83.
[51] Jung A, Huge A, Kuhlenbäumer G, Kempt S, Seehafer T, Evers S, Berger K, Marziniak M. Genetic TPH2 variants and the susceptibility for migraine: association of a TPH2 haplotype with migraine without aura. J Neural Transm 2010;117:1253–60.
[52] Kaiser EA, Kuburas A, Recober A, Russo AF. Modulation of CGRP-induced light aversion in wild-type mice by a 5-HT1B/D agonist. J Neurosci 2012;32:15439–49.
[53] Kim SJ, Yeo JH, Yoon SY, Kwon SG, Lee JH, Beitz AJ, Roh DH. Differential development of facial and hind paw allodynia in a nitroglycerin-induced mouse model of chronic migraine: role of capsaicin sensitive primary afferents. Biol Pharm Bull 2018;41:172–81.
[54] Kormos V, Gaszner B. Role of neuropeptides in anxiety, stress, and depression: from animals to humans. Neuropeptides 2013;47:401–19.
[55] Kormos V, Kecskés A, Farkas J, Gaszner T, Csernus V, Alomari A, Hegedüs D, Renner É, Palkovits M, Zelena D, Helyes Z, Pintér E, Gaszner B. Peptidergic neurons of the Edinger-Westphal nucleus express TRPA1 ion channel that is downregulated both upon chronic variable mild stress in male mice and in humans who died by suicide. J Psychiatry Neurosci 2022;47:E162–75.
[56] Kozicz T, Li M, Arimura A. The activation of urocortin immunoreactive neurons in the Edinger-Westphal nucleus following acute pain stress in rats. Stress 2001;4:85–90.
[57] Kozicz T, Bittencourt JC, May PJ, Reiner A, Gamlin PDR, Palkovits M, Horn AKE, Toledo CAB, Ryabinin AE. The Edinger-Westphal nucleus: a historical, structural, and functional perspective on a dichotomous terminology. J Comp Neurol 2011;519:1413–34.
[58] Kozicz T. Neurons colocalizing urocortin and cocaine and amphetamine-regulated transcript immunoreactivities are induced by acute lipopolysaccharide stress in the Edinger-Westphal nucleus in the rat. Neuroscience 2003;116:315–20.
[59] Kozicz T. On the role of urocortin 1 in the non-preganglionic Edinger-Westphal nucleus in stress adaptation. Gen Comp Endocrinol 2007; 153:235–40.
[60] Lassen LH, Haderslev PA, Jacobsen VB, Iversen HK, Sperling B, Olesen J. CGRP may play a causative role in migraine. Cephalalgia 2002;22: 54–61.
[61] Li J, Ryabinin AE. Oxytocin receptors in the mouse centrally-projecting Edinger-Westphal nucleus and their potential functional significance for thermoregulation. Neuroscience 2022;498:93–104.
[62] Lipton RB, Bigal ME, Rush SR, Yenkosky JP, Liberman JN, Bartleson JD, Silberstein SD. Migraine practice patterns among neurologists. Neurology 2004;62:1926–31.
[63] Lukkes JL, Staub DR, Dietrich A, Truitt W, Neufeld-Cohen A, Chen A, Johnson PL, Shekhar A, Lowry CA. Topographical distribution of corticotropin-releasing factor type 2 receptor-like immunoreactivity in the rat dorsal raphe nucleus: Co-localization with tryptophan hydroxylase. Neuroscience 2011;183:47–63.
[64] Ma W, Chabot JG, Powell KJ, Jhamandas K, Dickerson IM, Quirion R. Localization and modulation of calcitonin gene-related peptide-receptor component protein-immunoreactive cells in the rat central and peripheral nervous systems. Neuroscience 2003;120:677–94.
[65] Maciewicz R, Phipps BS, Foote WE, Aronin N, DiFiglia M. The distribution of substance P-containing neurons in the cat Edinger-Westphal nucleus: relationship to efferent projection systems. Brain Res 1983;270:217–30.
[66] Markovics A, Kormos V, Gaszner B, Lashgarara A, Szoke E, Sandor K, Szabadfi K, Tuka B, Tajti J, Szolcsanyi J, Pinter E, Hashimoto H, Kun J, Reglodi D, Helyes Z. Pituitary adenylate cyclase-activating polypeptide plays a key role in nitroglycerol-induced trigeminovascular activation in mice. Neurobiol Dis 2012;45:633–44.
[67] Marziniak M, Kienzler C, Kuhlenbäumer G, Sommer C, Mössner R. Functional gene variants of the serotonin-synthesizing enzyme tryptophan hydroxylase 2 in migraine. J Neural Transm 2009;116: 815–9.
[68] Mason BN, Kaiser EA, Kuburas A, Loomis MCM, Latham JA, Garcia-Martinez LF, Russo AF. Induction of migraine-like photophobic behavior in mice by both peripheral and central CGRP mechanisms. J Neurosci 2017;37:204–16.
[69] Mason BN, Wattiez AS, Balcziak LK, Kuburas A, Kutschke WJ, Russo AF. Vascular actions of peripheral CGRP in migraine-like photophobia in mice. Cephalalgia 2020;40:1585–604.
[70] Messlinger K. The big CGRP flood - sources, sinks and signaling sites in the trigeminovascular system. J Headache Pain 2018;19:22.
[71] Miller S, Liu H, Warfvinge K, Shi L, Dovlatyan M, Xu C, Edvinsson L. Immunohistochemical localization of the calcitonin gene-related peptide binding site in the primate trigeminovascular system using functional antagonist antibodies. Neuroscience 2016;328:165–83.
[72] Mitsikostas DD, Knight YE, Lasalandra M, Kavantzas N, Goadsby PJ. Triptans attenuate capsaicin-induced CREB phosphorylation within the trigeminal nucleus caudalis: a mechanism to prevent central sensitization? J Headache Pain 2011;12:411–7.
[73] Napadow V, Sclocco R, Henderson LA. Brainstem neuroimaging of nociception and pain circuitries. Pain Rep 2019;4:e745.
[74] Olesen J, Diener HC, Husstedt IW, Goadsby PJ, Hall D, Meier U, Pollentier S, Lesko LM; BIBN 4096 BS Clinical Proof of Concept Study

Group. Calcitonin gene–related peptide receptor antagonist BIBN 4096 BS for the acute treatment of migraine. N Engl J Med 2004;350: 1104–10.
[75] Olesen J. Headache Classification Committee of the International Headache Society (IHS) The International Classification of Headache Disorders, 3rd edition. Cephalalgia 2018;38:1–211.
[76] Ong WY, Stohler CS, Herr DR. Role of the prefrontal cortex in pain processing. Mol Neurobiol 2019;56:1137–66.
[77] Paxinos G. The mouse brain in stereotaxic coordinates. 2nd ed. San Diego: Academic Press, 2001. p. 105–120.
[78] Priest MF, Freda SN, Badong D, Dumrongprechachan V, Kozorovitskiy Y. Peptidergic modulation of fear responses by the Edinger-Westphal nucleus. bioRxiv 2021;2021.08.05.455317.
[79] Raddant AC, Russo AF. Calcitonin gene-related peptide in migraine: intersection of peripheral inflammation and central modulation. Expert Rev Mol Med 2011;13:e36.
[80] Razeghi Jahromi S, Togha M, Ghorbani Z, Hekmatdoost A, Khorsha F, Rafiee P, Shirani P, Nourmohammadi M, Ansari H. The association between dietary tryptophan intake and migraine. Neurol Sci 2019;40: 2349–55.
[81] Rea BJ, Wattiez AS, Waite JS, Castonguay WC, Schmidt CM, Fairbanks AM, Robertson BR, Brown CJ, Mason BN, Moldovan-Loomis MC, Garcia-Martinez LF, Poolman P, Ledolter J, Kardon RH, Sowers LP, Russo AF. Peripherally administered calcitonin gene-related peptide induces spontaneous pain in mice: implications for migraine. PAIN 2018; 159:2306–17.
[82] Rorden C, Brett M. Stereotaxic display of brain lesions. Behav Neurol 2000;12:191–200.
[83] Rossi MF, Tumminello A, Marconi M, Gualano MR, Santoro PE, Malorni W, Moscato U. Sex and gender differences in migraines: a narrative review. Neurol Sci 2022;43:5729–34.
[84] Rouwette T, Klemann K, Gaszner B, Scheffer GJ, Roubos EW, Scheenen WJJM, Vissers K, Kozicz T. Differential responses of corticotropin-releasing factor and urocortin 1 to acute pain stress in the rat brain. Neuroscience 2011;183:15–24.
[85] Sakai Y, Dobson C, Diksic M, Aubé M, Hamel E. Sumatriptan normalizes the migraine attack-related increase in brain serotonin synthesis. Neurology 2008;70:431–9.
[86] Salvatore CA, Mallee JJ, Bell IM, Zartman CB, Williams TM, Koblan KS, Kane SA. Identification and pharmacological characterization of domains involved in binding of CGRP receptor antagonists to the calcitonin-like receptor. Biochemistry 2006;45:1881–7.
[87] Shapiro SS, Wilk MB. An analysis of variance test for normality (complete samples). Biometrika 1965;52:591.
[88] Shibata Y. Migraine pathophysiology revisited: proposal of a new molecular theory of migraine pathophysiology and headache diagnostic criteria. Int J Mol Sci 2022;23:13002.
[89] Skorobogatykh K, Van Hoogstraten WS, Degan D, Prischepa A, Savitskaya A, Ileen BM, Bentivegna E, Skiba I, D'Acunto L, Ferri L, Sacco S, Hansen JM, Amin FM; European Headache Federation School of Advanced Studies EHF-SAS. Functional connectivity studies in migraine: what have we learned? J Headache Pain 2019;20:108.
[90] Smith GST, Savery D, Marden C, López Costa JJ, Averill S, Priestley JV, Rattray M. Distribution of messenger RNAs encoding enkephalin, substance P, somatostatin, galanin, vasoactive intestinal polypeptide, neuropeptide Y, and calcitonin gene-related peptide in the midbrain periaqueductal grey in the rat. J Comp Neurol 1994;350:23–40.
[91] Spina MG, Langnaese K, Orlando GF, Horn TFW, Rivier J, Vale WW, Wolf G, Engelmann M. Colocalization of urocortin and neuronal nitric oxide synthase in the hypothalamus and Edinger-Westphal nucleus of the rat. J Comp Neurol 2004;479:271–86.
[92] Szekeres-Paraczky C, Szocsics P, Erőss L, Fabó D, Mód L, Maglóczky Z. Reorganization of parvalbumin immunopositive perisomatic innervation of principal cells in focal cortical dysplasia type IIB in human epileptic patients. Int J Mol Sci 2022;23:4746.
[93] Tang Y, Liu S, Shu H, Yanagisawa L, Tao F. Gut microbiota dysbiosis enhances migraine-like pain via TNFα upregulation. Mol Neurobiol 2020; 57:461–8.
[94] Tepper SJ. Anti-calcitonin gene-related peptide (CGRP) therapies: update on a previous review after the American Headache Society 60th Scientific Meeting, San Francisco, June 2018. Headache 2018;58(suppl 3):276–90.
[95] Ujvári B, Pytel B, Márton Z, Bognár M, Kovács LÁ, Farkas J, Gaszner T, Berta G, Kecskés A, Kormos V, Farkas B, Füredi N, Gaszner B. Neurodegeneration in the centrally-projecting Edinger-Westphal nucleus contributes to the non-motor symptoms of Parkinson's disease in the rat. J Neuroinflammation 2022;19:31.
[96] Valentino RJ, Lucki I, Van Bockstaele E. Corticotropin-releasing factor in the dorsal raphe nucleus: linking stress coping and addiction. Brain Res 2010;1314:29–37.
[97] van der Doelen RHA, Robroch B, Arnoldussen IA, Schulpen M, Homberg JR, Kozicz T. Serotonin and urocortin 1 in the dorsal raphe and Edinger–Westphal nuclei after early life stress in serotonin transporter knockout rats. Neuroscience 2017;340:345–58.
[98] Vaughan J, Donaldson C, Bittencourt J, Perrin MH, Lewis K, Sutton S, Chan R, Turnbull AV, Lovejoy D, Rivier C. Urocortin, a mammalian neuropeptide related to fish urotensin I and to corticotropin-releasing factor. Nature 1995;378:287–92.
[99] Vila-Pueyo M, Hoffmann J, Romero-Reyes M, Akerman S. Brain structure and function related to headache: brainstem structure and function in headache. Cephalalgia 2019;39:1635–60.
[100] Walther DJ, Peter JU, Bashammakh S, Hörtnagl H, Voits M, Fink H, Bader M. Synthesis of serotonin by a second tryptophan hydroxylase isoform. Science 2003;299:76.
[101] Wang F, Flanagan J, Su N, Wang LC, Bui S, Nielson A, Wu X, Vo HT, Ma XJ, Luo Y. RNAscope: a novel in situ RNA analysis platform for formalin-fixed, paraffin-embedded tissues. J Mol Diagn 2012;14:22–29.
[102] Wang S, Wang H, Zhao D, Liu X, Yan W, Wang M, Zhao R. Grey matter changes in patients with vestibular migraine. Clin Radiol 2019;74:898.e1–e5.
[103] Waselus M, Nazzaro C, Valentino RJ, Van Bockstaele EJ. Stress-induced redistribution of corticotropin-releasing factor receptor subtypes in the dorsal raphe nucleus. Biol Psychiatry 2009;66:76–83.
[104] Wattiez AS, Wang M, Russo AF. CGRP in animal models of migraine. Handb Exp Pharmacol 2019;255:85–107.
[105] Wiley RG, Kline IV RH. Neuronal lesioning with axonally transported toxins. J Neurosci Methods 2000;103:73–82.
[106] Wood AJJ, Welch KMA. Drug therapy of migraine. N Engl J Med 1993; 329:1476–83.
[107] Xu L, Füredi N, Lutter C, Geenen B, Pétervári E, Balaskó M, Dénes Á, Kovács KJ, Gaszner B, Kozicz T. Leptin coordinates efferent sympathetic outflow to the white adipose tissue through the midbrain centrally-projecting Edinger-Westphal nucleus in male rats. Neuropharmacology 2022;205:108898.
[108] You Y, Park JS. A novel human brainstem map based on true-color sectioned images. J Korean Med Sci 2023;38:e76.
[109] Zuniga A, Ryabinin AE. Involvement of centrally projecting Edinger-Westphal nucleus neuropeptides in actions of addictive drugs. Brain Sci 2020;10:67.

frontiers | Frontiers in Cell and Developmental Biology

TYPE Original Research
PUBLISHED 10 January 2023
DOI 10.3389/fcell.2022.1046559

OPEN ACCESS

EDITED BY
Govindan Dayanithi,
Centre National de la Recherche Scientifique (CNRS), France

REVIEWED BY
Makoto Kawasaki,
University of Occupational and Environmental Health, Japan
Seungwoo Kang,
Augusta University, United States
Kabirullah Lutfy,
Western University of Health Sciences, United States

*CORRESPONDENCE
Miklós Kecskés,
kecskes.miklos@pte.hu
Viktória Kormos,
viktoria.kormos@aok.pte.hu

†These authors have contributed equally to this work and share first authorship

SPECIALTY SECTION
This article was submitted to Molecular and Cellular Pathology, a section of the journal Frontiers in Cell and Developmental Biology

RECEIVED 16 September 2022
ACCEPTED 21 December 2022
PUBLISHED 10 January 2023

CITATION
Al-Omari A, Kecskés M, Gaszner B, Biró-Sütő T, Fazekas B, Berta G, Kuzma M, Pintér E and Kormos V (2023), Functionally active TRPA1 ion channel is downregulated in peptidergic neurons of the Edinger-Westphal nucleus upon acute alcohol exposure.
Front. Cell Dev. Biol. 10:1046559.
doi: 10.3389/fcell.2022.1046559

Functionally active TRPA1 ion channel is downregulated in peptidergic neurons of the Edinger-Westphal nucleus upon acute alcohol exposure

Ammar Al-Omari[1†], Miklós Kecskés[2*†], Balázs Gaszner[3], Tünde Biró-Sütő[1], Balázs Fazekas[1], Gergely Berta[4], Mónika Kuzma[5], Erika Pintér[1] and Viktória Kormos[1*]

[1]Department of Pharmacology and Pharmacotherapy, Centre for Neuroscience, Szentágothai Research Centre, Medical School and Molecular Pharmacology Research Group, University of Pécs, Pécs, Hungary, [2]Medical School, Institute of Physiology, University of Pécs, Pécs, Hungary, [3]Department of Anatomy, Centre for Neuroscience, Medical School and Research Group for Mood Disorders, University of Pécs, Pécs, Hungary, [4]Department of Medical Biology, Medical School, University of Pécs, Pécs, Hungary, [5]Department of Forensic Medicine, Medical School, University of Pécs, Pécs, Hungary

Introduction: The centrally projecting Edinger-Westphal nucleus (EWcp) contributes to the control of alcohol consumption by its urocortin 1 (UCN1) and cocaine- and amphetamine-regulated transcript (CART) co-expressing peptidergic neurons. Our group recently showed that the urocortinergic centrally projecting EWcp is the primary seat of central nervous system transient receptor potential ankyrin 1 (TRPA1) cation channel mRNA expression. Here, we hypothesized that alcohol and its metabolites, that pass through the blood-brain barrier, may influence the function of urocortinergic cells in centrally projecting EWcp by activating TRPA1 ion channels. We aimed to examine the functional activity of TRPA1 in centrally projecting EWcp and its possible role in a mouse model of acute alcohol exposure.

Methods: Electrophysiological measurements were performed on acute brain slices of C57BL/6J male mice containing the centrally projecting EWcp to prove the functional activity of TRPA1 using a selective, potent, covalent agonist JT010. Male TRPA1 knockout (KO) and wildtype (WT) mice were compared with each other in the morphological studies upon acute alcohol treatment. In both genotypes, half of the animals was treated intraperitoneally with 1 g/kg 6% ethanol vs. physiological saline-injected controls. Transcardial perfusion was performed 2 h after the treatment. In the centrally projecting EWcp area, FOS immunohistochemistry was performed to assess neuronal activation. TRPA1, CART, and urocortin 1 mRNA expression as well as urocortin 1 and CART peptide content was semi-quantified by RNAscope *in situ* hybridization combined with immunofluorescence.

Results: JT010 activated TRPA1 channels of the urocortinergic cells in acute brain slices. Alcohol treatment resulted in a significant FOS activation in both genotypes. Alcohol decreased the *Trpa1* mRNA expression in WT mice. The assessment of urocortin 1 peptide immunoreactivity revealed lower basal urocortin 1 in KO mice compared to WTs. The urocortin 1 peptide content was affected genotype-dependently by alcohol: the peptide content decreased in WTs while it increased

in KO mice. Alcohol exposure influenced neither CART and urocortin 1 mRNA expression nor the centrally projecting EWcp/CART peptide content.

Conclusion: We proved the presence of functional TRPA1 receptors on urocortin 1 neurons of the centrally projecting EWcp. Decreased *Trpa1* mRNA expression upon acute alcohol treatment, associated with reduced neuronal urocortin 1 peptide content suggesting that this cation channel may contribute to the regulation of the urocortin 1 release.

KEYWORDS

alcohol, centrally projecting Edinger-Westphal nucleus, transient receptor potential ankyrin 1, urocortin 1, cocaine-and amphetamine-regulated transcript, JT010

1 Introduction

Alcohol use disorders are responsible for 3 million deaths worldwide each year, accounting for 5.3% of all deaths. The pathogenic role of alcohol exposure is known for more than 200 kinds of diseases (WHO 2018). Adverse consequences of addiction include mental and behavioral changes, mood disorders, and depression. Consequent social and economic damage, family and workplace conflicts highlight the importance of this research topic.

The midbrain Edinger-Westphal nucleus (EW) consists of two distinct cell populations. The preganglionic division provides cholinergic parasympathetic preganglionic fibers to the ciliary ganglion, to control pupil constriction and lens accommodation by the oculomotor nerve. The other division is peptidergic, designated as centrally projecting EW (EWcp) (for a review see Kozicz et al., 2011). Our research team has been investigating the role of the EWcp in stress adaptation response, mood control (Gaszner and Kozicz, 2003; Gaszner et al., 2004; Gaszner et al., 2007; Gaszner et al., 2012; Rouwette et al., 2011; Kormos and Gaszner, 2013; Kormos et al., 2022; Ujvári et al., 2022) and energy metabolism (Shah et al., 2013; Xu et al., 2014; Xu et al., 2022; Füredi et al., 2017) for many years.

The EWcp neurons express several reward-, stress- and energy expenditure-related neuropeptides, e.g., cholecystokinin, pituitary adenylate cyclase-activating polypeptide and substance P (Zuniga and Ryabinin, 2020; Priest et al., 2021), but the vast majority of peptidergic neurons co-express urocortin 1 (UCN1) and cocaine and amphetamine-regulated transcript peptide (CART) (Kozicz, 2003; Priest et al., 2021; Li and Ryabinin 2022). Numerous studies have provided evidence for the involvement of the latter two EWcp neuropeptides in the actions of alcohol and other drugs of abuse (Ong and McNally, 2020; Zuniga and Ryabinin, 2020).

UCN1 is a member of the corticotropin-releasing hormone (CRH) neuropeptide family. UCN1 binds both to the CRH1 and CRH2 receptors, and it shows higher affinity to the latter than CRH itself (Vaughan et al., 1995; Janssen and Kozicz, 2013). Interestingly, all efferent connections of the EWcp that project to addiction-related areas such as the ventral tegmental area (VTA), central nucleus of the amygdala (CeA), dorsal raphe nucleus (DRN), bed nucleus of the stria terminalis (BNST), lateral hypothalamus (LH) and lateral septum (LS) are urocortinergic (Zuniga and Ryabinin, 2020) and importantly, these areas were shown to express CRH receptors (Schreiber and Gilpin 2018). Multiple genetic studies have demonstrated that high alcohol preference in mouse and rat strains was associated with increased UCN1 levels (Bachtell et al., 2002; Bachtell et al., 2003; Turek et al., 2005; Fonareva et al., 2009; Ryabinin et al., 2012). Lesions of the rodent EW greatly attenuate ethanol preference (Bachtell et al., 2004; Ryabinin and Weitemier, 2006). UCN1 cells display a robust FOS (a marker of acute neuronal activity) response upon exposure to both passive and self-administered ethanol (Bachtell et al., 1999; Ryabinin et al., 2001; Weitemier et al., 2001; Zuniga and Ryabinin, 2020). The amount of consumed ethanol correlates positively with the number of FOS positive cells and *Fos* mRNA expression in the EWcp (Sharpe et al., 2005; Giardino et al., 2017). Additionally, increased level of FOSB (a marker of chronic neuronal activity) was observed in the EWcp after a seven-day-period of 24 h access to ethanol in mice (Bachtell et al., 1999; Ozburn et al., 2012).

CART is a neuropeptide, implicated in energy metabolism (Kristensen et al., 1998; Farzi, et al., 2018; Lau et al., 2018) and regulation of feeding, drug reward and addictive behaviors (Vicentic and Jones, 2007; Zuniga and Ryabinin 2020; Ong and McNally, 2020). CART is expressed in appetite, motivation and reward-related brain areas (e.g., EWcp, paraventricular nucleus of the hypothalamus, arcuate nucleus, dorsomedial hypothalamus, LH, nucleus accumbens, amygdala, locus coeruleus, nucleus of the solitary tract, medial accessory olive) (Koylu et al., 1998; Elias et al., 2001). Although several studies were published investigating the importance of CART in addiction, only few studies are available on the role of EWcp/CART in alcohol consumption. For instance, low alcohol preference DBA/2J mice show reduced CART expression at mRNA and peptide level in the EWcp compared to alcohol preferring C57BL/6J mice (Giardino et al., 2017). Moreover, reduced alcohol intake and preference was observed in *Cart* KO mice compared to the WTs in a 24 h 2-bottle-choice procedure (Salinas et al., 2014).

The fact that UCN1 and CART fully co-localize in the EWcp, and they show increased peptide and mRNA levels in alcohol preferring mice, suggests their important and probably common role in the regulation of alcohol intake and related behaviors.

The transient receptor potential ankyrin 1 (TRPA1) is a non-selective cation channel. The role of the peripheral TRPA1 in nociception and inflammatory responses has been well established (Kádková et al., 2017; Jannis et al., 2019; Talavera et al., 2020), in contrast, only limited knowledge has accumulated on its role in the central nervous system. In our recent studies, we proved that urocortinergic neurons in EWcp uniquely express significant amount of *Trpa1* mRNA in the mouse (Kormos et al., 2022). However, an earlier calcium imaging study described the link between ethanol and TRPA1, it was examined exclusively in the context of pain: ethanol activated the human TRPA1 on human embryonic kidney-derived 293 (HEK293) cells

(Komatsu et al., 2012). Alcohol is metabolized by alcohol dehydrogenase (ADH) into the reactive and toxic intermediate product acetaldehyde, which is rapidly converted into acetic acid (Cederbaum, 2012). Acetaldehyde is considered as the major contributor of the detrimental effects by acute and chronic alcohol consumption including flushing, headache, cirrhosis, and cancer (Eriksson, 2001). Human and mouse TRPA1 receptors were activated specifically by acetaldehyde both in a HEK293T cell heterologous expression system and cultured mouse trigeminal neurons and the pharmacological inhibition of the TRPA1 receptor prevented the acetaldehyde-induced activation (Bang et al., 2007). Acetic acid was also shown to acitivate TRPA1 in trigeminal neurons in patch clamp recordings and Ca^{2+} microfluorometry (Wang et al., 2011).

Since, we showed recently the presence of the *Trpa1* only at mRNA level in urocortinergic neurons (Kormos et al., 2022) in this study we aimed to investigate whether the ion channel is functionally active in the EWcp neurons. Considering the involvement of UCN1 in acute and chronic alcohol consumption (Schreiber and Gilpin, 2018; Zuniga and Ryabinin, 2020), in this study we aimed to test if TRPA1 contributes to the recruitment of EWcp/UCN1/CART neurons in acute alcohol exposure.

2 Materials and methods

2.1 Animals

Animals were housed in a temperature and humidity controlled 12 h light-dark cycle environment (lights on at 6 a.m.) in standard polycarbonate cages (365 mm × 207 mm × 144 mm) in four to six mice per cage groups, at the animal facility of the Department of Pharmacology and Pharmacotherapy, University of Pécs. Mice were provided *ad libitum* with standard rodent chow and tap water. All procedures were approved by the Animal Welfare Committee at Pécs University, National Scientific Ethical Committee on Animal Experimentation in Hungary (BA02/2000-25/2021) in agreement with the directive of the European Communities Council in 1986, and with the Law of XXCIII, in 1998, on Animal Care and Use in Hungary.

The original breeding pairs of *Trpa1* KO mice were obtained from Prof. P. Geppetti, University of Florence, Italy. *Trpa1* KO mice were bred on C57BL/6J background and crossed back after 10 generations (Kormos et al., 2022). WT and KO mice were selected from different litters. Offspring were genotyped for *Trpa1* gene by PCR (sequences of primers: ASM2: ATC ACC TAC CAG TAA GTT CAT; ASP2: AGC TGC ATG TGT GAA TTA AAT).

2.2 Experimental design

Acute coronal brain slices containing the EWcp from 4 to 5 week-old male C57BL/6J mice (n = 10) were used for the electrophysiological recordings to prove the presence of functional TRPA1 channel using the potent and selective agonist JT010.

In an independent experiment, 9–12 week-old male *Trpa1* knockout (KO) mice and their wildtype (WT) counterparts were assigned to four experimental groups: *Trpa1* KO (n = 7) and WT (n = 7) mice were intraperitoneally (i.p.) injected with 6% ethanol (D = 1 g/kg), while another set of *Trpa1* KO (n = 8) and WT (n = 6) mice were injected with the same volume of physiological saline as a control (Korkosz et al., 2006; Pradhan et al., 2013). Mice were euthanized 2 h after the treatment for the morphological studies, which is the time required after the onset of the stimuli to reach the peak of FOS protein expression (Chaudhuri et al., 2000; Zhong et al., 2014).

2.3 Acute brain slice preparation for electrophysiology

Electrophysiology experiments were performed in acute coronal brain slices containing the EWcp (from Bregma −2.92 to −4.04 according to Paxinos and Franklin, 2001) taken from C57BL/6J mice. Under deep isoflurane anesthesia, mice were decapitated and 300 µm thick coronal slices were cut in ice-cold external solution containing (in mM): 93 NMDG, 2.5 KCl, 25 Glucose, 20 HEPES, 1.2 NaH_2PO_4, 10 $MgSO_4$, .5 $CaCl_2$, 30 $NaHCO_3$, 5 L-ascorbate, 3 Na-pyruvate, 2 thiourea bubbled with 95% O_2 and 5% CO_2. Slices were transferred to artificial cerebrospinal fluid (ACSF) containing (in mM) 2.5 KCl, 10 glucose, 126 NaCl, 1.25 NaH_2PO_4, 2 $MgCl_2$, 2 $CaCl_2$, 26 $NaHCO_3$ bubbled with 95% O_2 and 5% CO_2. After an incubation period of 10 min at 34°C in the first solution, the slices were maintained at room temperature in ACSF until use. After recordings, the sections were immersed into fixative (4% paraformaldehyde in 0.1 M PB) for overnight fixation, then 50 µm thick coronal slices were re-sectioned using a Leica VT1000S vibratome (Leica Biosystems, Wetzlar, Germany) for further immunostaining.

2.4 *In vitro* electrophysiological recordings

Patch pipettes were pulled from borosilicate glass capillaries with filament (1.5 mm outer diameter and 1.1 mm inner diameter; Sutter Instruments, Novato, CA, United States) with a resistance of 2–3 MΩ. The pipette recording solution contained (in mM) 3.5 KCl, 40 CsCl, 90 K-gluconate, 1.8 NaCl, 1.7 $MgCl_2$, 0.5 EGTA, 10 Hepes, 2 Mg-ATP and .2% Biocytin, pH 7.3 adjusted with KOH; 290–300 mOsm. Whole-cell recordings were made with Axopatch 700B amplifier (Molecular Devices, San José, CA, United States) using an upright microscope (Eclipse FN1, Nikon) with 40× (NA: .8) water immersion objective lens equipped with differential interference contrast (DIC) optics. DIC images were captured with an Andor Zyla 5.5 s CMOS camera (Oxford Instruments, Abingdon, United Kingdom). All recordings were performed at 32°C, in ACSF bubbled with 95% O_2 and 5% CO_2. Cells with lower than 20 MΩ access resistance (continuously monitored) were accepted for analysis. Signals were low-pass filtered at 5 kHz and digitized at 20 kHz (Digidata 1550B, Molecular Devices). When it is indicated 5 µM JT010, 10 µM CNQX (Sigma) and 1 µM Gabazine (Sigma) were applied to the bath solution. In these experiments membrane potential was manually adjusted (max. −50 pA) to keep the neuron just below the threshold for action potential (AP) firing. This method allowed us the easily monitor the effect of TRPA1 activation since ~5 mV depolarization already induced AP firing.

2.5 Perfusion and tissue collection

WT and *Trpa1* KO mice were euthanized 2 h after the alcohol administration with an overdose of urethane (2.4 g/kg) injected

intraperitoneally. Then, tail clipping was performed to validate their genotype, and urine was collected by a urinary bladder puncture into a syringe. The samples were filled into pre-chilled tubes and stored at −20°C for urine alcohol concentration (UAC) measurements. Then, mice were perfused transcardially by 20 mL of ice-cold 0.1 M phosphate-buffered saline (PBS) (pH: 7.4) followed by 150 mL 4% paraformaldehyde (PFA) solution in Millonig buffer (pH 7.4).

Brain samples were dissected and post-fixed for 72 h at 4°C in PFA solution. The brains were coronally sectioned using a Leica VT1000S vibratome (Leica Biosystems, Wetzlar, Germany). Four series of 30 µm sections were collected and stored in PBS containing sodium-azide (.01%) at 4°C, and for long term storage at −20°C, they were transferred into antifreeze solution. Four representative sections of the EWcp (from Bregma −2.92 to −4.04 according to Paxinos and Franklin, 2001) per animal were selected for each staining.

2.6 Urine alcohol concentration measurement

The ethanol content of the urine samples was examined by headspace gas chromatography with flame-ionization detection (Agilent 7890A GC system, G1888 Network Headspace Sampler). 50 µL of sample was added to 500 µL of internal standard solution (tert-butanol solution with a concentration of 0.05 g/L) previously introduced into a 20-mL headspace vial. The vial was crimp sealed and thermostated at 75°C ± 0.1°C. After the equilibrium was established (15 min), 2 µL of vapor was injected directly into the chromatographic columns (DB-ALC1, Agilent J&W Scientific, 30 m × 0.32-mm i.d., 1.8-µm film thickness and DB-ALC2, Agilent J&W Scientific, 30 m × .32-mm i.d., 1.2-µm film thickness). The HS loop and transfer line temperatures were set at 75°C and 85°C, respectively. The injection port temperature was held at 150°C and used in split mode with a split ratio of 5:1. The flame ionization detector (FID) temperature was maintained at 260°C. Nitrogen was used as carrier gas. The GC oven temperature was kept at 35°C during the run time (4 min). The analytical method was validated for system suitability, selectivity, accuracy, linearity, repeatability, and intermediate precision in accordance with the current ICH guidelines [https://www.ema.europa.eu/en/documents/scientific-guideline/ich-guideline-q2r2-validation-analytical-procedures-step-2b_en.pdf (accessed 17 August 2022)]. Detector response was linear over the range of 0.025–2.5 g/L for both acetaldehyde and ethanol. The detection limit (DL) and quantitation limit (QL) values of both compounds were found to be 0.015 g/L and 0.025 g/L, respectively.

2.7 RNAscope *in situ* hybridization combined with immunofluorescence

RNAscope *in situ* hybridization (ISH) was performed to measure the expression of *Trpa1*, *Cart,* and *Ucn1* mRNA in EWcp. The pretreatment procedure was optimized for 30 µm-thick PFA-fixed sections (Kormos et al., 2022). Further steps of RNAscope (probe hybridization, signal amplification and channel development) were performed according to RNAscope Multiplex Fluorescent Reagent Kit v2 user manual (ACD, Hayward, CA, United States). Mouse *Trpa1* (ACD; Cat. No.: 400211), *Cart* (ACD; Cat. No.: 432001) and *Ucn1* probes (ACD; Cat. No.: 466261) were visualized by cyanine 3 (Cy3) (1:750 for *Trpa1* and 1:3000 for *Cart*) and fluorescein (1:3000 for *Ucn1*) dyes, respectively.

In case of the *Trpa1,* ISH was combined with immunofluorescence for UCN1 to examine the peptide content also. After the RNAscope procedure, slides were treated with polyclonal rabbit anti-UCN1 antibody (RRID: AB 2315527, gift from Prof. Wylie W. Vale, Salk Institute La Jolla, CA, United States) diluted to 1:20.000, for 24 h at 24°C. After 2 min × 15 min washes, Alexa 488-conjugated donkey anti-rabbit antibody (Jackson Immunoresearch Europe Ltd., Cambridgeshire, United Kingdom; Cat. No: 711-545-152, diluted to 1:500) was used for 3 h at 24°C. Sections were counterstained with DAPI (ACD) and covered with ProLong Gold Antifade (Thermo Fisher Scientific, Waltham, MA, United States) mounting medium.

Mouse 3-plex positive (ACD; Cat. No: 320881) control probes specific to *Polr2a* mRNA (fluorescein), *Ppib* mRNA (Cy3) and *Ubc* mRNA (cyanine 5, Cy5) and 3-plex negative (ACD; Cat. No: 320871) control probes to bacterial *dabP* mRNA were tested on the EWcp. The 3-plex positive control probes gave well-detectable signal in the EWcp, while the negative control probes did not give any recognizable fluorescence in the preparations (images not shown).

The specificity of the rabbit UCN1 (RRID: AB 2315527, gift from WW Vale, Salk Institute La Jolla, CA, United States) was tested earlier in mice (see our earlier work Kormos et al., 2016). In this study, omission or replacement of primary and secondary antibodies by non-immune sera abolished labeling in both WT and KO mice (images not shown).

2.8 Immunohistochemistry with diaminobenzidine

FOS immunohistochemistry was performed to assess the acute neuronal activity in EWcp. Sections were washed three times in PBS and treated with 1% H_2O_2 (Sigma Chemical, Zwijndrecht, Netherlands) to quench endogenous peroxidase activity of the tissue. After 3 min × 10 min washes, sections were treated with .5% Triton X-100 (Sigma Chemical, Zwijndrecht, Netherlands) in PBS to enhance the permeability. Then, non-specific binding sites were blocked using 2% normal goat serum in PBS. Sections were then incubated with rabbit anti-cFOS polyclonal antibody (1:2.000, RRID: AB, 2231974 Synaptic Systems GmbH, Cat. No: 226 003) in a dilution overnight at room temperature. After 3 min × 10 min washes with PBS, sections were incubated with biotinylated anti-rabbit gamma globulin for 1 h (VECTASTAIN® Elite ABC-HRP Kit, Peroxidase Rabbit IgG Vector Laboratories Cat. No: PK-6101). After washes again 3 times with PBS, sections were incubated in ABC (avidin-biotin complex) solution for 1 h. After washes they were treated with .05% diaminobenzidine (DAB) in Tris buffer with .003w/v% H_2O_2 (Sigma Chemical, Zwijndrecht, Netherlands), the latter reaction was controlled under a stereomicroscope and stopped with PBS. Sections were mounted on gelatin-coated glass slides, air-dried, treated with xylene (Merck, Leicester, United Kingdom) and coverslipped with DPX mounting medium (Merck, Leicester, United Kingdom).

The specificity of the FOS serum was tested in our recent work (Kovács et al., 2019) by preabsorption, using the respective blocking peptide (Synaptic Systems, Cat. No: 226-0P). Omission and replacement controls were performed also on some randomly selected sections collected in alcohol-treated mice, and no immunosignal was recognizable.

2.9 Immunofluorescence

In case of acute EWcp slices, Biocytin and UCN1 fluorescent labeling were performed to identify the electrophysiologically examined urocortinergic neurons. Sections were washed 2 min × 15 min with PBS then treated with .5% Triton X-100 (Sigma Chemical, Zwijndrecht, Netherlands) in PBS with Alexa 488-conjugated Streptavidin (Cat. No: 016-540-084 Jackson Immunoresearch Europe Ltd., Cambridgeshire, United Kingdom) diluted to 1:2.000, for 2 h. After washes, polyclonal rabbit anti-UCN1 antibody (RRID: AB 2315527, gift from Prof. Wylie W. Vale, Salk Institute La Jolla, CA, United States) was used diluted to 1:5.000, overnight at 24°C. After washes, Cy3-conjugated donkey anti-rabbit antibody (Cat. No: 711-165-152, Jackson) was used diluted to 1: 500 for 3 h. Sections were mounted on gelatin-coated glass slides then air-dried and coverslipped with glycerol-PBS (1:1).

In case of acute alcohol exposure model, CART immunofluorescence was performed to semi-quantify the peptide content of the EWcp neurons. Sections were washed 2 min × 15 min with PBS then treated with .5% Triton X-100 (Sigma Chemical, Zwijndrecht, Netherlands) in PBS for 30 min and blocked with 2% normal donkey serum in PBS. Sections were incubated with anti-CART rabbit antibody [Phoenix H-003-62 (55–102)] in 1: 10.000 dilution overnight at room temperature. After 2 min × 15 min washes with PBS, sections were incubated with Cy3-conjugated donkey anti-rabbit antibody (Cat. No.: 711-165-152 Jackson) in 1: 500 dilution for 3 h. After washes, sections were mounted on gelatin-coated glass slides, air-dried and coverslipped with glycerol-PBS (1:1).

The specificity of the rabbit CART antibody (RRID: AB 2313614 Phoenix Europe GmbH, Karlsruhe, Germany) was tested earlier (Armbruszt et al., 2015). In this study, omission or replacement of primary and secondary antibodies by non-immune sera abolished labeling in both WT and *Trpa1* KO mice (images not shown).

2.10 Microscopy, digital imaging and morphometry

The DAB-labeled sections were studied and digitalized by a Nikon Microphot FXA microscope with a Spot RT camera (Nikon, Tokyo, Japan). The number of FOS-positive nuclei was determined by manual cell counting on the whole cross section surface area of the EWcp.

Fluorescent labeled sections were digitalized by an Olympus FluoView 1000 confocal microscope (Olympus, Europa, Hamburg, Germany) in sequential scanning in analogue mode. We used 80 µm confocal aperture (optical thickness 3.5 µm), 1024 × 1024-pixel resolution, and a ×60 objective for scanning. The excitation and emission spectra for the respective fluorophores were selected using built-in settings of the FluoView software (FV10-ASW; Version 0102, Olympus, Europa, Hamburg, Germany). DAPI was excited at 405 nm, Fluorescein and Alexa 488 at 488 nm and Cy3 at 550 nm. Sections were scanned for the respective wavelengths at three channels. Digital images of the three channels, depicting the same area, were automatically superimposed and merged. Co-localization was assessed on digital images showing virtual blue (DAPI), green (fluorescein), and red (Cy3) colors representing the fluorescent signals of the three channels.

The UCN1 and CART signals showed a confluent or cluster-like patterns both at mRNA and peptide level. As counting of individual fluorescent dots was not possible, the intensity of the fluorescence was measured by ImageJ software (version 1.42., NIH, Bethesda, MD) in 5–10 cell bodies using four non-edited images of the corresponding channel. The region of interest was manually determined at cytoplasmic areas of neurons. The signal density was corrected for the background signal. The average of the specific signal density (SSD) of 5–10 neurons was determined in four sections per animal. The average of these four values represented the SSD value of one mouse. The SSD was expressed in arbitrary units (a.u.).

The *Trpa1* mRNA signal appeared as well distinguishable scattered fluorescent dots. The number of dots per cell was manually counted in the 5-10 *Trpa1*-expressing neurons, in four sections per animal. Finally, these values were averaged as described above.

2.11 Statistics

Data were expressed as mean ± standard error of the mean for each experimental group. Data sets were tested for normality (Shapiro–Wilk test; Shapiro and Wilk, 1965) and homogeneity (Bartlett's Chi-square test; Snedecor and Cochran, 1989) of variance. Outlier data beyond the two-sigma range were excluded. Data were evaluated by two-way analysis of variance (ANOVA). Tukey's *post hoc* tests were performed based on first or second order effects in ANOVA tests.

Student's *t*-test for independent samples was used to compare the *Trpa1* mRNA expression of alcohol treated vs. control WT mice. Analyses were conducted using Statistica 8.0 (StatSoft, Tulsa, OK) (alpha = 5%).

All statistical analyses of electrophysiological data were performed using Clampfit v. 10.7 (Molecular Devices) and OriginPro v. 8.6. Data were evaluated by Tukey's *post hoc* test upon one-way ANOVA.

3 Results

3.1 Electrophysiology

To test whether TRPA1 is functionally active on EWcp neurons we performed slice patch clamp recordings in whole cell configuration. All patched neurons were filled with biocytin and tested for UCN1 immunopositivity *post hoc* Figures 1A–C. Only UCN1-immunoreactive cells were used in statistical analysis. UCN1-immunoreactive neurons were tonically active at resting membrane potential Figure 1D as it was shown previously (Topilko et al., 2022). We used JT010, a potent and selective, covalently binding agonist to activate TRPA1 (Takaya et al., 2015). Since recording of a relatively small transmembrane current in neurons can be challenging, we decided to monitor membrane potential changes in current clamp mode upon application of JT010. Resting membrane potential of recorded cells were adjusted via the amplifier to keep the cells just below the threshold for AP firing (few AP still occurred). This strategy prevented spontaneous firing, however even a moderate membrane potential depolarization -by the activation of TRPA1- resulted in high frequency firing. Firing frequency was significantly increased during JT010 application in UCN1-immunoreactive neurons (Figures 1E, F).

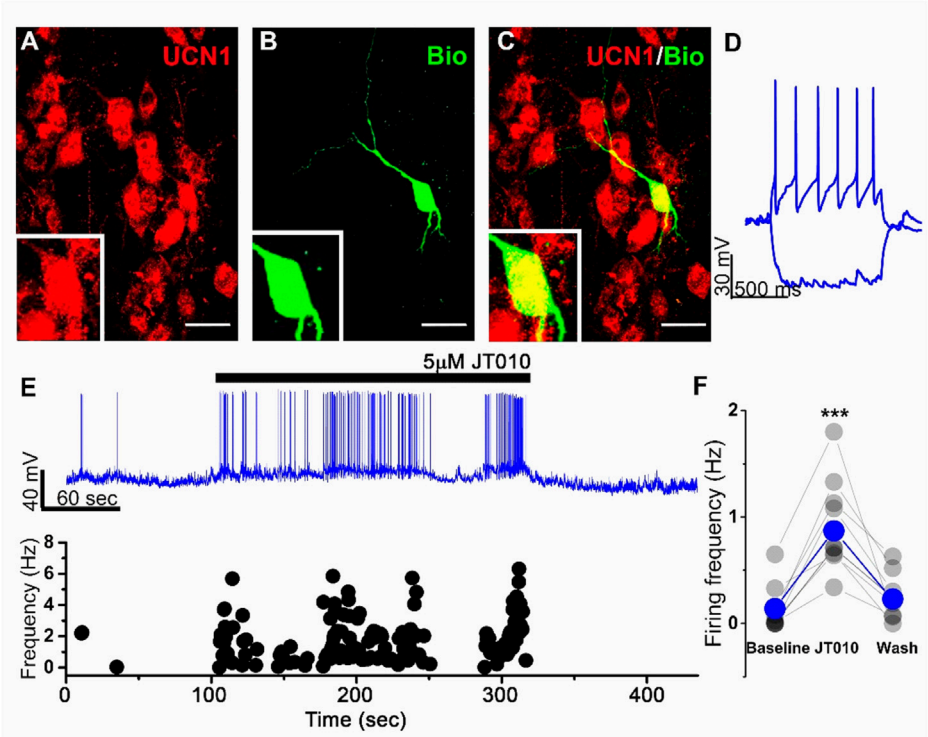

FIGURE 1
JT010 increases spontaneous firing frequency of UCN1-immunoreactive neurons in the EWcp nucleus. Representative confocal images of UCN1-immunoreactive (red) cells **(A)** and a biocytin (green) filled patched neuron **(B)** and the merged image **(C)**. Insets shows the magnified soma of the patched neuron. Scale bars: 40 μm. Response of the recorded cell **(D)** to 1 s current injection (–100 and +100 pA). Representative current clamp recordings (E, upper panel) showing the spontaneous activity of UCN1-immunoreactive neuron. Black bar represents JT010 application (5 μM). Instantaneous firing frequency **(E)**, lower panel] of each action potential in the upper recording is plotted. Statistics **(F)** showing the firing frequency at baseline (2 min before drug application) during JT010 application and after washing out the drug (n = 9 from 4 mice). ***p < .001; Tukey's *post hoc* test upon one-way ANOVA.

AP frequency was .14 ± .07 Hz at baseline, .87 ± .17 Hz during drug application and .22 ± .07 Hz after washing out the drug (n = 9/4 mice) (Figure 1F). Interestingly, after bath application of fast synaptic blockers (CNQX and Gabazine) the effect of JT010 was still present indicating that it acts directly on UCN1 positive neurons (Supplementary Figure S2). Notably UCN1-immunonegative neurons in the EW region showed no change in firing frequency or in membrane potential upon the application of JT010 (Supplementary Figure S1).

3.2 UAC measurement

The ethanol content of the urine samples was examined by headspace gas chromatography. As expected, no ethanol was detectable in the urine of the saline-treated groups. We detected similar ethanol concentration in the urine of both alcohol-treated WT and *Trpa1* KO animals (ANOVA, main effect of treatment: $F_{1,24} = 37.030$; $p < 10^{-6}$; main effect of genotype $F_{1,24} = .09$; $p = .76$) (Figure 2).

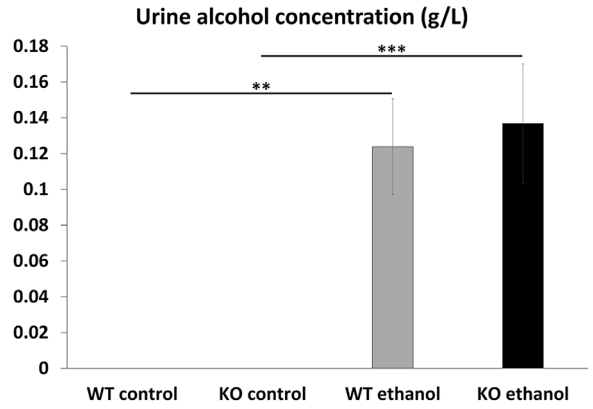

FIGURE 2
Urine alcohol concentration. Quantitative evaluation of alcohol concentration in the urine of wildtype (WT) and *Trpa1* knockout (KO) mice, 2 h after i.p., saline (control) or 1 g/kg ethanol injection. Columns show means ± SEM of alcohol concentration (g/L) (n = 6–8; **p = .002; ***p = .0009; Tukey's *post hoc* test upon two-way ANOVA).

3.3 FOS immunohistochemistry

FOS immunohistochemistry was performed to assess the acute neuronal activity in EWcp. Alcohol treatment resulted in an approximately 4-fold rise in the number of EWcp/FOS positive neurons in both WT and *Trpa1* KO animals compared to the respective controls (ANOVA, main effect of treatment: $F_{1,25} = 183.33$; $p < 10^{-6}$) without the main effect of genotype (Figures 3A, B).

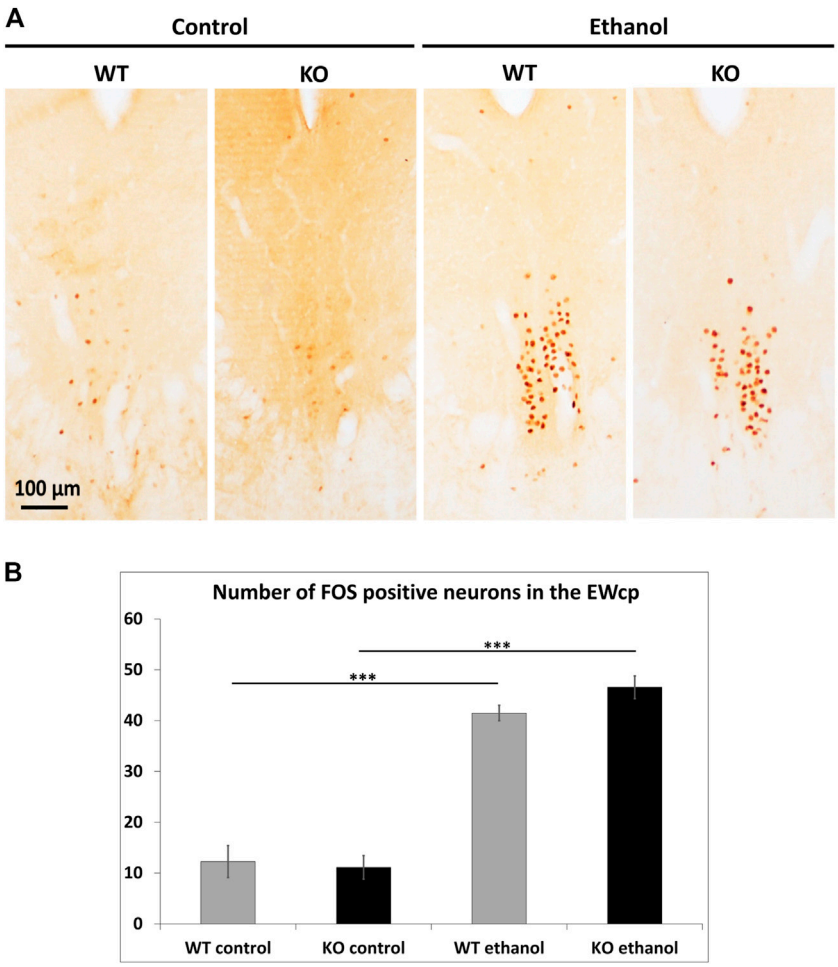

FIGURE 3
Quantitation of FOS immunoreactivity in the centrally projecting Edinger–Westphal nucleus (EWcp). **(A)** Representative immunohistochemical images showing the expression of FOS, as a marker of early neural activation, in the EWcp of wildtype (WT) and *Trpa1* knockout (KO) mice 2 h after i.p., saline (control) and 1 g/kg ethanol injection. Neuronal activation is represented by brown colored nuclei. **(B)** Quantitative evaluation of FOS immunostaining in the EWcp of WT and *Trpa1* KO mice, 2 h after i.p., saline (control) and 1 g/kg ethanol injection. Columns show means ± SEM of FOS positive neurons in the EWcp (n = 6–8; ***p = .0001; Tukey's *post hoc* test upon two-way ANOVA).

3.4 *Trpa1* RNAscope *in situ* hybridization

RNAscope ISH was performed to assess the effect of alcohol on the number of *Trpa1* mRNA transcripts in the EWcp/UCN1 neurons of WT animals. *Trpa1* mRNA showed a full co-localization with the UCN1 peptide immunosignal in the EWcp (Figure 4A). Alcohol-treated mice showed a significantly lower number of *Trpa1* transcripts compared to the controls (t_{12} = 5.345; p = .0001) (Figure 4B).

3.5 Dynamics of UCN1 mRNA and peptide upon alcohol treatment

To examine the effect of alcohol on *Ucn1* mRNA expression and UCN1 peptide content in the EWcp neurons, RNAscope ISH and immunofluorescence were performed, respectively.

There was a main effect of the genotype (ANOVA: $F_{1,23}$ = 6.758; p = .016) on *Ucn1* mRNA expression. In control groups, no difference was detected, however a lower *Ucn1* mRNA expression was observed in KO animals upon alcohol treatment (p = .030) (Figures 5A, C).

A strong effect of genotype × treatment interaction was observed (ANOVA: $F_{1,22}$ = 51.816; $p < 10^{-6}$) on UCN1 at peptide level. The basal UCN1 content of the EWcp neurons was significantly lower in *Trpa1* KO mice compared to WTs ($p < 10^{-4}$). Moreover, the UCN1 peptide content was differentially regulated by alcohol treatment in the two genotypes: it was significantly decreased in WT mice ($p < 10^{-3}$) while it increased in *Trpa1* KO animals (p = .002) (Figures 5B, D).

3.6 Dynamics of CART mRNA and peptide upon alcohol treatment

To study the effect of alcohol on *Cart* mRNA and CART peptide content in the EWcp neurons, RNAscope ISH and immunofluorescence were performed, respectively.

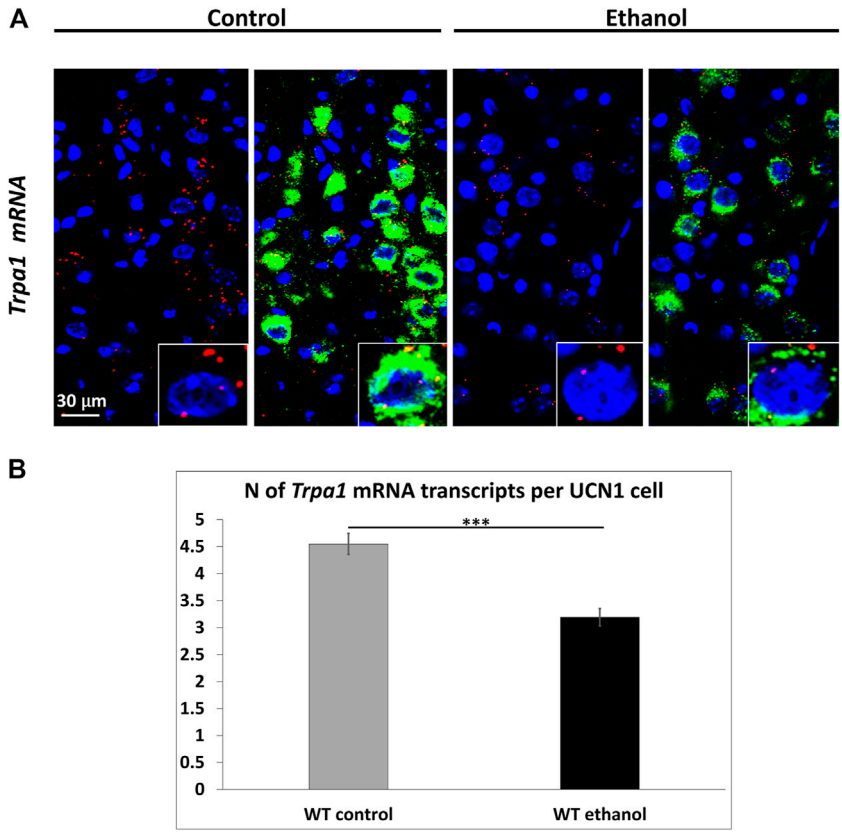

FIGURE 4
Trpa1 mRNA expression in the centrally projecting Edinger–Westphal nucleus (EWcp) of control and ethanol-treated mice. **(A)** Representative fluorescence images showing the expression of *Trpa1* mRNA (red) by RNAscope *in situ* hybridization and its co-localization with the urocortin1 (UCN1) peptide (green) by immunofluorescence, in the EWcp of *Trpa1* wildtype (WT) mice 2 h after i.p., saline (control) and 1 g/kg ethanol injection. For nuclei, the sections were counterstained with 4′,6-diamidino-2-phenylindole (DAPI) (blue). **(B)** Quantitative evaluation of *Trpa1* mRNA expression in the EWcp of WT mice, 2 h after i.p., saline (control) and 1 g/kg ethanol injection. Columns show means ± SEM of *Trpa1* mRNA transcripts in the EWcp (n = 6–8; ***p = .0001; Student's t-test).

There was a main effect of the genotype (ANOVA: $F_{1,21}$ = 10.37; p = .004) on *Cart* mRNA expression. In KO animals, a lower expression of *Cart* was observed regardless the treatment condition (Figures 6A, C).

The statistical evaluation found neither a main effect of alcohol treatment nor that of genotype on CART peptide content (Figures 6B, D).

4 Discussion

Our research group previously proved the presence of the *Trpa1* mRNA in mouse and human UCN1-immunoreactive neurons in the EWcp (Kormos et al., 2022). Here, we used an electrophysiological tool to prove the existence of the functionally active TRPA1 channel in the EWcp.

Presence of TRPA1 has been shown previously in cerebral blood vessels (Earley et al., 2009) and astrocytes (Shigetomi et al., 2012) of the mouse brain. However, the functional existence of TRPA1 in neurons of the brain was not shown before. Early studies suggested that pharmacological blockade of TRPA1 channel can be protective in granule cell degeneration (Koch et al., 2011) however this study did not prove the presence of the channel by histological experiments. Recently, we have shown using RNAscope *in situ* hybridization that *Trpa1* transcripts are present in urocortinergic neurons of the EWcp. Here, we suggest that TRPA1 is functionally active in these neurons. UCN1-immunoreactive neurons are spontaneously active and fire APs at resting membrane potential. Our hypothesis was that activation of TRPA1 in these neurons will result in Ca^{2+} influx and subsequent membrane potential depolarization which in turn will increase the frequency of spontaneous firing. Indeed, application of JT010, a selective and potent TRPA1 agonist, significantly increased the spontaneous firing frequency of UCN1-immunoreactive neurons while it was ineffective in neighboring neurons lacking UCN1. To our knowledge, this is the first evidence suggesting the functional role of TRPA1 in neurons of the mouse brain.

In our model for acute alcohol exposure, the measurement of urine alcohol concentration proved the reliability of the model as the absorption of ethanol was identical in WT and Trpa1 KO mice. Ethanol and all its metabolites efficiently pass through the blood-

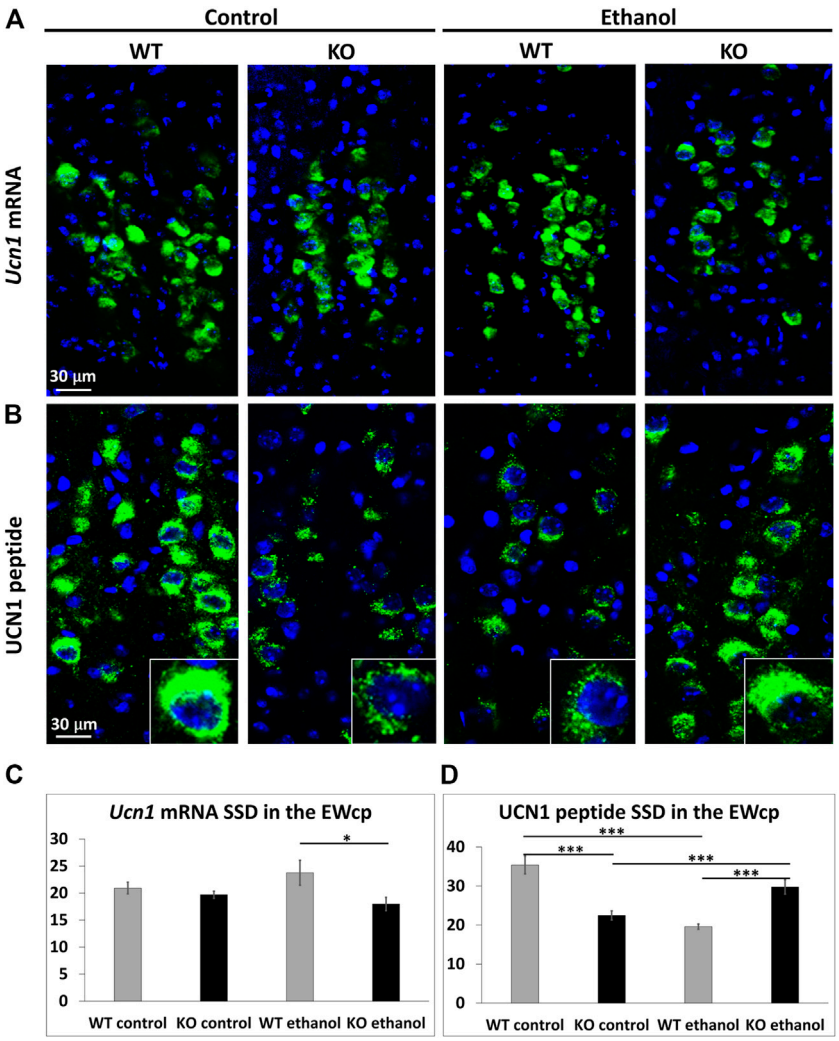

FIGURE 5
UCN1 mRNA and peptide content of the centrally projecting Edinger–Westphal nucleus (EWcp). Representative fluorescence images showing the expression of urocortin1 (*Ucn1*) mRNA (green) by RNAscope *in situ* hybridization **(A)** and the UCN1 peptide (green) by immunofluorescence **(B)**, in the EWcp of wildtype (WT) and *Trpa1* knockout (KO) mice 2 h after i.p., saline (control) and 1 g/kg ethanol injection. For nuclei, the sections were counterstained with 4′,6-diamidino-2-phenylindole (DAPI) (blue). Quantitative evaluation of *Ucn1* mRNA **(C)** and UCN1 peptide **(D)** specific signal density (SSD) in the EWcp of *Trpa1* WT and *Trpa1* KO mice, 2 h after i.p., saline (control) and 1 g/kg ethanol injection. Columns show means ± SEM of *Ucn1* mRNA **(C)** and UCN1 peptide **(D)** SSD in the EWcp (n = 6–8; *p = .03; ***p = .0001; two-way ANOVA and Tukey's *post hoc* test).

brain barrier (Nurmi et al., 1999; Quertemont and Tambour, 2004), and they were also shown to activate the TRPA1 *in vitro* (Bang et al., 2007; Wang et al., 2011; Komatsu et al., 2012) therefore, we propose that they may directly act on TRPA1 receptors in the EWcp. Increased FOS expression upon alcohol treatment further supports that alcohol could activate the EWcp urocortinergic neurons in WTs (Supplementary Figure S3), which is consistent with the literature (Bachtell et al., 1999; Ryabinin et al., 2001; Weitemier et al., 2001; Zuniga and Ryabinin, 2020). Our present finding, that the FOS activation was observed in alcohol-treated *Trpa1* KO mice also, suggests that besides the TRPA1 other receptors/ion channels may contribute to the alcohol-induced activation of urocortinergic cells. In line with this assumption, Bachtell et al. (2002) proposed that the alcohol-induced FOS response in EWcp is a result of signaling via GABA-A receptors, modified by α2A/D-adrenoceptors and dopamine receptors (Bachtell et al., 2002). Another possibility is that the alcohol-induced FOS activation in the EWcp is at least in part orchestrated through a TRPA1-independent mechanism by another alcohol-responsive brain area that innervates to the urocortinergic cells of the EWcp (Ryabinin et al., 1997; da Silva et al., 2013).

Because of the lack of genotype effect in the FOS cell counts, our data do not suggest unequivocally the role of TRPA1 in the EWcp, the reduced *Trpa1* mRNA expression in WT mice upon ethanol treatment, provides a further support for this assumption. Indeed, it is well-known that the effect of an agonist may downregulate its target (Finch et al., 2009). The fact that the *Trpa1* transcripts were restricted to the cells with UCN1 signal in both groups, on one hand replicated our recent finding that exclusively urocortinergic cells of the EWcp express the *Trpa1* (Kormos et al., 2022) on the other hand this indicates that acute alcohol treatment does not induce the

10.3389/fcell.2022.1046559

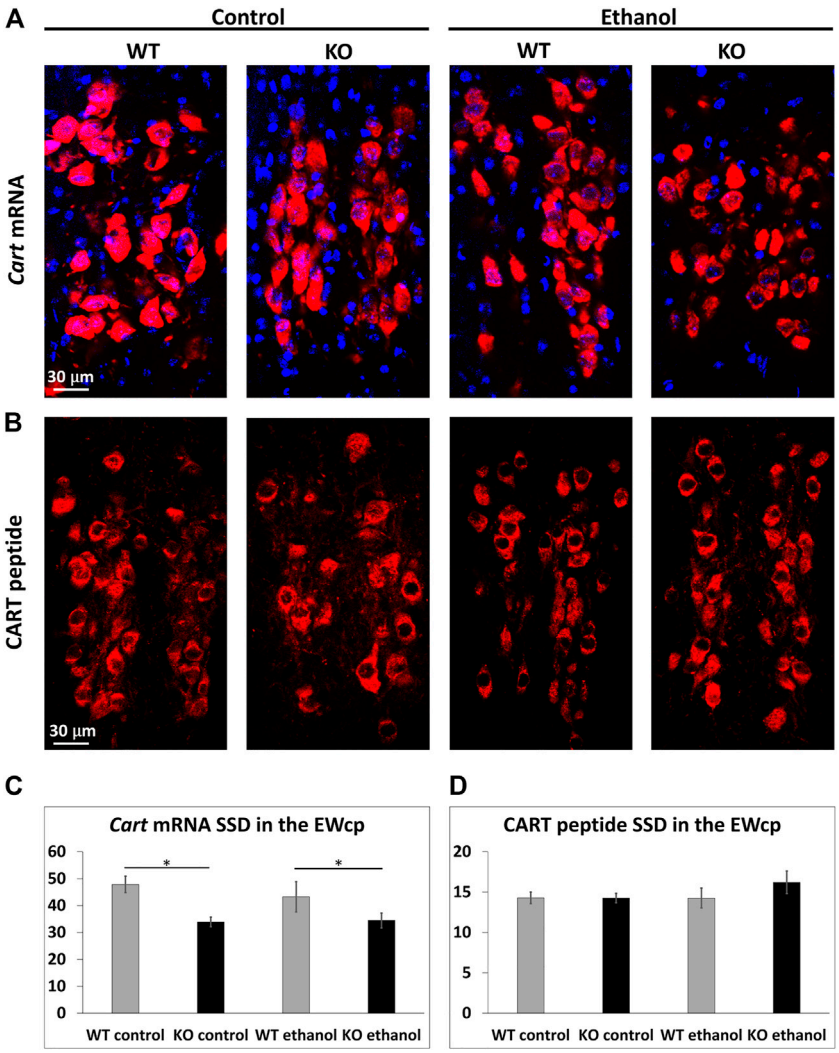

FIGURE 6
CART mRNA and peptide content of the centrally projecting Edinger–Westphal nucleus (EWcp). Representative fluorescence images showing the expression of cocaine- and amphetamine-regulated transcript (*Cart*) mRNA (red) by RNAscope *in situ* hybridization **(A)** and the CART peptide (red) by immunofluorescence **(B)**, in the EWcp of wildtype (WT) and *Trpa1* knockout (KO) mice 2 h after i.p., saline (control) and 1 g/kg ethanol injection. For nuclei, the sections were counterstained with 4′,6-diamidino-2-phenylindole (DAPI) (blue). Quantitative evaluation of *Cart* mRNA **(C)** and CART peptide **(D)** specific signal density (SSD) in the EWcp of WT and *Trpa1* KO mice, 2 h after i.p., saline (control) and 1 g/kg ethanol injection. Columns show means ± SEM of *Cart* mRNA **(C)** and CART peptide **(D)** SSD in the EWcp (n = 6–8; *p = .05; two-way ANOVA and Tukey's *post hoc* test).

transcription of *Trpa1* mRNA in non-urocortinergic EWcp cells, because we did not see any *Trpa1* mRNA transcripts outside the UCN1 neurons of the EWcp.

The UCN1 peptide content in EWcp differed between the two genotypes in saline-treated groups. The UCN1 content was much higher in WTs, compared to *Trpa1* KO mice. The comparison of the changes of UCN1 peptide content upon alcohol treatment revealed an opposite dynamics, with a decrease in WT mice, and an increase in *Trpa1* KO animals. This suggests that in WT mice the UCN1 is released from EWcp/UCN1 neurons in response to ethanol, while in *Trpa1* KO mice, increased UCN1 peptide content was observed suggesting the accumulation of the UCN1 peptide, possibly due to a reduced release. This was in part further supported by the RNAscope ISH, where we found lower *Ucn1* mRNA expression in the alcohol-treated *Trpa1* KO mice, compared to the WTs. This suggests that the peptide accumulation was associated with lower mRNA production due to the slower turnover (Gaszner et al., 2009).

Both control and alcohol-treated *Trpa1* KO animals showed lower *Cart* mRNA expression than the WT counterparts. Because the lower *Cart* mRNA expression is associated with reduced alcohol preference (Giardino et al., 2017), in our ongoing experiments we test if this is indeed characteristic for *Trpa1* KO mice. Neither the *Cart* mRNA expression, nor the CART peptide content of EWcp/UCN1 neurons was altered by acute alcohol treatment in any genotypes, suggesting that acute alcohol exposure does not have a deep impact on EWcp/CART. Based on the known role CART in addiction (Vicentic and Jones, 2007; Zuniga and Ryabinin 2020; Ong and McNally, 2020) we predict that, a chronic alcohol exposure model could prove its recruitment in alcohol abuse.

These above discussed observations together suggest that TRPA1 signaling may be involved in both the storage and release of UCN1 peptide from EWcp/UCN1 neurons. In our previous study we also found that the lack of functionally active TRPA1 affected the UCN1 content both in models of depression (Kormos et al., 2022) and posttraumatic stress disorder (Konkoly et al., 2022). In these models, we detected a genotype-related difference in the basal *Ucn1* mRNA (but not peptide) content in naïve control animals (Kormos et al., 2022; Konkoly et al., 2022). In contrast, in the present study saline-injected controls did not show a genotype difference in *Ucn1* mRNA expression but the peptide did. The discrepancy may be explained by the high acute stress sensitivity of the nucleus (Gaszner et al., 2004; Kormos et al., 2016) and by the stress effect of the ip., injection procedure.

The activation of TRPA1 in the membrane leads to calcium influx, triggering several intracellular pathways (Song and Guo, 2019). Indeed, our electrophysiological experiments showed that activation of TRPA1 increased the excitability and the rate of spontaneous firing of UCN1-expressing neurons leading to elevated calcium level. The increased intracellular calcium may cause exocytosis of the neuropeptide containing vesicles. Further experiments using pharmacological tools and electrophysiological recordings are required to the determine how exactly TRPA1 signaling contributes to the content and release of the UCN1 peptide. Considering the fact that lack of TRPA1 affected only UCN1 but not CART content of EWcp neurons regardless their co-localization (Kozicz, 2003; Priest et al., 2021; Li and Ryabinin 2022), which we also confirmed here (Supplementary Figure S4), it will be important to investigate the mechanism of UCN1-specific regulatory role of the TRPA1 channel.

5 Limitation

When assessing our present results, some limitations have to be considered. Because the functional TRPA1 receptor was deleted both in the periphery and the CNS in our global knockout mouse strain, we cannot exclude the possibility that peripheral or central compensatory mechanisms contributed to the alterations of the examined variables, observed in present study. We cannot exclude that possible litter differences influenced our results as WT and KO mice were not littermates. Because, at the moment, no reliable TRPA1 receptor antibody is available, we are unable to support our findings at protein level. The *in vivo* pharmacological manipulation on the TRPA1 receptor was also not possible due to the lack of information on the safety and pharmacokinetic profile of selective TRPA1 agonists and antagonists. We did not use alcohol for the electrophysiological experiment, because we assume, that the effect of the alcohol is not TRPA1 selective (Pozos and Oakes, 1987; Crews et al., 1996).

6 Conclusion and future perspective

With respect to the above listed limitations, in this study we proved the presence of functional TRPA1 receptors on UCN1 neurons of the EWcp. Decreased *Trpa1* mRNA expression upon acute alcohol treatment associated with reduced neuronal UCN1 peptide content suggests that this cation channel may contribute to the regulation of the UCN1 release. Taking the involvement of EWcp/UCN1 in chronic alcohol consumption and addiction in consideration (Schreiber and Gilpin, 2018; Zuniga and Ryabinin, 2020), in our ongoing research, we are investigating the recruitment of EWcp/TRPA1/UCN1/CART neurons in mouse models of chronic alcohol abuse.

Data availability statement

The raw data supporting the conclusion of this article will be made available by the authors, without undue reservation.

Ethics statement

The animal study was reviewed and approved by Animal Welfare Committee at Pécs University, National Scientific Ethical Committee on Animal Experimentation in Hungary (BA02/2000-25/2021).

Author contributions

VK planned the study. MK performed the electrophysiological investigations. VK and AA-O accomplished the animal experiments. VK, AA-O, and TB-S performed the ISH, and the immunostaining. VK, AA-O, and BF contributed to the morphometry, cell counting and statistical evaluations. MK conducted the UAC measurements. BG and GB helped with microscopy and digital images. VK, AA-O, and MK prepared the figures and wrote the manuscript. EP provided the *Trpa1* KO mice. BG and EP gave advice in the preparation of the manuscript. All authors have read and approved the final version of the manuscript.

Funding

VK was supported by the János Bolyai Research Scholarship of the Hungarian Academy of Sciences (BO/00750/22/5), by the New National Excellence Program of the Ministry for Innovation and Technology from the source of the National Research, Development and Innovation Fund (ÚNKP-22-5-PTE-1740) and the Research grant of Medical School, University of Pécs (KA-2022-29). MK was supported by the National Research Development and Innovation Office of Hungary (Grant Number: FK 135284). This project (TKP2021-EGA-16) has been implemented with the support provided from the National Research, Development and Innovation Fund of Hungary, financed under the TKP2021-EGA funding scheme and also under the 2020-4.1.1-TKP2020 funding scheme (Project No: TKP2020-IKA-08) to BG. EP was supported by the Hungarian Brain Research Programme (NAP3) 2022-2025.

Acknowledgments

Authors are grateful for the Reviewers and Editors of the Journal for their thorough work and valuable suggestions.

Conflict of interest

The authors declare that the research was conducted in the absence of any commercial or financial relationships that could be construed as a potential conflict of interest.

Publisher's note

All claims expressed in this article are solely those of the authors and do not necessarily represent those of their affiliated organizations, or those of the publisher, the editors and the reviewers. Any product that may be evaluated in this article, or claim that may be made by its manufacturer, is not guaranteed or endorsed by the publisher.

Supplementary material

The Supplementary Material for this article can be found online at: https://www.frontiersin.org/articles/10.3389/fcell.2022.1046559/full#supplementary-material

References

Armbruszt, S., Figler, M., and Ábrahám, H. (2015). Stability of CART peptide expression in the nucleus accumbens in aging. *Acta Biol. Hung.* 66 (1), 1–13. doi:10.1556/ABIOL.66.2015.1.1

Bachtell, R. K., Tsivkovskaia, N. O., and Ryabinin, A. E. (2002). Strain differences in urocortin expression in the Edinger-Westphal nucleus and its relation to alcohol-induced hypothermia. *Neuroscience* 113 (2), 421–434. PMID: 12127099. doi:10.1016/s0306-4522(02)00174-4

Bachtell, R. K., Wang, Y.-M., Freeman, P., Risinger, F. O., and Ryabinin, A. E. (1999). Alcohol drinking produces brain region-selective changes in expression of inducible transcription factors. *Brain Res.* 847, 157–165. doi:10.1016/s0006-8993(99)02019-3

Bachtell, R. K., Weitemier, A. Z., Galvan-Rosas, A., Tsivkovskaia, N. O., Risinger, F. O., Phillips, T. J., et al. (2003). The edinger-westphal-lateral septum urocortin pathway and its relationship to alcohol consumption. *J. Neurosci.* 23, 2477–2487. doi:10.1523/JNEUROSCI.23-06-02477.2003

Bachtell, R. K., Weitemier, A. Z., and Ryabinin, A. E. (2004). Lesions of the Edinger-Westphal nucleus in C57BL/6J mice disrupt ethanol-induced hypothermia and ethanol consumption. *Eur. J. Neurosci.* 20 (6), 1613–1623. doi:10.1111/j.1460-9568.2004.03594.x

Bang, S., Kim, K. Y., Yoo, S., Kim, Y. G., and Hwang, S. W. (2007). Transient receptor potential A1 mediates acetaldehyde-evoked pain sensation. *Eur. J. Neurosci.* 26 (9), 2516–2523. doi:10.1111/j.1460-9568.2007.05882.x

Cederbaum, A. I. (2012). Alcohol metabolism. *Clin. Liver Dis.* 16 (4), 667–685. doi:10.1016/j.cld.2012.08.002

Chaudhuri, A., Zangenehpour, S., Rahbar-Dehgan, F., and Ye, F. (2000). Molecular maps of neural activity and quiescence. *Acta Neurobiol. Exp.* 60, 403–410.

Crews, F. T., Morrow, A. L., Criswell, H., and Breese, G. (1996). Effects of ethanol on ion channels. *Int. Rev. Neurobiol.* 39, 283–367. PMID: 8894851. doi:10.1016/s0074-7742(08)60670-4

da Silva, A. V., Torres, K. R., Haemmerle, C. A., Cespedes, I. C., and Bittencourt, J. C. (2013). The Edinger-Westphal nucleus II: Hypothalamic afferents in the rat. *J. Chem. Neuroanat.* 54, 5–19. doi:10.1016/j.jchemneu.2013.04.001

Earley, S., Gonzales, A. L., and Crnich, R. (2009). Endothelium-dependent cerebral artery dilation mediated by trpa1 and CA2+-activated K+ channels. *Circulation Res.* 104 (8), 987–994. doi:10.1161/CIRCRESAHA.108.189530

Elias, C. F., Lee, C. E., Kelly, J. F., Ahima, R. S., Kuhar, M., Saper, C. B., et al. (2001). Characterization of CART neurons in the rat and human hypothalamus. *J. Comp. Neurol.* 432432, 1–19. doi:10.1002/cne.1085

Eriksson, C. J., Lau, J., Ip, C. K., Qi, Y., Shi, Y. C., Zhang, L., et al. (2001). The role of acetaldehyde in the actions of alcohol (update 2000). *Alcohol Clin. Exp. Res.* 25, 15S–32S. doi:10.1097/00000374-200105051-00005

Farzi, A., Lau, J., Lp, C. K., Qi, Y., Shi, Y. C., Zhang, L., et al. (2018). Arcuate nu*cleus* and lateral hypothalamic cart neurons in the mouse brain exert opposing effects on energy expenditure. *eLife* 7, 1–27. doi:10.7554/eLife.36494

Finch, A. R., Caunt, C. J., Armstrong, S. P., and McArdle, C. A. (2009). Agonist-induced internalization and downregulation of gonadotropin-releasing hormone receptors. *Am. J. Physiology - Cell Physiology* 297 (3), 591–C600. doi:10.1152/ajpcell.00166.2009

Fonareva, I., Spangler, E., Cannella, N., Sabino, V., Cottone, P., Ciccocioppo, R., et al. (2009). Increased perioculomotor urocortin 1 immunoreactivity in genetically selected alcohol preferring rats. *Alcohol. Clin. Exp. Res.* 33 (11), 1956–1965. doi:10.1111/j.1530-0277.2009.01033.x

Füredi, N., Nagy, Á., Mikó, A., Berta, G., Kozicz, T., Pétervári, E., et al. (2017). Melanocortin 4 receptor ligands modulate energy homeostasis through urocortin 1 neurons of the centrally projecting Edinger-Westphal nucleus. *Neuropharmacology* 118, 26–37. doi:10.1016/j.neuropharm.2017.03.002

Gaszner, B., Csernus, V., and Kozicz, T. (2004). Urocortinergic neurons respond in a differentiated manner to various acute stressors in the Edinger-Westphal nucleus in the rat. *J. Comp. Neurology* 480 (2), 170–179. doi:10.1002/cne.20343

Gaszner, B., Kormos, V., Kozicz, T., Hashimoto, H., Reglodi, D., and Helyes, Z. (2012). The behavioral phenotype of pituitary adenylate-cyclase activating polypeptide-deficient mice in anxiety and depression tests is accompanied by blunted c-Fos expression in the bed nucleus of the stria terminalis, central projecting Edinger-Westphal nucleus, ventral lateral septum, and dorsal raphe nucleus. *Neuroscience* 202, 283–299. doi:10.1016/j.neuroscience.2011.11.046

Gaszner, B., Korosi, A., Palkovits, M., Roubos, E. W., and Kozicz, T. (2007). Neuropeptide Y activates urocortin 1 neurons in the nonpreganglionic Edinger-Westphal nucleus. *J. Comp. Neurology* 500 (4), 708–719. doi:10.1002/cne.21177

Gaszner, B., and Kozicz, T. (2003). Interaction between catecholaminergic terminals and urocortinergic neurons in the Edinger-Westphal nucleus in the rat. *Brain Res.* 989 (1), 117–121. doi:10.1016/S0006-8993(03)03367-5

Gaszner, B., van Wijk, D. C. W. A., Korosi, A., Józsa, R., Roubos, E. W., and Kozicz, T. (2009). Diurnal expression of period 2 and urocortin 1 in neurones of the non-preganglionic Edinger-Westphal nucleus in the rat. *Stress* 12 (2), 115–124. doi:10.1080/10253890802057221

Giardino, W. J., Rodriguez, E. D., Smith, M. L., Ford, M. M., Galili, D., Mitchell, S. H., et al. (2017). Control of chronic excessive alcohol drinking by genetic manipulation of the Edinger-Westphal nucleus urocortin-1 neuropeptide system. *Transl. Psychiatry* 7 (1), e1021. doi:10.1038/tp.2016.293

Jannis, X., Meents, E., Ciotu, C. I., Michael, X., and Fischer, J. M. (2019). TRPA1: A molecular view. *Rev. Cell. Mol. Prop. Neurons J Neurophysiol* 121, 427–443. doi:10.1152/jn.00524.2018

Janssen, D., and Kozicz, T. (2013). Is it really a matter of simple dualism? Corticotropin-releasing factor receptors in body and mental health Frontiers in endocrinology. *Front. Endocrinol.* 4, 28. doi:10.3389/fendo.2013.00028

Kádková, A., Synytsya, V., Krusek, J., Zímová, L., and Vlachová, V. (2017). Molecular basis of TRPA1 regulation in nociceptive neurons. A review. *Physiological Res.* 66 (3), 425–439. doi:10.33549/physiolres.933553

Koch, M., Kreutz, S., Böttger, C., Grabiec, U., Ghadban, C., Korf, H. W., et al. (2011). The cannabinoid WIN 55, 212-2-mediated protection of dentate gyrus granule cells is driven by CB 1 receptors and modulated by TRPA1 and Ca v2.2 channels. *Hippocampus* 21 (5), 554–564. doi:10.1002/hipo.20772

Komatsu, T., Uchida, K., Fujita, F., Zhou, Y., and Tominaga, M. (2012). Primary alcohols activate human TRPA1 channel in a carbon chain length-dependent manner. *Pflugers Archiv Eur. J. Physiology* 463 (4), 549–559. doi:10.1007/s00424-011-1069-4

Konkoly, J., Kormos, V., Gaszner, B., Correia, P., Berta, G., Biró-Sütő, T., et al. (2022). Transient receptor potential ankyrin 1 ion channel expressed by the Edinger-Westphal nucleus contributes to stress adaptation in murine model of posttraumatic stress disorder. *Front. Cell Dev. Biol.* 10. doi:10.3389/fcell.2022.1059073

Korkosz, A., Zatorski, P., Taracha, E., Plaznik, A., Kostowski, W., and Bienkowski, P. (2006). Effects of ethanol on nicotine-induced conditioned place preference in C57BL/6J mice. *Prog. Neuro-Psychopharmacology Biol. Psychiatry* 30 (7), 1283–1290. doi:10.1016/j.pnpbp.2006.04.024

Kormos, V., Gáspár, L., Kovács, L., Farkas, J., Gaszner, T., Csernus, V., et al. (2016). Reduced response to chronic mild stress in PACAP mutant mice is associated with blunted FosB expression in limbic forebrain and brainstem centers. *Neuroscience* 330, 335–358. doi:10.1016/j.neuroscience.2016.06.004

Kormos, V., and Gaszner, B. (2013). Role of neuropeptides in anxiety, stress, and depression: From animals to humans. *Neuropeptides* 47 (6), 401–419. doi:10.1016/j.npep.2013.10.014

Kormos, V., Kecskés, A., Farkas, J., Gaszner, T., Csernus, V., Alomari, A., et al. (2022). Peptidergic neurons of the Edinger-Westphal nucleus express TRPA1 ion channel that is downregulated both upon chronic variable mild stress in male mice and in humans who died by suicide. *J. Psychiatry & Neurosci. JPN* 47 (3), E162–E175. doi:10.1503/jpn.210187

Kovács, L. Á., Berta, G., Csernus, V., Ujvári, B., Füredi, N., and Gaszner, B. (2019). Corticotropin-releasing factor-producing cells in the paraventricular nucleus of the

hypothalamus and extended amygdala show age-dependent FOS and FOSB/deltaFOSB immunoreactivity in acute and chronic stress models in the rat. *Front. Aging Neurosci.* 11, 274. doi:10.3389/fnagi.2019.00274

Koylu, E. O., Couceyro, P. R, Lambert, P. D, and Kuhar, M. J (1998). Cocaine- and amphetamine-regulated transcript peptide immunohistochemical localization in the rat brain. *J. Comp. Neurology* 391 (1), 115–132. doi:10.1002/(SICI)1096-9861(19980202)391:1<115:AID-CNE10>3.0

Kozicz, T., Bittencourt, J. C., May, P. J., Reiner, A., Gamlin, P. D. R., Palkovits, M., et al. (2011). The edinger-westphal nucleus: A historical, structural, and functional perspective on a dichotomous terminology. *J. Comp. Neurology* 519 (8), 1413–1434. doi:10.1002/cne.22580

Kozicz, T. (2003). Neurons colocalizing urocortin and cocaine and amphetamine-regulated transcript immunoreactivities are induced by acute lipopolysaccharide stress in the Edinger-Westphal nucleus in the rat. *Neuroscience* 116 (2), 315–320. doi:10.1016/S0306-4522(02)00772-8

Kristensen, P., Judge, M. E., Thim, L., Ribel, U., Christjansen, K. N., Wulff, B. S., et al. (1998). Hypothalamic CART is a new anorectic peptide regulated by leptin. *Nature* 393393 (6680), 668072–668076. doi:10.1038/29993

Lau, J., Farzi, A., Qi, Y., Heilbronn, R., Mietzsch, M., Shi, Y. C., et al. (2018). CART neurons in the arcuate nucleus and lateral hypothalamic area exert differential controls on energy homeostasis. *Mol. Metab.* 7, 102–118. doi:10.1016/j.molmet.2017.10.015

Li, J., and Ryabinin, A. E. (2022). Oxytocin receptors in the mouse centrally-projecting edinger-westphal nucleus and their potential functional significance for thermoregulation. *Neuroscience* 498, 93–104. doi:10.1016/J.NEUROSCIENCE.2022.07.002

Nurmi, M., Kiianmaa, K., Sinclair, J. D., Nurmi, M., Kiianmaa, K., and Brain, J. D. S. (1999). Brain ethanol levels after voluntary ethanol drinking in AA and Wistar rats. *Alcohol* 19, 113–118. doi:10.1016/s0741-8329(99)00022-1

Ong, Z. Y., and McNally, G. P. (2020). CART in energy balance and drug addiction: Current insights and mechanisms. *Brain Res.* 1740, 146852. doi:10.1016/j.brainres.2020.146852

Ozburn, A. R., Larson, E. B., Self, D. W., and McClung, C. A. (2012). Cocaine self-administration behaviors in ClockΔ19 mice. *Psychopharmacology* 223 (2), 169–177. doi:10.1007/s00213-012-2704-2

Paxinos, G, and Franklin, K (2001). *The mouse brain in stereotaxic coordinates*. San Diego, California, USA: Academic Press. 0-12-547636-1.

Pozos, R. S., and Oakes, S. G. (1987). The effects of ethanol on the electrophysiology of calcium channels. *Recent Dev. Alcohol* 5, 327–345. PMID: 2436259. doi:10.1007/978-1-4899-1684-6_13

Pradhan, A., McGuire, B., and Charles, A. (2013). Characterization of a novel model for chronic migraine. *J. Headache Pain* 14 (S1), P81. doi:10.1186/1129-2377-14-s1-p81

Priest, M. F., Freda, S. N., Badong, D., Dumrongprechachan, V., and Kozorovitskiy, Y. Peptidergic modulation of fear responses by the Edinger-Westphal nucleus. 2021, doi:10.1101/2021.08.05.455317

Quertemont, E., and Tambour, S. (2004). Is ethanol a pro-drug? The role of acetaldehyde in the central effects of ethanol. *Trends Pharmacol. Sci.* 25 (3), 130–134. doi:10.1016/j.tips.2004.01.001

Rouwette, T., Klemann, K., Gaszner, B., Scheffer, G. J., Roubos, E. W., Scheenen, W. J. J. M., et al. (2011). Differential responses of corticotropin-releasing factor and urocortin 1 to acute pain stress in the rat brain. *Neuroscience* 183, 15–24. doi:10.1016/j.neuroscience.2011.03.054

Ryabinin, A. E., Bachtell, R. K., Freeman, P., and Risinger, F. O. (2001). ITF expression in mouse brain during acquisition of alcohol self-administration. *Brain Res.* 890, 192–195. doi:10.1016/S0006-8993(00)03251-0

Ryabinin, A. E., Criado, J. R., Henriksen, S. J., Bloom, F. E., and Wilson, M. C. (1997). Differential sensitivity of c-Fos expression in hippocampus and other brain regions to moderate and low doses of alcohol. *Mol. Psychiatry* 2 (1), 32–43. doi:10.1038/sj.mp.4000206

Ryabinin, A. E., Tsoory, M. M., Kozicz, T., Thiele, T. E., Neufeld-Cohen, A., Chen, A., et al. (2012). Urocortins: CRF's siblings and their potential role in anxiety, depression and alcohol drinking behavior. *Alcohol* 46 (4), 349–357. doi:10.1016/j.alcohol.2011.10.007

Ryabinin, A. E., and Weitemier, A. Z. (2006). The urocortin 1 neurocircuit: Ethanol-sensitivity and potential involvement in alcohol consumption. *Brain Res. Rev.* 52, 368–380. doi:10.1016/j.brainresrev.2006.04.007

Salinas, A. G., Nguyen, C. T. Q., Ahmadi-Tehrani, D., and Morrisett, R. A. (2014). Reduced ethanol consumption and preference in cocaine- and amphetamine-regulated transcript (CART) knockout mice. *Addict. Biol.* 19 (2), 175–184. doi:10.1111/j.1369-1600.2012.00475.x

Schreiber, A. L., and Gilpin, N. W. (2018) Corticotropin-releasing factor (CRF) neurocircuitry and neuropharmacology in alcohol drinking, *Handb. Exp. Pharmacol.*, 248, 435–471. doi:10.1007/164_2017_86

Shah, N. S., Pugh, P. C., Nam, H., Rosenthal, D. T., van Wijk, D., Gaszner, B., et al. (2013). A subset of presympathetic-premotor neurons within the centrally projecting Edinger-Westphal nucleus expresses urocortin-1. *J. Chem. Neuroanat.* 52, 25–35. doi:10.1016/j.jchemneu.2013.04.004

Shapiro, S. S., and Wilk, M. B. (1965). An analysis of variance test for normality (complete samples). *Biometrika* 52, 591–599. doi:10.2307/2333709

Sharpe, A. L., Tsivkovskaia, N. O., and Ryabinin, A. E. (2005). Ataxia and c-Fos expression in mice drinking ethanol in a limited access session. *Alcohol. Clin. Exp. Res.* 29 (8), 1419–1426. doi:10.1097/01.alc.0000174746.64499.83

Shigetomi, E., Tong, X., Kwan, K. Y., Corey, D. P., and Khakh, B. S. (2012). TRPA1 channels regulate astrocyte resting calcium and inhibitory synapse efficacy through GAT-3. *Nat. Neurosci.* 15 (1), 70–80. doi:10.1038/nn.3000

Snedecor, G. W., and Cochran, W. G. (1989). *Statistical methods*. Ames, Iowa: Iowa State University Press.

Song, F., and Guo, J. (2019). [Progress on structural biology of voltage-gated ion channels]. *Zhejiang Da Xue Xue Bao Yi Xue Ban.* 48 (1), 25–33. Chinese. PMID: 31102354. doi:10.3785/j.issn.1008-9292.2019.02.05

Takaya, J., Mio, K., Shiraishi, T., Kurokawa, T., Otsuka, S., Mori, Y., et al. (2015). A potent and site-selective agonist of TRPA1. *J. Am. Chem. Soc.* 137 (50), 15859–15864. Epub 2015 Dec 15. PMID: 26630251. doi:10.1021/jacs.5b10162

Talavera, K., Startek, J. B., Alvarez-Collazo, J., Boonen, B., Alpizar, Y. A., Sanchez, A., et al. (2020). Mammalian transient receptor potential TRPA1 channels: From structure to disease. *Physiol. Rev.* 100 (2 725), 725–803. doi:10.1152/physrev.00005.2019

Topilko, T., Diaz, S. L., Pacheco, C. M., Verny, F., Rousseau, C. V., Kirst, C., et al. (2022)., 110. PMC9090132: PMCID, 1385–1399. Epub 2022 Feb 4. PMID: 35123655. doi:10.1016/j.neuron.2022.01.012Edinger-Westphal peptidergic neurons enable maternal preparatory nesting*Neuron*8

Turek, V. F., Tsivkovskaia, N. O., Hyytia, P., Harding, S., Lê, A. D., and Ryabinin, A. E. (2005). Urocortin 1 expression in five pairs of rat lines selectively bred for differences in alcohol drinking. *Psychopharmacology* 181 (3), 511–517. doi:10.1007/s00213-005-0011-x

Ujvári, B., Pytel, B., Márton, Z., Bognár, M., Kovács, L. Á., Farkas, J., et al. (2022). Neurodegeneration in the centrally-projecting Edinger–Westphal nucleus contributes to the non-motor symptoms of Parkinson's disease in the rat. *J. Neuroinflammation* 19 (1), 31. doi:10.1186/s12974-022-02399-w

Vaughan, J., Donaldson, C., Bittencourt, J., Perrin, M. H., Lewis, K., Sutton, S., et al. (1995). Urocortin, a mammalian neuropeptide related to fish urotensin I and to corticotropin-releasing factorThe CART (cocaine- and amphetamine-regulated transcript) system in appetite and drug addiction. *NatureJournal Pharmacol. Exp. Ther.* 378320 (65542), 287499–292506. doi:10.1038/378287a0

Vicentic, A., and Jones, D. C. (2007). The CART (cocaine- and amphetamine-regulated transcript) system in appetite and drug addiction. *J. Pharmacol. Exp. Ther.* 320 (2), 499–506. doi:10.1124/jpet.105.091512

Wang, Y. Y., Chang, R. B., Allgood, S. D., Silver, W. L., and Liman, E. R. (2011). A TRPA1-dependent mechanism for the pungent sensationof weak acids. *J. General Physiology* 137 (6), 493–505. doi:10.1085/jgp.201110615

Weitemier, A. Z., Woerner, A., Bäckström, P., Hyytiä, P., and Ryabinin, A. E. (2001). Expression of c-fos in alko alcohol rats responding for ethanol in an operant paradigm. *Alcohol Clin. Exp. Res.* 25, 704–710. doi:10.1111/j.1530-0277.2001.tb02270.x

WHO, (2018). health-topics alcohol, Available at: https://www.who.int/health-topics/alcohol#tab=tab_1 (Accessed 16 November, 2018).

Xu, L., Füredi, N., Lutter, C., Geenen, B., Pétervári, E., Balaskó, M., et al. (2022). Leptin coordinates efferent sympathetic outflow to the white adipose tissue through the midbrain centrally-projecting Edinger-Westphal nucleus in male rats. *Neuropharmacology* 205, 108898. doi:10.1016/j.neuropharm.2021.108898

Xu, L., Janssen, D., van der Knaap, N., Roubos, E. W., Leshan, R. L., Myers, M. G., et al. (2014). Integration of stress and leptin signaling by CART producing neurons in the rodent midbrain centrally projecting Edinger-Westphal nucleus. *Front. Neuroanat.* 8 (MAR), 8. doi:10.3389/fnana.2014.00008

Zhong, J., Liang, M., Akther, S., Higashida, C., Tsuji, T., and Higashida, H. (2014). C-Fos expression in the paternal mouse brain induced by communicative interaction with maternal mates. *Mol. Brain* 7 (1), 66. doi:10.1186/s13041-014-0066-x

Zuniga, A., and Ryabinin, A. E. (2020). Involvement of centrally projecting edinger– westphal nucleus neuropeptides in actions of addictive drugs. *Brain Sci.* 10 (2), 67–14. doi:10.3390/brainsci10020067